



This work has been submitted to **NECTAR**, the **Northampton Electronic Collection of Theses and Research**.

Thesis

Title: Investigation into the development of a gelatin-based biocomposite for wound-management

Creator: Poursamar, S. A.

Example citation: Poursamar, S. A. (2015) *Investigation into the development of a gelatin-based biocomposite for wound-management*. Doctoral thesis. The University of Northampton.

Version: Accepted version

<http://nectar.northampton.ac.uk/8878/>





Investigation into the Development of a Gelatin-based Biocomposite for Wound-management

Submitted in partial fulfillment for the Degree of Doctor of Philosophy

At the University of Northampton

2015

Seyed Ali Poursamar,

© Seyed Ali Poursamar, 2015

This thesis is copyright material and no quotation from it may be published without
proper acknowledgement

Disclaimer:

The content of this dissertation describes the original work by the candidate, except where specific reference is made to the work of others. No part of this dissertation has been submitted for a higher degree to any other university.

Northampton, January 2015

Seyed Ali Poursamar

Acknowledgments:

First and foremost I would like to recognise the support and the leadership that Dr. Paula Antunes showed during my research. She patiently corrected my broken English, showed exceptional leadership, and rushed to rescue my sinking spirit in the darkest days of my PhD. I cannot thank her enough. I wish her all of the world happiness wherever she ends up in the future.

I cannot express my gratitude enough towards my second Supervisor and the director of study Dr. Alexander N. Lehner, he believed in me even when I did not. He lifted me up each and every step of the way. By sharing the story of his personal journey towards academic career, he showed me that if one do everything possible, work his hardest, and stay positive, a shot at the silver lining would be in sight.

How can I not recognise tremendous help by Mrs. Tanya Haynes in the last 3 years. She was a great helping hand in the lab and she is also a great violinist that I really enjoyed her play at her concerts in numerous occasions.

I want to recognise my dear friend Mr. Hira Lal Paul (a.k.a. Bengali Tiger). I am proud to call him a friend. He is all and all a great human being, he is by far the most humble man I have ever known and he is a darn good badminton player, I wish him the health and happiness for many days to come.

Finally I want to acknowledge my beloved family. Chances are that they never read these lines, but I want the record to show how much integral they were for me to make it to this point. Their spirit kept me going. You made me a better man. So long as lord sees fit to keep on this Earth, I shall do my best to make you all proud.

Abstract:

The application of wound dressings is the most common method of wound management. In the past two decades, a novel type of wound dressing has been introduced that functions according to tissue engineering principles and provides an implantable platform for wound regeneration. The focus of this thesis was to develop such a wound dressing with multi-layer architecture that would be capable of absorbing wound exudates, be flexible with adequate contact with the wound bed, and have desirable porosity to allow cell migration. This thesis concludes with the development of a wound dressing which is comprised of three separate layers bonded together.

The first layer, which would be directly in contact with the wound bed, was a gelatin scaffold of uniform porosity produced through an optimised gas foaming method. In this part of the research, in addition to optimising the gas foaming process parameters, a comprehensive comparison between applying four different crosslinking agents (glutaraldehyde, hexamethylene diisocyanate, poly ether epoxide, and genipin) was carried out. The scaffolds, although showing a uniform porosity, had the tensile strength (240 kPa) lower than the reported value for natural skin (850 kPa). To strengthen the porous scaffold, a middle layer was applied and bonded to it.

The middle layer with a thickness of 120 μ m was adhered to the gelatin scaffold, functioning as a mechanical support and exudate absorbent. This layer comprised of a chitosan-gelatin composite which exhibited a tensile strength of 26 MPa. The chitosan-gelatin membrane bonded to the gelatin scaffold had a combined tensile strength of 644 kPa, approaching natural skin tensile properties.

The wound dressing assembly was completed by applying a plasticised gelatin membrane as the third and final layer above the chitosan-gelatin composite. This membrane with a thickness of 130 μ m, was plasticised using glycerol. It was designed with the primary function of covering the wound against debris, bacteria, and excessive manipulation, but also safeguarding the chitosan-gelatin membrane from disintegration once the wound exudate had been absorbed.

The presented multi-layer design architecture provides a combination of a conventional wound dressing occlusive functionality with a modern tissue engineering approach in one product. Application of gas foaming resulted in a pore system that had an optimised porosity in comparison with commercially available wound dressings, by providing a more spherical pore system with pore size distribution closer to desirable values for skin tissue engineering (125 μ m). It is anticipated that the design of the biomaterial would result in accelerated wound healing and reducing long term care in a cost-effective manner.

Table of Contents

Table of Contentsiii
List of Abbreviationsviii
List of Figures.....	.ix
List of Tables.....	.xi
Chapter 1 - Introduction.....	.1
1. Natural Skin Structure of Humans1
1.1. Skin Structure1
1.2. Skin Components.....	.1
2. Wound Healing Biochemistry3
2.1. Haemostasis3
2.2. Inflammation4
2.3. Proliferation Phase5
2.4. Wound Remodeling.....	.6
3. Wound Types.....	.6
3.1. Acute Wounds6
3.2. Chronic Wounds7
4. Wound Management9
5. Wound Dressings.....	.10
5.1. Foams12
5.2. Films12
5.3. Alginates13
5.4. Hydrogels.....	.13
5.5. Hydrocolloids.....	.13
5.6. Biological Wound Dressings14
6. Biomaterials Used in Wound Management16
6.1. Collagen16
6.2. Gelatin19
7. <i>In-Vivo</i> Stabilisation of Biomaterials.....	.21
7.1. Glutaraldehyde22
7.2. Polyepoxides.....	.25
7.3. Isocyanates / Di-isocyanates27
7.4. Genipin28
8. Research Overview30

Chapter 2 - Materials and Methods	32
1. Materials.....	32
2. Samples Characterisation Methods.....	32
2.1. Chemical Characterisation Methods	32
2.1.1. Fourier Transform Infra Red Spectroscopy (FT-IR).....	32
2.1.2. Thermal Analysis of Samples	32
2.1.3. Free Amine Groups Assessment (Ninhydrin Assay).....	34
2.1.4. <i>In-Vitro</i> Biodegradation Assay	35
2.2. Physical Characterisation Methods	36
2.2.1. Mechanical Properties Analysis.....	36
2.2.2. Water Absorption Analysis	37
2.2.3. Adhesion Test	37
2.2.4. Water Vapour Permeability Test	38
2.3. Visual Analysis	40
2.3.1. Visual Analysis of Samples.....	40
2.3.2. Scanning Electron Microscopy (SEM)	40
3. The Statistical Analysis	40
Chapter 3 - Preparation of Porous Gelatin Scaffolds.....	41
1. First Generation Scaffolds	42
1.1. Scaffold Preparation Method.....	42
1.2. Results	43
1.2.1. Visual Description of Scaffolds	43
1.2.2. Fourier Transform Infra-Red Spectroscopy (FT-IR).....	43
1.2.3. Mechanical Properties of the Scaffolds.....	45
1.2.4. Scaffolds Thermal Analysis	48
1.2.5. Scaffolds Microstructure Analysis	50
1.2.6. Scaffold Water Absorption	52
1.3. Summary.....	54
2. Second Generation Scaffold	55
2.1. Scaffold Preparation Method	55
2.2. Results	56
2.2.1. Visual Description of Scaffolds	56
2.2.2. Fourier Transform Infra-Red Spectroscopy (FT-IR).....	57
2.2.3. Mechanical Properties of the Scaffolds.....	58
2.2.4. Scaffolds Thermal Analysis	61

2.2.5. Scaffolds Microstructure Analysis	63
2.2.6. Scaffold Water Absorption	66
2.3. Summary.....	67
3. Third Generation Scaffold.....	68
3.1. Scaffold Preparation Method.....	68
3.2. Results	69
3.2.1. Visual Description of Scaffolds	69
3.2.2. Fourier Transform Infra-Red Spectroscopy (FT-IR).....	71
3.2.3. Mechanical Properties of the Scaffolds.....	72
3.2.4. Scaffolds Thermal Analysis	74
3.2.5. Scaffolds Microstructure Analysis	75
3.2.6. Scaffold Water Absorption	77
3.3. Summary.....	78
4. Fourth Generation Scaffold	80
4.1. Scaffolds Preparation Method.....	80
4.2. Results	82
4.2.1. Visual Description of Scaffolds	82
4.2.2. Fourier Transform Infra-Red Spectroscopy (FT-IR).....	82
4.2.3. Mechanical Properties of the Scaffolds.....	84
4.2.4. Scaffolds Thermal Analysis	86
4.2.5. Scaffolds Microstructure Analysis	88
4.2.6. Scaffold Water Absorption	91
4.2.7. <i>In-Vitro</i> Biodegradation Analysis	92
4.2.8. The Degree of Crosslinking Analysis	94
5. Conclusion	95
Chapter 4 - Stabilisation of Scaffolds.....	98
1. Hexamethylene Diisocyanate (HMDI)	98
1.1. Introduction.....	98
1.2. Crosslinking Method.....	99
1.3. Results	100
1.3.1. Visual Description of Scaffolds	100
1.3.2. Fourier Transform Infra-Red Spectroscopy (FT-IR).....	101
1.3.3. Mechanical Properties of the Scaffolds.....	104
1.3.4. Scaffolds Thermal Analysis	105
1.3.5. Scaffolds Microstructure Analysis	107

1.3.6. Scaffold Water Absorption	109
2. Poly (ethylene glycol) di-glycidyl ether (Epoxy).....	110
2.1. Introduction.....	110
2.2. Crosslinking Method.....	110
2.3. Results	111
2.3.1. Visual Description of Scaffolds	111
2.3.2. Fourier Transform Infra-Red Spectroscopy (FT-IR).....	112
2.3.3. Mechanical Properties of the Scaffolds.....	114
2.3.4. Scaffolds Thermal Analysis	116
2.3.5. Scaffolds Microstructure Analysis	117
2.3.6. Scaffold Water Absorption	119
3. Iridoid Glucosides (Genipin)	121
3.1. Introduction.....	121
3.2. Crosslinking Method.....	122
3.3. Results	122
3.3.1. Visual Description of Scaffolds	122
3.3.2. Fourier Transform Infra-Red Spectroscopy (FT-IR).....	123
3.3.3. Mechanical Properties of the Scaffolds.....	126
3.3.4. Scaffolds Thermal Analysis	128
3.3.5. Scaffolds Microstructure Analysis	129
3.3.6. Scaffold Water Absorption	131
4. Conclusion	132
Chapter 5 - Mechanical Support, (Middle Layer)	134
1. Introduction.....	134
2. Membrane Preparation Method	135
3. Results	136
3.1. Visual Descriptions of Membranes.....	136
3.2. Fourier Transform Infra-Red Spectroscopy (FT-IR).....	137
3.3. Mechanical Properties of the Membrane	139
3.4. Membrane Thermal Analysis.....	140
3.5. Membrane Water Absorption	143
4. Conclusion	144
Chapter 6 - Plasticised Cover, (Top Layer).....	145
1. Introduction.....	145
2. Membrane Preparation Method	146

3. Results	146
3.1. Fourier Transformed Infrared Spectroscopy (FT-IR).....	146
3.2. Mechanical Properties of the Gelatin Membrane	147
3.3. Membrane Thermal Analysis.....	149
3.4. Water Vapour Permeability.....	150
Chapter 7 - Final Assembled Wound Dressing	152
1. Preparation Method.....	152
2. Results	152
2.1. Visual Description of Wound Dressing	152
2.2. Mechanical Properties of the Assembled Wound Dressing	154
2.3. Adhesion Force of the Membranes	155
2.4. Wound Dressing Microstructure Analysis	156
Chapter 8 - Conclusion and Future Research Studies	158
Conclusion	158
Future Research Studies.....	160
Chapter 9 - References	162

List of Abbreviations

GT	Glutaraldehyde
HMDI	Hexamethylene diisocyanate
Epoxy	Poly(ethylene glycol) di-glycidyl ether epoxy
GAG	Glycosaminoglycan
ECM	Extra Cellular Matrix
WHO	World Health Organization
FT-IR	Fourier Transform Infra-Red Spectroscopy
DSC	Differential Scanning Calorimeter
SEM	Scanning Electron Microscope
MMP	Matrix MetalloProtease
cP	centi-Poise (Viscosity Unit)

List of Figures

Figure 1–1: Wound healing phases and relevant incidents in each phase..	3
Figure 1–2: Schematic correlation between collagen synthesis and wound strength.....	5
Figure 1–3: Assembly of collagen peptides	17
Figure 1–4: Gelatin fragments.....	20
Figure 1–5: GT reaction with collagen macromolecules	22
Figure 1–6: Proposed reaction of aldehyde groups with hydroxyl groups	23
Figure 1–7: Proposed mechanism of crosslinking for the poly epoxy compound under acidic pH's	25
Figure 1–8: Proposed mechanism of crosslinking for the poly epoxy compound under basic pH's	26
Figure 1–9: The reaction mechanism for epoxy groups with carboxylic, amino, and hydroxyl groups.	26
Figure 1–10: The reaction between hexamethylene diisocyanate (HMDI) and gelatin	28
Figure 1–11: Proposed genipin molecule reaction with gelatin	29
Figure 1–12: Proposed genipin molecule reaction with gelatin (2).	29
Figure 2–1: The wound dressing sample was glued on adhesion test.....	38
Figure 2–2: The water permeability testing apparatus.....	39
Figure 3–1: The first generation gelatin scaffold visual characteristics.	43
Figure 3–2: FT-IR spectra of the first generation gelatin scaffolds.	44
Figure 3–3: How gelatin form gel at room temperature.....	46
Figure 3–4: SEM images of the first generation gelatin scaffolds.	51
Figure 3–5: SEM image of the control samples surface at the 80x magnification. with unreacted NaHCO ₃	52
Figure 3–6: Water absorption profile of the first generation gelatin scaffolds..	53
Figure 3–7: Visual characteristics of second generation gelatin scaffold.	56
Figure 3–8: FT-IR spectra of the second generation gelatin scaffolds.	58
Figure 3–9: The impact of pH on the mechanical properties of the second generation gelatin scaffolds.	60
Figure 3–10: A comparison between second generation scaffolds thermal stability.	63
Figure 3–11: SEM images of the second generation gelatin scaffolds.	65
Figure 3–12: Water absorption profile of second generation gelatin scaffolds.....	66
Figure 3–13: The viscosity of 10% w/v gelatin solution as a function of solution temperature.	69
Figure 3–14: The third generation of gelatin scaffolds visual characteristics.	70
Figure 3–15: FT-IR spectra of the third generation gelatin scaffold.....	71
Figure 3–16: SEM images taken from the third generation of gelatin scaffolds.....	76
Figure 3–17: Water absorption properties of the third generation scaffolds.....	78
Figure 3–18: A comparison of sample preparation methods for each of four scaffold generations.	81
Figure 3–19: The visual features of the fourth generation gelatin scaffolds	82
Figure 3–20: The FT-IR spectra of the fourth generation gelatin scaffolds.....	83
Figure 3–21: A side by side comparison between amide bands of 4 different generations scaffolds.	84
Figure 3–22: A comparison of mechanical properties of different generations of gelatin scaffolds.	86
Figure 3–23: Comparison amongst the thermal characteristics of different generations of scaffolds.....	87
Figure 3–24: SEM images taken from fourth generation gelatin scaffolds.....	89
Figure 3–25: The comparison between the pore size distribution for various generations of scaffolds.	90
Figure 3–26: The water absorption characteristics of fourth generation gelatin scaffolds.	91
Figure 3–27: Comparison of water absorption capability of four generations of gelatin scaffolds.	92
Figure 3–28: Results of biodegradation analysis.....	93
Figure 3–29: The crosslinking index of fourth generation scaffolds as a function GT concentration.....	94

Figure 3-30: The low magnification SEM image of 4 th generation scaffolds.....	97
Figure 4-1: The chemical configuration of urethane and urea bonds.....	99
Figure 4-2: Visual description of the 4 th generation gelatin scaffolds crosslinked using HMDI.	101
Figure 4-3: FT-IR spectra of the 4 th generation gelatin scaffolds crosslinked with HMDI.	102
Figure 4-4: SEM analysis of the 4 th generation scaffolds crosslinked using HMDI.	107
Figure 4-5: A comparison between control gelatin samples prepared in de-ionised water and Propan-2-ol. .	108
Figure 4-6: Water absorption capability of 4 th generation scaffolds crosslinked using HMDI.	109
Figure 4-7: Visual features of the 4 th generation gelatin scaffolds crosslinked with epoxy compound.....	112
Figure 4-8: The FT-IR spectrum of 4 th generation gelatin scaffolds crosslinked using Epoxy.....	113
Figure 4-9: SEM analysis of 4 th generation scaffolds crosslinked with Epoxy.....	118
Figure 4-10: Water absorption capability of 4 th generation scaffolds crosslinked with epoxy compound.....	119
Figure 4-11: Visual features of the 4 th generation gelatin scaffolds crosslinked with genipin.....	123
Figure 4-12: The FT-IR spectrum of 4 th generation gelatin scaffolds crosslinked with genipin.....	124
Figure 4-13: The mechanical properties of gelatin scaffolds crosslinked with 4 different crosslinking agents.	126
Figure 4-14: SEM images of 4 th generation scaffolds crosslinked with genipin.	130
Figure 4-15: Water absorption ability of 4 th generation scaffolds crosslinked by genipin.....	131
Figure 4-16: A comparison amongst the crosslinking index and tensile strength.....	132
Figure 5-1: Chitosan-based membranes visual descriptions	136
Figure 5-2: FT-IR spectra of pure chitosan and chitosan-gelatin composites.	137
Figure 5-3: A typical thermograph of chitosan	141
Figure 5-4: Water absorption capability of chitosan and chitosan-gelatin membranes.	143
Figure 6-1: The FT-IR spectra of gelatin membranes with and without glycerol.	147
Figure 7-1: Images of prepared multi-layer wound dressing.	153
Figure 7-2: Tensile properties of final wound dressing.	154
Figure 7-3: The recorded force required for peeling off the gelatin scaffold.....	156
Figure 7-4: The SEM images of the final assembled wound dressing cross section.....	157

List of Tables

Table 1–1: A selected list of commercially available wound dressings.....	11
 Table 2–1: The list of DSC methods used for different specimens in this study.....	33
 Table 3–1: Mechanical properties of the first generation gelatin scaffolds.	45
Table 3–2: The results of thermal analysis of the first generation gelatin scaffold.	49
Table 3–3: Tensile strength, Young's modulus, and tensile strain of second generation gelatin scaffolds.	59
Table 3–4: Thermal analysis results of second generation gelatin scaffolds.	62
Table 3–5: Thermal analysis results of second generation gelatin scaffolds.	62
Table 3–6: Tensile properties of the third generation gelatin scaffolds.	72
Table 3–7: Thermal analysis of third generation gelatin scaffolds.....	75
Table 3–8: Tensile strength, Young's modulus, and strain of the fourth generation gelatin scaffolds.....	85
Table 3–9: Thermal characteristics of the fourth generation gelatin scaffolds.	87
 Table 4–1: Mechanical properties of 4 th generation gelatin scaffolds crosslinked using HMDI.	104
Table 4–2: Thermal analysis of HMDI-crosslinked gelatin scaffolds.	105
Table 4–3: Mechanical properties of 4 th generation gelatin scaffolds crosslinked using epoxy.	114
Table 4–4: The results of thermal analysis of 4 th generation gelatin scaffolds crosslinked using Epoxy.	116
Table 4–5: Mechanical properties of 4 th generation gelatin scaffolds crosslinked with genipin.	126
Table 4–6: A comparison between the molecular structure of crosslinking agents used in this study	128
Table 4–7: The results of thermal analysis of the 4 th generation gelatin scaffolds crosslinked using genipin... .	129
 Table 5–1: Mechanical strength of pure chitosan.....	139
Table 5–2: The results of thermal analysis of chitosan membranes.....	142
 Table 6–1: Mechanical properties of non-crosslinked and crosslinked gelatin membranes	148
Table 6–2: Thermal properties of gelatin membrane	149
 Table 7–1: Tensile properties of final assembled gelatin wound dressing and its individual components.	155

Chapter 1:

Introduction

Chapter 1 - Introduction

1. Natural Skin Structure of Humans

The skin is the largest organ in body and accounts for 15% of the body mass (Sezer *et al.*, 2011). Skin guards the underlying organs and protects the body against micro-organisms, mechanical disturbances, and UV radiation. It is also preventing the substantial dehydration of body, plays an important role in stabilising body temperature, and its embedded touch receptors facilitate its ability to sense the environment (Kamel *et al.*, 2013; Supp and Boyce, 2005).

1.1. Skin Structure

Skin is a complex multi-structural organ with substantial regional variations. It is divided into three layers: epidermis, dermis, and hypodermis (Pereira *et al.*, 2013). The epidermis is the most external layer and is avascular and thin (Böttcher-Haberzeth *et al.*, 2010). Immediately below the epidermis, is the dermis, which constitutes the bulk of the skin. The top portion of dermis is mainly collagen, elastin, and glycosaminoglycans (GAGs). Fibroblasts cells in the dermis adhere to the collagen fibres and blood arteries (Brohem *et al.*, 2011). The hypodermis is the deepest skin layer, which is composed of mainly loose connective tissue and fat (Kamel *et al.*, 2013), and provides mechanical and thermal insulating properties to the skin (Baroni *et al.*, 2012).

1.2. Skin Components

Major cell types within the skin include fibroblasts, melanocytes, and keratinocytes (MacNeil, 2007). The cells are supported by a three-dimensional matrix called the Extra Cellular Matrix (ECM). It provides tissue with structural support and modulates important process such as: development, migration, attachment, differentiation, and repair of cells (Griffith and Swartz, 2006). The ECM has five major components: collagen, a basement membrane, structural proteins, elastin, and proteoglycans (Linares, 1996). Collagen is the most abundant component of ECM (Zhao *et al.*, 2013) and will be discussed in detail in Section 6.1 of this Chapter. The basement

membrane is the interface between epidermis and dermis. It controls the diffusion between these two regions and binds to a variety of cytokines and growth factors (Brohem *et al.*, 2011). Structural proteins are a group of different proteins such as fibronectin, laminin, and thrombospondin. They link the components of the ECM to one another and to the cells (Enoch and Leaper, 2008). Elastin provides elastic recoil, controls stiffness, and resists tension. Proteoglycans resist external compression forces and hinder water and macromolecule transport in tissue (Griffith and Swartz, 2006). These five building blocks of skin are working together in order to repair damage to the skin through a process, known as *Wound Healing*.

2. Wound Healing Biochemistry

A wound is a break in the skin integrity (Sezer *et al.*, 2011). The wound healing process includes a set of diverse components: several cell types (such as fibroblasts, endothelial, macrophages), inter-cellular messengers (such as cytokines, hormones, growth factors), synthetic products (such as collagen, proteoglycans), and enzymes (such as collagenase, elastase, and their inhibitors) (Menke *et al.*, 2007). In general, the wound healing process can be divided into 4 phases occurring in chronological order: Haemostasis, Inflammation, Proliferation phase, and Wound Remodelling (Hardwicke *et al.*, 2008). Figure 1–1 summarises wound healing phases along with the incidents taking place in each phase.

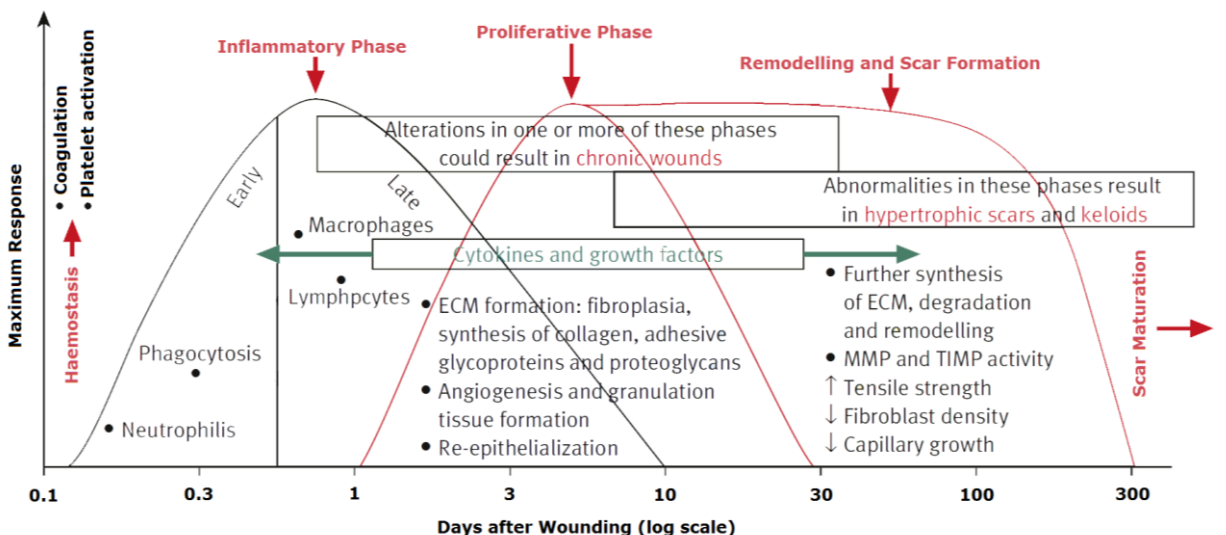


Figure 1–1: Wound healing phases and relevant incidents in each phase. The wound healing processes can be divided into 4 separate phases which overlap with each other (Enoch and Leaper, 2008).

2.1. Haemostasis

The immediate response to skin injuries is bleeding and formation of blood clots. As a result of injury, blood vessels leading to the injury sites constrict to decrease blood flow (Williamson and Harding, 2004). This includes a 5 to 10 minutes period of intense artery constriction that contributes to haemostasis (Garrison, 2001). Bleeding is halted through the formation of the blood clots by platelet aggregation and the formation of

haemostatic plugs (Gurtner *et al.*, 2008). Platelets release a variety of growth factors into the injury site. The growth factors initiate the wound healing cascade by attracting fibroblast, endothelial, and immune system cells (Vincent, 2005). The attraction of immune cells to the wound site initiates the next phase of wound healing known as the *Inflammation Phase*.

2.2. Inflammation

The Inflammation Phase is highlighted by the aggregation of white blood cells (known as neutrophils), macrophages and lymphocytes in the injury site (Hardwicke *et al.*, 2008). The neutrophils clear the wound environment from foreign bodies and bacteria (Gurtner *et al.*, 2008). By the end of this phase, neutrophils undergo apoptosis (programmed cell death) or digestion by another cell type, called macrophages. Arrival of macrophages at the wound site initiates another step into the inflammation phase progress. These cellular components can tolerate a lower oxygen pressure at the edges of the wound and have a longer life span than neutrophils. Macrophages eradicate the remaining bacteria, remove damaged tissue fragments, and produce a variety of different growth factors such as Fibroblast Growth Factor (FGF) and Endothelial Growth Factor (EGF) (Enoch and Leaper, 2008; Williamson and Harding, 2004; Pauline, 2010). The earlier-formed haemostatic plug must be removed to allow formation of new tissue. Macrophages undertake this task by releasing wound digestive enzymes known as Matrix MetalloProtease (MMP's) (such as collagenases, and gelatinases) (Gorgieva and Kokol, 2011). Healing processes in the dermis are dependent on a dense network of capillaries (De Carvalho and Grosso, 2004). Macrophages stimulate the endothelial cells in the blood vessels near the wound site to migrate and form small, finger-like capillaries (Loretta, 2007). Macrophages also produce extracellular molecules and transform the lower part of haemostatic plug to become granulation tissue (Linares, 1996). The granulation tissue mainly sets the stage for the next phase of wound healing known as *the proliferation phase* (Williamson and Harding, 2004).

2.3. Proliferation Phase

The proliferation phase commences on day 3 after injury and lasts for 2-4 weeks (Enoch and Leaper, 2008). Fibroblasts are recruited from the surrounding tissue by macrophage-derived growth factors. Fibroblasts migrate into the wound granulation tissue where they proliferate and begin depositing ECM (Brohem *et al.*, 2011). Fibroblasts dominate the wound cell population within the first week (Garrison, 2001). They produce a variety of substances essential for wound repair, including fibronectin, hyaluronan, proteoglycans, and collagen (Enoch and Leaper, 2008). Collagen production level rises constantly for approximately 3 weeks after injuries. During this phase, the wound tensile strength continues to rise (Williamson and Harding, 2004; Stadelmann *et al.*, 1998b). Figure 1–2 shows the schematic correlation between collagen synthesis and wound tensile strength.

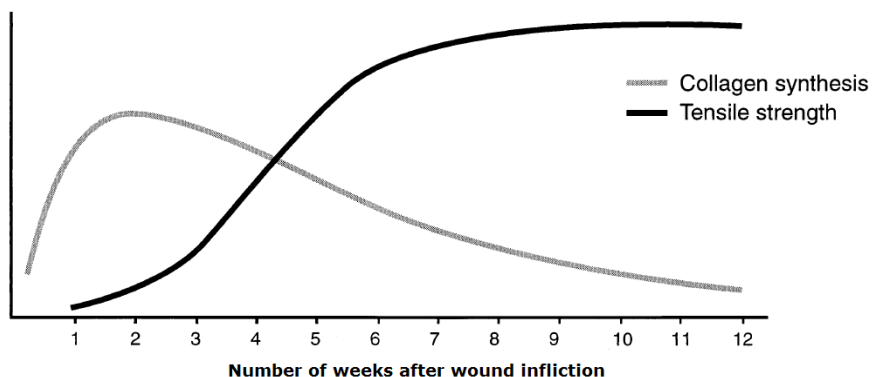


Figure 1–2: Schematic correlation between collagen synthesis and wound tensile strength (Williamson and Harding, 2004).

Whilst the fibroblasts are active underneath the blood clot, on the surface of the clot, the skin epithelial cells begin a mass migration to close the wound surface (Gurtner *et al.*, 2008) Epithelialisation of the wound represents the final part of the proliferation phase (Enoch and Leaper, 2008). It is the last visible segment of wound healing and delayed until the wound defect is filled (Pauline, 2010). The epithelial migration ceases when the advancing epithelium meets its counterpart from the opposite direction (Saint *et al.*, 1998).

2.4. Wound Remodeling

The last phase of wound healing is wound remodeling. It will be initiated after skin collagen content has reached a stable level, usually by the third week after the injury. This process continues for up to 2 years after the injury (Gurtner *et al.*, 2008). Typically the new dermal tissue varies from the original skin tissue and is known as *scar tissue*. The scar tissue is inelastic and relatively brittle. The remodeling includes an increased crosslinking of collagen fibres, removal of the newly formed blood vessels that are not necessary, and re-orientation of collagen fibres in response to mechanical stresses. During remodeling, collagen fibre orientation of the scar tissue will become similar to the natural skin. In the normal dermis, the collagen fibres are arranged in a random, basket-weave form, whereas in a scar, there is an isotropic orientation of the collagen fibre alignment (Sherratt and Dallon, 2002). During the wound re-modeling phase, the collagen fibres reorganise into a more ordered lattice structure (Stadelmann *et al.*, 1998b).

3. Wound Types

Wounds can be categorised into two groups: acute and chronic wounds. In the acute wounds the skin structure and function is restored through a normal multi-phase healing process within an expected time frame (Li *et al.*, 2007; Strodtbeck, 2001; Franz *et al.*, 2007). Most superficial and surgically-induced wounds fit into this category. However, if a wound does not heal in an orderly or timely manner, or if the healing process does not result in desirable structural integrity, then the wound is considered as a chronic wound (Stadelmann *et al.*, 1998b). The chronic wounds are long lasting wounds where the healing process may take up to 6 weeks or longer (Gilkes, 2002; Werdin *et al.*, 2008; Fonder *et al.*, 2008). A leg ulcer and a severe burn injury are two examples of the chronic wounds.

3.1. Acute Wounds

Acute wounds heal in an orderly progression, maturing through defined phases of coagulation, inflammation, matrix synthesis and deposition, angiogenesis,

fibrolasia, epithelialisation, contraction, and remodeling (Hardwicke *et al.*, 2008). In acute wounds, the end result of uncomplicated healing is a fine scar with little fibrosis, minimal wound contraction, and a return to near normal tissue architecture and organ function (Stadelmann *et al.*, 1998b). The healing process in the acute wounds follows the procedure described in Section 2.

3.2. Chronic Wounds

As it was discussed in Section 2, the healing of the wound requires a delicate balance of opposing actions: cell proliferation versus cell apoptosis, collagenosis versus collagenolysis, and angiogenesis versus angiolysis (Linares, 1996). Any disruption of the delicate balance between these actions may cause a chronic wound and results in a delay in healing beyond the anticipated time (Enoch and Leaper, 2008; Werdin *et al.*, 2008). The most common causes of the chronic wounds include: infection and prolonged inflammation, presence of free radicals and micro-organisms, vascular insufficiency (blood flow), mechanical stress, long term tissue hypoxia (lack of tissue oxygen), and foreign bodies presence in the wound (Enoch and Leaper, 2008; Wong and Gurtner, 2012; Stadelmann *et al.*, 1998a), or systemic conditions such as: aging, obesity, malnutrition, diabetes, renal diseases, poor cardiac output, lack of physical activities, drugs and tobacco use (Stadelmann *et al.*, 1998b). Below, two major physiological causes of the chronic wounds are elucidated.

Chronic or non-healing wounds are often stalled in the inflammation phase (Ovington, 2007). In term of duration, the inflammatory process should be a self-limiting process, however in a chronic wound this is not the case, which causes further injury in a self-perpetuated cycle (Menke *et al.*, 2007). As described in Section 2.2, the presence of digestive MMP's enzymes such as collagenase and gelatinase is essential for blood clots removal and damaged tissue debridement (Williamson and Harding, 2004; Abramo *et al.*, 2008); In an acute wounds, the cells that secrete these enzymes are virtually nonexistent after the first 72 hours; whereas in a chronic wound, not only these cells exist, they are the dominant cell types (Stadelmann *et al.*, 1998b). In two separate

studies, certain enzymes, such as gelatinase-2 and collagenase, were detected in over 90% of the chronic wound samples, whilst they were absent in the fluid of acute wounds (Enoch and Leaper, 2008; Garrison, 2001). This over-supply of digestive enzymes causes excessive protein degradation and the inactivation of wound growth factors (Hardwicke *et al.*, 2008; Loretta, 2007). As a result, fibroblasts would be unable to make progress in depositing the ECM as degradation is greater than its synthesis (Menke *et al.*, 2007) and angiogenesis and endothelial cell precursor migration is inhibited (Ji *et al.*, 2011).

Apart from the inflammation phase stagnation, another physiological cause of chronic wounds is the imbalance in the growth factors concentration. Growth factors are peptides that regulate the wound healing process by binding to cell receptors (Groeber *et al.*, 2011). Quantitatively, it was demonstrated that in the chronic wounds, the level of growth factors may be below (Hardwicke *et al.*, 2008) or above the average level depending on the wound type (Garrison, 2001). It was speculated that the concentration of growth factors may not be the only cause of chronic wounds and may be the indirect consequence of the wound environment. The available growth factors may be trapped within the fibrin cuffs that surround capillaries and become inactive (Hardwicke *et al.*, 2008; Vincent, 2005). Moreover, the proteinases of chronic wounds may neutralise the influence of the growth factor or degrade them (Menke *et al.*, 2007; Loretta, 2007). If growth factors are under-secreted or rapidly metabolised, wound healing will be retarded. To add to the complexity, it was shown that the cells isolated from chronic wounds response poorly to certain growth factors (Ovington, 2007). Lack of regular responsive cells within chronic wounds is another element that makes available growth factors ineffective.

In addition to the physiological causes, the chronic wounds may occur as a result of accident or burn injuries. If the skin damaged area is large or deeper than 4 cm, then the natural repairing mechanisms of the skin would not be enough for healing to proceed autonomously (MacNeil, 2007). No matter what is the origin of the chronic

wound, a timely and efficient medical intervention to avoid exacerbation of condition is vital. Such an intervention is known as *wound management*.

4. Wound Management

Modern wound management was initiated through the discovery of the sterilisation and aseptic wound dressings (Lionelli and Lawrence, 2003). Today, wound management has evolved into an important sector of the medical industry. As of 2012, in the UK it is estimated that approximately 4 out of every 1000 people covered by the NHS suffered from at least one wound. This includes all types of wounds from superficial scratches to chronic wounds (Dowsett *et al.*, 2012). Out of this number, chronic wounds have a high incidence rate amongst British patients, where one in every three is suffering from chronic wounds (Drew *et al.*, 2007). Conservative estimation regarding the cost of chronic wounds treatment for the UK National Health Service (NHS) is between £1 to 3.1 billion per year in direct costs (Hardwicke *et al.*, 2008; Harding, 2010). This includes £168-198 million to treat leg ulcers, £300 million for diabetic foot ulcers and £1760-2640 million for pressure ulcers (Dowsett *et al.*, 2012). According to WHO, 6 million patients worldwide suffer from chronic ulcer wounds and 300,000 dies annually due to burn injuries. Just in the US, 3 million individual are suffering from chronic wounds which imposes a cost of US\$25 billion to the US national healthcare budget annually (Pereira *et al.*, 2013; Brem *et al.*, 2007).

There are different strategies to combat chronic wounds such as: direct administration of growth factors to the wounds (Wong and Gurtner, 2012), debridement and infection control (Marston *et al.*, 2003), improving the life style of the patients (Steed *et al.*, 1995), nutritional support (Supp and Boyce, 2005); but application of wound dressings is a common complimentary element to the majority of them and sometime is the sole remedy to confront chronic wounds. The efficiency of wound dressings directly affect the efficiency of the healing process, the efforts to improve the life quality of the patients, and bringing the wound management costs under control (Kamel *et al.*, 2013). Thus designing a more effective wound dress is indispensable in

the path towards a more efficient wound management practice. Following section provides a brief introduction to different types of wound dressings systems.

5. Wound Dressings

Wound dressings have undergone an evolutionary progress from the materials that simply cover the wounds, to the materials that interact with, and in the last two decades, integrate with the skin. Certain functions are expected from any wound dressings: they should protect wounds from trauma and intrusion by foreign materials (Chvapil, 1982), have enough bio-adhesiveness to remain in place (Sezer *et al.*, 2011), minimise scar formation, provide adequate exchange of gas (Pereira *et al.*, 2013), and prevent the loss of fluid, especially in wounds covering a large surface area, such as burns (Boyce *et al.*, 1988). Other expected wound dressing functions (such as having anti-bacterial ability, being water absorbent or hydrating) are more wound-type-specific.

Advanced wound dressings may be divided into two major categories: non-biological and biological (Lionelli and Lawrence, 2003; Gregg, 2001). Non-biological dressings interact but do not integrate with skin after healing. Amongst others, this group includes foams, films, and hydrogels. Biological dressings both interact and integrate with skin during healing and will become part of skin after healing. They include allograft skin (graft taken from another person), xenograft (grafts taken from an animal), and skin substitutes (artificial skins implants and synthetic tissue engineering scaffolds). There are hundreds of different brands in the wound management market. A survey of wound care product buyer's guide in 2005 listed more than 400 individual advanced wound dressings (Ovington, 2007). Table 1-1 lists a selected number of wound dressings from each of these categories. The following Sections briefly introduce some of the well known advance wound dressings types.

Table 1-1: A selected list of commercially available wound dressings (Kamel *et al.*, 2013; Supp and Boyce, 2005; Gregg, 2001; Landsman *et al.*, 2009; Abdelrahman and Newton, 2011).

Wound Dressing Type	Brand	Composition
Foam	Prisma™	55% Collagen, 44% Cellulose, and 1% Ionic silver
Foam	Primatrix™	Collagen sponge
Film	Tegaderm™	Poly-urethane transparent film
Film	Biobrane™	Thin silicon membrane bonded to nylon fabric
Alginate	Algosterile™	-
Hydrocolloid	Comfeel™	-
Hydrogel	Tegagel™	-
Biological Wound Dress, Cell Free	Integra™	Pulverized bovine collagen bonded to a silicon sheet
Biological Wound Dress, Cell Free	Terudermis™	Silicon and crosslinked collagen sponge
Biological Wound Dress, Cell Free	Transcyte™	Nylon mesh with dermal matrix secreted by eradicated fibroblasts
Biological Wound Dress, Cell Seeded	DermaGraft™	Neonatal fibroblasts in silicon film, nylon mesh, and collagen scaffold
Biological Wound Dress, Cell Seeded	Epicel™	Patients biopsy cells cultured and seeded on gauze sheet support
Biological Wound Dress, Cell Seeded	MySkin™	Synthetic silicon layer along with autologous keratinocytes
Biological Wound Dress, Cell Seeded	CellSpray™	Cultured or non-cultured autologous keratinocytes
Biological Wound Dress, Cell Seeded	Apligraf™	Fibroblasts, and keratinocytes cultured in collagen sponge
Biological Wound Dress, Natural Tissue	AlloDerm™	Acellular human dermis
Biological Wound Dress, Natural Tissue	Surederm™	Human acellular pre-meshed dermis

5.1. Foams

Foam dressings may consist of polyurethane or silicon base foam sheets which enable them to handle large volumes of fluid (Gregg, 2001; Abdelrahman and Newton, 2011). Foams are also available in composite form, made up of two separate membranes. For instance they are composed of a polyurethane mesh inner layer and an outer semi-permeable membrane of polyurethane, polyester, silicone, or Gore Tex™. Foams provide thermal insulation to a wound (Ramos-e-Silva and Ribeiro de Castro, 2002). These dressings have good water absorbency and after hydration make an intimate contact with uneven wound surfaces. This causes the dressing to eliminate dead spaces and thus reduces the potential sites for bacterial infection (Chvapil, 1982). Due to these features, foam dressings are recommended for use throughout the proliferation phase of wound healing (Werdin *et al.*, 2008).

5.2. Films

Film dressings are generally clear, thin (0.2 mm in thickness) polyurethane or co-polystyrene membranes with an acrylic adhesive on one side for adherence (Lionelli and Lawrence, 2003; Gregg, 2001; Ramos-e-Silva and Ribeiro de Castro, 2002). Transparency of these dressings usually offers a window into wound healing progress and complications may be readily be diagnosed (Chvapil, 1982) and due to being extremely thin and highly elastic, they do not interfere with patient daily activities (Ramos-e-Silva and Ribeiro de Castro, 2002). Films are waterproof and impermeable to bacteria but allow the transmission of oxygen, carbon dioxide, and water vapour (Lionelli and Lawrence, 2003; Gregg, 2001). They do not absorb wound exudates and their vapour transmission rates vary between 30 and 80 mg/cm²/24 hours and may remain in place for up to 7 days. These dressings may be used as a primary dressing for dry, superficial wounds or a secondary dressing along with foams, alginates, and hydrogel dressings (Abdelrahman and Newton, 2011).

5.3. Alginates

These dressings are composed of soft, non-woven fibres of a cellulose-like polysaccharide derived from the calcium or sodium salt of alginic acid (seaweed) (Lionelli and Lawrence, 2003; Gregg, 2001). Alginates primary application is in heavily exuding and bleeding wounds (Abdelrahman and Newton, 2011). In application as a wound dressing, the alginate undergo a mild gelation in the presences of cations exist in the wound exudates (Kim *et al.*, 2011). In addition, alginate fibres release calcium ions and thus have blood coagulation properties suitable for bleeding wounds. Alginates dressings may remain in place for up to 7 days or changed when secondary dressings covering the alginate dressings require removal once become soaked (Ramos-e-Silva and Ribeiro de Castro, 2002). Alginates are packaged in a variety of form factors, including sponges for filling cavities, thin films for narrow wounds, and pads for flat surfaces (Lionelli and Lawrence, 2003).

5.4. Hydrogels

Hydrogels can enhance debridement of dead and dry wound tissue by creating a moist environment above the wound surface (Chvapil, 1982). Hydrogels dressings are semi solid systems formed by combination of one or more hydrophilic polymers such as: polyvinyl alcohol, polyacryl amide, polyethylene oxide, polyvinyl pyrrolidone, or carboxymethylcellulose (Sezer and Cevher, 2011). These polymer matrices have a high water absorbent capacity and can absorb up to 80% of their dry weight (Lionelli and Lawrence, 2003). It does not adhere to the wound and lowers the temperature of wound surface which reduces pain and inflammation (Ramos-e-Silva and Ribeiro de Castro, 2002). This type of wound dressing is applied for dry wounds or battling heavily infected wounds. Hydrogels are shown to accelerate the rate of cellular migration and vascularisation (Yannas and Burke, 1980).

5.5. Hydrocolloids

The term Hydrocolloid is used to describe a family of dressings containing a hydrophilic matrix composed of materials such as gelatin, pectin, and

carboxymethylcellulose attached to an adhesive membrane (Lionelli and Lawrence, 2003). The outer layer of these dressings is composed of an impermeable material such as polyurethane which is attached to gelling agents (Ramos-e-Silva and Ribeiro de Castro, 2002). The dressing absorbs wound exudates, forming a viscous, colloidal gel that prevents adherence of the dressing to the wound base (Abdelrahman and Newton, 2011). Hydrocolloids are suitable for application throughout epithelialisation of the wound and may be left in place as long as 7 days (Werdin *et al.*, 2008). Hydrocolloids have a low moisture transmission rate of less than 30 mg/cm²/24 hours (Abdelrahman and Newton, 2011). These dressings are generally opaque and are slightly bulkier than films. This increased size may provide more protection for the wound, though it may interfere with patient daily life activities (Lionelli and Lawrence, 2003). These dressings have shown to stimulate angiogenesis and increased speed of healing by as much as 40% when compared with open-air controls (Gregg, 2001). They also help mitigate pain through keeping nerve endings moist (Abdelrahman and Newton, 2011).

5.6. Biological Wound Dressings

This group of wound dressings can be divided into three sub-categories:

1. Wound dressing scaffolds made up of a wide range of biocompatible polymers. They can actively interact with the wound tissue and may be embedded into wound tissue after the service period has been completed,
2. Similar to the previous category but wound dressings in this subcategory contain live cells. This type of wound dressings is offered in mono- or bi-layer configurations and contains one or more cell types,
3. Living skin substitute, which are harvested from deceased human or animal dead bodies.

All of these three categories function according to tissue engineering principles (Wong and Gurtner, 2012). They provide the cells with a microenvironment which is favorable for cell adhesion, proliferation, and differentiation to enhance regeneration of

the damaged tissue (Natesan *et al.*, 2010). These wound dressings may be composed of more than one layer. As an example, Integra™ approved by FDA in 1996, consists of matrix of bovine collagen, chondroitin-6-sulfate, and a shark-derived GAG's as an artificial dermis. On top of this layer, there is a bonded disposable silicon sheet (as an artificial epidermis) (Böttcher-Haberzeth *et al.*, 2010). The multi layered structure is easy to handle and can be sutured over the wound site. The silicone material is left in place whilst the collagen material is gradually solubilised or incorporated into the wound bed. Once the collagen matrix in the wound bed is vascularised, the silicon layer will be removed from the skin leaving behind, the collagen matrix embedded into skin (MacNeil, 2007).

Transcyte™ is another example of advanced biological dressing. This wound dressing takes a radical approach towards producing a collagen matrix. Fibroblasts are cultured in the laboratory and allowed to proliferate on a nylon mesh. After synthesising enough collagen extracellular matrix and growth factors, the fibroblasts will be eradicated through a freezing process. This brand of wound dressing is easily stored and has immediate availability for burn injuries (Supp and Boyce, 2005).

Incorporating live cells into the wound dressing structure offers several advantages such as new matrix deposition, increased availability of cytokines and growth factors to the wound bed, and recruitment of stem cells to the wound site (Groeber *et al.*, 2011). There are several commercially available skin substitutes such as brands like Apligraf™ and OrCel™ that are mainly composed of collagen type I matrix seeded with human fibroblasts and keratinocytes cells (Kamel *et al.*, 2013). Cells used in these wound dressings may be obtained either from the patient body or from available tissue bank stocks. Dermagraft™ is one the oldest FDA approved biological dressing commercially available. To manufacture the wound dressing, human fibroblasts are cultured on a biodegradable PLGA mesh (Kim *et al.*, 2011). This wound dressing will be delivered in a frozen condition, and contain fibroblasts-derived dermal substitutes containing collagen, ECM proteins, and growth factors (Marston *et al.*, 2003). Although these advanced wound management systems are more expensive compared to

conventional treatments, but they may in fact ultimately lead to reduction in costs if the number of procedure, length of hospitalisation, the required amount of physical therapy, and number of reconstructive procedures can all be reduced (Supp and Boyce, 2005). A more advanced type of wound dressings comes in two layers representing the natural skin epidermis and dermis. Offered under the trade name of OrCel™, this skin equivalent consists of allogeneic fibroblasts and keratinocytes grown on the reverse side of a bovine collagen bi-layered matrix. The collagen matrix consists of a crosslinked bovine collagen sponge coated with an overlay of pepsinised, dense collagen membrane. Keratinocytes are seeded on one side of sponge whilst the fibroblasts are seeded on the other (Pereira *et al.*, 2013).

Living human or animal skin samples are alternatives to laboratory-created skin equivalents. AlloDerm™ is one example for such types of wound dressings which is acellular dermis from deceased human body and is administered for dermal replacement (Kim *et al.*, 2011). These products contain the full array of components found in native skin (Badylak *et al.*, 2009). Questions have been arisen with respect to tissue rejection, transmission of disease, and stimulation of immune system response regarding the application of this type of wound dressing (Yannas and Burke, 1980).

6. Biomaterials Used in Wound Management

The biomaterials which are used in advanced wound dressings usually are either the components of ECM or their derivatives. Application of these components in the wound dressing increases the chance of having a positive impact on the wound healing process. In the following section two prominent examples of these biomaterials which have relevancy to this study will be discussed:

6.1. Collagen

Collagen is the most abundant family of fibrous proteins in the body (Zhao *et al.*, 2013; Abraham *et al.*, 2008) and accounts for approximately 30% of all body proteins and 50% of skin (Ruszczak, 2003; Friess, 1998). As it provides strength and

integrity to all tissues, collagen plays a vital role in maintaining the flexibility and functionality of skin (Brohem *et al.*, 2011).

Collagen has a peculiar structure. Collagen polypeptide chains wind upon itself in a left-handed helix (Gorgieva and Kokol, 2011). Three polypeptide helices then join each other to form a super helix known as *tropocollagen*. The individual chains are able to inter-twine tightly because each polypeptide has one glycine molecule at every third position (Enoch and Leaper, 2008). Tropocollagens are stabilised by inter chain hydrogen bonds and water bridged crosslinks (Gelse *et al.*, 2003). By stacking together, collagen helices form a collagen filament. The collagen filaments then, in turn, adjoin to form collagen fibrils, which aggregate to form collagen fibres (Stadelmann *et al.*, 1998b).

Figure 1–3 illustrates collagen molecules assembly into collagen bundles.

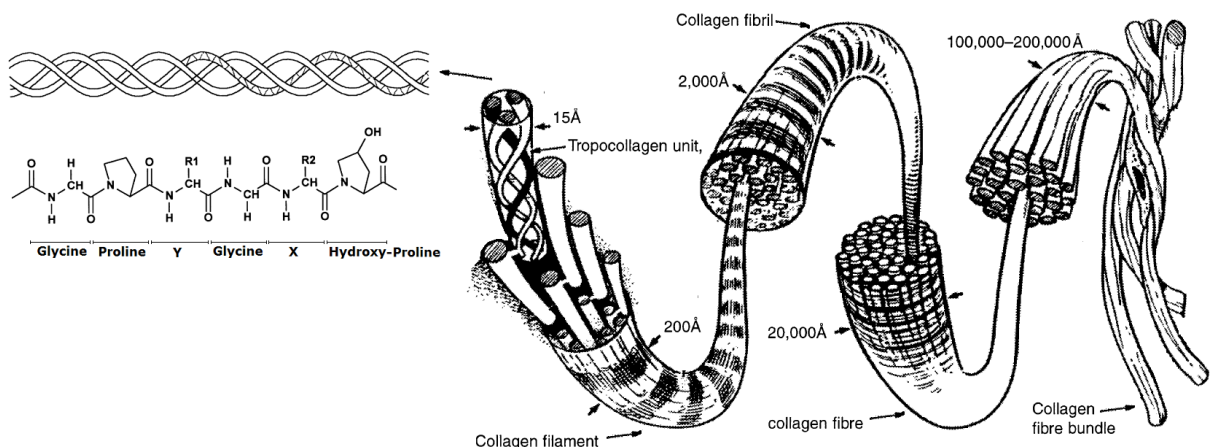


Figure 1–3: Assembly of collagen peptides into, tropocollagen, filaments, fibrils, fibres, and collagen bundles. The numbers show the approximate width of each component (Stadelmann *et al.*, 1998b). The amino acid structure of collagen macromolecule is shown on the left hand side. Repetition of Glycine amino acids is critical for formation of triple helical structure of collagen (Friess, 1998).

Unique structure of collagen is due to its unique amino acid composition. Based on difference in polypeptide structure, almost 30 different collagen types have been reported so far (Reich, 2007). Collagen type I makes for over 90% of body collagen

content and is found in bone and skin. In addition to type I collagen, skin is composed of type III collagen which together contribute significantly to the tissue tensile strength (Gorgieva and Kokol, 2011). Type IV and V are also the components of the skin and are found in the basement membrane and ECM structure (Stadelmann *et al.*, 1998b).

Due to abundance of collagen in variety of human tissue, collagen is frequently used as a starting material in soft tissue engineering scaffolds, heart valve prostheses, and wound dressings (Charulatha and Rajaram, 2003). Collagen matrices can also serve as a drug delivery carrier (Ruszczak, 2003). Absorbable collagen sponges were developed for use as haemostats or for guided tissue re-generation after dental surgery and as a coating on artery stents to improve their biocompatibility (Olsen *et al.*, 2003). Collagen can be easily manipulated into various physical forms such as: powders, sponge, scaffolds, pellets, and sheets (Zeugolis *et al.*, 2009). In wound healing, implanting a collagen matrix significantly speeds up skin reconstruction. The record about applications of collagen as a wound dress dates back to as early as 1943 (Yannas and Burke, 1980). Deep implantation of collagen pads can be used to strengthen the underneath tissues and reducing the local pressure associated with diabetic foot ulcers. Foamed collagens are also shown to be effective for controlling exudates and reducing MMP's concentration (Such as collagenase or gelatinase) in the wound environment (Pauline, 2010). Injection of collagen suspension has reported for wound management (Sezer and Cevher, 2011).

Gelatin is a derivative of collagen. It retains some of collagen peptide sequences, such as RGD (Zhao *et al.*, 2013), which can promote cells differentiation (Kim *et al.*, 2011), adhesion, and migration (Steed *et al.*, 1995; Hajiali *et al.*, 2011). Thus gelatin can be an effective, low cost, and readily available substitute for collagen applications in tissue engineering (Olsen *et al.*, 2003). Following section presents a brief introduction to Gelatin.

6.2. Gelatin

Gelatin is a protein that has no existence in nature and is derived from its precursor protein, collagen (Bigi *et al.*, 2004). Gelatin is traditionally isolated from porcine or bovine bone and skin by acid or basic extraction by denaturing the collagen molecules that are available in these tissues (Olsen *et al.*, 2003). Two types of gelatin are available and commercially known as type-A or type-B gelatin obtained under acid or alkaline pre-treatment conditions, respectively (Gómez-Guillén *et al.*, 2011). To produce gelatin, tissue collagen is extracted by heating with water at a temperature higher than 60°C. Subsequent heat treatment cleaves the hydrogen and covalent bonds to derive the triple helix-to-coil transition and convert the collagen into soluble gelatin. Higher temperature and processing time increases gelatin production yield from the precursor tissue, though, such increase in yield comes at a price of lower molecular weight fragments (Kittiphattanabawon *et al.*, 2010). Higher molecular weight gelatin can offer better gel strength, thus increasing the temperature for increasing the production yield should be done with cautious (Gómez-Guillén *et al.*, 2009). Gelatin products consist of polypeptide fragments of different molecular weights, iso-electric points, and gelling properties. It is shown that by measuring iso-electric point of gelatin fragments, the number of amino acids in gelatin fragments may be deduced and the portion of collagen helical chain from which they are originated (Olsen *et al.*, 2003). Figure 1–4 lists the iso-electric points of gelatin fragments, the number of amino acids in each fragment, and the regions from which in the collagen helical chain, they are originated from.

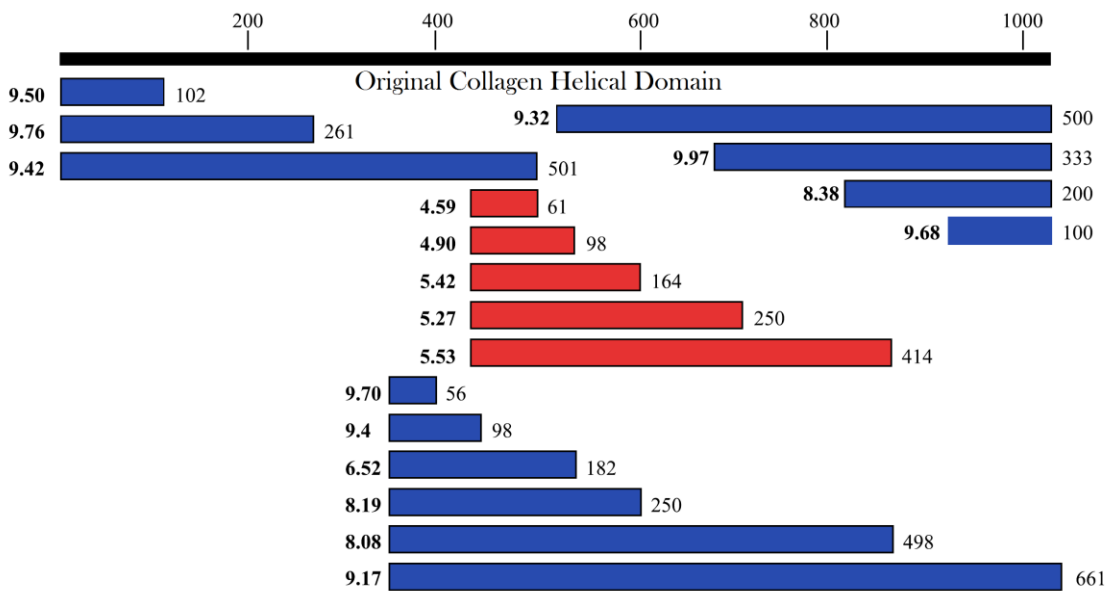


Figure 1–4: Gelatin fragments and the relation between iso-electric point of gelatin solution and the number of amino acids in each fragment. The numbers to the left of each bar shows the iso-electric points and the number to the right shows the number of amino acids in each fragments (Olsen *et al.*, 2003).

Recent reports show that annual world output of gelatin is approximately 320,000 tonnes (Koli *et al.*, 2012). Approximately 55,000 metric tons of gelatin are produced annually for medical purposes (Gorgieva and Kokol, 2011). Pig skin derived-gelatin accountings for 46% of global gelatin output, followed by bovine hide (29.4%) and bone (23.1%) derived gelatin (Koli *et al.*, 2012). Scientific interest in biopolymers such as gelatin originates from several mechanical functionalities, physiological similarities with collagen, along with some additional features such as low immunogenicity, biodegradability, as well as simple preparation (Koob and Hernandez, 2003). Formation of thermo-reversible gels is one of the most peculiar features of gelatin.

Gelatin is unique amongst hydrocolloids in forming thermo-reversible gels with a melting point close to body temperature (Achet and He, 1995). Upon cooling, gelatin molecules undergo reverse coil-to-helix transition triggered by cooling below 30°C (Gorgieva and Kokol, 2011). Helical formation is derived by weak energetic interactions

(Van der Waals forces or hydrogen bonding between N-H of glycine and C=O of proline). It develops an extensive, non-covalent, interconnected network and results in gel formation (Chen *et al.*, 2003; Dardelle *et al.*, 2011). Ability of gelatin to form a strong thermally reversible gel depends on total content of two amino acids: proline and hydroxyproline. Higher hydroxyproline content leads to higher thermal stability and stronger gels (Olsen *et al.*, 2003). Before being considered for using *in-vivo*, both gelatin and collagen require crosslinking in order to increase their thermal stability (Giraudier *et al.*, 2004), mechanical strength (De Carvalho and Grosso, 2004), and their water resistance (Farris *et al.*, 2010). Following section is dedicated to an introduction about the crosslinking compounds that were used in this study to stabilise gelatin.

7. In-Vivo Stabilisation of Biomaterials

In-vivo stabilisation of biomaterials can be achieved either by chemical or physical crosslinking methods (Khor, 1997). During chemical method the biomaterial become mechanically stronger through establishment of covalent bonds between adjoining polymer chains (Farris *et al.*, 2010). Apart from increasing mechanical strength, such a new arrangement increases the resistance of samples to enzymatic degradation (Giraudier *et al.*, 2004) and extends life time *in-vivo*. 4 Different crosslinking agents were used in this study that will be discussed in the following Sections:

7.1. Glutaraldehyde

Amongst chemical crosslinking agents, the aldehydes bind relatively rapidly to proteins amine groups (Huang *et al.*, 1998). Glutaraldehyde (GT) is one of the major types of aldehydes that are used frequently to stabilise biomaterials. As of the end of the 90's, GT was extensively used and became one of the main commercially viable reagents for crosslinking collagen (Khor, 1997). However, application of GT-crosslinked materials *in-vivo* has the potential of releasing cytotoxic agents (Speit *et al.*, 2008; Jayakrishnan and Jameela, 1996). GT is a five-carbon aliphatic molecule with an aldehyde functional group at each end of the chain. Although during crosslinking reaction it may react with several different functional groups in protein (Wine *et al.*, 2007), GT mainly establishes covalent bonds within the matrix between the amine groups of lysine (hydroxylysine) (Charulatha and Rajaram, 2003). In a comprehensive review, Damink *et al.* have put together a list of potential reactions of GT with proteins functional groups, which included different possible oligo- and polymeric structures of GT (Damink *et al.*, 1995). One possible reaction mechanism of GT with proteins such as gelatin includes establishing carbon and nitrogen double bonds (C=N) formation between GT and gelatin molecules (Knaul *et al.*, 1999). Figure 1-5 illustrates GT molecules reaction with a gelatin macromolecule and the formation of carbon, nitrogen double bonds.

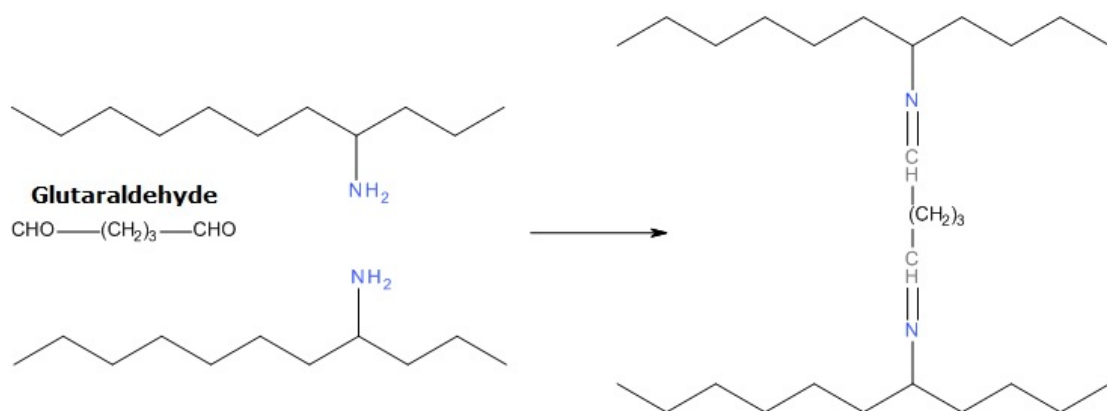


Figure 1-5: Glutaraldehyde reaction with collagen macromolecules (Khor, 1997).

The kinetics of GT crosslinking will be affected under acidic conditions and become slower than neutral or alkaline conditions (Damink *et al.*, 1995). This mainly happens as a result of amine group protonation at low pH's, in addition to the fact that Schiff bases, which are produced during crosslinking reaction, are considered to be unstable under acidic conditions (Wine *et al.*, 2007). However, Farris *et al.*, (2010) suggested an alternative procedure for GT reaction with protein under acidic pH's. Figure 1–6 illustrates the proposed aldehyde reaction with hydroxyproline at the acidic pH's. They suggested that at low pH's the crosslinking may still be possible through the protonation of carbon of aldehyde groups and subsequent attack of -OH groups of hydroxyproline and hydroxylsines (Farris *et al.*, 2010).

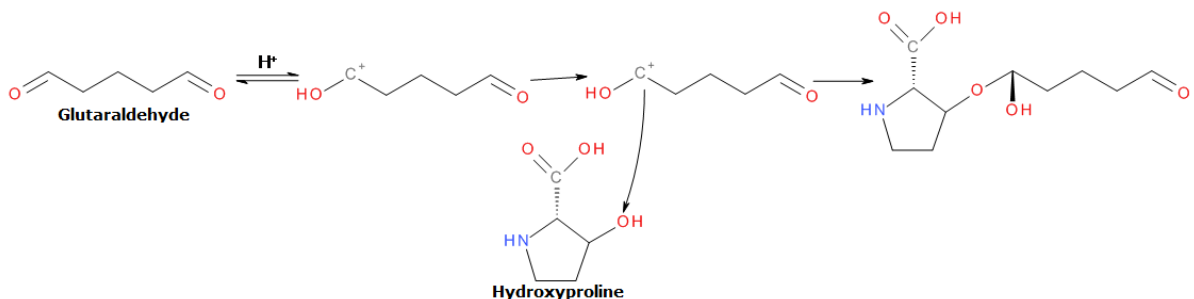


Figure 1–6: Proposed reaction of aldehyde groups with hydroxyl groups of hydroxyproline at the acidic pH's (Farris *et al.*, 2010).

Crosslinking using GT causes an increase in the Young's modulus and tensile strength, lower water absorption, and higher thermal stability. Increase in mechanical strength of the structure may be due to the establishment of covalent bonds and Schiff bases that are formed between the amine groups of lysine residues (Giraudier *et al.*, 2004; Farris *et al.*, 2010). Less water absorption is due to fewer sites for hydrogen bonding (Knaul *et al.*, 1999) or lower ability of the structure to expand and accommodate water molecules (Tasselli *et al.*, 2013). Higher thermal stability of the structure after crosslinking with GT is caused by the structural changes which require higher heat energy for the task of unfolding protein comparing with non-crosslinked state (Miles *et al.*, 2005).

GT was first applied successfully for manufacturing bio-prostheses in the late 1960's. It is easily available, inexpensive, and forms aqueous solutions that can effectively crosslink in a relatively short time. In clinical practice, GT has been used extensively as a crosslinking agent for fixation of prosthetic heart valves (Khor, 1997), patches for repairing heart (Jayakrishnan and Jameela 1996), and vascular vessels (Sung *et al.*, 1996). Concerns about GT toxicity recently raised serious reservations in its application (Speit *et al.*, 2008; Koob *et al.*, 2001). Glutaraldehyde crosslinking may lead to the presence of unreacted functional groups in the matrix which can result in a cytotoxic reaction upon degradation of the matrix (Olde Damink *et al.*, 1996). In addition, calcification of GT-treated tissue is another concern for its application (Sung *et al.*, 1999b; Gratzer *et al.*, 1996). Another side effect of GT application is excessive hydrophobicity and stiffness that it causes in the structure. These changes can be so intense that the samples cannot adapt to the host tissue conditions after implantation (Lohre *et al.*, 1993). This leads to tissue hardening and flexibility reduction. Regardless of these reservations, due to excellent reactivity of GT, it is commonly used as a reference crosslinking agent to measure the performance of other crosslinkers in research studies.

7.2. Polyepoxides

As early as 1980's, reports about applications of poly-epoxy compounds began to appear in the scientific publications (Khor, 1997). An epoxy is any compound with three-membered cyclic ether functional groups (Figure 1–7). The three-atom ether rings are thermodynamically unstable due to strained covalent bonds and it favors ring opening to relieve this strain. This makes the epoxy rings more reactive than other ethers (Sung *et al.*, 1996b). This is the driving force for the cross-linking reaction. The epoxy functionality predominantly reacts with the amine groups on lysine. The amine groups on lysine act as the nucleophile (ready to donate electron), substituting the oxygen bond on the epoxy terminal carbon to give a carbon-nitrogen stable bond (Khor, 1997). Additionally, Epoxide groups may react with carboxyl and hydroxyl functional groups, depending on the reaction pH (Sung *et al.*, 1996a). Figure 1–7 shows the proposed mechanism of epoxy crosslinking in acidic pH's. Acidic pH's catalyse the reaction by converting the epoxy into the highly reactive protonated compound. Under acidic conditions, the epoxy is first protonated by acidic medium, the protonated epoxy may undergo attack by the nucleophilic reagent, the lysyl amino group.

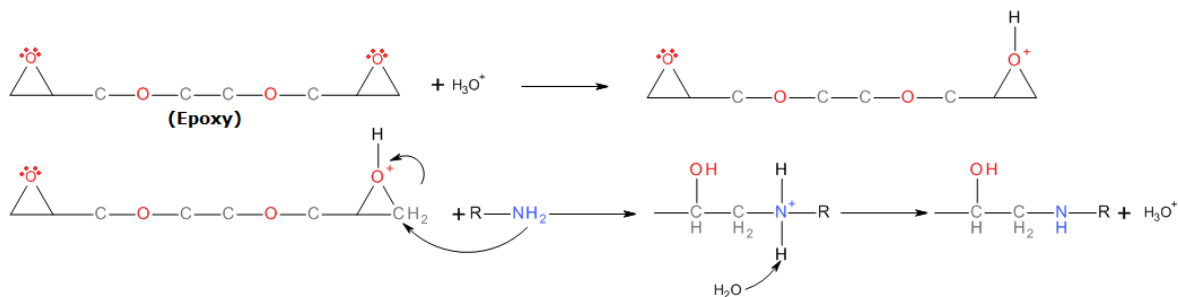


Figure 1–7: Proposed mechanism of crosslinking for the poly epoxy compound under acidic pH's (Sung *et al.*, 1996b).

Figure 1–8 illustrates the reaction of epoxy with amine groups in the alkaline pH's. High pH's catalyse the reaction by converting the lysyl amino group into a stronger nucleophilic reagent (Sung *et al.*, 1996b). Under basic conditions, the epoxy is the target

of nucleophilic attack by the lysyl amino group. In both conditions, a covalent bond would be formed between the epoxy carbon and the nitrogen of protein.

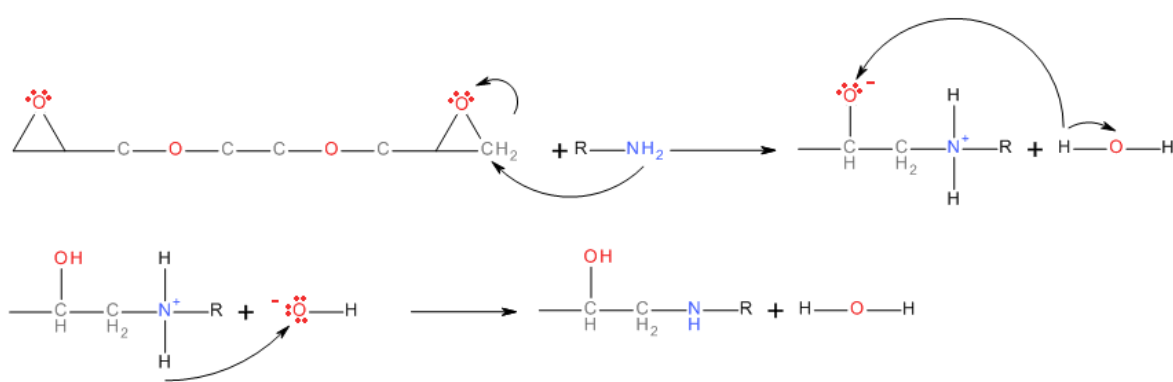


Figure 1-8: Proposed mechanism of crosslinking for the poly epoxy compound under basic pH's (Sung *et al.*, 1996b).

Apart from reacting with amino groups, epoxy is capable of reacting with carboxylic and hydroxyl groups of a protein. It is suggested that epoxy reaction with each of these functional groups is pH-dependant. Reaction with carboxylic groups occurs in acidic pH's, whilst in alkaline conditions the reaction would form an ether bond between the hydroxyl groups and epoxy ring, and finally at neutral pH the reaction between epoxy and amine groups would take place and form a amide bond (Leach *et al.*, 2005). Figure 1-9 shows the schematic diagram related to each reaction.

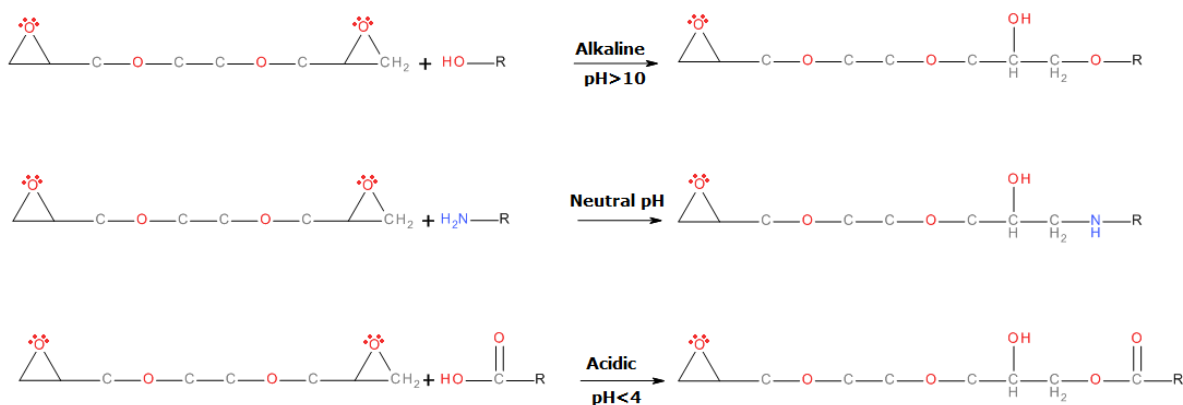


Figure 1-9: The reaction mechanism for epoxy groups with carboxylic, amino, and hydroxyl functional groups at different pH's (Leach *et al.*, 2005).

The epoxy molecules are larger when compared with the straight-chain, five-carbon GT molecules (Sung *et al.*, 1996). The larger molecular mass allows slower diffusion of epoxy compound within the structure than GT. The difference in molecular mass and diffusion rate will have substantial impacts on final product properties that will be addressed in Chapter 4 of this thesis. The cytotoxicity of the epoxy compounds has been evaluated and showed to be lower than GT (Huang *et al.*, 1998).

7.3. Isocyanates / Di-isocyanates

This group of crosslinkers is a bifunctional molecule with terminal isocyanate groups (Zeugolis *et al.*, 2009). They react with the amine groups of lysine on gelatin to form a urea bond (Huang *et al.*, 2007). Apart from urea bonds, as a result of isocyanate functional groups reaction with hydroxyl groups, urethane links can be formed (Deible *et al.*, 1998). A urethane link is relatively more stable than a urea linkage *in-vivo*. Due to the reactivity of isocyanate groups with hydroxyls, isocyanates compounds are thus reactive with water. This is the main obstacle against practical applications of isocyanate, because crosslinking needs to be carried out in anhydrous conditions. To tackle this restriction a water/diisocyanate/surfactant system is reported to crosslink dermal collagen. As an alternative to the use of surfactant, the crosslinking reaction was carried out in an anhydrous organic solvent such as Propan-2-ol (Gratzer *et al.*, 1996). However, the short half life of isocyanates in water ensures that the reactive groups will not be released from the treated surface whilst implanted in the body (Zeugolis *et al.*, 2009). The toxicity effects of isocyanate appear to be much more tolerable than GT (Khor, 1997). In this dissertation Hexamethylene Diisocyanate (HMDI) was used as one type of isocyanate to crosslink gelatin. HMDI structure is shown in Figure 1-10. This bi-functional reagent has been used extensively as an alternative for GT crosslinking (Zeugolis *et al.*, 2009). Figure 1-10 displays the reaction between isocyanate and gelatin molecules schematically.

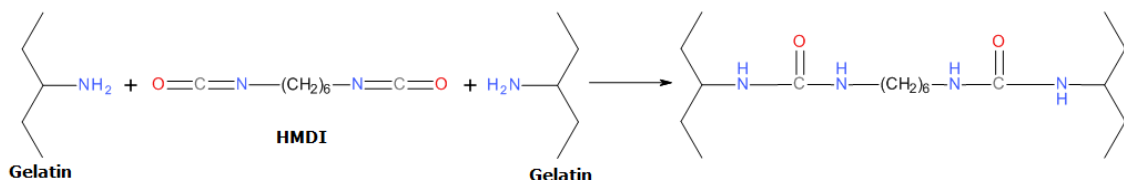


Figure 1–10: The reaction between hexamethylene diisocyanate (HMDI) and gelatin molecules (Khor, 1997).

It was shown that collagen samples crosslinked using HMDI showed a denaturation temperature of 66°C . In comparison with GT-crosslinked collagen, collagen samples crosslinked with HMDI show lower swelling properties (Zeugolis *et al.*, 2009). The application of HMDI has been advocated since the reaction of isocyanates with amines does not involve any potentially toxic side products and it does not leave any residues within the product after reaction (Chvapil, 1982).

7.4. Genipin

Genipin is extracted from its parent compound, Geniposide. This compound is isolated from the fruits of *Genipa Americana* (found widely in Latin America from Mexico to Argentina) and *Gardenia Jasminoides Ellis* (found in the Far East Asia). Previously, genipin have been widely used in Chinese herbal medicine (Butler *et al.*, 2003). Genipin is also known to react spontaneously with amino acids or proteins to form dark blue pigments. These pigments have been used as an edible dye in the food industry (Touyama *et al.*, 1994). Genipin can be used as a bridge between amino groups of lysine, hydroxylysine, or arginine residues of different polypeptide chains by monomeric or oligomeric crosslinks. It is proposed that genipin reacts spontaneously with an amino acid to form a nitrogen-iridoid bond. As illustrated in Figure 1–11, genipin has a cyclic hemi-acetal skeleton. In the presence of water, genipin becomes the structurally equivalent to a dialdehyde by forming two aldehydic functional groups. It is suggested that the two carbonyl functional groups in genipin readily react with the free amine groups in proteins (Sung *et al.*, 1999a; Sung *et al.*, 1998). Dimerisation occurs at the second stage, perhaps by a radical reaction (Sung *et al.*, 2000).

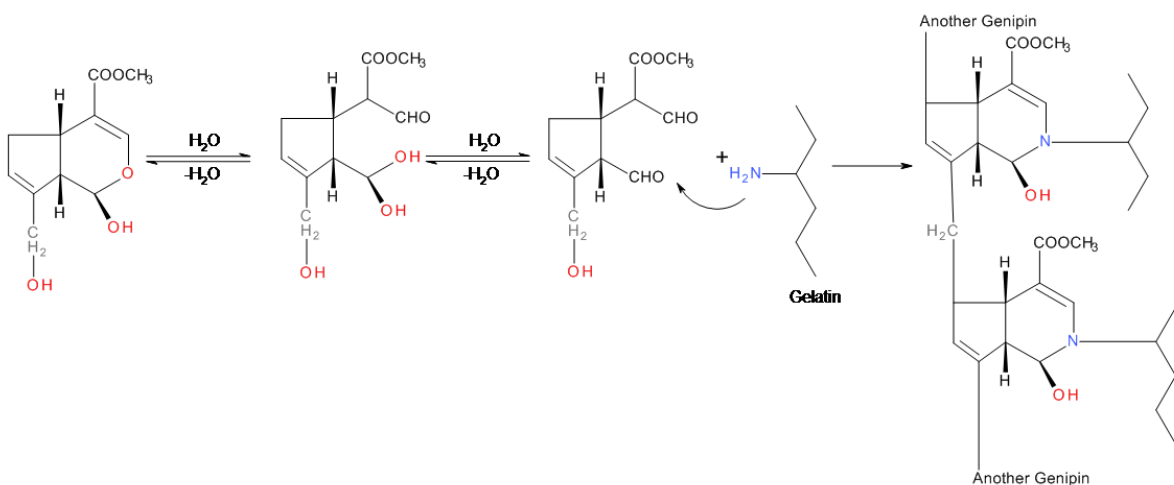


Figure 1-11: Proposed genipin molecule reaction with gelatin that includes ring opening (Sung *et al.*, 1999a; Sung *et al.*, 1998).

Another proposed mechanism of genipin reaction with biopolymers is illustrated in Figure 1-12. Similar to previous mechanism, this reaction also includes the conversion of the biopolymer primary amine functional groups to a secondary amine and it results the release of methanol as a byproduct. The second reaction occurs during the later stages of the crosslinking processes (Butler *et al.*, 2003). Genipin appears to have the biocompatibility advantage of being a biological molecule (Koob and Hernandez, 2003). Genipin is reported to be significantly less cytotoxic than GT (Huang *et al.*, 1998; Liu *et al.*, 2003). However, the effects of the degradation products from the materials crosslinked with genipin may be antigenic (Koob and Hernandez, 2003).

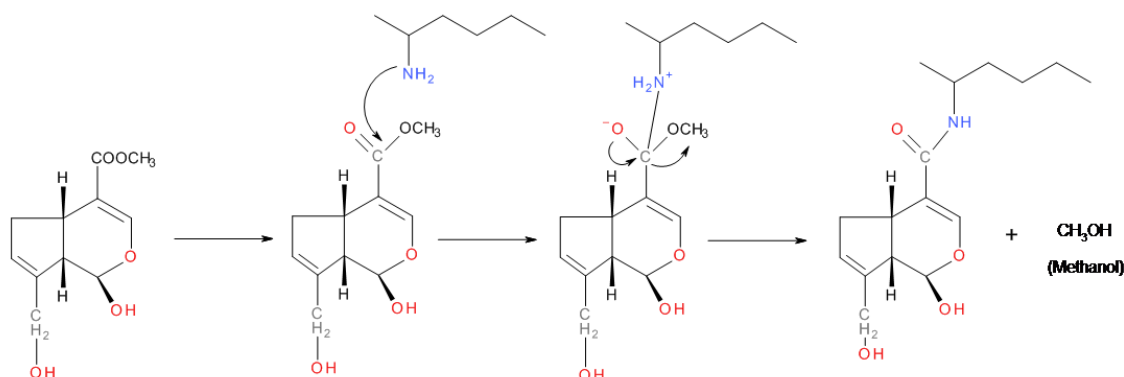


Figure 1-12: Proposed genipin molecule reaction with gelatin that results in release of methanol as a byproduct (Butler *et al.*, 2003).

8. Research Overview

This study was aimed at preparing an advanced biological wound dressing. An ideal wound dressing requires porosity at the area in contact with wound bed for better cell penetration and needs to be mechanically strong enough for handling and staying in place during use. In order to achieve desirable combination of porosity and mechanical strength, different modifications to manufacturing techniques were investigated and multiple crosslinking agents were explored to stabilise the samples. Aims and objectives of this study can be classified into three main areas: manufacturing of each of three layers, assembling and bonding layers together, and understanding the behaviour of these assembled structures as a single product.

Aim1: To develop and produce 3 separate gelatin-based layers with different characteristics which complement each other weaknesses

- Layer 1: to produce a biodegradable and porous gelatin material to be placed in direct contact with the wound.
- Layer 2: to produce a gelatin composite incorporating additive hydrophilic material(s) to be used as a mechanical support for layer 1 and an absorbent for wound exudates.
- Layer 3: to produce a covering layer with more elasticity to be used as a cover on the top of wound dressing.
- To characterise the physical and chemical properties of the prepared layers.
- To assess the biodegradation rate of prepared layer using collagenase enzyme.

Aim2: To bond and assemble prepared layers

- To develop, implement and characterise a bonding mechanism which allows adhesion of individual layers together.
- To investigate a method of bonding that allows detachment of porous layer from the covering layer after completion of treatment.

Aim3: To characterise the properties of the completed wound dressing as a fully bonded multi layer structure

- To study the microstructural and mechanical properties of completed wound dressing and compare its properties with natural skin features and commercially available wound dressings.

Chapter 2:

Materials

&

Methods

Chapter 2 - Materials and Methods

1. Materials

The list of the materials used in this dissertation and their suppliers is as follow:

- Bovine Gelatin, Type B, Sigma Aldrich (MO, USA), (**Detailed characterisations of gelatin used in this dissertation are reported in Appendix 1**)
- Sodium Hydrogen Carbonate, BDH Chemical, (Poole, UK),
- Acetic Acid Glacial, Fisher Scientific, (Leicestershire, UK),
- Glutaraldehyde aqueous solution (50% v/v), Density: 1.1 g/ml, Fisher Scientific, (Leicestershire, UK),
- Hexamethylene diisocyanate (HMDI), Sigma life science, (MO, USA),
- Poly(ethylene glycol) diglycidyl ether [Epoxy], Sigma life science, (Japan),
- Genipin, Challenge Bioproducts, (Taiwan),
- Chitosan, Medium molecular weight, 75-85% deacetylated, Aldrich, (MO, USA),
- Collagenase (From *Clostridium Histolyticum*), Type IA, ≥ 125 CDU/mg solid, Sigma, (MO, USA),
- Glycerol, 92%, Prime Chemicals, (South Yorkshire, UK),
- Ninhydrin, Indanetrione Hydrate, BDH Chemical, (Poole, UK),
- Glycine, Reagent Plus™, $\geq 99\%$, Sigma, (Steinheim, Germany),
- Hydrindantin, Sigma, (Austria),
- Lithium acetate, Dihydrate, Sigma, (Steinheim, Germany),
- Ethyl acetate, Bayer, (Germany),
- Desmocoll 400, Bayer, (Germany).

2. Samples Characterisation Methods

2.1. Chemical Characterisation Methods

2.1.1. Fourier Transform Infra Red Spectroscopy (FT-IR)

Fourier Transform Infra Red spectroscopy (FTIR/ATR-4800s, Shimadzu, Japan) was employed to examine the samples intermolecular structure. All spectra were obtained from 4000 to 1000 cm^{-1} at a nominal resolution of 4 cm^{-1} using 256 scans. The results were normalised against a background scan collected at ambient temperature. The samples were conditioned in a 0% RH desiccator containing self-indicating silica gel at 20 °C prior to analysis.

2.1.2. Thermal Analysis of Samples

Thermal analysis observes the denaturation of protein structure as the sample is heated by a Differential Scanning Calorimeter (DSC). The heat flow variation detected by DSC corresponds to the energy necessary to melt the crosslink zones and advance protein unfolding (Michon *et al.*, 1997). In evaluating the crosslinking of the samples, denaturation temperature (T_d) is used as an indicator of crosslinking degree (Miles *et al.*, 2005). Denaturation temperature is an indirect measure of degree of crosslinking: the

higher the T_d value is, the greater the degree of crosslinking will be (Gratzer *et al.*, 1996). Within the context of collagen, denaturation temperature is also known as *shrinkage temperature* or melting point (Miles and Ghelashvili, 1999). Heat-induced denaturation of tropocollagen causes a dramatic and sudden shrinkage of collagen or gelatin samples within a narrow temperature range (Porter, and Vollrath, 2012; Loke and Khor, 1995). In addition thermal analysis was used to assess the phase stability of chitosan-gelatin composites (Gill *et al.*, 2010).

Water is the most ubiquitous plasticiser of hydrophilic polymers such as gelatin and its presence is reported to have a significant impact on their thermal behaviour (Arvanitoyannis *et al.*, 1997). Furthermore, in the case of gelatin, water is necessary to allow the rebuilding of the collagen triple helix structure (Achet and He, 1994). Thus it was important that all possible effort be made to ensure the studied samples been conditioned at the same humidity so that they can be directly compared with each other throughout the study. In the case of this study, prior to analysis, all samples were conditioned for 2 days at 65% RH and 20°C. This combination of humidity and temperature was chosen in light of available facilities. The samples weighing between 4 to 16 mg were placed in 40 μ l aluminum pans and hermetically sealed. The thermal analysis was performed under nitrogen gas flow of 100 cm³.min⁻¹. The samples were analysed using a DSC-822e (Mettler-Toledo, Switzerland). Each specimen in this study was analysed using specific thermal regime according to its chemical characterisation. The thermal analysis methods used in this dissertation are provided in Table 2-1.

Table 2-1: The list of thermal analysis methods used for different specimens in this study.

Samples	Start Temperature (°C)	End Temperature (°C)	Heating Rate (°C. min ⁻¹)
Gelatin Scaffolds	15	100	5
Chitosan Membranes	25	350	10
Gelatin Membranes	15	100	5

For each detected thermal transition, two entries were recorded: the peak temperature (the point at which the derivative of heat flow - temperature diagram is zero) and the enthalpy of transition (the integrated area under the transition peak normalised according to the sample weight (Gill *et al.*, 2010)).

2.1.3. Free Amine Groups Assessment (Ninhydrin Assay)

The degree of crosslinking using chemical crosslinking agents was assessed according to the Ninhydrin assay reported by Sun *et al.*, with minor modifications (Sun *et al.*, 2006). As part of this assay, the reaction of Ninhydrin with a primary amine group forms a coloured reaction product known as *Ruhemann's Purple* which is detectable by UV-Vis-spectroscopy (Prochazkova *et al.*, 1999). Since chemical crosslinking of gelatin compound involves reaction with amine groups, the intensity of light absorption correlates with the number of available free amine groups in the sample. The control samples were used to estimate the number of free amine groups available per mass unit of gelatin sample ($N_{control}$). The number of free amine groups available in crosslinked samples was measured and recorded as $N_{crosslinked}$. The crosslinking index is defined as $N_{crosslinked}$ normalised to $N_{control}$ and reported in percentage (Equation 2-1):

$$\text{Crosslink Index (\%)} = \frac{N_{crosslinked}}{N_{control}} \times 100 \quad (\text{Equation 2-1})$$

To perform the assay, gelatin scaffolds were weighed and was added to 2 ml of 50% v/v Ninhydrin reagent aqueous solution. The mixture was heated in boiling water for 20 minutes. Then the test tubes were transferred into 4 °C water bath and after temperature adjustment, 5 ml of 50% v/v ethanol-water solution was added to the test tubes. The excess non-reacted Ninhydrins were oxidised by vortex for 15 seconds. The absorption was measured at 570 nm (UV-250IPC, Shimadzu, Japan). Glycine aqueous solutions with known concentrations were used to plot the calibration curve. Complete test protocol, the method for plotting the calibration curve, and the recipe for Ninhydrin reagents solution are reported in the Appendix 2.

2.1.4. In-Vitro Biodegradation Assay

Assessing the resistance of a wound dressing against enzymatic degradation may be helpful in estimating its lifetime after administration. MMP's (such as collagenase and gelatinase) are important components of the wound healing (Chapter 1, Section 2.2). Acting like a molecular scissors, the MMP's help regulate matrix degradation and cellular movement however excessive concentration of these components is a common cause of chronic wound and therefore resistance of wound dressings against these compound need to be determined. Biodegradation assays were performed to assess the rate of degradation of crosslinked gelatin scaffolds in contact with collagenase and the effect of crosslinking on the scaffold stability. *In-vitro* biodegradation assay was performed according to the method described by Melling *et al.*, with some modifications (Melling *et al.*, 2000). Scaffolds blocks were cut and their dry weights were recorded. Collagenase, from *Clostridium Histolyticum* (125 CDU/mg, Sigma, USA) was dissolved in PBS to obtain 5 and 2.5 mg/ml solution providing an enzymatic concentration of 625 and 317.5 CDU/ml, respectively. From the prepared enzyme solution, 300 μ l was diluted 2.67 times by addition of 500 μ l CaCl₂ solution (from 100 mMol CaCl₂ stock solution). The mixture was diluted to 5 ml total volume by addition of 4.2 ml PBS. A set of control samples was prepared by incubating the samples in plain de-ionised water for comparison. The samples were incubated in the solutions at 37°C for 20 hours at 40 rpm. The solutions were centrifuged for 5 minutes at 1000 g at 5°C (Megafuge 16R, Thermo Scientific, Germany). Through manual filtration, the non-digested samples were collected using filter paper No. 541. The collected solid residues were dried in 100°C oven. The samples were periodically weighed until a constant weight to 2 decimal places occurred. This number was recorded as the remaining mass (non-degraded). The degradation index was calculated for each sample as the ratio of non-degraded mass to initial mass (Pok *et al.*, 2013) (Equation 2-2):

$$\text{Degradation Ratio (\%)} = \frac{\text{Non-degraded Mass}}{\text{Initial Mass}} \times 100 \quad (\text{Equation 2-2})$$

2.2. Physical Characterisation Methods

2.2.1. Mechanical Properties Analysis

The native skin mechanical strength varies depending on which part of body it protects. The skin that covers load bearing surface of the body such as the surface of heel is tougher than the skin covering the area such as face and forearm (Diridollou *et al.*, 2000). Natural skin mechanical characteristics can be a suitable benchmark for designing an artificial skin substitutes and grafts.

In this dissertation uni-axial tensile tests were used to characterise the mechanical strength of samples. The scaffolds were conditioned in a 95% RH desiccator containing saturated copper sulphate at 20°C prior to mechanical tests for 2 days. It should be noted that water molecules act as a plasticiser for gelatin macromolecules (Díaz *et al.*, 2011) and have noticeable impacts on the structure mechanical properties. Thus, the results of his study cannot be directly compared with similar studies but with samples conditioning performed at different humidity conditions. Axial tensile strength tests were performed using a TA.XT-Plus texture analyser (Stable Micro Systems, Surrey, UK).

$$\sigma = \frac{F}{A_0} \quad (\text{Equation 2-3})$$

$$\varepsilon = \frac{\delta}{L_0} \times 100 \quad (\text{Equation 2-4})$$

Rectangular strips measuring 10x20mm were cut from the conditioned samples. The thickness of the samples was measured at 3 points using a digital caliper and the average value was recorded. The test specimens pulled with a cross head speed of 0.033 mm.sec⁻¹ until the sample failure was detected. Tensile strength (σ) was computed from the Stress-Strain plot using Equation 2-3, where σ is the scaffold tensile strength (Pa), F is the highest force recorded during the test (N), A_0 is the theoretical cross section area of the sample (m²). Tensile strain of samples (ε) was computed using Equation 2-4, where (ε) is tensile strain (%), δ is the change in gauge length at the rupture (mm) and L_0 is initial gauge length (mm). The sample Young's modulus was

calculated as the gradient of the linear segment of Stress-Strain plot and is reported in kPa.

2.2.2. Water Absorption Analysis

Prior to analysis, the samples were conditioned in a 0% RH desiccator containing self-indicating silica gel at 20°C for 2 days. Dry samples were weighed and soaked in de-ionised water. Soaked samples were taken out of water at regular intervals of 1, 3, and 6 hours after start of soaking and their hydrated weights recorded. Before weighing, the samples were blot-dried 10 times using No. 540 filter papers. Each measurement was carried out in duplicate and the average value of the two results was reported. The degree of swelling was calculated using Equation 2-5, where W_H and W_D are the sample hydrated and initial dry weights, respectively.

$$\text{Swelling Ratio(%)} = \frac{W_H - W_D}{W_D} \times 100 \quad (\text{Equation 2-5})$$

2.2.3. Adhesion Test

The adhesion between the different components of wound dressing was measured using standard method BS EN ISO 11644. Rectangular strips of triple layer wound dressings were cut with dimensions of 10x25mm. The strips were glued on to the standard poly ethylene test stubs measuring 20x70mm. The glue was prepared by mixing 20g of Desmocoll 400 and 80g of Ethyl Acetate. Just before applying the glue, Desmodur L75 was added to the mixture as a hardener. The ratio of Glue:Hardener was 20g:1g. The glued samples were left overnight (16 hours) at 20°C and a 95% RH desiccator containing saturated copper sulphate to cure.

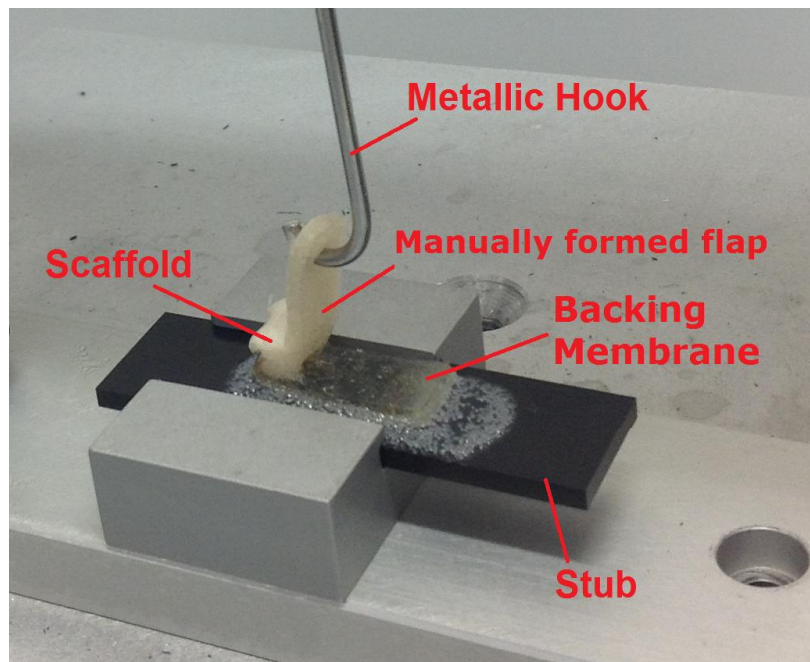


Figure 2-1: The wound dressing sample was glued on to the plastic test stub and installed on the test apparatus railing. The metallic hook was engaged to the upper portion of the sample and moved upward and measured the adhesion force between upper and lower portions of the wound dressing.

The stubs were fixed on the standard test apparatus railing. The upper portion of the sample was detached from its backing membrane manually to form a flap. The flap was engaged to the metallic hook as shown in Figure 2-1. The TA.XT-Plus texture analyser (Stable Micro Systems, Surrey, UK) probe was programmed to move upward and away from the stub by the crosshead speed of $1.2 \text{ mm}.\text{min}^{-1}$ and the resistance force was recorded as a function of distance.

2.2.4. Water Vapour Permeability Test

Gelatin membranes water vapour permeability was measured according to the standard test method SLP-25. An image of the testing instrument is shown in Figure 2-2.

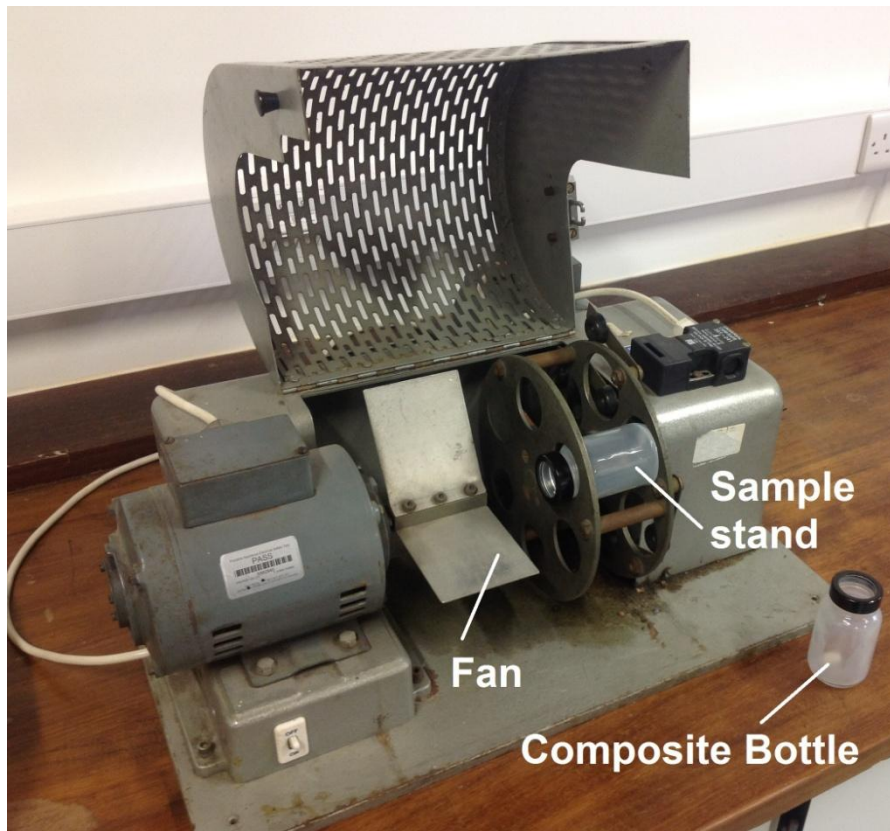


Figure 2-2: The water permeability testing apparatus. On the left, the metallic fan is visible as connected to an electric motor. On the right, the circular stands for the samples with one bottle inserted are visible.

To perform the test, the standard composite bottles were half-filled with dry self-indicating silica gel. The test membranes were cut in circle and placed on the top of the composite bottle. Before screwing the plastic cap, the internal diameter of the hole cut into the cap was measured and recorded. The cap was screwed in place. The bottle and samples were weighed. The bottle was placed in the testing stand. The stand was located in front of a rotating metallic fan. The sample was directly exposed to the air flow generated by the fan through the hole in the bottle cap. After 6 hours, the bottles were re-weighed and the secondary weights were recorded. The water permeability (P) was calculated according to Equation 2-6, where (P) is water vapour permeability, (m) is the difference between final and initial weight in mg, (d) is bottle internal diameter in mm, and (t) is time in hours:

$$P = \frac{7639 \text{ m}}{d^2 t} \quad (\text{Equation 2-6})$$

2.3. Visual Analysis

2.3.1. Visual Analysis of Samples

To record the visual appearance of the samples, they were photographed using a 5MP digital camera against a blue background and in the ambient light.

2.3.2. Scanning Electron Microscopy (SEM)

The samples were conditioned in a 0% RH desiccator containing self-indicating silica gel at 20 °C for 2 days prior to testing. The samples were sectioned and attached to an aluminium SEM stub using carbon tabs. Samples were gold-coated using a sputter coater (SC500, Mscope, UK) and the structural texture examined using a Variable Pressure Scanning Electron Microscope (VP-SEM, S-3000N, Hitachi, Japan). The acceleration voltage of the examination was individually chosen for each sample batch to obtain the best image quality and it is included in the caption of SEM image. The average pore size of the samples was determined using Quartz PCI image processing software package (Quartz Image Corp., Vancouver, Canada). The size calibration was performed before each measurement using an internal digital scale bar which was part of the software package.

3. The Statistical Analysis

The presence of significant difference between results was verified using non-parametric tests according to Kruskal-Wallis method using SPSS Statistics software (Version 20, International Business Machine, USA). The differences between results were accepted as significant at $p \leq 0.05$.

Chapter 3:

Gelatin Scaffold

Chapter 3 - Preparation of Porous Gelatin Scaffolds

The objective of this study is to prepare a wound dressing that is able to act as a platform for attracting skin cells from the wound surrounding, fostering their proliferation, infusion of blood arteries, and closure of the wound. In the biomedical engineering terminology, such a platform is called *Scaffold*, a hollow matrix suitable for cells migration and proliferation. There are certain requirements that are necessary for the scaffold to function desirably (Kamel *et al.*, 2013). It needs to be porous so that cells can easily penetrate, migrate, and conglomerate in it. Porosity is also vital for diffusion of vital nutrients to surrounding area of the cells (Dagalakis *et al.*, 1980). Finally, having a porous system with pore size of more than 80 μm is essential for formation of capillaries and blood arteries (Chvapil, 1982). The scaffold also needs to be degradable so that it is gradually removed from the wound site and replaces by regenerated skin (Kim *et al.*, 2011). In this study, gelatin was chosen as the building block of the scaffold due its similarity to the collagen, the main component of skin (Olsen *et al.*, 2003). Previous experience with freeze drying proved it to be an effective in preparing porous structure (Poursamar *et al.*, 2011). Considering this and the fact that precursor of the scaffold would be a biopolymer, freeze drying was selected over drying at high temperature for final product processing. However it has been shown that there is a limit with the respect to porosity distribution in the depth of porous structure that can be prepared solely through freeze drying (Azami *et al.*, 2010). This is due to reliance of freeze drying on vacuum for creating porous structure. In order to improve the porosity of the structure and having a foam block suitable for practical applications, it was decided to apply a combination of freeze drying with a supplementary method to create maximum possible porosity within the structure. Some of the industrially established methods that can be used in combination with freeze drying include: whisking or bubbling with gas input (Kiran, 2010). In this study a combination of freeze drying and gas foaming was used due to its simplicity and effectiveness in producing highly porous

structure (Dehghani and Annabi, 2011). In this Chapter, the gas foaming process started at a very basic level and it was refined in an iterative manner to lead to a better structure. All and all, 4 generations of gelatin scaffolds were prepared which would be discussed in chronological order in this Chapter.

1. First Generation Scaffolds

1.1. Scaffold Preparation Method

Sodium hydrogen carbonate is unstable in heated gelatin solution and it decomposes into carbon dioxide, water, and sodium carbonate. Monitoring 20% w/v gelatin solution pH shows that it has a mild acidic pH ($\text{pH} = 4.9$) and displays strong buffering capacity. First generation of gelatin scaffolds were prepared by taking advantage of mild acidic pH of gelatin solution and instability of carbonate particles in heated medium.

Gelatin solution with concentration of 20% w/v was prepared by dissolving 3.2g gelatin powder in 16ml de-ionised water at 60°C for 1 hour. Sodium hydrogen carbonate (0.9g) was added to 16 ml of the prepared gelatin solution. Shortly after carbonate addition due to its decomposition, CO_2 bubbles were formed in the liquid. Gelatin has a good surfactant ability which results in its ability in retaining formed bubbles and generating foam (Gómez-Guillén *et al.*, 2011). From the gelatin and carbonate mixture, 10 gram was cast in a stainless steel mold measuring 6 cm in diameter and 1.5 cm in height. Shortly after casting, the samples froze in -25°C freezer. The samples were extracted from the molds after 1 hour. Glutaraldehyde (GT) was used as the crosslinker agent throughout this Chapter. For better diffusion of GT within the samples, the frozen samples were thawed before crosslinking by incubation in 4°C de-ionised water for 1 hour. In order to crosslink the samples, the thawed gelatin samples were incubated in GT solution for 3 hours with no pH adjustment. The scaffolds were crosslinked using 0.25, 0.50, 0.75, and 1.00% v/v GT aqueous solutions. A set of non-crosslinked samples were prepared as control. After crosslinking, the samples were washed over night in de-

ionised water, frozen, and lyophilised for 24 hours. Lyophilisation was done under vacuum pressure of 0.250 mbar and temperature of -40°C.

1.2. Results

1.2.1. Visual Description of Scaffolds

Prepared scaffolds visual characteristics are shown in Figure 3-1-(A-C). Noticeable difference was observed between upper and lower surfaces of the scaffolds. The upper surface had a scattered porosity distribution (Figure 3-1-A). The porosity distribution was not uniform across the scaffolds surface. The lower surface contained elongated, tubular holes that may have been formed as a result of ice crystal formation through lyophilisation process (Figure 3-1-B). Figure 3-1-C shows the cross section of scaffolds with average thickness of 2.7mm based on the average of 3 measurements using digital caliper with the tolerance of ± 0.3 . The cross section of the scaffold showed linear pores grew laterally from the lower side of the scaffold to the top side.

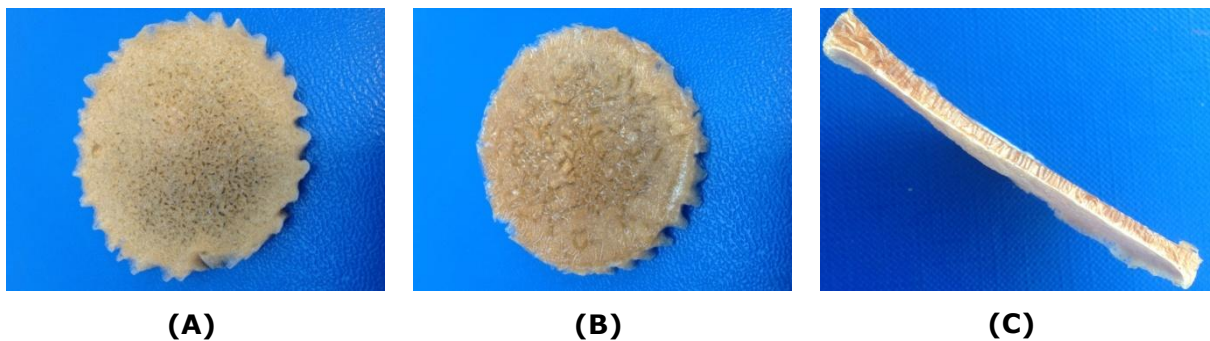


Figure 3-1: The first generation gelatin scaffold visual characteristics: (A) the upper surface of the scaffold; (B) the lower surface of the scaffold; (C) the cross section view of prepared scaffolds, the cross section of the scaffolds showed linear pores grew laterally from the down to top side.

1.2.2. Fourier Transform Infra-Red Spectroscopy (FT-IR)

The main purpose of performing FT-IR spectroscopy was to investigate the gelatin macromolecules structure in the atomic level. Figure 3-2 compares FT-IR spectra of scaffolds crosslinked by 0.25, 0.50, 0.75, and 1.00% v/v GT solutions with the control samples. Gelatin FT-IR spectra comprise of 5 amide bands. Absorption bands at 1631,

1541, and 1235 cm^{-1} correspond to the amide I, II, and III respectively (Haroun and El Toumy, 2010; Hashim *et al.*, 2010; Payne *et al.*, 1988; Jackson *et al.*, 1995). At longer wave numbers, gelatin amide A and amide B bands close to 3300 and 3080 cm^{-1} were noticeable, respectively (Abdelrahman and Newton, 2011; Yang *et al.*, 2010). Carbon and oxygen atoms interactions as part of carbonyl groups ($\text{C}=\text{O}$) are responsible for the Amide I absorption (Haroun and El Toumy, 2010; Hashim *et al.*, 2010; Payne *et al.*, 1988; Jackson *et al.*, 1995). Amide II absorption band originates from N-H bending and N=C stretching (Jackson *et al.*, 1995), and amide III band is caused by weak N=C stretching and N-H bending (Haroun and El Toumy, 2010). Finally, amide A and amide B are assigned to the vibrations of hydroxyl groups (O-H) and N-H stretching vibrations, respectively (Kanmani and Rhim, 2014; Muyonga *et al.*, 2004).

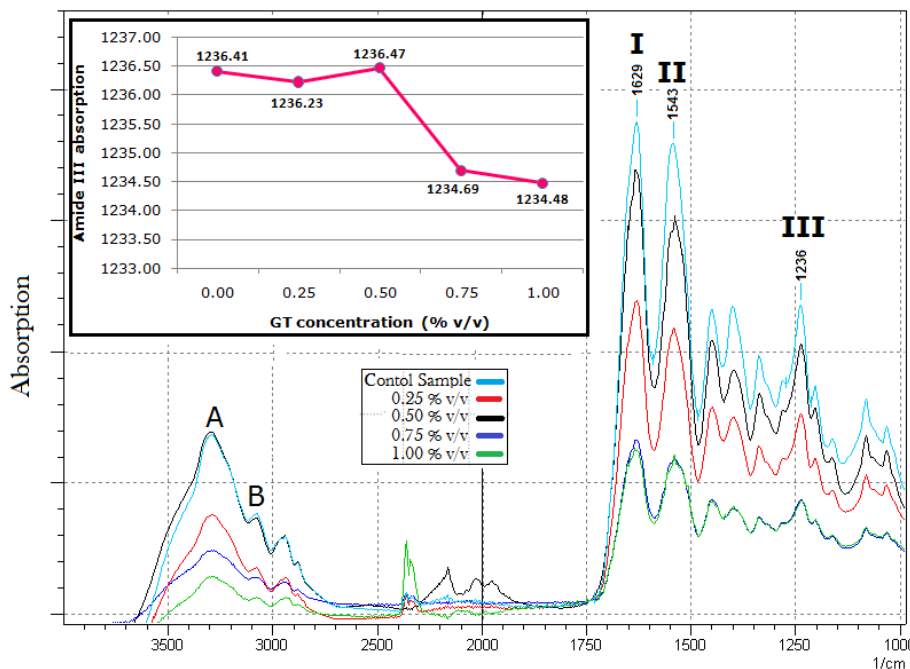


Figure 3-2: FT-IR spectra of the first generation gelatin scaffolds crosslinked with 0.25, 0.50, 0.75, and 1.00% v/v GT aqueous solution. The inset figure shows the absorption bands for amide III at different concentrations of GT.

All samples showed three major absorption bands associated with the gelatin spectrum. The FT-IR spectrums of crosslinked scaffolds and control sample show the

same pattern which may be indicative of intact gelatin structure at the atomic level during foaming. Shift of the amide A absorption to longer wave numbers may be indicative of molecular structure breakdown (Rabotyagova *et al.*, 2008). The absence of such a shift indicates that the scaffold preparation method was nondestructive to gelatin macromolecules.

The shift in amide I and III bands to lower wave numbers may correlate to a more stable helical structure as a result of the crosslinking (Payne *et al.*, 1988; Muyonga *et al.*, 2004; Susi *et al.*, 1971). There was slight shift of amide III band in crosslinked scaffolds compared with the control samples. The absorption bands of amide III shifted from 1236.4 cm⁻¹ in the control sample to 1234.5 cm⁻¹ in scaffolds crosslinked at 1.00% v/v GT. This may be indicative of subtle structural impacts of GT crosslinking on gelatin macromolecules. However, the degree of this shift was minute and a decisive argument about its impact is not prudent.

1.2.3. Mechanical Properties of the Scaffolds

The change in the tensile properties of the first generation gelatin scaffolds as a function of GT concentration was investigated and the results are listed in Table 3-1.

Table 3-1: Mechanical properties of the first generation gelatin scaffolds as a function of GT concentration. As a result of crosslinking, the scaffolds tensile strength increased from 139.4 kPa for the control samples to as high as 198.5 kPa for scaffolds crosslinked with 0.50% v/v GT.

GT Concentration (% v/v)	Tensile Strength (kPa)	Young's Modulus (kPa)	Tensile Strain (%)
0 (Control)	139.4 (± 4)	5.1 (± 5)	95.2 (± 42)
0.25	163.8 (± 64)	12.9 (± 7)	23.9 (± 2)
0.50	198.5 (± 81)	13.0 (± 5)	24.1 (± 2)
0.75	186.4 (± 52)	13.6 (± 7)	23.2 (± 4)
1.00	175.5 (± 123)	12.7 (± 11)	25.7 (± 12)

Gelatin is denatured collagen in which the inter-chain bonds in a thermally labile region have to be broken before the whole molecule can unzip. Thus, unlike fibrillar collagen, in gelatin the inter-chain interaction has been significantly weaken. When a gelatin solution temperature is reduced, gelatin molecules form junction zones through physical crosslinking, although the strength of formed structure is not high (Achet and He, 1995). Chemical crosslinking therefore stabilises the collagen molecules in a fibre by reducing the separation of the molecules. As a result of crosslinking, scaffolds tensile strength increased comparing with the control samples. Figure 3-3 shows the schematic view of physical and chemical crosslinking formation in the gelatin structure. Chemical crosslinking using reactant agents such as GT forms intra-molecular covalent bonds that drastically strengthen the already formed weak physical crosslinking (Giraudier *et al.*, 2004; Farris *et al.*, 2010). By reducing the mobility of the chains, crosslinking increases the tensile strength of the structure and reduces its elasticity and malleability (Farris *et al.*, 2010; Bigi *et al.*, 2001).



Figure 3-3: How gelatin form gel at room temperature. Upon reduction of gelatin solution temperature the physical junction zones formed by pulling polypeptide chains together and formation of partial helical structure. During chemical crosslinking, reactive agents such as GT increase the strength of already formed weak physical crosslinks by forming intra-molecular covalent bonds by connecting adjacent polypeptides and thus increasing the overall strength of structure (Giraudier *et al.*, 2004).

Although numerical values of the tensile strength listed in Table 3-1 increased upon crosslinking, the changes in tensile strength proved to be statistically insignificant

($p \geq 0.05$). The increase of tensile strength continues up to crosslinking in 0.50% v/v GT solution. From this point, the tensile strength began to decrease. Decrease of the tensile strength as a result of a higher crosslinking concentration has been observed by other researchers (Knaul *et al.*, 1999; Bigi *et al.*, 2001; Price, 1986; Wu *et al.*, 2010; Chiou *et al.*, 2008). Reduction of tensile strength can be the result of *over-crosslinking*. Price (1986) showed that at higher concentrations of crosslinking agents, polymeric materials can become so fragile that they fracture at noticeably smaller forces. Wu *et al.*, (2010) showed that such a decrease of mechanical strength is much more significant for porous gelatin scaffolds. Knaul *et al.*, (1999) suggested that the decrease in mechanical strength at high concentrations of GT may be due to local mechanical stress concentrations with increasing crosslink density. Irregular porosity has also been suggested as a source of structural defects and the cause of strength reduction (Nussinovitch, 1992). The pores may contribute to elevated local stress at their sharp edges, leading to reduced mechanical resistance against crack initiation (Liu *et al.*, 2006). It is suggested that mechanical properties of the brittle material with higher Young's modulus may be very sensitive to internal flaws and defects and may fracture prematurely (Allen *et al.*, 2006). In summary, porosity and a more brittle bio-polymeric network together may have caused the reduction of tensile strength in the scaffolds crosslinked with 0.75 and 1.00% v/v GT aqueous solution.

Crosslinking increased the Young's modulus of the scaffolds by as much as 2.7 times. Increase of Young's modulus represents the reduction in plasticity and tensile strain before fracture. Crosslinking caused a significant reduction in the tensile strain of the scaffolds ($p \leq 0.05$). This decrease occurred at the lowest concentration of GT and subsequent increase of GT concentration did not change the strain values noticeably. Reduction in strain and elongation as a result of crosslinking is observed by other researchers (Bigi *et al.*, 2001). The main cause for this reduction is inter-molecular covalent bonds formation by crosslinking agent which restricts molecular mobility (Martucci *et al.*, 2006). It should be noted that Bigi's study has been carried out at

relative humidity of 75%. High sensitivity of mechanical properties is highlighted for the collagen-derived materials and it is reported that the tensile strength of such materials can be significantly impacted in a water saturated atmosphere (Meyer, *et al.*, 2010, Klüver and Meyer, 2014).

1.2.4. Scaffolds Thermal Analysis

Table 3-2 shows the results of the first generation gelatin scaffolds thermal analysis. The main purpose of performing thermal analysis on the gelatin structure was to verify chemical crosslinking and stabilisation. Denaturation temperature (T_d) is an indirect measurement of the crosslinking degree: higher denaturation temperature value delineates a greater degree of crosslinking or stabilisation (Gratzer *et al.*, 1996). Denaturation temperature is usually associated with the loss of proteins activity through unfolding, aggregation, and loss of bound water (Porter, and Vollrath, 2012). Unfolding of protein structure in thermodynamic terms is a *work* which the energy required for its progress is measureable as Gibbs Free Energy (ΔG). Gibbs Free Energy is defined through Equation 3-1, where ΔH is the Enthalpy of transition in Joules, T is temperature in Kelvin, and ΔS is the entropy of transition in Joules per Kelvin.

$$\Delta G = \Delta H - T\Delta S \quad (\text{Equation 3-1})$$

At least two factors may be considered as potentially important in explaining the increase in the denaturation temperature of samples after crosslinking. Crosslinking might dehydrate the structure by closer binding of the molecules. Since water molecules can act as plasticiser (Díaz *et al.*, 2011), the water mass in the structure determines the degree of freedom that the molecules have in their relative movement against each other (van den Bosch *et al.*, 2003). Such stabilisation is consistent with the polymer-in-a-box mechanism which is suggested to explain the increase in denaturation temperature brought about by dehydration (Miles and Ghelashvili, 1999). By removing water, the degree of freedom and entropy of molecular movements decreases. In

addition, covalent bonds formation as a result of crosslinking will cause loss of chain entropy brought about by the reduced number of molecular configurations (Martucci *et al.*, 2006; Usha and Ramasami, 2000). Reduction of entropy value in Equation 3-1 increases the Gibbs energy which means doing the same amount of work (in this case unfolding gelatin molecules) requires more energy. This translates into higher temperature (T) to compensate for reduction in entropy (Miles *et al.*, 2005). The peak temperature was assigned as the denaturation temperature in this and all future studies. The control samples showed an endothermic peak of 54°C; upon crosslinking at the lowest concentration of GT (0.25 %v/v), the denaturation temperature increased to 80°C and remains stable as the GT concentration increased. According to Equation 3-1, another element of determining ΔG is the enthalpy of transition (ΔH). In the GT-crosslinking systems the changes in the enthalpy value is not determinant in the value of ΔG (Covington, 2009). However, enthalpy value can offer valuable information about the extent of covalent bonds formation in the structure after crosslinking.

Table 3–2: The results of thermal analysis of the first generation gelatin scaffold crosslinked at different concentrations of GT.

GT concentration (% v/v)	Peak Temperature (T_d) (°C)	Enthalpy of Transition (ΔH) (J.g ⁻¹)
0 (Control)	53.8	-22.3
0.25	80.0	-15.1
0.50	79.1	-14.6
0.75	80.4	-12.8
1.00	79.5	-12.6

Along with an increase in T_d , the enthalpy of transition (ΔH) reduces as GT concentration increased. The change of ΔH is determined by the balance between two balancing thermal phenomena: cleavage of hydrogen bonds which is an endothermic phenomena (Achet and He, 1995; Gill *et al.*, 2010), and formation of new bonds to give

less order in addition with cleavage of covalent bonds which are both exothermic (Dardelle *et al.*, 2011; Gill *et al.*, 2010). De Carvalho and Grosso (2004) reported that reduction in enthalpy is caused by a reduction in the number of hydrogen bonds in favour of an increase in the number of covalent bonds. Chemical crosslinking consumes amines groups which are the sites suitable for hydrogen bonds establishment at the expense of covalent bonds formation. Such structural changes tilt the balance towards thermal transitions which are more exothermic and less endothermic. This justifies the overall decrease in the ΔH after crosslinking with GT solution. The negative values of enthalpy of transition was reduced from -22.3 J.g^{-1} in the control samples to -12.6 J.g^{-1} in the samples crosslinked with 1.00% v/v GT. Considering these results, thermal analysis showed that stabilisation by crosslinking was occurred in the scaffolds structure.

1.2.5. Scaffolds Microstructure Analysis

Figure 3-4, (A-F) displays the SEM images of the first generation gelatin scaffolds. The control samples and scaffolds crosslinked at GT concentration of 0.50, and 1.00% v/v were examined using Scanning Electron Microscopy at 20 kV acceleration voltage. The prepared scaffolds showed scattered porosity on the surface which is similar to the visual observation made in Section 1.2.1. The structural profile of the surface of all three specimens was flat and smooth, without any noticeable sharp edges. The average pore size of the scaffolds in the control samples was $188 \mu\text{m}$ (Figure 3-4, A and B). The scaffolds crosslinked using 0.50% v/v GT showed an average pore size of $214 \mu\text{m}$ (Figure 3-4, C and D), and at 1.00% v/v, the average pore size of the scaffolds was $240 \mu\text{m}$ (Figure 3-4, E and F). An increase in the pore size as GT concentration increased may be the result of GT effectiveness in stabilising the gelatin foam during synthesis. Gelatin foam tends to collapse after foam casting in the mold (*Barbetta et al.*, 2009). Collapse of foam after casting may be caused by either the phenomena known as *Ostwald ripening* (growth of large bubbles due to higher internal pressure) and/or drainage (downward movement of liquid on the bubble surfaces as a result of gravity force) (Stevenson, 2010). Improving the mechanical strength may have caused the

foam become stable more rapidly at higher concentrations of GT. Therefore at such concentrations, higher number of bigger pores was left in the structure after synthesis.

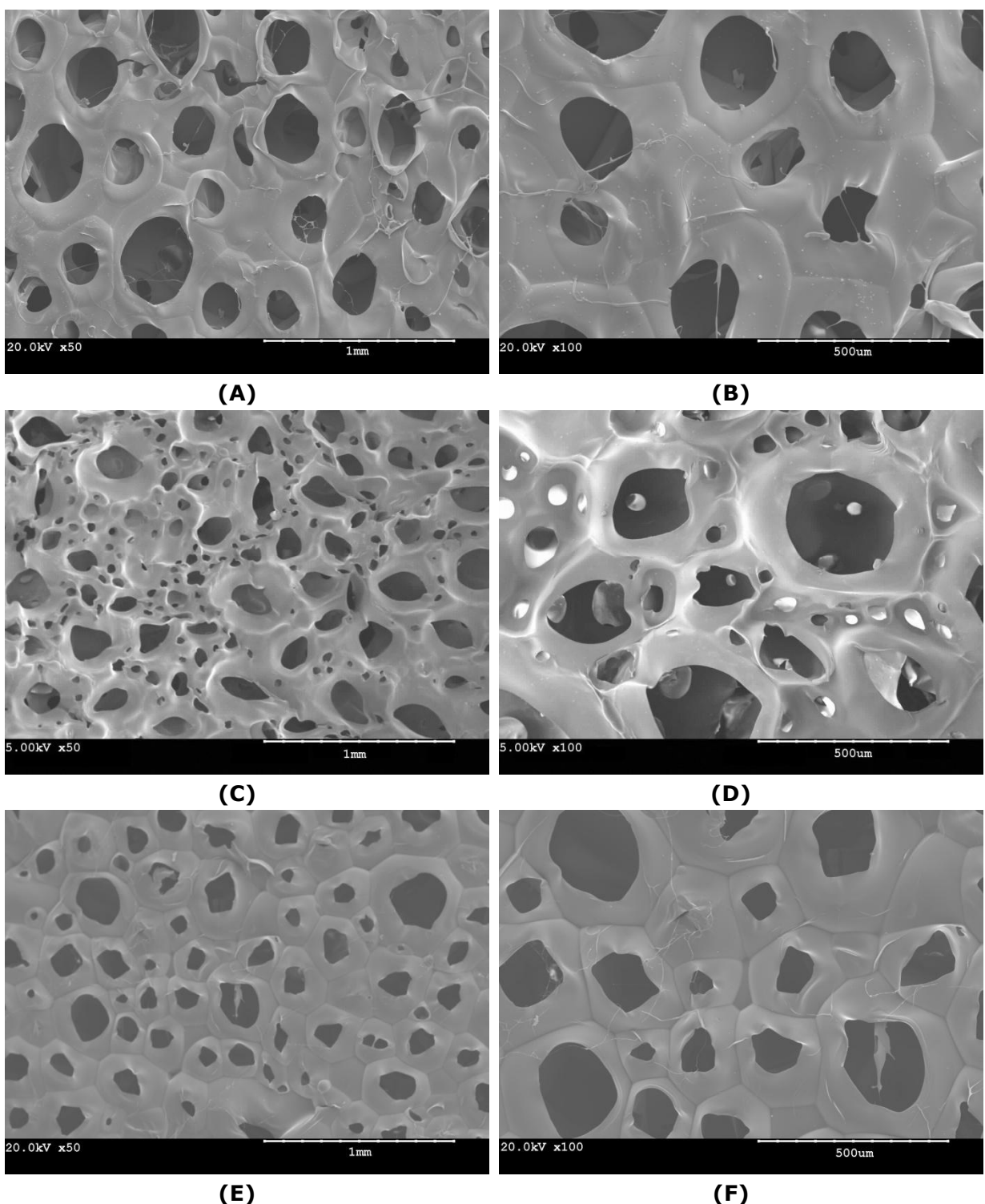


Figure 3-4: SEM images of the first generation gelatin scaffolds at 50x and 100x magnifications, (A) and (B) control samples; (C) and (D) scaffolds crosslinked with 0.50% v/v GT solution; (E) and (F), scaffolds crosslinked with 1.00% v/v GT solution. All images are captured at 20 kV acceleration voltage.

Figure 3-5-(A) shows the surface of the control sample which may contain residual NaHCO_3 once the synthesis was completed. To study this hypothesis, EDX analysis were performed on the control sample. Figure 3-5-(B) shows the EDX result with a strong sodium peak that may have originated from unreacted NaHCO_3 . This may be due to insufficiency of high temperature, mildly acidic gelatin solution to cause the complete decomposition of the added carbonate.

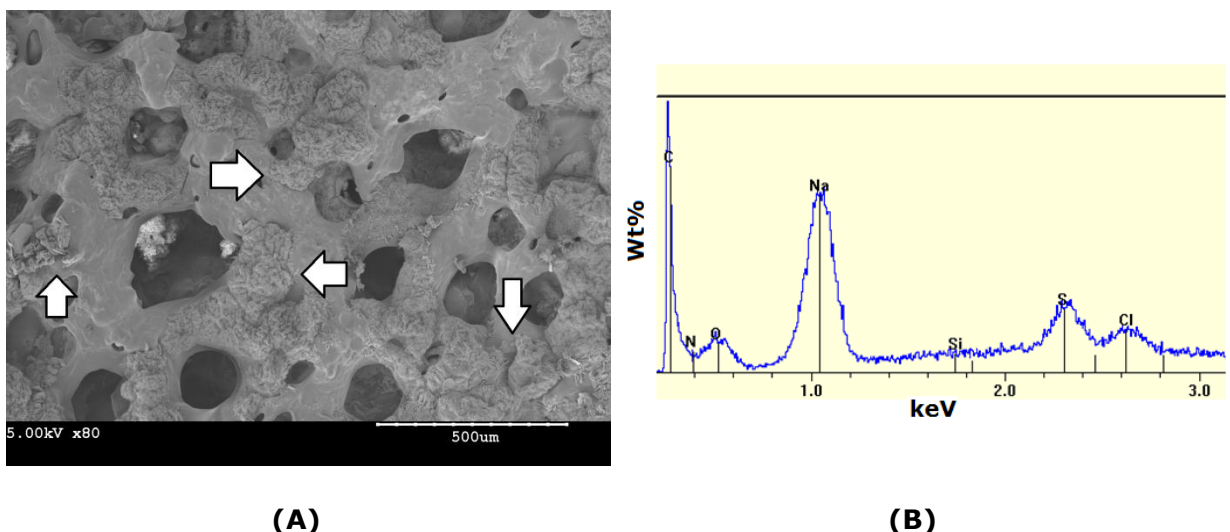


Figure 3-5: (A) SEM image of the control samples surface at the 80x magnification. The white arrows point towards compact powder compounds which may be unreacted NaHCO_3 , (B) The EDX result of control sample analysis shows a strong sodium peak which may be originated from NaHCO_3 , the SEM image is obtained at 5kV acceleration voltage.

Gelatin has a good foaming ability (Gómez-Guillén *et al.*, 2011), it is plausible to believe that some of the pores shown in the SEM images was originated not because of CO_2 emission but as a result of such an intrinsic feature in gelatin. Thus to obtain better porous structure, it is necessary to employ a mechanism to accelerate carbonate decomposition and release of CO_2 gas.

1.2.6. Scaffold Water Absorption

Figure 3-6 displays water absorption capabilities of the crosslinked scaffolds compared with the control samples. The control samples showed the highest water

absorption capacity and the scaffolds crosslinked with 1.00% v/v GT solution had the lowest. All crosslinked scaffolds reached a water saturation level within the first hour. An increase in GT concentration reduces water absorption capability of the scaffolds (Charulatha and Rajaram, 2003; Knaul *et al.*, 1999). This may be due to a reduction in the bonding of water molecules to amine groups in gelatin, since these functional groups were already consumed during the reaction with GT. Thus, crosslinked scaffolds become weaker in establishing hydrogen bonds with water molecules and this leads to less water absorption. However, Miles *et al.*, (2005) argued that reduction of water content as a result of crosslinking has few to do with water bounding mechanism and is mainly caused as a result of configurationally restricted and tightly packed crosslinked structure. This is observed by other researchers who attributed the dehydration to the reduced elasticity of the structure which hinders expansion in water and thus preventing water absorption (Tasselli *et al.*, 2013). Together, these two elements cause the reduction of water absorption as a result of GT crosslinking that was observed in Figure 3–6.

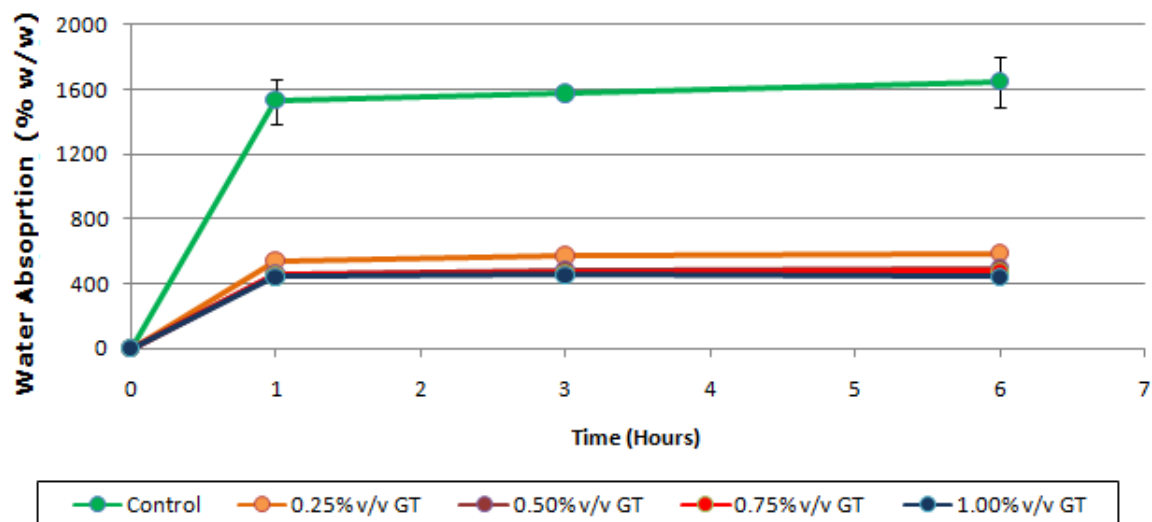


Figure 3–6: Water absorption profile of the first generation gelatin scaffolds. The scaffolds which were crosslinked using the highest concentration of GT (1.00% v/v) showed the lowest water absorption ability.

1.3. Summary

The first generation gelatin scaffolds had scattered and irregular distribution of porosity throughout the structure. Although the gas foaming method managed to produce some pores within the structure, the pore distribution was not sufficiently high to establish an interconnected network of pore system. This may be due to the limited amount of gas emission in the gelatin solution prior to scaffold casting and freezing.

Therefore, it is necessary to employ a modification into fabrication method in order to increase the CO₂ emission in gelatin solution. Lower pH's can cause more decomposition of carbonate and better porosity in the structure. Direct addition of acetic acid to the gelatin solution is reported for improving the foaming ability of gelatin (Leffler and Müller, 2000). Thus, increasing the pH of the gelatin solution was explored in the next generation of gelatin scaffolds.

2. Second Generation Scaffold

2.1. Scaffold Preparation Method

The first generation of gelatin scaffold described in Section 1.1 had scattered and irregular distribution of porosity throughout the structure. Low gas emission was assumed to be the potential cause for this. To address the problem, in this generation, acetic acid was manually added as a reactant to enhance CO₂ gas emission. The reaction between acetic acid and sodium hydrogen carbonate is shown in Equation 3-2. In order to implement this enhancement, the synthesis procedure described in Section 1.1 was modified as follows:



Gelatin solution with concentration of 20% w/v was prepared using a hot plate magnetic stirrer at 60 °C. Sodium hydrogen carbonate particles (1.2g) were added to 16ml of gelatin solution. Shortly after the NaHCO₃ addition, gelatin solution (8g) was cast in a stainless steel mold. The samples were kept in 5 °C fridge for 5 minutes. At this point, the material was solidified to allow its extraction from the mold. 50ml of 10% v/v acetic acid aqueous solution was prepared. By addition of adequate volume of GT to acetic acid solution, 4 aqueous solutions of GT with 0.25, 0.50, 0.75, and 1.00% v/v concentrations were prepared. Solidified gelatin samples that were extracted from the molds were crosslinked by immersing into GT/acetic acid aqueous solutions for 3 hours. A set of non-crosslinked samples were prepared as controls. To study the impact of pH on the properties of the scaffolds, crosslinking were performed at two different pH's of 2.5 and 4.5. Crosslinked samples were washed in de-ionised water for 2 hours. The samples were frozen and then lyophilised for 24 hours. Lyophilisation was performed under vacuum pressure of 0.250 mbar and temperature of -40 °C.

2.2. Results

2.2.1. Visual Description of Scaffolds

The visual features of the second generation gelatin scaffold are shown in Figure 3-7-(A). As a result of direct acetic acid addition, more pores with more uniform circular shapes and regular distribution throughout the structure were formed. The edges of the scaffold were sharp and irregular similar to the first generation samples (Figure 3-1). Figure 3-7-(B) shows the cross section view of the scaffold with an average thickness of 2.3mm based on three measurements with the tolerance of ± 0.3 . To study how much the foaming is actually effective on the final properties of the scaffold, a gelatin membrane was prepared only with lyophilisation and without the gas foaming. The result is shown in Figure 3-7-(C). The membrane prepared through lyophilising showed scattered areas of compact gelatin that were brighter and more distinguishable from the surrounding areas. Scaffolds prepared without foaming also showed more grooves and tubular textures within its structure which may be the result of ice crystal formation and evaporation during lyophilisation. Thus, it is shown that gas foaming has a positive impact on porosity of the scaffold.

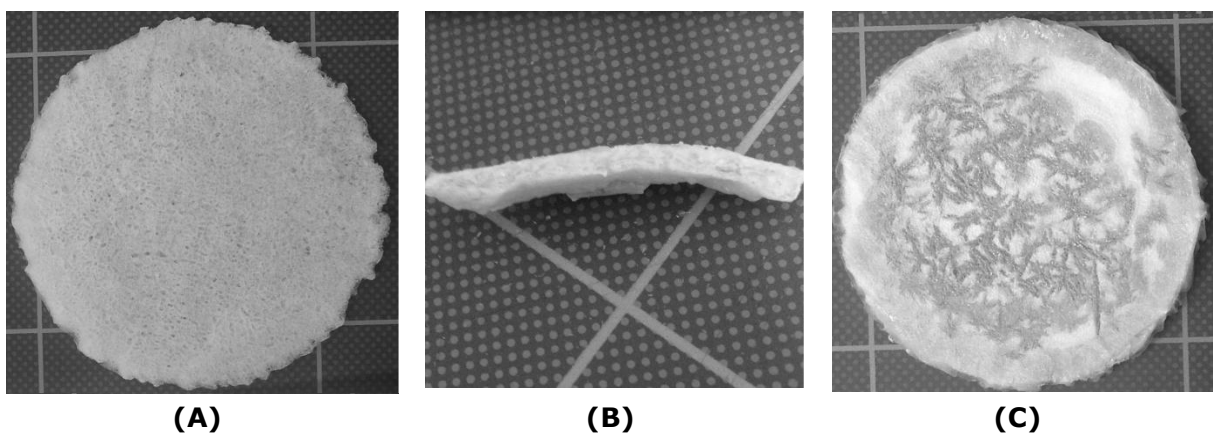


Figure 3-7: Visual characteristics of second generation gelatin scaffold, (A) the top surface view of the scaffold, (B) the cross section of the scaffolds, (C) the gelatin sample prepared through lyophilisation and without any foaming procedure for the sake of comparison.

2.2.2. Fourier Transform Infra-Red Spectroscopy (FT-IR)

Direct addition of acetic acid may have had a detrimental impact on gelatin molecules which can be investigated through FT-IR spectroscopy. Figure 3-8 shows a comparison amongst the second generation gelatin scaffolds crosslinked at various concentrations of GT. With respect to the main gelatin absorption peaks, the FT-IR spectra of the samples are not noticeably different from the previous generation results. The amide I, II, and III absorption bands appeared at 1631, 1537, and 1234 cm^{-1} , respectively (Haroun and El Toumy, 2010; Hashim *et al.*, 2010; Payne *et al.*, 1988; Jackson *et al.*, 1995). At longer wave numbers, absorptions at 3277 and 3075 cm^{-1} are assigned to amide A and B, respectively (Abdelrahman and Newton, 2011; Yang *et al.*, 2010). Strong absorption bands at 2350 cm^{-1} may be a result of strong CO_2 presence within the samples, which can be a sign of increased gas emission as result of the method modification.

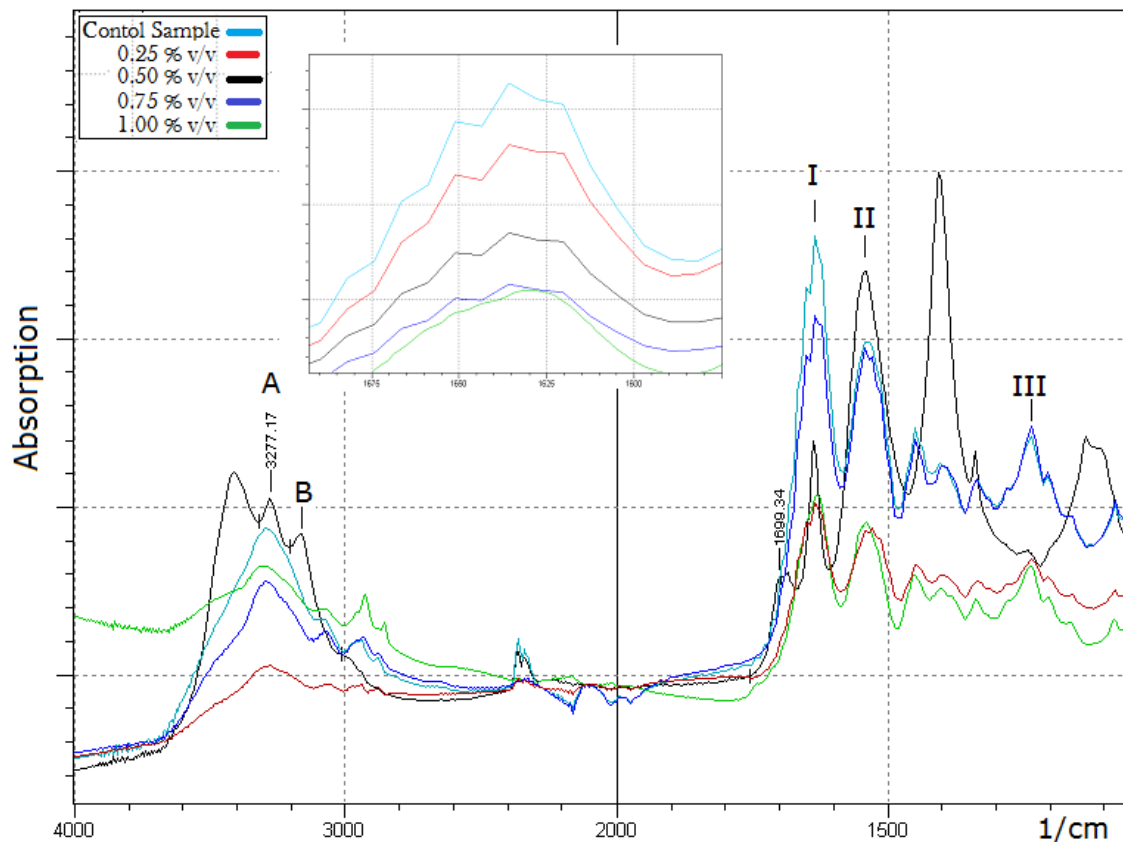


Figure 3–8: FT-IR spectra of the second generation gelatin scaffolds and crosslinked with 0, 0.25, 0.50, 0.75, and 1.00% v/v GT aqueous solutions. The inset figure shows the magnified view of amide I peaks for all 5 samples (Amides I, II, III, A, and B are marked on the chart).

The absorption at 1699 cm^{-1} can be originated from protonated carboxylic acid groups in acetic acid (Butler *et al.*, 2003). This absorption band may have been caused due to residual acetic acid in the scaffold after preparation. In comparison with *the first generation scaffolds*, main absorption wave numbers of gelatin did not show noticeable changes. This shows that method modifications did not have any significant impacts on the crosslinked and control sample molecular structures.

2.2.3. Mechanical Properties of the Scaffolds

Table 3–3 lists the values for the tensile strength, Young's modulus, and tensile strain of the second generation gelatin scaffolds. As mentioned in Section 1.2.3, high sensitivity of mechanical properties in the collagen-derived materials should be taken

into account before considering the listed values in Table 3-3 (Meyer, *et al.*, 2010, Klüver and Meyer, 2014). Crosslinking significantly reduced both the tensile strength and strain of the structure in comparison with the control samples ($p \leq 0.05$). Decrease of strain as a result of crosslinking is an expected phenomenon that is reported by another researcher (Bigi *et al.*, 2001). However, decrease of strength upon crosslinking was a surprising result. Such a reduction may be the result of excessive brittleness within the structure. Zeugolis *et al.*, (2008) reported a significant reduction of tensile strength in collagen samples as a result of crosslinking with GT. As discussed for the first generation scaffolds, the reduction of tensile strength can be the result of over-crosslinking (Wu *et al.*, 2010). This effect in conjunction with irregular porosity within the structure may have led to failure of the structure at lower tensile strength (Liu *et al.*, 2006).

Table 3-3: Tensile strength, Young's modulus, and tensile strain of second generation gelatin scaffolds prepared at pH 2.5. Crosslinking significantly reduced the tensile strength of scaffolds.

GT Concentration (% v/v)	Tensile Strength (kPa)	Young's Modulus (kPa)	Tensile Strain (%)
0 (Control)	117.9 (± 45)	1.4 (± 0.3)	148.2 (± 30)
0.25	67.2 (± 7)	1.1 (± 0.1)	73.6 (± 18)
0.50	39.7 (± 8)	1.4 (± 0.6)	52.3 (± 28)
0.75	42.9 (± 16)	2.1 (± 0.6)	18.7 (± 4)
1.00	42.1 (± 2)	1.8 (± 0.1)	24.6 (± 2)

In comparison with its predecessor, current generation showed lower tensile strength. Due to modifications to fabrication methods, second generation scaffolds appeared to be more porous. Nussinovitch *et al.*, (1992) showed that porous structures prepared by gas foaming had significantly lower tensile strength in comparison with non-porous samples made of the same ingredients. In addition to more porosity, the inferior tensile strength may have caused as a result of molecular scission and degradation. Considering the hydrolysing effect of acetic acid and its potential impact on gelatin helical sections cleavage (Achet and He, 1995) and the impact of GT crosslinking on the

molecular disintegration (Knaul *et al.*, 1999) lower tensile strength of second generation scaffolds may partly be due to prolong interaction with acetic acid. The third possible cause for lower tensile strength of these sets of samples relative to their predecessors may be in-effective crosslinking. As discussed in Chapter 1, Section 7.1., the activity of GT is a pH-dependant value. The efficiency of GT reaction would be reduced as a result of acidic pH's (Damink *et al.*, 1995).

To study how much effective chemical crosslinking was on the scaffold tensile strength, synthesis, and crosslinking of scaffolds were carried at a higher adjusted pH of 4.5. Figure 3-9 shows the results of the comparing two sets of experiments.

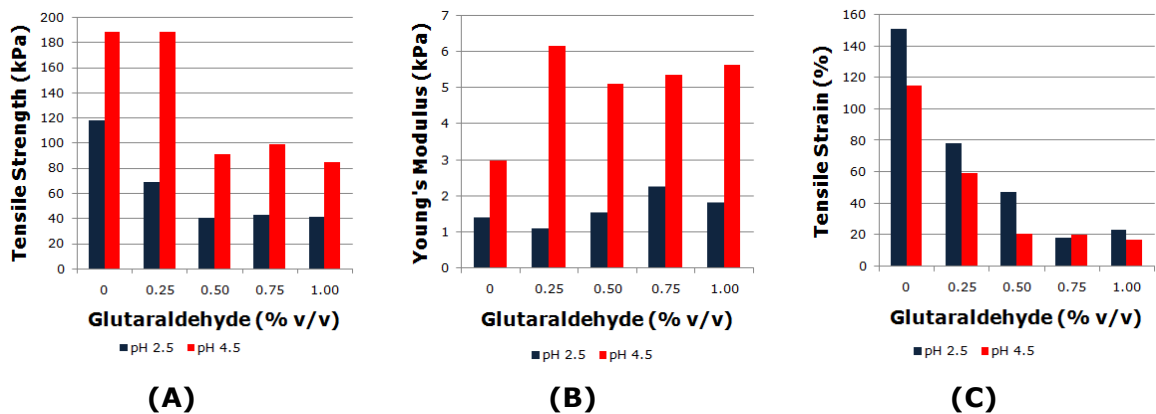


Figure 3-9: The impact of pH on the mechanical properties of the second generation gelatin scaffolds: (A) tensile strength, (B) Young's modulus, and (C) tensile strain. The crosslinking was carried out using GT which its reaction is pH-dependent. Lower pH led to a lower tensile strength regardless of GT concentration. A higher pH caused the scaffold to become less plastic with higher Young's modulus and lower tensile strain.

Scaffolds prepared at pH 4.5 had significantly higher tensile strength ($p \leq 0.05$). This may point towards detrimental impact of acidic pH's on gelatin but upon further scrutiny one would notice that the scaffolds prepared at lower pH showed significantly higher tensile strain ($p \leq 0.05$). If the acidic pH was degrading, then the affected samples could not stretched longer than other sets of samples. This points towards the fact that lower tensile strength of the second generation scaffolds may be the result of incomplete crosslinking by GT. It is assumed that the lower pH may lead to an inefficient GT

reaction and hence a lower tensile strength of the scaffold. Thus when the pH was increased from 2.5 to 4.5 (Figure 3-9), the strength of the scaffolds was increased and the strain was decreased. Lack of crosslinking and inefficiency in GT crosslinking may be verified from thermal analysis and the study of denaturation temperature. The results obtained by thermal analysis are discussed in the next section.

2.2.4. Scaffolds Thermal Analysis

Due to addition of acetic acid to the ingredients and its potential effect on GT reaction, it was necessary to investigate the influence of pH on the thermal stability of the scaffolds. Table 3-4 and Table 3-5 show the results of the thermal analysis of the scaffolds prepared at pH 2.5 and 4.5, respectively. The denaturation temperature values did not increase as a result of GT crosslinking at pH 2.5. The denaturation temperature of the control sample was 56.3°C whilst the denaturation temperature of the scaffolds crosslinked at 1.00% v/v showed the value of 56.7°C. These values suggest that crosslinking and stabilisation did not occur at pH 2.5. Farris *et al.*, (2010) reported the absence of increase in denaturation temperature as a result of crosslinking gelatin with GT in the acidic pH's.

Table 3-4: Thermal analysis results of second generation gelatin scaffolds prepared and crosslinked at pH 2.5. The results showed little change in denaturation temperatures as a result of GT concentration changes.

GT concentration (% v/v)	Denaturation Temperature (T_d) (°C)	Enthalpy of Transition (ΔH) (J.g ⁻¹)
0 (Control)	56.3	-32.2
0.25	54.2	-29.1
0.50	56.8	-35.2
0.75	56.7	-33.8
1.00	56.6	-40.0

As explained in Chapter 1, Section 7.1, GT crosslinking reaction cannot proceed efficiently at acidic pH's as the amine groups of the gelatin macromolecules are protonated and the Schiff base reaction between carbon and nitrogen atoms in GT and gelatin molecules is not favorable (Farris *et al.*, 2010). Thus to enhance the rate of scaffold crosslinking, it was necessary to increase the pH of crosslinking solution. Lack of crosslinking is in agreement with the results of low tensile strength at the pH 2.5 (Table 3-4).

Table 3-5: Thermal analysis results of second generation gelatin scaffolds prepared and crosslinked at pH 4.5. The data showed an increase in the denaturation temperature as the GT concentration was increased.

GT concentration (% v/v)	Denaturation Temperature (T_d) (°C)	Enthalpy of Transition (ΔH) (J.g ⁻¹)
0 (Control)	56.3	-32.2
0.25	81.9	-10.0
0.50	82.0	-14.4
0.75	79.0	-13.1
1.00	84.9	-12.3

Table 3-5 lists the results of thermal analysis of the scaffolds prepared at pH 4.5. The increase in pH improved the efficiency of the GT reaction within the solution and as a result, the denaturation temperature increased as the GT concentration was raised. The comparison between the thermal properties of scaffolds at each pH of 2.5 and 4.5 is shown in Figure 3-10. Increase in denaturation temperature as a result of an increase in pH substantiates that pH adjustment is indispensable for scaffold stabilisation. Thus preparing scaffolds without pH adjustment at 4.5 or higher was not possible and for the rest of the remaining sets of experiments the results for pH 4.5 are presented.

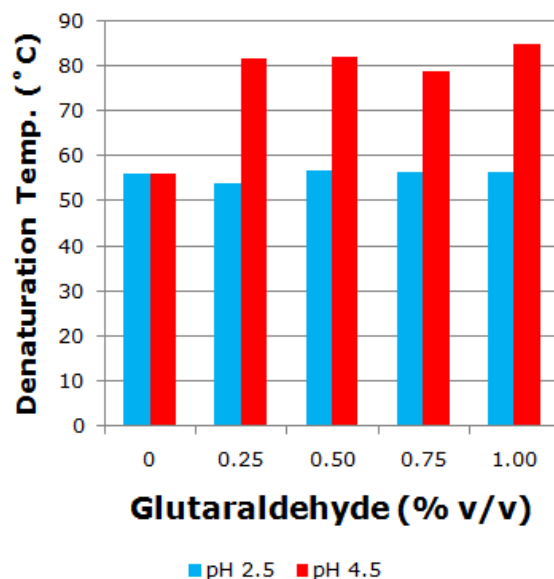


Figure 3-10: A comparison between second generation scaffolds thermal stability (denaturation temperature) that were prepared at pH 2.5 and 4.5.

2.2.5. Scaffolds Microstructure Analysis

Figure 3-11 shows the SEM images of crosslinked and control samples of second generation scaffolds. The SEM images show an array of pores with fairly uniform circular or elliptical shapes. The diameters of these pores range from 180 to 250 μm . The porous texture was limited to the top surface of the scaffolds and the pores were not interconnected. This structure is similar to the first generation scaffolds. The average pore size for the control samples was 188 μm . Crosslinked scaffolds showed a higher

average pore size. The average pore size of scaffolds crosslinked using 0.50% and 1.00% v/v GT solution were 192 μ m and 229 μ m, respectively. In comparison with first generation of scaffolds the average pore sizes did not show noticeable difference. Lack of difference/improvement from the first generation may be the result of compromising the benefit of acetic addition by the necessity of increasing the pH. Brittleness is apparent in Figure 3-11-(E) where crack propagation from one pore to the other is visible in 1.00% v/v GT crosslinked sample. Gas foaming method is an effective technique for producing highly porous structure (Dehghani and Annabi, 2011). This method is reported to produce structures with pore size distributions as high as 400 to 500 μ m (Nam *et al.*, 2000; Park, 2002). Comparison between SEM results in this Section and reported data by other researchers showed that obtained scaffolds did not benefit from full potential of gas foaming and method modification is necessary to improve porous structure of the samples. This is taken into consideration in designing the following generation of scaffolds in the next.

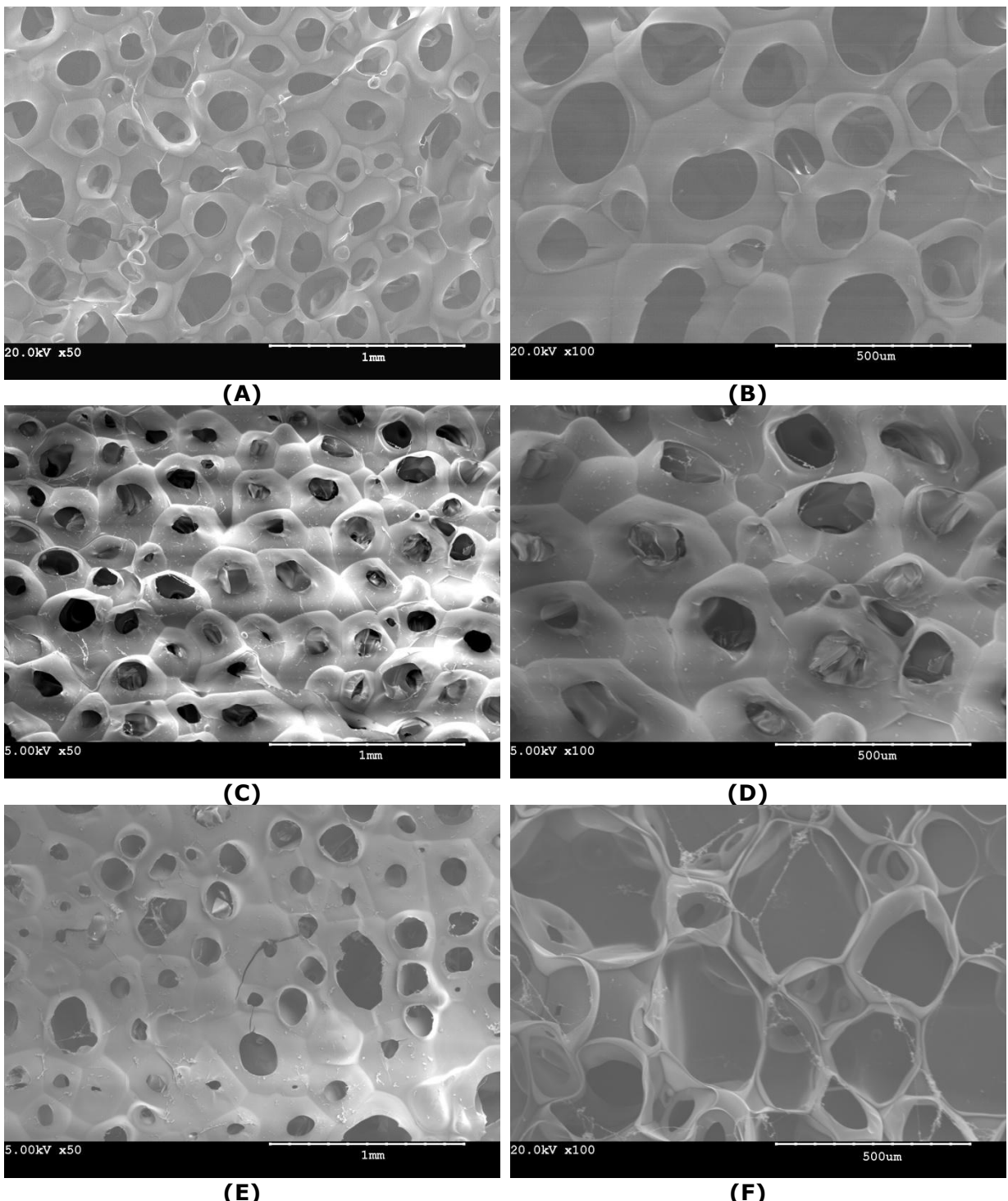


Figure 3-11: SEM images of the second generation gelatin scaffolds (prepared at pH 4.5): (A) and (B) control samples both at 50x and 100x magnifications, respectively; (C) and (D) scaffolds crosslinked with 0.50% v/v GT solution, at 50x and 100x magnifications, respectively; (E), and (F), scaffolds crosslinked with 1.00% v/v GT solution at 50x and 100x magnifications, respectively. All images are captured at 5kV acceleration voltage.

2.2.6. Scaffold Water Absorption

Figure 3-12 shows the water absorption properties of the second generation gelatin scaffolds. Crosslinking using GT noticeably reduced the ability of gelatin scaffolds to absorb water. The control sample absorbed over 1500% of its initial dry weight within 6 hours of incubation in de-ionised water, whilst crosslinked scaffolds absorbed between 370 - 460 % of their initial dry weights after 6 hours. There was no noticeable difference amongst the scaffolds crosslinked at different concentrations of GT. Reduction of water absorption ability of the scaffolds as a result of crosslinking shows a similar trend as the first generation samples (Section 1.2.6). This was caused by reduction in the number of amine groups after crosslinking which makes the samples less capable in bonding with water molecules and also more restriction after crosslinking in the intermolecular mobility which leads to less swelling and water absorption (Tasselli *et al.*, 2013; Miles and Ghelashvili, 1999). The water absorption capabilities did not show any noticeable differences in comparison with first generation of scaffolds: 408% for the second generation (crosslinked at 1.00% v/v GT), 450% for the first generation (crosslinked at 1.00% v/v GT); this is in agreement with observation made through SEM analysis and similarities in pore structure in both generations.

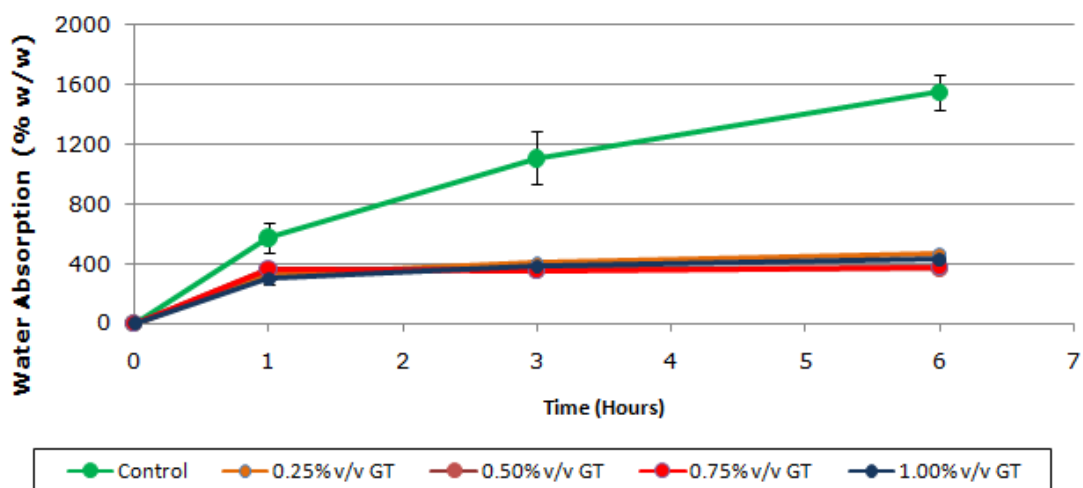


Figure 3-12: Water absorption profile of second generation gelatin scaffolds. Crosslinked scaffolds absorbed a similar mass of water and collectively were less water absorbent than the control samples.

2.3. Summary

The main objective of experiment design in the second generation was to increase the amount of gas formed in the structure and to obtain a better porous structure. Direct addition of acetic acid increased CO₂ production but after acid addition a pH adjustment was needed for an effective GT crosslinking. Increase of pH subsequently compromised the porous structure of the scaffolds. As a conclusion, it must be noted that although manual addition of acetic acid can produce more porosity, it requires a separate processing stage from GT crosslinking so that both foaming and GT reaction can proceed as efficiently as possible.

3. Third Generation Scaffold

3.1. Scaffold Preparation Method

In the second generation, decreasing of reaction pH was inhibiting the GT crosslinking. Therefore, the gas foaming procedure was modified as follows: 20% w/v gelatin solution was prepared by dissolving gelatin powder in de-ionised water using a hot plate magnetic stirrer at 60°C for 10 minutes at 600 rpm (Stuart Magnetic Stirrer, SD162, UK). Before gelatin casting, the bottom surface of the mold was covered with 0.88g sodium hydrogen carbonate with particle size of 400 μ m.

In the gas foaming method, the viscosity of gelatin solution is decisive in determining the properties of the sample. The formed bubbles in the foam tend to rise to the solution surface due to having lower density than the surrounding liquid. Gelatin solution higher viscosity prolongs the duration of this travel to surface. However the viscosity of solution cannot be increased infinitely, as such a viscous solution cannot be cast in the mold. The viscosity of the solution is a function of its temperature. Colder temperature leads to higher viscosity. Figure 3-13 shows the change of gelatin solution (10% w/v) viscosity as a function of temperature measured using Brookfield DV-III viscometer (Massachusetts, USA). The viscosity of gelatin solution began to measure at 25 cP at the highest temperature. As the temperature was reduced, the viscosity rose and eventually the solution turned into gel as temperature approached 30°C. At this point the viscosity increased rapidly. For this study, it was decided that optimum casting temperature was 33°C with a solution viscosity of 35 cP. This is the lowest temperature technically feasible for casting and the closest to gelling point of gelatin solution where the solution has the highest possible viscosity.

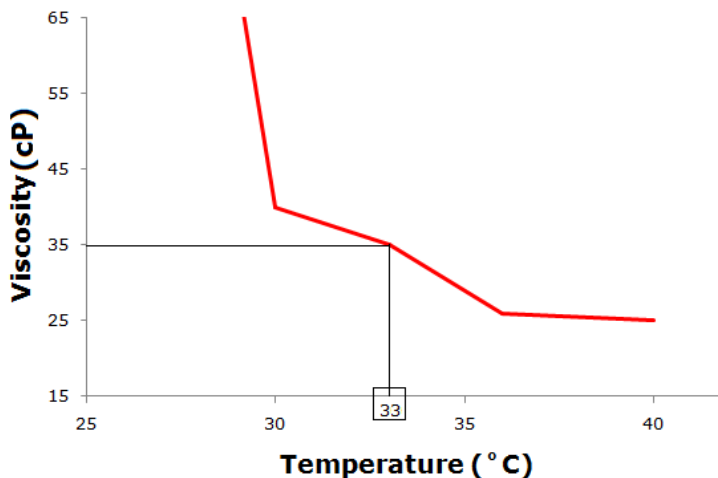


Figure 3–13: The viscosity of 10% w/v gelatin solution as a function of solution temperature.

Gelatin solution (8g) was cast in the mold containing sodium hydrogen carbonate. Shortly after casting, 0.63 ml of acetic acid was added to mold. Acetic acid reacts with carbonate salt particles to produce CO₂ gas as a byproduct (Equation 3-2). The samples froze in -25 °C freezer for 1 hour.

The frozen samples were extracted from the metallic molds and instantly plunged into 4 °C water bath for 3 hours to remove unreacted carbonate particles and acid in the scaffolds.

The gelatin scaffolds were subsequently crosslinked by incubation in 0.25, 0.50, 0.75, and 1.00 % v/v GT solutions for 3 hours. Control samples were left non-crosslinked. Samples were then washed with de-ionised water overnight (16 hours), frozen, and then lyophilised for 24 hours. Lyophilisation was performed under vacuum pressure of 0.250 mbar and temperature of -40 °C.

3.2. Results

3.2.1. Visual Description of Scaffolds

The third generation gelatin scaffold is shown in Figure 3–14. Comparing with the two previous generations, the latest generation showed an increased thickness. This increase was not due to an increase of gelatin mass as this remained constant from

previous generation. However, increased gas formation caused a relatively thicker sample in the 3rd generation. Figure 3-14-(B) shows the cross section of the scaffold with an average thickness of 12.4mm based on the average of three measurements and with the tolerance of $\pm 2.6\text{mm}$. The side of the scaffolds which was in contact with the mold was smoother than the upper surface which was in contact with air. This may be due to faster cooling rate as a result of gelatin contact with the mold sides (Boyce *et al.*, 1988; Schoof *et al.*, 2001). The top surface of the scaffold, however, was prone to have macro pores and grooves (Figure 3-14-C). These macro pores may be due to excessive gas emission as a result of NaHCO_3 decomposition, Ostwald ripening, and drainage as discussed in Section 1.2.5 (Stevenson, 2010). Ostwald ripening causes as a result of higher air pressure in smaller bubbles than larger neighbouring bubbles which drives the air transfer from former to latter. The end result of this transfer is further growing of larger bubble at the price of smaller bubbles disappearance (Britan *et al.*, 2009). The drainage is driven by gravity force generating a downward flow of liquid in the foam leading to dense layer at the bottom and high porosity at the top (Dehghani and Annabi, 2011).

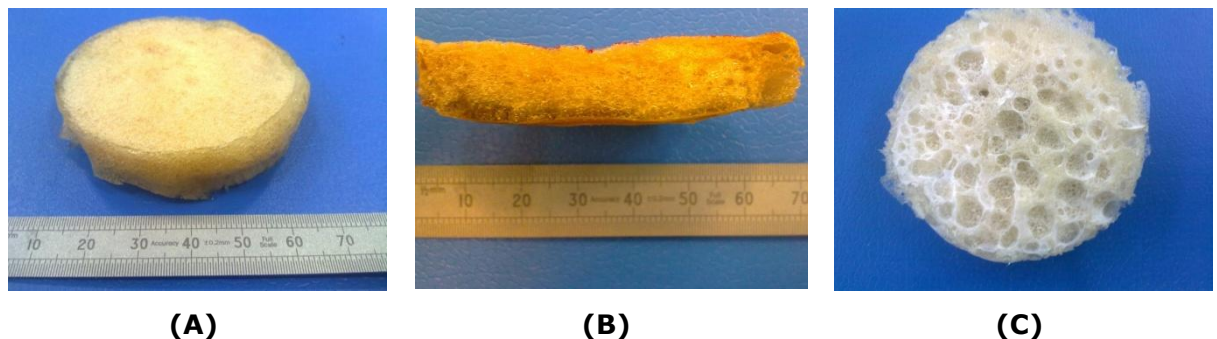


Figure 3-14: The third generation of gelatin scaffolds visual characteristics; (A) The top view of the scaffold; (B) The cross section view of the scaffold; (C) The result of excessive gas emission may have caused occasional formation of macro pores, pits, and grooves on the surface of scaffold.

3.2.2. Fourier Transform Infra-Red Spectroscopy (FT-IR)

Figure 3-15 compares the FT-IR spectra of scaffolds crosslinked with 0, 0.25, 0.50, 0.75, and 1.00% v/v GT solutions. FT-IR spectra of all 5 samples included the gelatin amide I, II, and III peaks around 1629, 1544, and 1239 cm⁻¹. Amide A and amide B bands were located in the region between 3290 and 3060 cm⁻¹, respectively (Muyonga *et al.*, 2004).

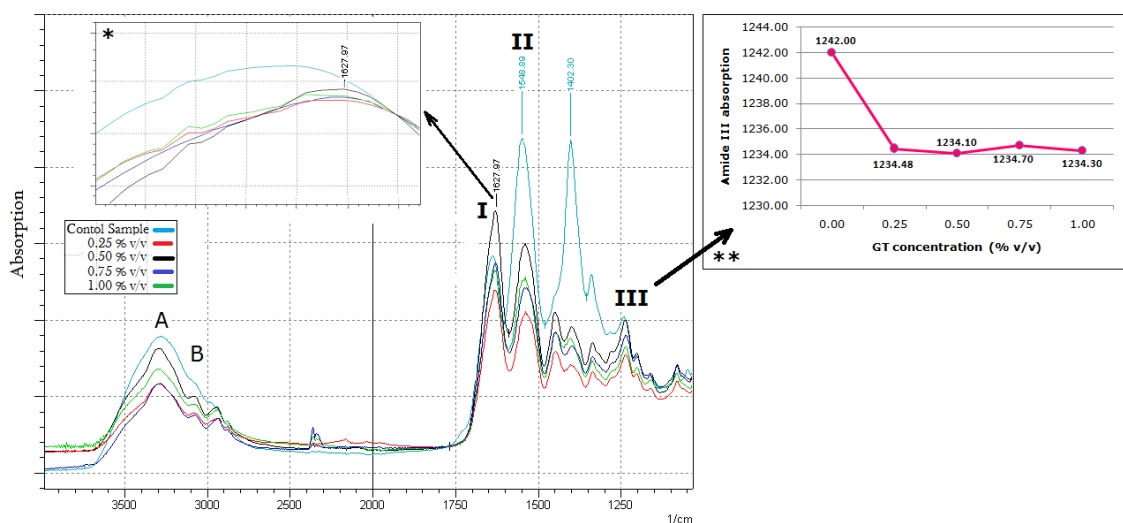


Figure 3-15: FT-IR spectra of the third generation gelatin scaffold crosslinked in 0, 0.25, 0.50, 0.75, and 1.00% v/v GT aqueous solutions. The crosslinked samples showed a slight shift towards lower wave numbers when compared with the control sample in the amide I and III bands. The inset marked by * shows the area of amide I band in higher magnification. The inset marked by ** shows the shift of amide III absorption as a function of GT concentration.

A slight shift of amide I and III peaks to a lower wave numbers in all crosslinked samples was noticeable. The amide III absorption in the scaffold shifted from 1242 cm⁻¹ in the control samples to 1234 cm⁻¹ in the scaffolds crosslinked with 1.00% v/v GT (Inset frame Figure 3-15). As it was discussed in the first generation FT-IR results, change in the amide to lower wave number peak may be indicative of a structural change in the gelatin macromolecular structure arising from GT crosslinking as discussed in the first generation FT-IR results (Payne *et al.*, 1988). One notes that, in the absence of cross-linker, there is a shoulder-like peak centred at around 3500 cm⁻¹ which corresponded to

-OH stretching band (Kanmani and Rhim, 2014). However, for the crosslinked samples it nearly disappear suggesting the -OH group may have been involved in the reaction with GT. As discussed in Chapter 1, Section 7.1, as an alternative mechanism of GT reaction with gelatin, in acidic pH's aldehyde groups react with hydroxyl groups of gelatin (Farris *et al.*, 2010). Figure 3–15 shows that in this set of samples this reaction may have been part of crosslinking process.

3.2.3. Mechanical Properties of the Scaffolds

Table 3–6 lists the tensile properties of 3rd generation gelatin scaffolds. The tensile strength of the scaffolds significantly increased with GT concentration up to 0.50% v/v GT solution ($p \leq 0.05$). Crosslinking with concentrations above 0.50% v/v caused the tensile strength to decrease. However this reduction was proved to be statistically not significant ($p \geq 0.05$). An arrest of increase in tensile strength upon further increase of GT above 0.50% v/v may have the root causes such as over-crosslinking and excessive brittleness of polymeric structure at relatively high GT concentration as explained for the first generation in Section 1.2.3 (Knau et al., 1999; Price, 1986; Wu *et al.*, 2010).

Table 3–6: Tensile properties of the third generation gelatin scaffolds. The tensile strain of the scaffolds was reduced as a result of crosslinking. The strength of scaffolds reached a maximum at 0.50% v/v GT and was reduced upon further increase of GT concentration.

GT Concentration (% v/v)	Tensile Strength (kPa)	Young's Modulus (kPa)	Tensile Strain (%)
0 (Control)	1.09 (± 0.3)	0.94 (± 0.0)	53.43 (± 15)
0.25	4.1 (± 0.6)	2.7 (± 0.0)	231.2 (± 38)
0.50	5.4 (± 1.9)	12.2 (± 0.0)	158.9 (± 50)
0.75	4.3 (± 0.9)	13.1 (± 0.0)	102.8 (± 38)
1.00	3.8 (± 0.6)	8.0 (± 0.0)	39.6 (± 14)

Tensile strength of 3rd generation scaffolds is significantly lower than its predecessors ($p \leq 0.05$). Nussinovitch *et al.*, (1992) reported drastic decrease in the strength of porous structure prepared through gas foaming method in comparison with non-porous control samples. These researchers attributed such a reduction to local rupture and pores growth which act as sites of failure propagation (Nussinovitch, 1992). Porosity can exacerbate the negative impact of over-crosslinking on gelatin structure. Recently Sarem *et al.*, (2013) reported a similar declining trend in the mechanical strength of a porous gelatin scaffold after increased crosslinking. It was proposed that two inter-competing factors may determine the structural strength of the crosslinked porous structure: pore size and crosslinker concentration. At low concentrations, the crosslinker is the dominating element in determining the structural integrity of the scaffold, however as the concentration increases the impact of increasing pore size becomes the dominating factor in reducing the structural strength (Sarem *et al.*, 2013). Since the 3rd generation scaffolds had an increased porosity therefore its impact was more pronounced than in the previous generations.

There was a significant difference between the Young's modulus of non-crosslinked samples and crosslinked samples up to a GT concentration of 0.50% v/v ($p \leq 0.05$). Similar to the tensile strength, the changes in the Young's modulus values were not statistically significant above 0.50% v/v GT ($p \geq 0.05$). In comparison with first and second generations of the scaffolds, third generation showed lower Young's modulus. This difference in the Young's modulus values can be explained easier in the context of tensile strain.

Crosslinking reduced the tensile strain of the gelatin scaffolds (Table 3-6). In comparison with control sample, this decrease of tensile strain in crosslinked scaffolds was significant for the scaffolds crosslinked with GT concentrations above 0.25% ($p \leq 0.05$). In comparison with previous generation current scaffolds were noticeably more plastic and stretched longer. Whilst minimum tensile strain for the first and second generation scaffolds was 20%, the minimum tensile strain for the third generation was

136%. As mentioned in Section 1.2.3, the mechanical properties of the collagen-derived materials such as gelatin have high sensitivity to humidity (Meyer, *et al.*, 2010, Klüver and Meyer, 2014). Higher tensile strain can be explained in the context of higher water absorption. Water molecules, due to their low molecular weight and the ability to disrupt the hydrogen bonds between gelatin molecules, act as a plasticiser for gelatin molecules (Díaz *et al.*, 2011; Patil *et al.*, 2000). Larger number of pores in the third generation may have caused more empty volume available for water absorption. This consequently can cause the ability of the scaffold to deform more plastically which reflected in high tensile strain and low Young's Modulus of the scaffolds.

3.2.4. Scaffolds Thermal Analysis

Table 3–7 lists the thermal characteristics of control and crosslinked scaffolds at various concentrations of GT. The control samples showed the denaturation temperature of 44 °C. The denaturation temperature values for the crosslinked samples were between 73.5 - 77.9 °C. This is similar to what was seen in response of previous generations to crosslinking. The negative values of enthalpy of transition (ΔH) decreased as crosslinking concentration increased. Enthalpy of transition (which is significantly lower in gelatin with respect to collagen (Bigi *et al.*, 2002)) represents the energy necessary to transform the re-natured gelatin helix to random coil by breaking hydrogen bonds between gelatin strands (Achet and He, 1995). Reduction in the negative value of enthalpy is caused by a reduction in the number of hydrogen bonds in favour of increase in the number of covalent bonds as a result of crosslinking (De Carvalho and Grosso, 2004; Achet and He, 1995; Dardelle *et al.*, 2011). From -14.2 J.g^{-1} in the control samples, the normalised enthalpy of transition was shifted to -9.7 J.g^{-1} in the scaffolds crosslinked with 1 % v/v GT solution. Thermal analysis results confirmed chemical crosslinking of gelatin scaffolds prepared in this study.

Table 3-7: Thermal analysis of the third generation gelatin scaffolds crosslinked at different concentrations of GT.

GT concentration (% v/v)	Denaturation Temperature (T_d) (°C)	Enthalpy of Transition (ΔH) (J.g ⁻¹)
0 (Control)	44.0 (± 1.3)	-14.2 (± 1.2)
0.25	77.5 (± 0.3)	-13.7 (± 0.2)
0.50	73.5 (± 1.8)	-12.0 (± 0.3)
0.75	77.9 (± 0.7)	-10.6 (± 0.9)
1.00	76.3 (± 1.9)	-9.7 (± 0.8)

3.2.5. Scaffolds Microstructure Analysis

Figure 3-16 (A-F) displays the SEM images of the control samples and scaffolds crosslinked with 0.50 and 1.00% v/v GT solution. Varying the GT concentration affected both the pore size and textural structure of the scaffolds. In general, the control samples showed a flat and smoother surface as compared with both of the crosslinked scaffolds shown in Figure 3-16. The structure in the control samples appeared to have collapsed with less pore interconnectivity, whilst the crosslinked structures showed more pore interconnectivity. As shown in Figure 3-16-(B), the pores in the control samples showed signs of distortion which may be due to lack of mechanical strength.

Average pore size in scaffolds crosslinked using 0.50% v/v GT solution (Figure 3-16-(C) and (D)) was 280µm. Scaffolds crosslinked with 1.00% v/v GT showed more interconnectivity when compared with the flat structure of the control scaffolds (Figure 3-16-(A) and (B)). The average pore size in 1.00% v/v GT crosslinked scaffolds was 550µm. Increase of pore size with increase of GT concentration was a trend seen in the previous generations as well. Crosslinking with GT appears to be responsible for the stable porous microstructure and may have led to a more effective crosslinking, as explained for the previous generations.

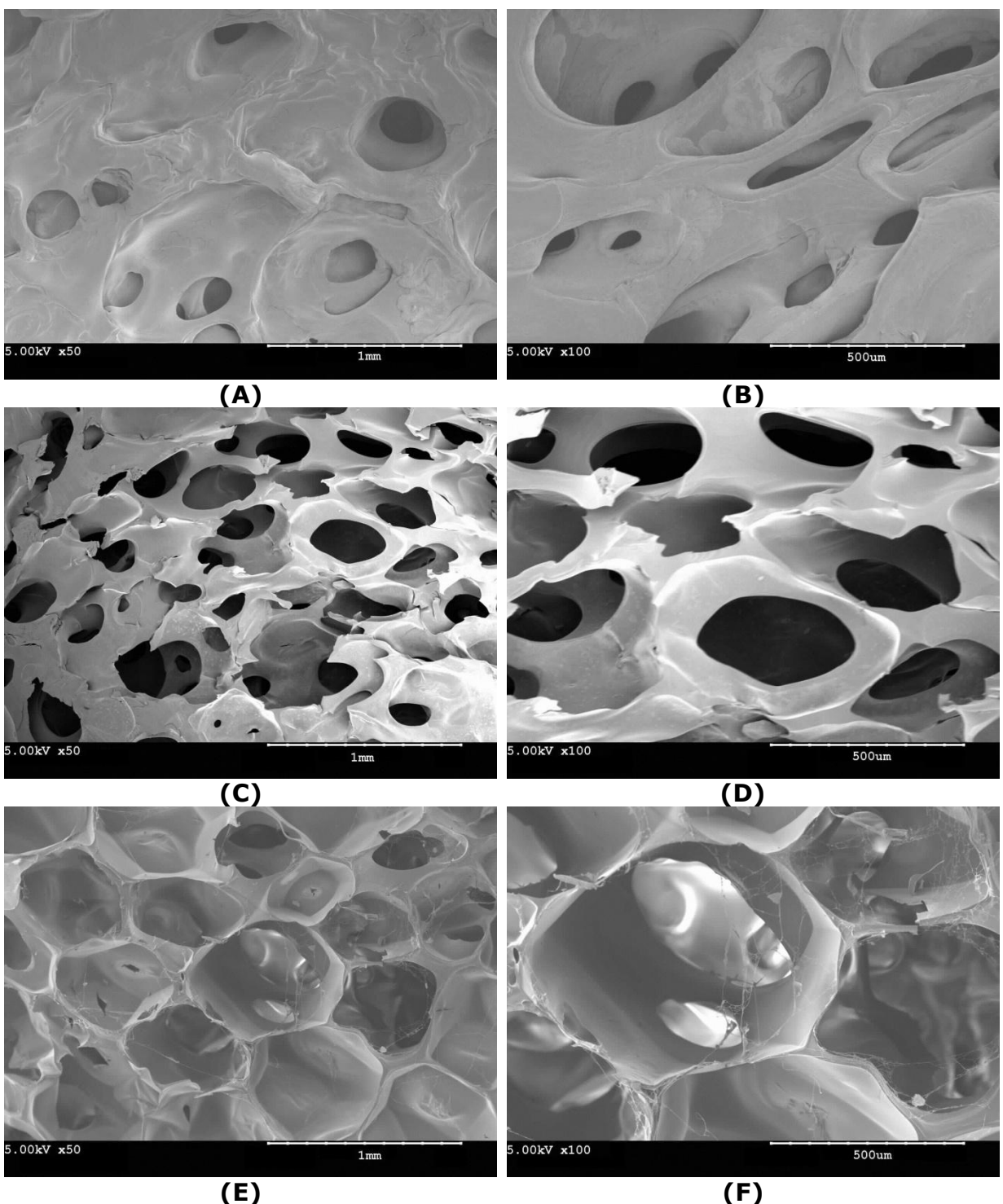


Figure 3-16: SEM images taken from the third generation of gelatin scaffolds, (A) and (B) control samples both at 50x and 100x magnifications, respectively; (C) and (D) scaffolds crosslinked with 0.50% v/v GT solution, at 50x and 100x magnifications, respectively; (E) and (F), scaffolds crosslinked with 1.00% v/v GT solution at 50x and 100x magnifications, respectively. The images are obtained at 5kV acceleration voltage.

Current generation showed higher average pore size than the previous ones. This difference was the biggest for the scaffolds crosslinked with 1.00% v/v GT. Whilst the previous generations of scaffolds had the average pore size of 280 μ m at this crosslinking concentration, current generation showed the average pore size of 550 μ m. Larger pore size may be one of the main reasons behind the relatively low mechanical strength of the third generation scaffold in comparison with its predecessors.

Irregularity was noticeable amongst the prepared scaffolds. Such an irregularity is mostly inherent part of the gas foaming method. Complex events that occur at the interface of gas-liquid during foaming process may make the foaming process highly unpredictable and complex (Stevenson, 2010). This complexity in turn makes control of pore size within structure more difficult.

3.2.6. Scaffold Water Absorption

Figure 3-17 displays water absorption properties of the crosslinked scaffolds compared with the control samples. All prepared scaffolds reached water saturation level within the first one hour of the experiment. Increase of GT concentration reduced water absorption capability of the scaffolds. In comparison with other two generations of scaffold, the structure showed a higher capacity in absorbing water. Whilst the previous generation absorbed between 400 to 500% of their initial dry weight after 6 hours of immersion in water, current generation absorbed more than 1000% of their initial dry weight after 1 hour. This may be due to a larger number of pores and porosity within the structure that increased the available space for water storage within the structure (Miles *et al.*, 2005).

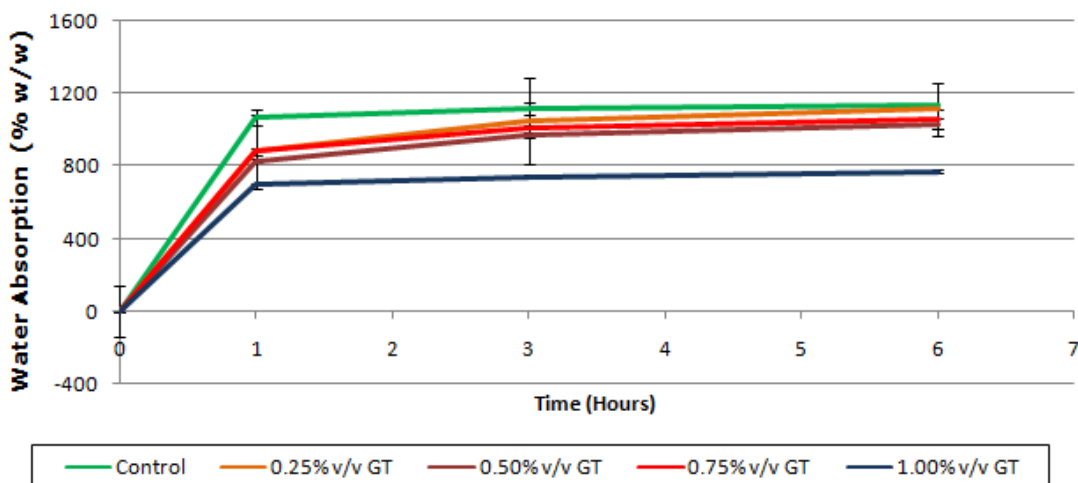


Figure 3-17: Water absorption properties of the third generation scaffolds. Absorption of the scaffold was reduced as the GT concentration increased. The third generation scaffolds showed higher water absorption in comparison with two earlier generations.

3.3. Summary

This generation of scaffolds showed an increased porosity and larger pore structure when compared with the previous two generations (Section 3.2.5). The modifications made to the synthesis procedure, such as direct addition of acetic acid and carbonate to the casting mold instead of GT solution, produced a larger emission of CO₂ gas within the gelatin solution (Section 3.1). Average pore size of the scaffold was noticeably increased in comparison with the two previous generations of scaffolds. A more porous structure of the scaffold directly affected its water absorption ability. Together, larger pores and higher water content influence the tensile strength of the scaffold. Based on SEM analysis, it was shown that crosslinking was crucial for having a stable porous structure and preventing pores collapse. Crosslinking, however, failed to improve the mechanical strength of the scaffold as compared with the two previous generations (Section 3.2.3). Tensile strength of the scaffold changed as a function of GT concentration with a pattern similar to the previous generations; tensile strength increased and then decreased upon further increase of the GT concentration. Crosslinking of the samples using GT lowered the scaffolds tensile strength above 0.50%

v/v of GT concentration. Even at its peak, the tensile strength values achieved by third generation were significantly weaker in comparison with its predecessor.

To summarise, although the third generation of scaffold showed better porous structure, the high levels of released CO₂ and the produced porosity reduced the mechanical integrity of the structure. Hence, it was necessary to implement some modifications to control the gas emission and consequently reduce the scaffold pore size and improve mechanical integrity of the structure.

4. Fourth Generation Scaffold

4.1. Scaffolds Preparation Method

During preparation of the previous generation scaffolds, more CO₂ emission was achieved but this achievement indirectly led to two following disadvantages:

- Excessive thickness of the scaffolds which impaired ease of use of a wound dressing by interfering with patient daily life activities.
- Increased CO₂ release led to increased pore size, above optimal size required for skin tissue engineering purpose (125µm for adult mammalian skin (Dehghani and Annabi, 2011)). This in turn led to low mechanical strength.

To lower the rate of CO₂ emission, the following modifications were implemented in the gas foaming procedure. Gelatin solution (20% w/v) was prepared by dissolving the appropriate mass of gelatin powder in de-ionised water. A hot plate containing a magnetic stirrer was used to stir the mixture until complete dissolution. As discussed for the 3rd generation, having optimum viscosity and solution temperature is crucial for obtaining desirable gelatin foam. To prepare the condition for the ideal foaming following sequence of sample treatment was executed:

1. Gelatin mixture with de-ionised water was carried out at 33°C;
2. The temperature of the mixture was increased to 60°C at the heating rate of 5.4 degree.min⁻¹ whilst stirring was carried out at 200 rpm (Stuart Magnetic Stirrer, SD162, UK);
3. At 60°C the gelatin mixture was stirred for a further 5 minutes at 600 rpm;
4. The solution temperature was reduced to 33°C at the cooling rate of 2.07 degree.min⁻¹. The foaming was performed immediately after the temperature reached to 33°C. This temperature was chosen based on the viscosity measurements described in Figure 3-13.

Foaming was carried out by addition of NaHCO₃ (0.32g) to every 16 ml of gelatin solution. Shortly thereafter carbonate addition, 360 µl of acetic acid was added to

the solution, as a result turned gelatin solution into foam (Equation 3-2). This gelatin solution (8g) was cast in a petri dish with 5.5cm in diameter and 0.7cm in height. The foam was frozen in a -25°C freezer for 1 hour. Frozen samples were extracted from the petri dishes and plunged in de-ionised water for 1 hour to extract unreacted acetic acids and carbonate and to ensure neutral pH for the optimised crosslinking. The scaffolds were then incubated in GT aqueous solution with four various concentrations ranging from 0 to 1% v/v GT at 0.25 increments for 3 hours. A set of non-crosslinked samples were prepared as control. The samples were washed in de-ionised water overnight (16 hours) to remove unreacted GT. The samples were frozen and then lyophilised for 24 hours. Lyophilisation was performed under vacuum pressure of 0.250 mbar and temperature of -40°C. Figure 3-18 shows a comparison of sample preparation methods presented in this Chapter. The addition of acid to the synthesis protocol was introduced in the second generation to improve foaming. In the third generation, the acid addition stage was separated from crosslinking to improve GT efficiency. In the fourth generation, to prevent excessive foaming the acid addition was executed before casting of gelatin in the molds.

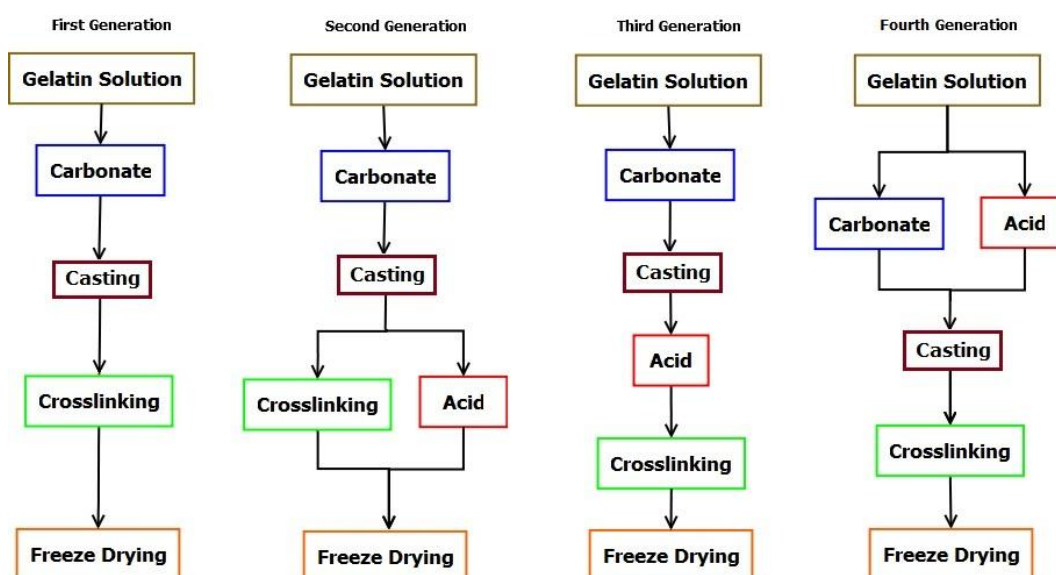


Figure 3-18: A comparison of sample preparation methods for each of four scaffold generations. The acid addition in the second generation and the point at which this addition would be done was refined at each consecutive generation.

4.2. Results

4.2.1. Visual Description of Scaffolds

Figure 3-19 (A-B) shows the visual characteristics of the fourth generation gelatin scaffolds. The samples showed a more compact structure with sharper edges. In comparison with its predecessor, the top surface of the scaffold is uniform and did not show ridges. In this generation good film forming ability of gelatin (Alves *et al.*, 2011) was better demonstrated as the edges of gelatin scaffold replicated the outer contour of petri dish in the form of circular rims on the edges (Figure 3-19-A). The cross section of the scaffolds is shown in Figure 3-19-(B). The scaffold thickness was 5mm based on the average of 3 measurements with ± 0.4 tolerance. The scaffold inner texture appeared to be compact and with porosity distribution that cannot be noticed at this magnification and would be discussed in detail in SEM analysis Section.



Figure 3-19: The visual features of the fourth generation gelatin scaffolds; (A) the rear view of gelatin scaffold, (B) The cross section of prepared scaffolds. The scaffolds inner texture appeared to be compact with uniform thickness.

4.2.2. Fourier Transform Infra-Red Spectroscopy (FT-IR)

Figure 3-20 shows the comparison amongst the FT-IR spectra of the fourth generation scaffold crosslinked at different GT concentrations. All spectra showed the fingerprint absorption regions of the gelatin FT-IR spectra. This includes amide I, II, and III at 1633, 1540, and 1238 cm^{-1} , respectively. The amide A and B absorptions are

evident at 3400 and 3050 cm^{-1} , respectively. The detail discussion regarding the origins of these absorptions is presented in Section 1.2.2.

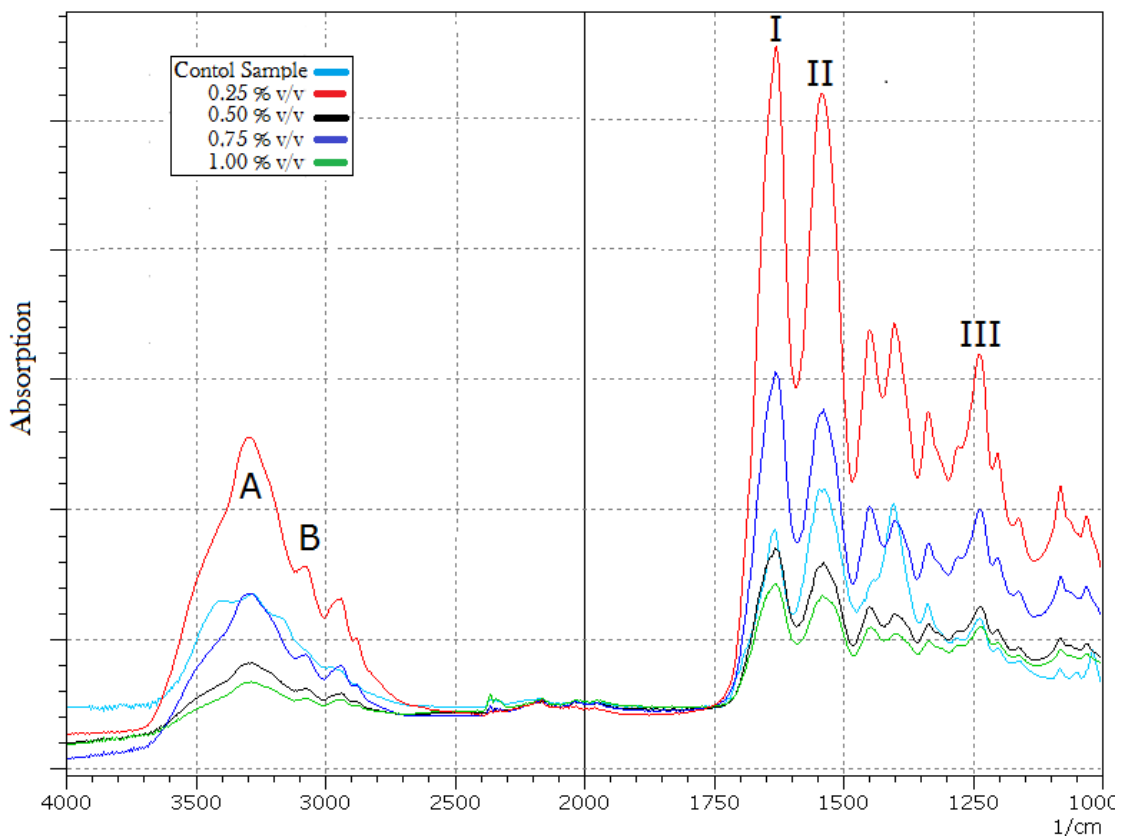


Figure 3–20: The FT-IR spectra of the fourth generation gelatin scaffolds. Amide I, II, III, and A & B are marked in the Figure.

Similar to previous generation, the shoulder-like peak close to 3500 cm^{-1} which corresponded -OH stretching band (Kanmani and Rhim, 2014) appeared for the control samples but in the crosslinked samples it nearly disappeared suggesting reaction of aldehyde functional group with hydroxyl groups in acidic pH's was part of crosslinking process (Farris *et al.*, 2010).

Regarding amide I, II, and III, the 4th generation scaffolds showed similar FT-IR spectra to its previous predecessors. In fact, the FT-IR spectra of the all 4 generations of the scaffolds that are presented in this Chapter showed values that were falling in the similar range. Figure 3–21 makes a side by side comparison amongst amide I, II, and III

absorptions of gelatin in different generations of scaffolds. The pattern in the change of the absorption bands of Amide I was similar in 4 generations. The amide bands absorption shifted towards smaller lower wave number as results of crosslinking. However the degree of difference in the absorption changes was not high enough for drawing a definitive conclusion from them.

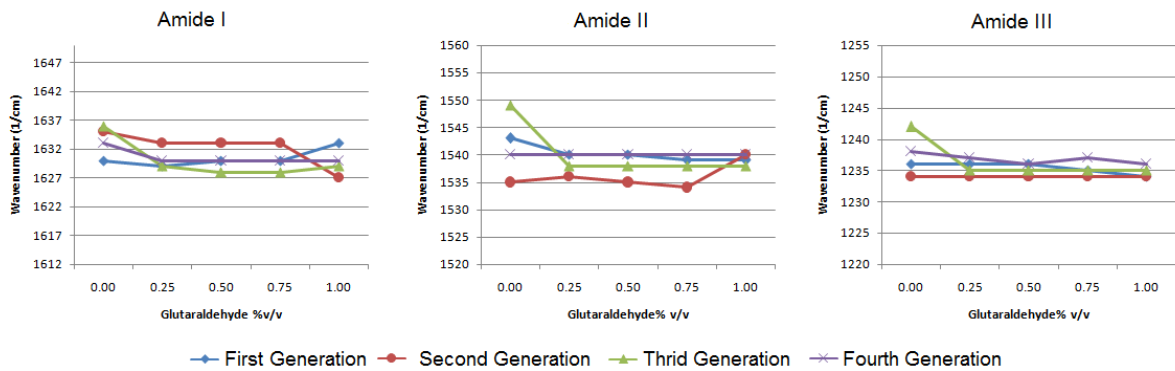


Figure 3-21: A side by side comparison between amide I, II, and III bands of 4 different generations of gelatin scaffolds.

4.2.3. Mechanical Properties of the Scaffolds

Table 3-8 lists the tensile properties of the scaffolds crosslinked at different concentrations of GT. In comparison with the control samples, crosslinking the scaffolds with 0.50% v/v GT solution significantly increased the tensile strength of the scaffolds ($p \leq 0.05$). The increase of tensile strength for the scaffolds crosslinked at lower concentrations (0.25% v/v) was not significant comparing with control samples ($p \geq 0.05$). As the concentration of the GT increased to 1.00% v/v, the tensile strength of the scaffolds decreased significantly in comparison with the control samples ($p \leq 0.05$). The justification behind increase and then decrease of tensile strength as result of mounting GT concentrations can be attributed to over-crosslinking and excessive fragility of structure at high GT concentrations as discussed in Section 1.2.3 (Price, 1986; Wu *et al.*, 2010).

The Young's modulus of the scaffolds increased as a result of crosslinking in comparison with the control samples. The scaffolds crosslinked with 1% v/v GT had the highest Young's modulus which was significantly higher than the control samples ($p \leq 0.05$). The tensile strain of the scaffolds decreased significantly as a result of crosslinking. The control samples showed elongation as high as 114.8% whilst the scaffold crosslinked with 1.00% v/v GT showed the lowest value of elongation at 17.9%. This amount was significantly lower than the control samples ($p \leq 0.05$). The reduction of tensile strain as result of crosslinking is attributed to establishment of covalent bonds and restriction in mobility of gelatin molecules as discussed in Section 1.2.3 (Martucci *et al.*, 2006).

Table 3–8: Tensile strength, Young's modulus, and strain of the fourth generation gelatin scaffolds.

GT Concentration (% v/v)	Tensile Strength (kPa)	Young's Modulus (kPa)	Tensile Strain (%)
0 (Control)	80.76 (± 4)	0.84 (± 0.1)	114.83 (± 9)
0.25	100.10 (± 13)	2.09 (± 0.1)	38.57 (± 1)
0.50	239.48 (± 70)	2.44 (± 0.4)	30.23 (± 5)
0.75	59.22 (± 14)	1.80 (± 0.1)	30.02 (± 0.4)
1	15.46 (± 5)	4.07 (± 1.3)	17.88 (± 5)

Figure 3–22 shows a comparison amongst all of the four generation scaffolds that are reported in this Chapter. According to Figure 3–22-(A), the 3rd generation relatively showed the lowest tensile strength whilst the first generation showed the highest, which may be the direct result of relative pore size distributions in each of these generations, respectively. The modification in preparation methods managed to improve the fourth generation scaffolds tensile strength from its previous precedent. Whilst the tensile strength of the 3rd generation scaffolds (at all tested concentrations of GT) did not exceed 10 kPa, the minimum value for tensile strength for the fourth generation gelatin scaffolds was 15.5 kPa.

The latest generation of scaffolds showed a mechanical behaviour more similar to the first and second generations scaffolds that were discussed at the beginning of this Chapter. Figure 3-22-(C) shows that the 3rd generation had the highest tensile strain which may be the result of higher water content in these samples and since water acts as a plasticiser in gelatin structure (Díaz *et al.*, 2011). This is in agreement with the reported sensitivity of collagen-derived compounds such as gelatin to humidity (Meyer, *et al.*, 2010, Klüver and Meyer, 2014).

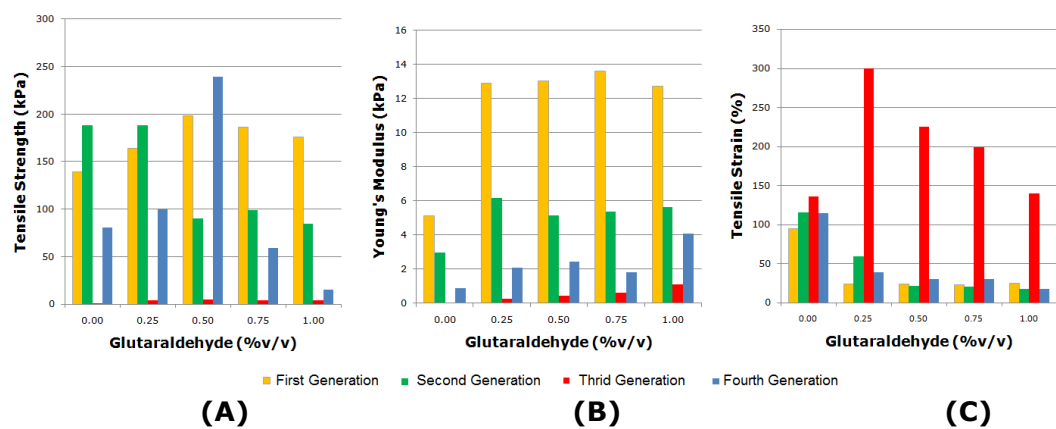


Figure 3-22: A comparison of mechanical properties of different generations of gelatin scaffolds:
 (A) Tensile Strength, (B) Young's Modulus, (C) Tensile Strain.

4.2.4. Scaffolds Thermal Analysis

Table 3-9 lists the thermal characteristics of the fourth generation gelatin scaffolds at different GT concentrations. The denaturation temperature of the scaffolds increased as the GT concentration increased from 0 to 1.00% v/v GT. As a result of crosslinking the denaturation temperature increased from 48 °C in the control samples to the values higher than 80 °C in the crosslinked scaffolds. Similar to what was seen for previous generations, the enthalpy of transition was reduced as a result of crosslinking. The enthalpy of transition in the scaffolds was reduced from -25.7 J.g⁻¹ in the control samples to -12.3 J.g⁻¹ in the scaffolds crosslinked with 1.00% v/v GT. As discussed earlier, formation of covalent bonds during crosslinking and restriction of intra molecular mobility are responsible for the increase of denaturation temperature (Martucci *et al.*, 2006; Usha and Ramasami, 2000). Detail discussion about the thermodynamic principles

of crosslinking and its impact on thermal stability of the samples is provided in Section 1.2.4 of this Chapter.

Table 3–9: Thermal characteristics of the fourth generation gelatin scaffolds.

GT concentration (% V/V)	Denaturation Temperature (T_d) (°C)	Enthalpy of Transition (ΔH) (J.g ⁻¹)
0.00 (Control)	48.1 (± 6.9)	-25.7 (± 16.7)
0.25	82.0 (± 3.5)	-16.4 (± 0.4)
0.50	84.5 (± 1.5)	-16.3 (± 0.9)
0.75	86.2 (± 1.6)	-13.2 (± 3.2)
1.00	83.8 (± 1.4)	-12.3 (± 1.8)

Figure 3–23 further compares the thermal characteristics of all gelatin scaffolds presented in this Chapter. Regardless of the scaffolds generation, the denaturation temperature increased as a result of crosslinking. Similarly the enthalpy of transition approach toward lower negative values as a result of crosslinking in all samples.

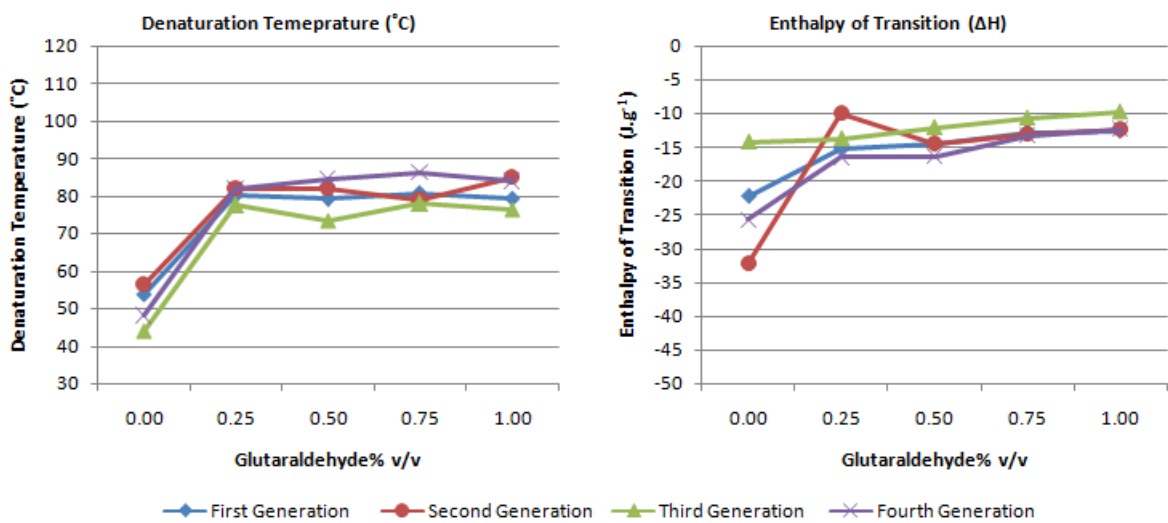


Figure 3–23: Comparison amongst the thermal characteristics of different generations of gelatin scaffolds crosslinked with a range of GT concentrations from 0 to 1.00% v/v. As a result of crosslinking the denaturation temperature increased and the negative values of enthalpy of transition was decreased.

4.2.5. Scaffolds Microstructure Analysis

Figure 3-24 shows the surface morphology of the fourth generation gelatin scaffolds. The porosity recorded in this set of Figures was similar to the 3rd generation scaffolds with round, spherical and inter-connected pores distributed throughout the structure. The control sample portrayed a lower mechanical integrity and more elastic nature, as it appeared to be deformed during the scaffold sectioning (Figure 3-24-B). Gradual increase of the pore size as the GT concentration increased was seen in the fourth generation scaffolds. The average pore size in the control samples was 180 μm whilst the average pore size for the scaffolds crosslinked in 0.50 and 1.00% v/v GT solutions were 226 and 306 μm , respectively.

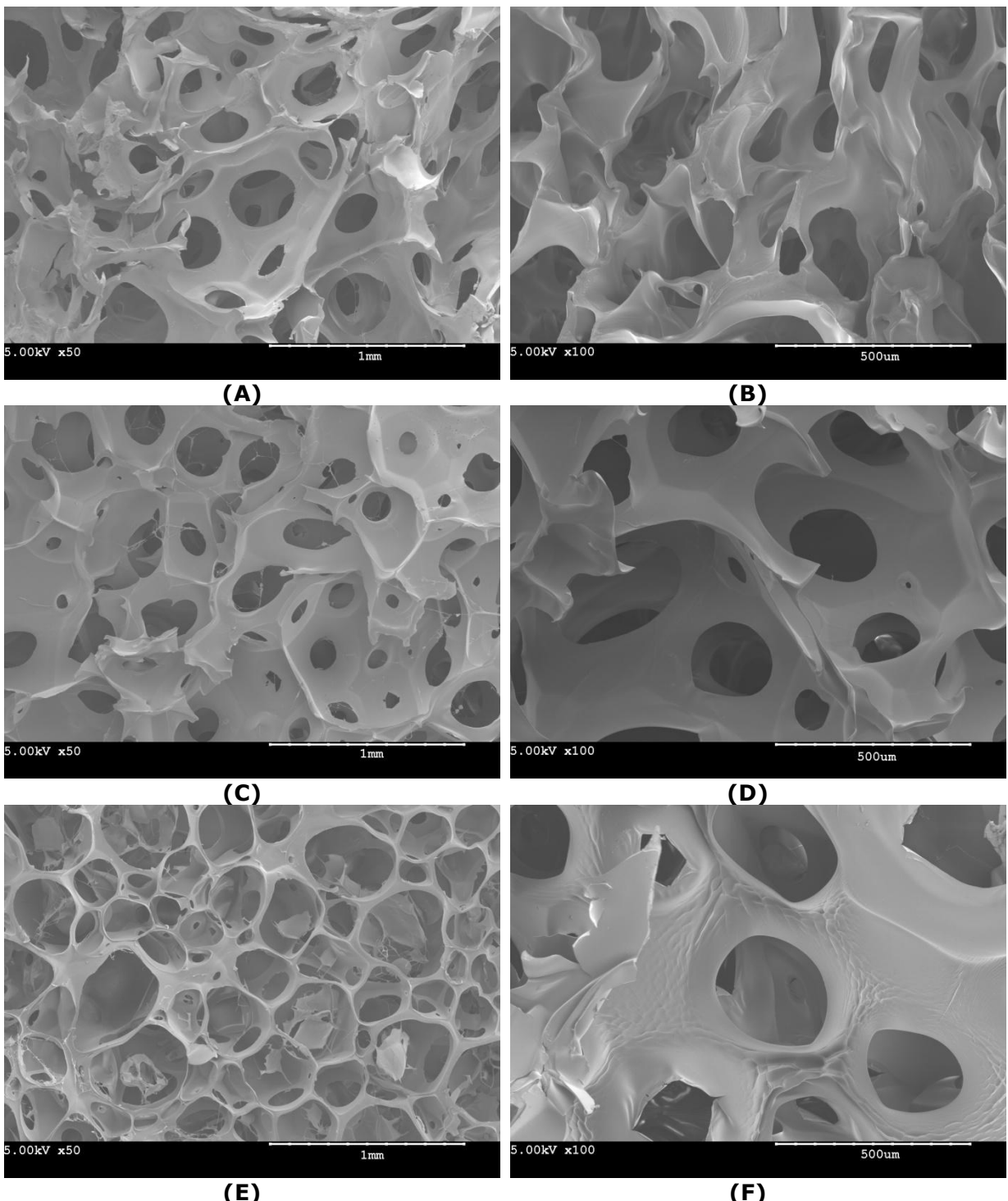


Figure 3-24: SEM images taken from fourth generation gelatin scaffolds: (A) and (B) control samples, at 50x and 100x magnifications, respectively; (C) and (D) scaffolds crosslinked with 0.50% v/v GT solution, at 50x and 100x magnifications, respectively; (E) and (F), scaffolds crosslinked with 1.00% v/v GT solution at 50x and 100x magnifications, respectively. The images are obtained at 5kV acceleration voltage.

Figure 3–25 further compares all four generations of gelatin scaffolds pore sizes. The fourth generation scaffold average pore size showed a reduction in comparison with the previous generation. This reduction is more noticeable at 1% v/v GT concentration. For successful tissue engineering application, the optimum porosity size in the scaffold depends on the type of cell tissue that would grow on it. For the skin cells growth, the optimum scaffold pore size is reported to be between 20 to 125 μm (Dehghani and Annabi, 2011). Although the average pore size of none of the presented samples in this chapter did not include this range, the modification in the synthesis method of fourth generation scaffolds managed to reduce the average pore size values from its predecessor. The pore size distribution shown in the fourth generation of scaffold was similar to the average pore size shown in the first and second generation scaffolds. This similarity may be the reason for the improvement of the scaffold tensile strength in comparison with the third generation. These results suggest that there may be a correlation between pore size of the scaffold and the mechanical strength of structure.

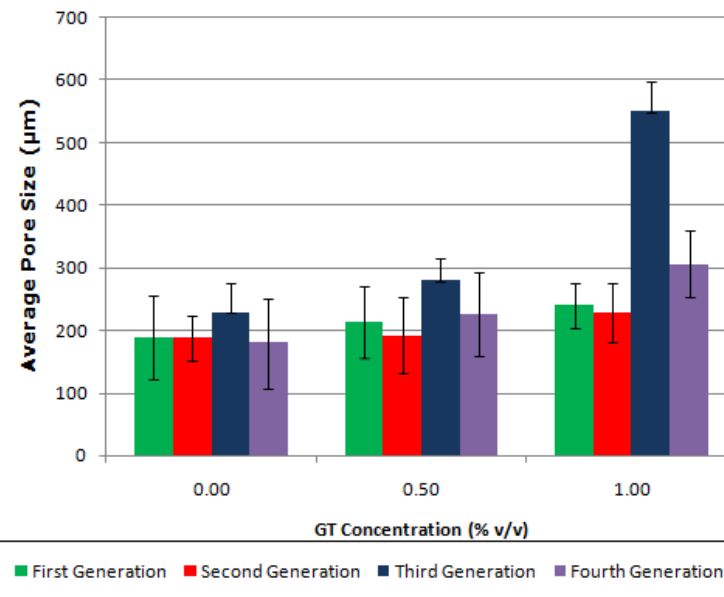


Figure 3–25: The comparison between the average pore size distribution for various generations of gelatin scaffolds.

4.2.6. Scaffold Water Absorption

Figure 3–26 displays the water absorption characteristics of fourth generation gelatin scaffolds. Similar to the previous observations in this Chapter, the ability of scaffolds to absorb water was reduced as the concentration of GT increased. The water absorption ability of the control scaffold reduced from 1900% of dry weight after 6 hours immersion to 537% for the scaffolds crosslinked with 1.00% v/v GT. As discussed in Section 1.2.6, reduction of water absorption ability after crosslinking may be due to reduction in the number of available amine groups for bonding with water molecules (Knaul *et al.*, 1999) or due to further restrictions in the expansion of gelatin molecules and less swelling in water as a result of covalent bonds formation (Tasselli *et al.*, 2013).

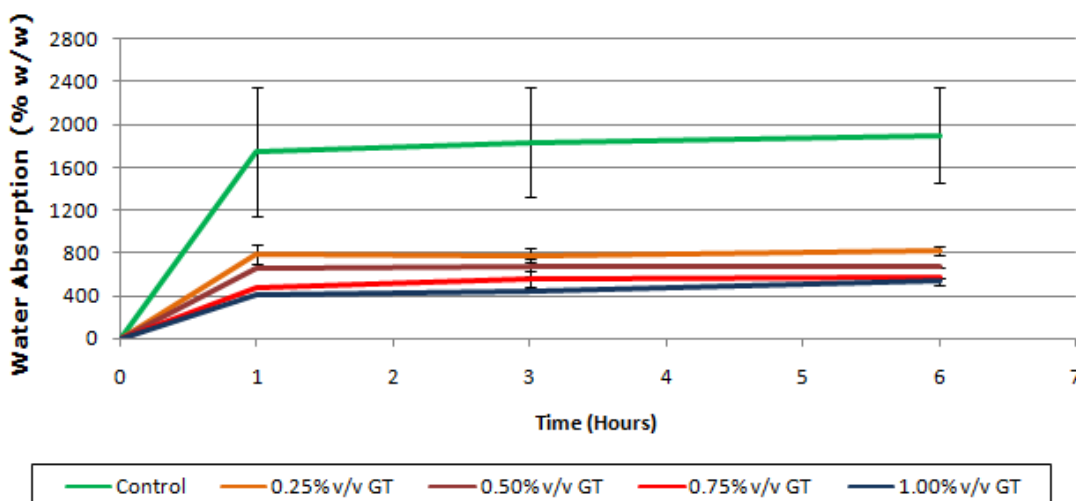


Figure 3–26: The water absorption characteristics of fourth generation gelatin scaffolds.

Figure 3–27 shows how much water each generation of gelatin scaffolds absorbed after 6 hours incubation in de-ionised water. Regardless of method of preparation, the water absorption capacity of the scaffolds decreased as the crosslinking occurred. The first and second generations scaffolds showed the lowest water absorption capacity and the third generation showed the highest. As discussed in the previous section, the third generation scaffold showed the higher porosity amongst presented results in this Chapter and Figure 3–27 shows the relation that exists between the degree of porosity and the ability of structure in absorbing water.

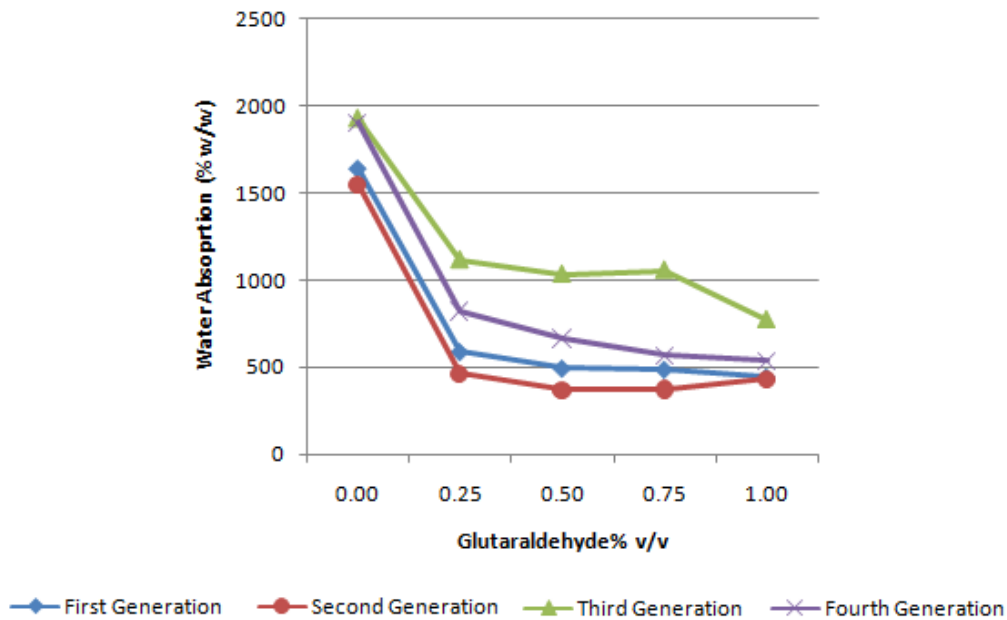


Figure 3-27: Comparison of water absorption capability of four generations of gelatin scaffolds. Crosslinking reduced the water absorption capacity of the scaffolds regardless of scaffolds preparation method.

4.2.7. In-Vitro Biodegradation Analysis

In this study, the gelatin scaffold will come into direct contact with the chronic wound environment and thus it was important to assess their biodegradation rate against collagenase (one of the main digestive enzymes in chronic wounds (Gorgieva and Kokol, 2011)). Figure 3-28 shows the results of biodegradation analysis performed on the gelatin scaffolds at 2 different concentrations of collagenase as compared with the set of control samples incubated in de-ionised water. Crosslinking samples with GT was enough to stabilise gelatin scaffolds in de-ionised water at 37°C without any enzyme presence. However, upon addition of enzyme to the solution, there was a meaningful difference between different concentrations of GT. At collagenase concentration of 2.5 mg/ml, the degradation rate of samples crosslinked with 0.25% v/v GT was 39.5%. Increase of GT concentration above this value improved the stability of crosslinked scaffolds close to nil degradation level. At the highest concentration of collagenase (5mg/ml), 91% of initial mass of scaffolds crosslinked at 0.25% v/v GT was degraded and only the scaffolds crosslinked with 1% v/v GT showed the degradation rate less than

30% of initial mass. Higher crosslink density of the scaffolds at more concentrated solutions of GT is reported to cause lower degradation rate (Sung *et al.*, 1997a). Complete degradation of control sample shows the indispensable necessity of chemical crosslinking to increase *in-vivo* stabilisation of structure.

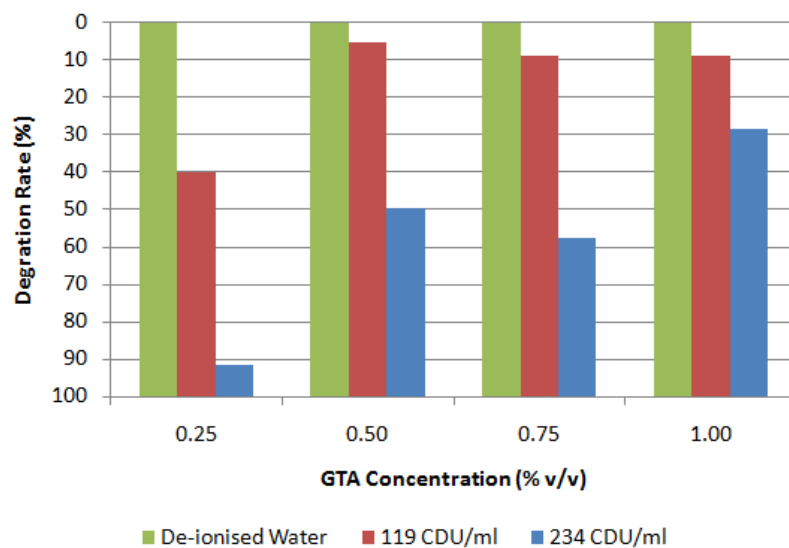


Figure 3–28: Results of biodegradation analysis at two concentrations of enzyme as a function of GT concentration at 37°C.

As it was discussed in Chapter one, Section 2.3, third phase of wound healing, known as *proliferation* will reach its peak of activities 3 days after injuries. After applying the wound dressing on the first day of injury, it is desirable that scaffold be able to resist degradation at injury site for at least 3 days in order to initiate the proliferation phase of wound healing and cell growth. For this to occur, the wound dressing needs to lose less than 30% of its mass per day. According to Figure 3–28 the rate of scaffold degradation was a function of enzyme concentration in the solution. Current scaffold preparation and crosslinking method were suffice for slowing the degradation rate below 30% per day for the collagenase concentration of 2.5 mg/ml, however this combination of crosslinking and scaffold manufacturing technique was not effective for collagenase concentration of 5 mg/ml where only GT concentrations of 1% v/v had the degradation rate of less than 30%. These results showed that selection of crosslinking agent concentration needs to

be considered alongside the type of wounds that the final product would be administered to.

4.2.8. The Degree of Crosslinking Analysis

The degree of GT crosslinking was assessed for the fourth generation of gelatin scaffold by Ninhydrin assay (Sun *et al.*, 2006). Figure 3-29 shows the scaffolds crosslinking index as a function of GT concentration. Crosslinking index is defined in Chapter 2, Section 2.1.3.

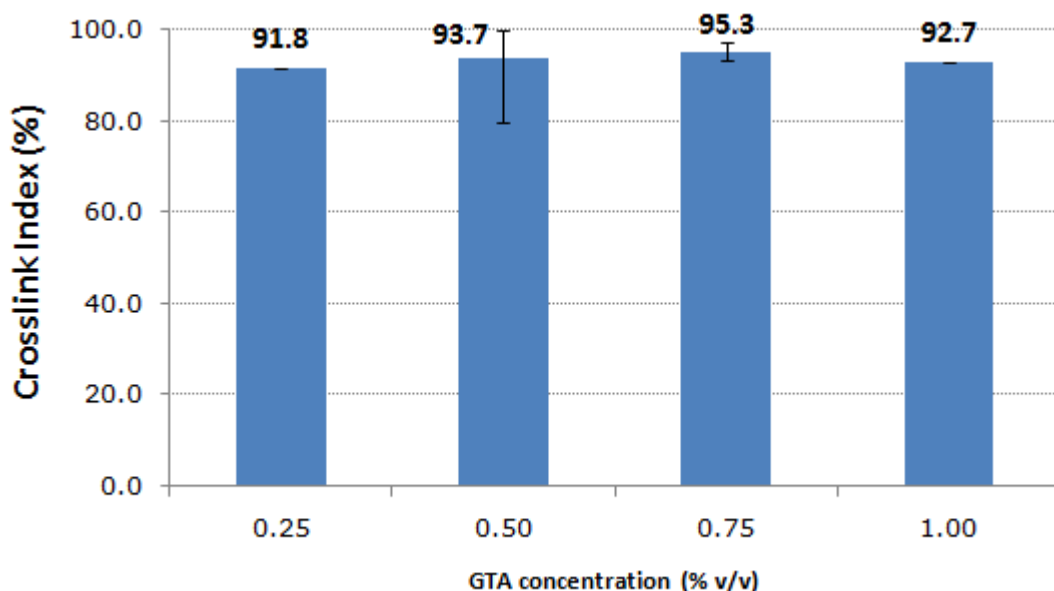


Figure 3-29: The crosslinking index of fourth generation scaffolds as a function GT concentration. Crosslinking index is measured by normalising number of free amine groups in crosslinked samples with respect to pure gelatin.

GT solution with the concentration of 0.25% v/v is capable of binding 92% of free amine groups available in gelatin scaffold. Further increase of GT concentration did not significantly changed the crosslinking index ($p \geq 0.05$). These results are in agreement with the thermal analysis results in Table 3-9 which showed the denaturation temperature increased to 82°C after crosslinking at 0.25% v/v GT and later formed a plateau at higher concentration values. Thus, the mid range values between 0.25 and 0.50% v/v GT can be recommended as optimal GT concentration. Bigi *et al.*, (2001)

reported that crosslinking the gelatin films with 1.00% GT aqueous solution is capable of consuming up to 98% of free amino groups. Lower crosslinking index in the case of present study in comparison with Bigi's results may be due to longer reaction time and higher pH, which were 24 hours and 7.4, respectively, in the case of the referred study.

5. Conclusion

Amongst all four generations of the scaffolds prepared through gas foaming method, the latest generation shows the best combination of microstructure and mechanical properties. As a result of modifications that were made to the preparation method, fourth generation scaffolds showed the pore size distribution closer to the desirable value for skin tissue engineering scaffold (Section 4.2.5), whilst showing multi layer inter-connected porous structure. Based on result of thermal analysis and FT-IR spectroscopy, the synthesis procedure was compatible with the crosslinking agents and did not cause a disruptive impact on the gelatin macromolecular structure as seen in the second generation of the scaffold (Section 2.2.2).

If only the control samples tensile strength of each of 4 generations of gelatin scaffolds prepared as part of this Chapter are compared individually, a relative correlation between the porosity presence within the structure and the tensile strength of the final samples can be noticed. The tensile strength of control samples in the 1st, 2nd, 3rd, and 4th generation scaffolds were 139, 180, 1.09, and 80.7 kPa respectively (the tensile strength of the second generation was reported for the samples that are prepared at pH 4.5 which was the same pH as the rest of generations). The third generation control samples had the lowest tensile strength amongst this group of scaffolds and at the same time it had the highest amount of porosity within the structure. On the contrary, the two first generations of scaffolds had the lowest porous structure generated as a result of gas foaming method, which was reflected in the higher tensile strength amongst the reported batches. As it was mentioned in the Section 1.2.3, porosity within the structure acts as the point of crack propagation and can cause weakening of the structure (Liu *et al.*, 2006). These results once again highlight the

delicate balance that exists between optimised porous structure and desirable mechanical strength for the structure.

The reported mechanical properties for some of the samples in this Chapter showed high values of standard deviation. In particular, the first generation scaffolds crosslinked with 1% v/v GT showed greater than 50% standard deviation (Section 1.2.3). High standard deviation in the mechanical properties of the structure has been reported for the tensile strength of collagen fibres at certain synthesis conditions (Zeugolis, *et al.*, 2008). Although the fibrillar collagen is used in the synthesis procedure of the cited study, the root cause behind such high standard deviation may be the same. High standard deviation may have been caused by high brittleness of the structure and functioning of gaps, sharp edges, and porosity within the samples as the site of crack initiation and premature failure of the structure.

Gas foaming method is an extremely chaotic process. As it was discussed in Sections 1.2.1 and 2.2.1, the distribution of porosities within the structure was not homogenous and uniform for the first two generation of the samples. However, along with improvement of synthesis process, the uniform distribution of the porosity was enhanced and became more regulated and evenly spread throughout the structure. The fourth generation scaffolds showed the most uniform distribution of porosity amongst the prepared sets of scaffolds. Figure 3-30 shows the low-magnification SEM image of the foam blocks produced through fourth generation gas foaming process. However, it should be noted that even with the improvement made in the fourth generation synthesis method, the frequency of macro pores inclusion and uneven distribution of porosity in the structure was reduced. Having access to industrial scale hardware and custom-made moulding systems can improve the reproducibility rate of the process even further.

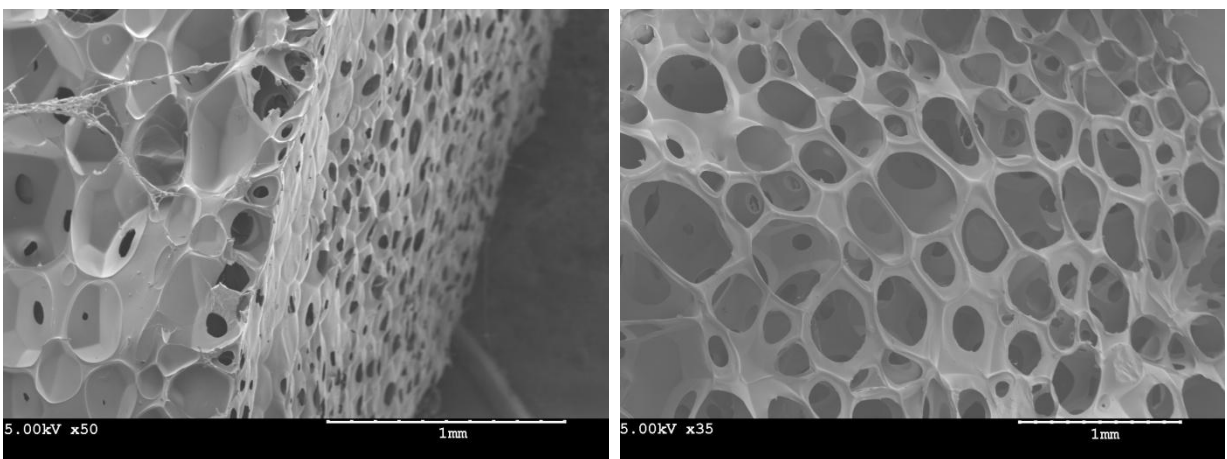


Figure 3-30: The low magnification SEM image of 4th generation scaffolds. The images are displaying the overall porosity distribution of samples throughout the sample cross section.

In the range of GT concentration that was studied in this Chapter (0.25%, 0.50%, 0.75%, and 1.00% v/v), the median value of 0.50% was proved to be an optimum range for crosslinking gelatin scaffolds. At higher concentrations of GT, over-crosslinking resulted in a brittle structure and reduction of strength (Section 4.2.3). Crosslinking index test results showed that using 0.25% GT solution would lead to consumption of 92% of gelatin free amine groups and showed that increasing GT concentration beyond this level was not necessary (Section 4.2.8). Concern over toxicity of GT is another factor that calls for using the lowest possible concentration of GT (Speit *et al.*, 2008). Thus the 4th generation scaffold crosslinked with 0.50% GT solution may be reported as the optimal combination for gelatin scaffold applications.

Considering the potential cytotoxic impact of unreacted GT, it was necessary to study the effectiveness of other potential crosslinking agents as alternatives to GT. In the following Chapter, three potential crosslinking agents were experienced to stabilise the 4th generation gelatin scaffold at the molar concentration equivalent to 0.50% v/v GT.

Chapter 4: Stabilisation of Scaffolds

Chapter 4 - Stabilisation of Scaffolds

As it was discussed in Chapter 1, Section 7, crosslinking gelatin is necessary for increasing its *in-vivo* stability (Giraudier *et al.*, 2004), strength (Farris *et al.*, 2010), and thermal stability (Bigi *et al.*, 2001). In this chapter, 3 alternative crosslinking agents were used to stabilise gelatin scaffolds. The main criterion in selecting these crosslinkers was to avoid the concerns over cytotoxicity of the GT (Speit *et al.*, 2008). To directly compare the effectiveness of these alternatives with GT, all three choices were prepared at an equivalent molar concentration of 0.005% mol/v and the results were compared with GT crosslinking at the same concentration (Chapter 3). The chemical nature and principles of reaction of these crosslinking agents were discussed in the First Chapter, here a concise review of their applications in biomedical engineering field is offered prior to discussing the results.

1. Hexamethylene Diisocyanate (HMDI)

1.1. Introduction

Hexamethylene Diisocyanate (HMDI) is capable of establishing urea or urethane bonds in contact with polymers containing amine or hydroxyl groups, respectively (Dong *et al.*, 2001). Figure 4-1 shows the subtle difference between urethane and urea bonds. Considering the abundance of both amine and hydroxyl groups in gelatin formation of either of these bonds is probable. Polyurethanes can provide a broad range of mechanical, biological, and physical properties. Crosslinked gelatin using HMDI is reported to be administered intravenously as plasma expander (Chvapil, 1982). The applications of HMDI are reported both in bone and cartilage tissue engineering (Puppi *et al.*, 2010). Polyurethane bone substitute is studied as a replacement for bone tissue (Gogolewski *et al.*, 2007). Due to flexible chemistry of polyurethane fabrications, HMDI-crosslinked polyurethane has been used in conjunction with brittle hydroxyapatite bioceramic to enhance biocompatibility of the structure (Laschke *et al.*, 2010).



Figure 4-1: The chemical configuration of urethane and urea bonds. The cyanate functional group will form a urethane bonds in reaction with hydroxyl functional groups and urea bond in reaction with amine groups.

HMDI can be used as a coupling agent for grafting organic polymers onto the surface of the metals (Chuang *et al.*, 2008) and ceramics (Dong *et al.*, 2001). Out of two cyanate groups available on each HMDI molecule, one can react with a hydroxyl group of the surface whilst the other can be converted into an active amine group after exposure to air (Chuang *et al.*, 2008). HMDI can be employed to graft organic polymers on the surface of the bioceramics such as hydroxyapatite. Dong *et al.*, (2001) used this concept to graft Osteogenetic growth factors to the surface of bio-ceramic and increase bone repair rate. They studied the efficiency of the grafting at the temperature between 20 and 70 °C and concluded that the amount of HMDI grafting on the surface tipped at 60 °C and decrease afterward as HMDI become pre-polymerised at higher temperature (Dong *et al.*, 2001). Catalina *et al.*, (2010) compared HMDI application with several other crosslinking agents (including GT and epoxy compound) in order to crosslink bovine gelatin films. They showed that gelatin films crosslinked with HMDI had lower thermal stability but it showed higher water absorption as compared with GT (Catalina *et al.*, 2011).

1.2. Crosslinking Method

As discussed in Chapter 1, Section 7.3, the major restriction in applying HMDI as a crosslinker is the fact that it has undesirable reaction with an aqueous medium, thus it is imperative that the scaffolds be dehydrate before crosslinking. Crosslinking was performed according to the method described by Catalina *et al.*, (2011). Briefly, the soaked samples (prepared after foaming) were dehydrated in gradient Propan-2-ol

aqueous solutions of 25, 50, 75, and 100% v/v. In each step of the dehydrating process, the scaffolds were immersed in Propan-2-ol solution for 30 minutes with agitation. At the last stage, the scaffolds were incubated in Propan-2-ol solution of HMDI with a concentration of 0.005% mol/v overnight (16 hours) whilst kept at 4°C. This molar concentration is equivalent to the molar value of 0.50% v/v GT solution used in Chapter 3 and allows direct comparison of these two crosslinkers based on their molar activity. The calculation for determining necessary volume for preparing HMDI solution with this concentration is provided in Appendix 3. After crosslinking, the samples were rehydrated back in gradient Propan-2-ol aqueous solutions in the reverse order used in pre-crosslinking preparation. The scaffolds were frozen and lyophilised for 24 hours. Lyophilisation was performed under vacuum pressure of 0.250 mbar and temperature of -40°C.

1.3. Results

1.3.1. Visual Description of Scaffolds

Figure 4–2 shows the visual features of 4th generation gelatin scaffold crosslinked using HMDI. Comparing with GT-crosslinked scaffold, these sets of samples had a more whitish colour. The edges and the peripheral surfaces of the scaffold were smooth and comparable with GT-crosslinked scaffolds (Chapter 3, Figure 3–19), however the top surface of the sample showed more wrinkling and superficial creases. This may have been due to Propan-2-ol interaction with gelatin compound. There was an accumulation of localised wrinkled texture on the top side centre of the scaffold (Figure 4–2-A, marked by arrows). The gelatin structure shrinks when in contact with the alcoholic solvents such as Propon-2-ol. This phenomenon is due to the impact of alcohol-based medium on peptide chains of protein. Alcohol-based solvents would expose hydrophobic amino acid residues of protein and allow its structure to unfold (Herskovits *et al.*, 1970). As a result the structure collapse, water is removed from its core centre which causes gelatin to shrink and became more compact comparing with GT-crosslinked

scaffolds. The shrinkage may have caused formation of the compact and wrinkled regions shown in Figure 4-2-A by arrows.

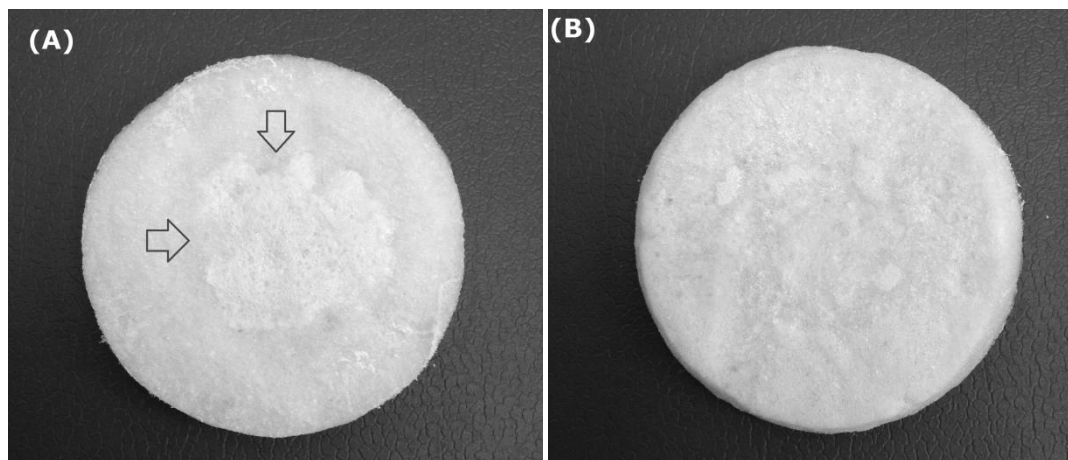


Figure 4-2: Visual characteristics of the 4th generation gelatin scaffolds crosslinked using HMDI; (A) the top side of the scaffold. The area marked by arrows showed a localised wrinkled-texture and may have formed as a result of propan-2-ol interaction with gelatin. (B) The bottom side of the scaffold where it was in contact with mold showed a much smoother texture.

1.3.2. Fourier Transform Infra-Red Spectroscopy (FT-IR)

Figure 4-3 shows the FT-IR spectra of the fourth generation gelatin scaffolds crosslinked using HMDI and the control sample. The gelatin reaction with HMDI and crosslink network formation includes the formation of urethane bonds (Vijayakumar and Subramanian, 2014). As discussed in Introduction Section, the cyanate functional groups can react with hydroxyl groups to form urethane bonds. Figure 4-3 shows an absorption band close to 3500cm^{-1} in a form of shoulder close to amide A band which did not exist in the crosslinked sample (Kanmani and Rhim, 2014). This shoulder like absorption is assigned to hydroxyl functional groups which its disappearance can show their consumption during crosslinking. This coincides with appearance of urethane bonds in the crosslinked sample. In the crosslinked scaffolds, there is an absorption peak at 1255 cm^{-1} which is attributed to urethane bonds (Chuang *et al.*, 2008). Other urethane bond peaks in the crosslinked scaffolds spectra was at 1077 cm^{-1} . Presence of an absorption peak at 1470 cm^{-1} can suggest the presence of urea linkage in addition to

urethane in the sample structure (Dong *et al.*, 2001). This absorption can be intensified by the absorption peak at 1450 cm^{-1} which is assigned to backbone vibrations of HMDI molecules (Chuang *et al.*, 2008) Which is related to CH_3 symmetrical deformation mode both in gelatin and HMDI (Sarem *et al.*, 2013; Chuang *et al.*, 2008). In addition to 1470 cm^{-1} peak, the amide I peak of crosslinked samples showed a shoulder-like broadness at 1720 cm^{-1} which was in contrast with the sharp amide I peak of control samples. This phenomenon may be an additional sign of urea linkage presence in the crosslinked samples (Chuang *et al.*, 2008). The presence of urea linkage may be caused as a result of cyanate reaction with amine groups of gelatin. These transformations in the FT-IR spectra of the samples can show potential crosslinking reaction mechanism.

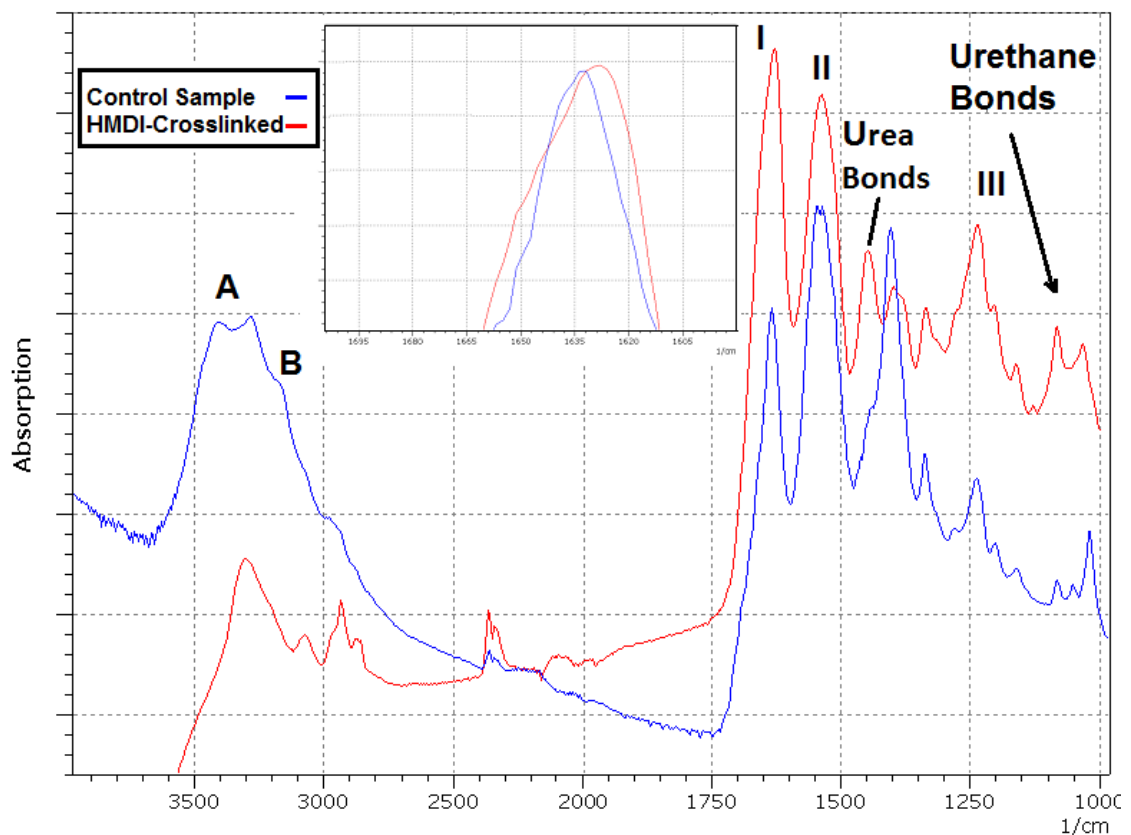


Figure 4-3: FT-IR spectra of the 4th generation gelatin scaffolds crosslinked with HMDI and control samples. The inset figure shows the magnified area of spectra corresponding to amide I.

The formation of urea and urethane bonds allows establishment of hydrogen bonds in the structure. Two types of hydrogen bonds may be established: (1) bonds

between the hydrogen atoms of amine groups and the oxygen atoms in the carbonyl groups (-N-H \cdots O=C-), and (2) bonds between hydrogen atoms within one amine group and nitrogen atom within another amine group (-N-H \cdots N-H-) (Yilgör *et al.*, 2000). These hydrogen bonds interact with the gelatin amide I and III. Gelatin amide I band originates from carbon and oxygen atoms interaction as part of gelatin carbonyl groups (C=O) (Payne *et al.*, 1988). In comparison with the control samples, the crosslinked scaffold showed shifts of these peaks to lower wave numbers. This shift was the most obvious for amide I. Absorption for amide I in the control samples occurred at 1633 cm⁻¹ whilst this absorption occurred at 1622 cm⁻¹ for the crosslinked scaffolds. These shifts may have resulted from the weakening of the covalent bonds between nitrogen and hydrogen atoms in amine (N-H) and carbon and oxygen in carbonyl (C=O) due to establishment of additional hydrogen bonding (Yilgör *et al.*, 2000). Other researchers suggested that this shift may be the result of HMDI incorporation within the structure since HMDI shows an absorption at 1620 cm⁻¹ associated with its amide band (Liu *et al.*, 1998). Inset section of Figure 4-3 shows a magnified view of gelatin amide I peaks for both the control and the crosslinked scaffolds.

No absorption at 2260 cm⁻¹ was found in the crosslinked scaffolds. This absorption is assigned to the isocyanate functional groups and its absence shows that no unreacted isocyanate groups exist within the structure (Kadnaim *et al.*, 2008; Stankus *et al.*, 2004). This is important in the context of biocompatibility where unreacted agents may result in irritation or inflammatory response in the wound. Strong absorptions at 2850 and 2940 cm⁻¹ in the crosslinked scaffold in comparison with control sample are caused by CH₂ groups of HMDI (Liu *et al.*, 1998). At longer wave numbers, there was another shift to a lower value similar to what was seen for amide I peak. The control scaffolds showed an absorption band at 3402 cm⁻¹ which is assigned to free amine (-N-H) groups (Vijayakumar and Subramanian, 2014; Kadnaim *et al.*, 2008). As a result of crosslinking and establishment of hydrogen bonds, this absorption shifted to 3318 cm⁻¹.

in the crosslinked scaffolds. These results may have been caused as a result of hydrogen bonds formation that discussed earlier and are indicative of crosslinking in the structure.

1.3.3. Mechanical Properties of the Scaffolds

Tensile properties of 4th generation gelatin scaffolds crosslinked using HMDI are listed in Table 4-1 and were compared with control samples and scaffolds crosslinked using 0.50% v/v GT.

Table 4-1: Mechanical properties of 4th generation gelatin scaffolds crosslinked using HMDI as compared with GT-crosslinked scaffolds and control sample.

Sample	Tensile Strength (kPa)	Young's Modulus (kPa)	Tensile Strain (%)
Control	80.8 (± 4)	0.9 (± 0.1)	114.8 (± 11)
HMDI	157.5 (± 13)	2.6 (± 0.4)	101.2 (± 16)
GT	239.48 (± 70)	2.44 (± 0.4)	30.23 (± 5)

The tensile strength of HMDI-crosslinked gelatin scaffolds was significantly increased in comparison with control samples ($p \leq 0.05$). In comparison with GT, scaffold crosslinked using HMDI showed a significantly lower tensile strength ($p \leq 0.05$).

Higher tensile strength showed by the GT-crosslinked structure in comparison with HMDI-crosslinked samples may be due difference in crosslinker molecular length and crosslinking index caused as a result of crosslinking. Glutaraldehyde molecules are shorter than HMDI molecules (Catalina *et al.*, 2011). Price (1986) showed that the molecular length of crosslinking agent may be decisive in determining the mechanical strength and elongation of the structure. Shorter crosslinking molecules can establish higher crosslink density in the structure (Allen *et al.*, 2006). Shorter crosslinking agents such as GT can form more intra-molecular covalent bonds than longer crosslinker chains such as HMDI. Since intra-molecular covalent bonds are the main reason for the increase of tensile strength after crosslinking (Farris *et al.*, 2010). Higher number of these bonds

at a given volume of network in the GT-crosslinked samples may have been contributed to significantly higher tensile strength than HMDI-crosslinked sample ($p \leq 0.05$).

There was no significant difference between the Young's modulus values of the HMDI and GT-crosslinked samples, however HMDI-crosslinked scaffolds showed significantly higher tensile strain than GT-crosslinked scaffolds ($p \leq 0.05$) and showed a more plastic nature. Crosslinking agents with longer molecular chains result in a more flexible network. This may be evident in the molecular structure of gelatin allowing partial freedom of movement resulting in a semi-flexible structure (Catalina *et al.*, 2011). A higher Young's modulus is indicative of a more rigid structure which is more prone to more crack initiation and propagation (Bigi *et al.*, 2001; Martucci *et al.*, 2006). Compared to the control samples, crosslinking with HMDI significantly increased the Young's modulus of the scaffold ($p \leq 0.05$). This is a direct result of covalent bonds establishment during chemical crosslinking (Farris *et al.*, 2010).

1.3.4. Scaffolds Thermal Analysis

Table 4-2 further compares thermal analysis results for the 4th generation gelatin scaffolds crosslinked using HMDI with the control sample and GT-crosslinked scaffolds. The control samples showed the denaturation temperature of 48.1 °C; crosslinking the gelatin scaffolds with HMDI increased the denaturation temperature to 76.5 °C. Patil *et al.*, (2000) reported the value of 78 °C for the denaturation temperature for isocyanate-crosslinked gelatin films with 68% water content (the water content of samples in this study was 65%).

Table 4-2: Thermal analysis of HMDI-crosslinked gelatin scaffolds compares with the corresponding results for scaffolds crosslinked with GT and control samples.

Sample	Denaturation Temperature (°C) (T_d)	Enthalpy of Transition (ΔH) (J.g ⁻¹)
Control	48.1 (±7)	-25.7 (±17)
HMDI	77.8 (±1)	-15.4 (±1)
GT	84.5 (±2)	-16.3 (±1)

The increase of denaturation temperature from 48°C to 78°C confirms crosslinking of gelatin with HMDI. At 84.5°C, the denaturation temperature of GT-crosslinked scaffolds was higher than HMDI-crosslinked samples. Catalina *et al.*, (2011) suggested that the denaturation temperature of crosslinked gelatin is influenced by crosslinking molecules length. The longer crosslinker molecules provide flexibility (Patil *et al.*, 2000) and shorter crosslinkers draw the fibres closer together. Closer fibres reduce their axial separation, thus more energy would be necessary to unfold the protein structure which require higher temperature (Miles *et al.*, 2005; Miles and Ghelashvili, 1999). It is shown that as the crosslinking agent length increases, the crosslinking density of the overall molecular structure diminishes (Allen *et al.*, 2006). Reduction of crosslink density consequently reduces the denaturation temperature of the sample, since a higher denaturation temperature often indicates a higher crosslinking density (Sung *et al.*, 1996; Nakka *et al.*, 2011). Thus, shorter GT molecules have led to higher crosslinking density and less flexible molecular structure, which in turn led to higher denaturation temperature than HMDI-crosslinked scaffolds. Decrease in the enthalpy of transition as result of crosslinking showed the similar pattern as it was noticed in Chapter 3, Section 1.2.4. and can be explained in the context of more covalent bonds establishment at the expense of hydrogen bonds elimination (De Carvalho and Grosso, 2004; Achet and He, 1995).

1.3.5. Scaffolds Microstructure Analysis

Figure 4-4 (A-D) shows the SEM results of the 4th generation scaffolds crosslinked using HMDI. In comparison with the microstructures of GT-crosslinked scaffolds discussed in Chapter 3, Section 4.2.5, HMDI-crosslinked scaffolds showed smaller pore sizes with some distortion. Figure 4-4-(D) is taken parallel to the surface of the scaffold whilst the sample was tilted 45° relative to the electron beam to better show the distortion of the surface.

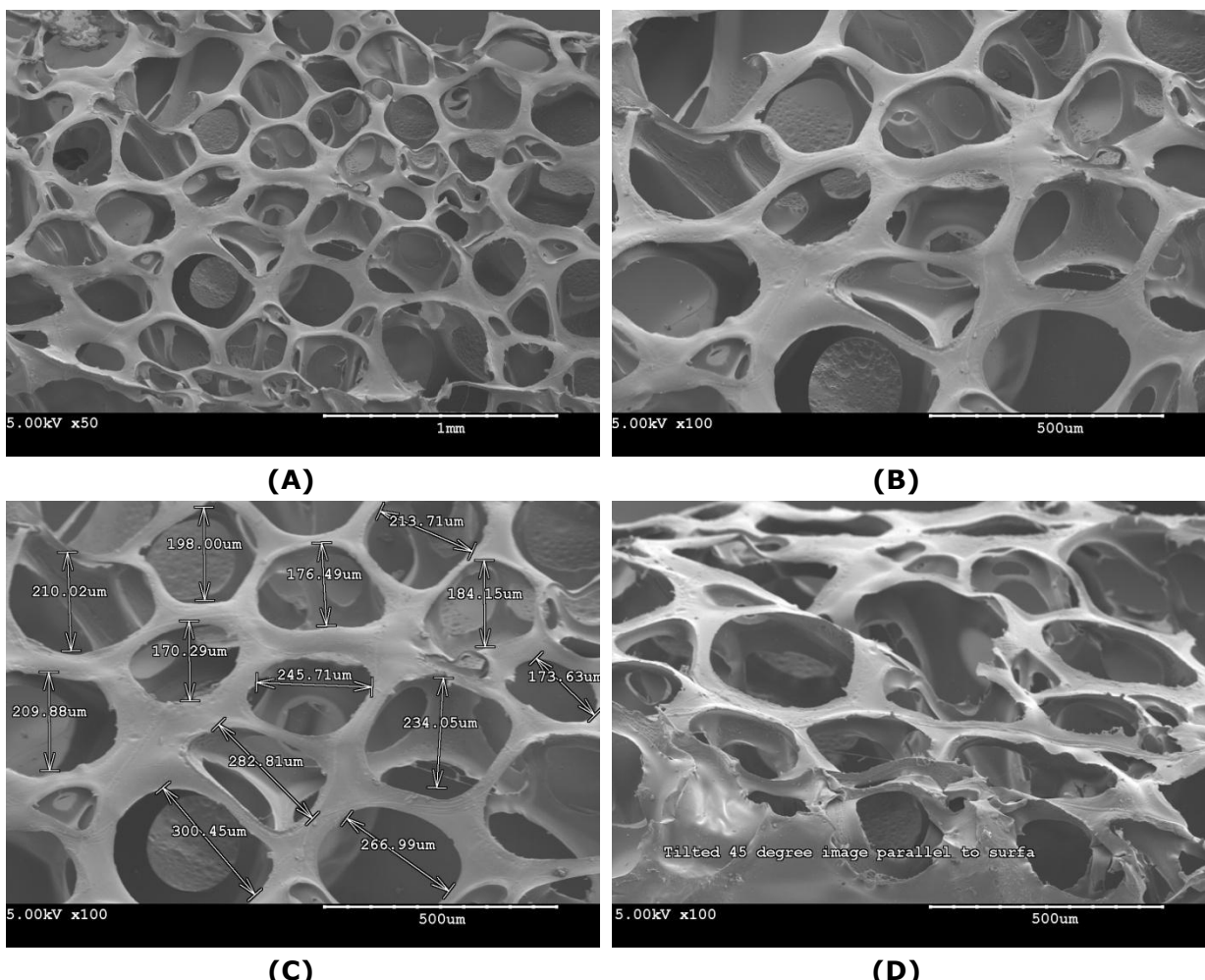


Figure 4-4: SEM analysis of the 4th generation scaffolds crosslinked using HMDI: (A) 50x, (B - D) 100x magnifications. The average pore size of the crosslinked gelatin scaffold was 220 μm (± 56). The acceleration voltage used for scanning was 5kV. Figure (D) shows the surface of scaffold whilst it was tilted 45° relative to the electron beam to show the distortion of the scaffold.

The average pore size of HMDI-crosslinked scaffolds was 220 μm (± 41). The average pore size of 4th generation scaffold crosslinked using 0.50% v/v GT was 245 μm .

Reduction of the average pore size in the structure may be due to contraction caused by Propan-2-ol (solvent used) during the crosslinking reaction. As discussed earlier, alcohol solvents are shown to cause increased hydrophobicity, removal of water, and collapse and contraction of molecular structure (Herskovits *et al.*, 1970). To investigate the sole effect of solvent on the structure, a gelatin scaffold was incubated in the solvent (Propan-2-ol) in the absence of HMDI. Figure 4-5 compares the scaffold prepared in de-ionised water and Propan-2-ol. The average pore size of the scaffold immersed in Propan-2-ol was 69 µm. This value for sample incubated in de-ionised water was 180 µm which was significantly higher than the sample prepared in Propan-2-ol ($p \leq 0.05$). The gelatin scaffold prepared in Propan-2-ol produced a more contracted structure with sharp edges and fragmented structures surrounding the pore area, whilst the sample prepared in de-ionised water showed relatively smoother surface with more expanded pores throughout the sample. This comparison showed the effect of solvent on porous structure of gelatin and provided visual confirmation about shrinkage and collapse of gelatin sample upon contact with Propon-2-ol.

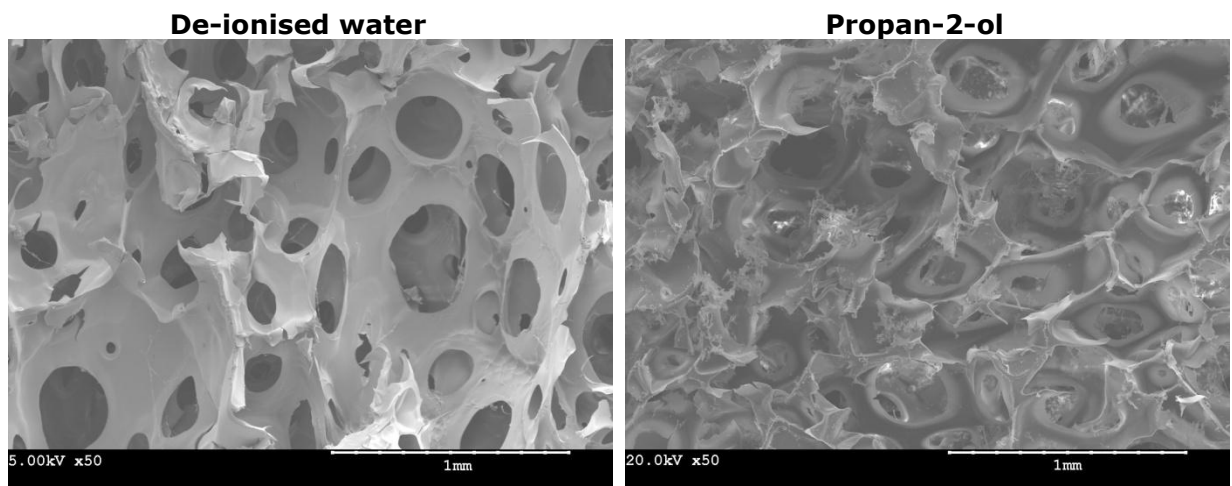


Figure 4-5: A comparison between control gelatin samples prepared in de-ionised water and Propan-2-ol. Alcoholic solvents were reported to cause removal of water from protein structure and contraction of sample. In this comparison, the sample prepared in de-ionised water showed smoother surface with more expanded pores comparing with sample prepared in Propon-2-ol. The images are obtained at 5kV acceleration voltage.

1.3.6. Scaffold Water Absorption

Figure 4–6 displays the water absorption characteristics of gelatin scaffolds crosslinked using HMDI. In comparison with the control sample, scaffolds crosslinked using HMDI showed less ability to absorb water. However, in comparison with GT, scaffolds crosslinked using HMDI showed a higher percentage of water absorption. These samples absorbed 1567% of their dried weight after 3 hours incubation in de-ionised water with 665% for the GT-crosslinked scaffolds. Higher water absorption ability of structure crosslinked by HMDI in comparison with GT may be attributed to the fact that HMDI molecules are longer than GT molecules. Longer crosslinking molecules lead to lower crosslink density (Allen *et al.*, 2006). This consequently leads to a less compact polymeric network (Miles *et al.*, 2005). It is suggested that since the equilibrium degree of swelling of polymer structure depends on the elastic force of the polymer structure, thus longer crosslinking chain may bring more elasticity and consequently more swelling to the structure (Mabilleau *et al.*, 2006). As discussed in Chapter 3, Section 1.2.6, crosslinking mainly reduced the amount of water absorption as a result of more restriction against network expansion in water and less subsequent swelling (Tasselli *et al.*, 2013). More compact and tighter structure in GT-crosslinked samples would subsequently lead to less water absorption relative to their HMDI-crosslinked counterparts.

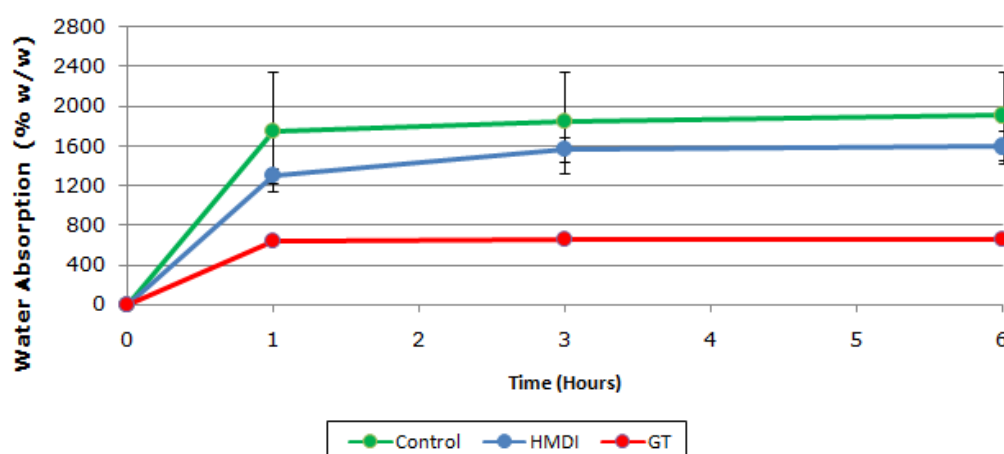


Figure 4–6: Water absorption capability of 4th generation scaffolds crosslinked using HMDI. The results are further compared with GT-crosslinked scaffolds and the control samples.

2. Poly (ethylene glycol) di-glycidyl ether (Epoxy)

2.1. Introduction

Poly-(ethylene glycol) di-glycidyl ether (as would be referred to as *epoxy compound*) has two epoxide functional groups located at both ends of each molecule (Khor, 1997). The epoxy compounds are used for fixing biological tissue prosthesis like arterial grafts as an alternative to GT and other aldehydic crosslinking agents (Lohre *et al.*, 1993). In addition to fixing capability, epoxy compounds may be used for sterilisation of biological tissue prosthesis (Sung *et al.*, 1997b). The epoxy compound is reported to graft the enzymes on chitosan/alginate to increase enzyme durability on the surface (Mendes *et al.*, 2013). Another practical application of epoxy is its ability to react with carboxylic acid functional groups (Tillet *et al.*, 2011). As a result of such reaction ester bonds will be formed which has the ability to be hydrolysed in an aqueous environment. It is therefore used to prepare a biodegradable structure that dissolves after service in the body in applications such as bio-absorbable membranes containing chitosan or gelatin and Poly-siloxane (Ren *et al.*, 2001; Shiroasaki *et al.*, 2009).

Another practical feature of the epoxy is its ability to function within a range of acidic and alkaline pH's (Sung *et al.*, 1996b). Leach *et al.*, (2005) used epoxy compound to crosslink and prepare vascular tissue engineering scaffolds from bovine elastin and studied the effect of pH on the final product characteristics. It was reported that higher pH's resulted in a more stable specimen in contact with elastase and aqueous media (Leach *et al.*, 2005). Zeugolis *et al.*, (2008) studied the application of epoxy compounds to crosslink collagen fibres to be used as medical sutures. It was shown that collagen fibres crosslinked using an epoxy showed a higher tensile strength in comparison with fibres crosslinked using GT (Zeugolis *et al.*, 2009).

2.2. Crosslinking Method

Crosslinking of scaffolds with the epoxy compound was carried out according to the method described by Catalina *et al.*, with some modifications (Catalina *et al.*, 2011). The prepared scaffolds were immersed in an aqueous solution of epoxy at a molar

concentration of 0.005% mol/v. This molar concentration is equivalent to the molar value of 0.50% v/v GT solution used in Chapter 3 and allows direct comparison of these two crosslinkers based on their molar activity. The calculation for determining necessary volume for preparing solution with this concentration is provided in Appendix 3. The fourth generation gelatin scaffolds were incubated in the epoxy aqueous solution for 3 hours without any pH adjustment whilst kept at 4 °C fridge. After crosslinking, the scaffolds were transferred into de-ionised water and washed overnight (16 hours). Washed scaffolds were frozen and then lyophilised for 24 hours. Lyophilisation was performed under vacuum pressure of 0.250 mbar and temperature of -40 °C.

2.3. Results

2.3.1. Visual Description of Scaffolds

Figure 4–7 shows the visual features of gelatin scaffolds crosslinked using the epoxy compound. Crosslinking with epoxy produced a white coloured scaffold which was different from a yellow-coloured GT-crosslinked scaffold seen in Chapter 3. It is reported that since epoxy is a colourless compound, it does not have any colouring effect on the final product (Sung *et al.*, 1996). One noticeable difference that existed between scaffolds crosslinked with epoxy and the ones crosslinked with GT was the level of smoothness that existed on the surfaces of the former. The edges of the scaffolds were sharp and well-defined. The scaffold showed soft and elastic texture upon touching. In contrast with the HMDI-crosslinked scaffold, these samples did not show any sign of contraction, or wrinkled texture on the surface.



Figure 4-7: Visual features of the 4th generation gelatin scaffolds crosslinked with epoxy compound. The surfaces of the scaffold were smooth. The white colour of scaffold was different from yellow GT-crosslinked scaffolds seen in Chapter 3.

2.3.2. Fourier Transform Infra-Red Spectroscopy (FT-IR)

Figure 4-8 shows the FT-IR spectrum of gelatin scaffolds crosslinked using epoxy compounds. Since the peaks assigned to the epoxy functional groups were located at wave-numbers shorter than 1000 cm^{-1} , the FT-IR scan for this set of samples was performed from 700 cm^{-1} . Epoxide functional groups absorptions bands are located at 972 and 1081 cm^{-1} with these bands correspond with the C-O-C and C-O-H functional groups, respectively (Shirosaki *et al.*, 2009; Vargas *et al.*, 2008). Epoxy-crosslinked scaffolds showed the both of these peaks in comparison with the control sample. The absorption intensity at 972 cm^{-1} was lower in comparison with 1081 cm^{-1} . The crosslinked samples also showed an intense peak at 1237 cm^{-1} which is assigned to the diethyl ether (C-O-C) in the epoxy compound (Vargas *et al.*, 2008). The above mentioned data showed crosslinking and the incorporation of the epoxy within the scaffolds. According to Ren *et al.*, (2010), the acidic pH's may have a positive impact on the epoxy crosslinking for that the epoxy functional group may be hydrolysed and undergo ring opening (Chapter 1, Section 7.2). The protonated epoxy groups are now activated and attack the neutrophilic groups on the side chain of gelatin (Ren *et al.*, 2001; Ren *et al.*, 2010). Effective function of epoxy in an acidic pH is in contrast with the ineffectiveness of GT at a low pH as seen in Chapter 3, Section 2.

Apart from the peaks that directly indicate epoxy presence in the scaffold, another impact of crosslinking was the shift of gelatin amide I absorption towards lower wave numbers (shown in the inset of Figure 4–8). This shift is similar to what was seen for HMDI-crosslinked scaffolds. The shift in amide bands to lower wave numbers may be due to formation of a stronger helical structure, as discussed in Section 1.3.2 (Yilgör *et al.*, 2000; Lee *et al.*, 2005; Lim *et al.*, 2008; Warren, 1997).

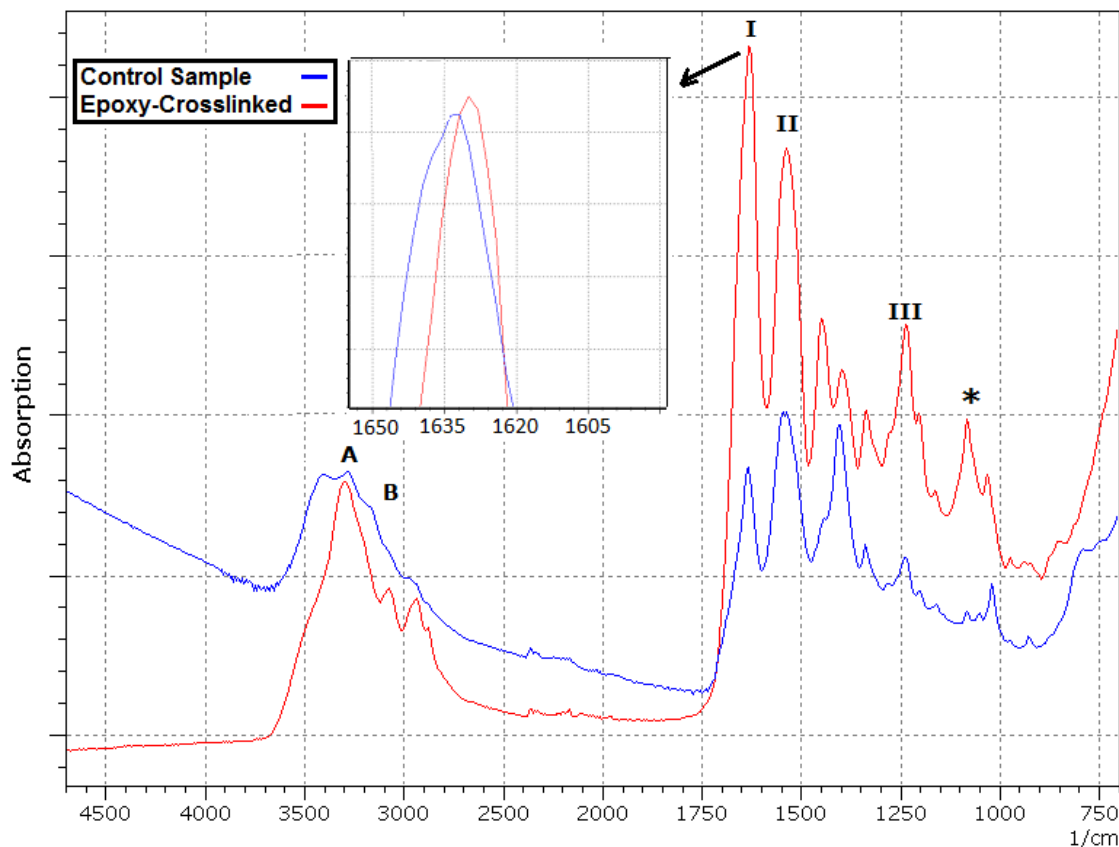


Figure 4–8: The FT-IR spectrum of 4th generation gelatin scaffolds crosslinked using Epoxy. The inset shows the magnified view of amide I region of gelatin spectra. The peak marked by * is assigned to C-O-H groups formed in crosslinking of gelatin by epoxy in acidic pH. Gelatin Amide I, II, III, A, and B are indicated in the Figure.

In Figure 4–8, control samples showed a shoulder-like peak centred at around 3500 cm⁻¹ which corresponds -OH stretching band (Kanmani and Rhim, 2014). However, for the crosslinked samples it disappeared suggesting that the -OH group may have been involved in the reaction with Epoxy. As discussed in Chapter 1, Section 7.2, epoxy

compounds has the capability of reacting with hydroxyl groups and formation of ether bonds (Leach *et al.*, 2005). Figure 4–8 shows that such a reaction may have been took place resulting in consumption of hydroxyl functional groups during crosslinking of gelatin with Epoxy.

2.3.3. Mechanical Properties of the Scaffolds

Epoxy compound was used to crosslink the 4th generation gelatin scaffolds and the product mechanical features are listed in Table 4–3. The samples properties are compared against the control samples and scaffolds crosslinked with a molar equivalent of GT.

Table 4–3: Mechanical properties of 4th generation gelatin scaffolds crosslinked using epoxy. The epoxy-crosslinked scaffold showed the lowest mechanical values amongst studied samples.

Sample	Tensile Strength (kPa)	Young's Modulus (kPa)	Tensile Strain (%)
Control	80.8 (± 4)	0.9 (± 0.1)	114.8 (± 9)
Epoxy	20.3 (± 10)	0.5 (± 0.2)	53.9 (± 16)
GT	239.5 (± 70)	2.44 (± 0.4)	30.2 (± 5)

The mechanical properties of epoxy-crosslinked scaffolds were found to be lower than the control samples. Tensile strength of the epoxy-crosslinked scaffold was 25% of the control samples. Young's modulus of the crosslinked scaffolds was 56% lower than the values for the control samples and crosslinking using epoxy allowed the scaffold to elongate half the value showed by control samples before their failure.

In comparison with GT and HMDI, scaffolds crosslinked with epoxy showed the lowest mechanical strength. HMDI-crosslinked samples had the tensile strength of 157.5 kPa (Section 1.3.3). Huang *et al.* (1998) reported a reduction of biological tissue (collagen-based porcine pericardia) tensile strength as a result of crosslinking with epoxy-compound (Huang *et al.*, 1998). It is reported that upon absorbing water, the mechanical strength of epoxy crosslinked samples can deteriorate severely (Li *et al.*,

2009a). This deterioration is a result of infiltration of water molecules between epoxy polymer chains and establishing hydrogen bonds between them and polar functional groups, such as hydroxyl functional groups in the polymer (Zhou and Lucas, 1999). Reaction of amine functional groups with epoxy compounds results in formation of additional hydroxyl groups (Chapter 1, Section 7.2) (Leach *et al.*, 2005). Considering that the samples were conditioned at 95% relative humidity prior to tensile testing (Chapter 2, Section 2.2.1), these additional hydroxyl groups may have had contributed to further deterioration of epoxy-crosslinked scaffolds. Epoxy compound has an oxygen atom at every third site of its chain (Chapter 1, Section 7.2). It is reported that increasing the number of oxygen atoms in the backbone of a molecule increases the flexibility features of the structure (Thomazine *et al.*, 2005). In a molecular level, it is suggested that the repetition of triple combination of -C-C-O- atom units increases the flexibility of the chain (Price, 1986; Mabilleau *et al.*, 2006). It is shown that crosslinkers possessing such molecular structure are prone to cause reduction of tensile strength after crosslinking due to chain flexibility (Caycik and Jagger, 1992). This may justify the reduction of tensile strength of the scaffold after crosslinking with epoxy compound in this study. Apart from chain flexibility of the crosslinking agent, the reduction of the tensile strength may have been intensified due to an increase in porosity in the structure. Epoxy-crosslinked scaffolds showed a better interconnectivity within the structure in comparison with both GT and the HMDI-crosslinked scaffolds (Section 1.3.5). It is well known that porosity can contribute to an elevated local stress at sharp pores edges, leading to a reduced mechanical resistance against crack initiation (Liu *et al.*, 2006). An increase in the number of pores may ultimately contribute to a lower mechanical strength. The pore size and microstructure of the scaffolds are discussed in further details in the Section 2.3.5.

In terms of elasticity, epoxy crosslinking caused an increased flexibility as the Young's modulus was the lowest when compared with control and GT-crosslinked scaffolds (Table 4-3). Epoxy-crosslinked tissues are reported to show better flexibility

than GT-fixed tissue (Sung *et al.*, 1996a). Improved flexibility of the crosslinked scaffolds may be due to molecular structure of epoxy and impact of oxygen atoms in this structure as discussed above. In addition to the impact of oxygen atoms presence in the backbone of epoxy, it is suggested that crosslinking the polymeric structure with a long chain length crosslinking agent may increase more elasticity in the structure compared to the control samples (Patil *et al.*, 2000; Catalina *et al.*, 2011). Reduction of Young's modulus as a result of crosslinking with a long chain crosslinking agent has been reported for polymeric structure (Mabilleau *et al.*, 2006). Allen *et al.*, (2006) showed that increasing the length of crosslinking chain reduces the Young's modulus and the strength of polymeric structure. It was reported that an increase of the crosslinking chain length from 2 atoms to 12 atoms may reduce the Young's modulus of the structure by approximately 40% (Allen *et al.*, 2006). This may justify the low Young's modulus of the scaffolds crosslinked with epoxy compound.

2.3.4. Scaffolds Thermal Analysis

Table 4-4 shows the results of thermal analysis for the 4th generation gelatin scaffolds crosslinked with the epoxy compound. These results further compared thermal characteristics of scaffolds crosslinked with 0.50% v/v GT and the control samples.

Table 4-4: The results of thermal analysis of 4th generation gelatin scaffolds crosslinked using Epoxy and GT in addition to control samples.

Sample	Denaturation Temperature (°C) (T _d)	Enthalpy of Transition (ΔH) (J.g ⁻¹)
Control	48.1 (±7)	-25.7 (±17)
Epoxy	80.4 (±2.3)	-19.1 (±0.9)
GT	84.5 (±2)	-16.3 (±0.9)

Crosslinking the gelatin scaffolds using epoxy increased the denaturation temperature from 48.1 °C for the control samples to 80.4 °C. Catalina *et al.*, (2011) reported the denaturation temperature of 73.9 °C for crosslinked gelatin using epoxy. In a study using porcine collagen tissue, Sung *et al.*, (1996) compared the denaturation temperature of epoxy-crosslinked collagen with GT-crosslinked collagen. They reported

that GT-crosslinked collagen showed the denaturation temperature (T_d) of 86.7°C whilst the epoxy-crosslinked sample showed the T_d of 78.7°C. However, it is argued that lower T_d cannot be a result of crosslinking efficiency since both crosslinking agents showed similar crosslinking index in the tissue (Sung *et al.*, 1996). The lower denaturation temperature in epoxy-crosslinked scaffold may be the direct result of relatively longer molecular chain of epoxy in comparison with GT. A longer molecular chain can lead to more elastic polymer network and a lower denaturation temperature (Allen *et al.*, 2006; Nakka *et al.*, 2011). When polymeric structure is more packed and there are spatial restrictions against unzipping of helical structure, the transition from helix to coil occurs at higher temperature to procure enough energy for this transition (Miles and Ghelashvili, 1999). This may explain lower denaturation temperature of epoxy-crosslinked scaffold in comparison with the GT-crosslinked sample in Table 4-4. The negative value of scaffolds enthalpy of transition was reduced from -25.7 J.g⁻¹ in the control samples to -20.0 J.g⁻¹ as a result of epoxy crosslinking. Decrease of enthalpy of transition as a result of crosslinking is caused by establishment of covalent bonds and was discussed in Chapter 3, Section 1.2.4 (De Carvalho and Grosso, 2004; Achet and He, 1995; Dardelle *et al.*, 2011).

2.3.5. Scaffolds Microstructure Analysis

Surface microstructure of epoxy-crosslinked scaffolds is shown in Figure 4-9 (A-D). In comparison with the microstructures of the 4th generation scaffolds discussed in Chapter 3, Section 4.2.5, epoxy-crosslinked scaffold showed an increased porosity and interconnectivity. Relative to the microstructure shown in the aforementioned Chapter, the surface surrounding the pores was reduced and the edges of the pores were thinner. The surface of the scaffold was smoother which may be the result of epoxy crosslinking. It is shown that longer molecular chains in the crosslinking agent can increase the smoothness of the scaffold (Mabilleau *et al.*, 2006). The pore shape appeared more regular in comparison with the 4th generation scaffolds described in Chapter 3, Section 4.2.5. The average pore size of epoxy-crosslinked scaffolds was 389μm (±117). The

average pore size of 4th generation scaffold crosslinked with 0.50% v/v GT (molar equivalent of used epoxy), was 245 μm . This value for scaffolds crosslinked using HMDI was 182 μm . The pores of the epoxy-crosslinked scaffolds showed a significant increase in size in comparison with the scaffolds crosslinked with GT and the control samples ($p \leq 0.05$). Increase in pore size and reduction in the surface that surround the pores may be one of the main reasons behind noticeable reduction in scaffolds tensile strength and lack of mechanical integrity observed in the mechanical testing results.

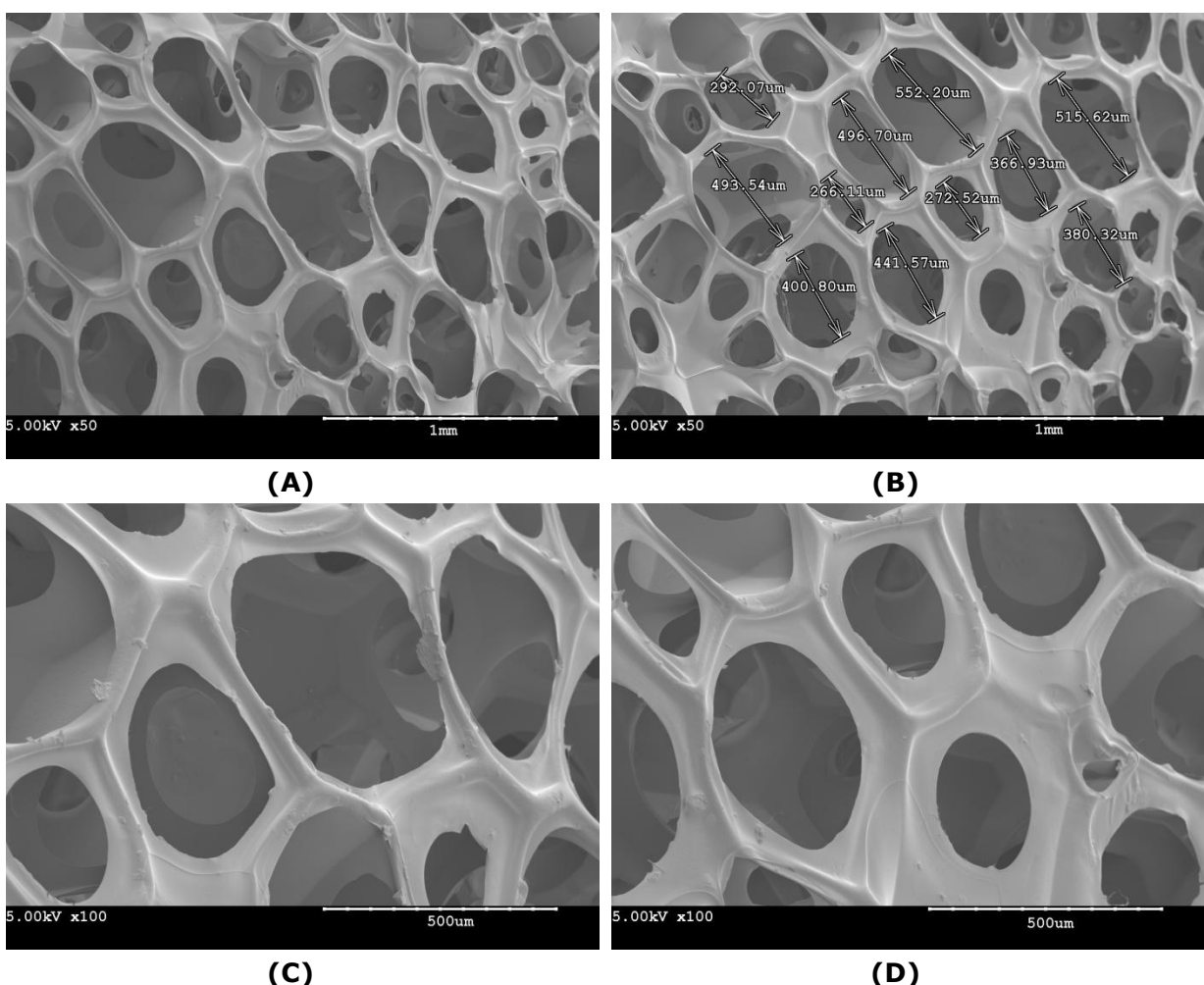


Figure 4-9: SEM analysis of 4th generation scaffolds crosslinked with epoxy: crosslinked scaffolds at: (A & B) 50x, and (C & D) 100x magnifications. The average pore size of the epoxy-crosslinked scaffold was 389 μm (± 117). The images are obtained at 5kV acceleration voltage.

2.3.6. Scaffold Water Absorption

The results for the water absorption capability of the 4th generation gelatin scaffolds crosslinked with epoxy compounds are shown in Figure 4-10. Comparison between the control samples and GT-crosslinked scaffolds are included in the same Figure.

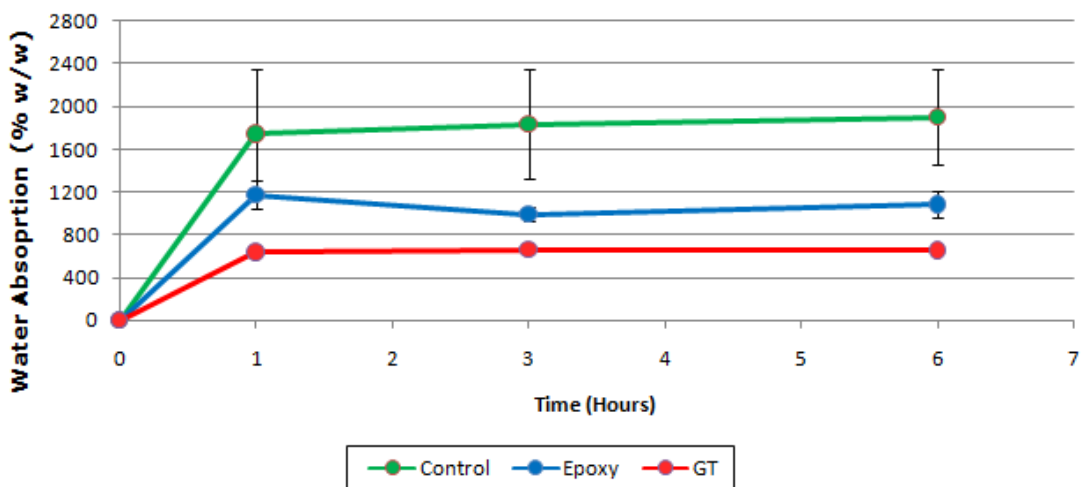


Figure 4-10: Water absorption capability of 4th generation scaffolds crosslinked with epoxy compound. The results of 4th generation GT-crosslinked scaffold are included for comparison.

As a result of crosslinking with the epoxy compound, the scaffolds absorbed less water in comparison with the control samples. The epoxy-crosslinked scaffolds absorbed 1084.4% of initial dry weight after 6 hours immersion in de-ionised water, whilst the control samples absorbed 1903.9% of their initial dry weight. The reduction of water absorption capacity may be the result of crosslinking and was in agreement with the results reported in the literature (Sung *et al.*, 1996a; Vargas *et al.*, 2008). Vargas *et al.*, (2008) suggested that a decrease in water absorption may be caused by the chemical crosslinking of lysyl amino functional groups and a phenomenon known as *masking*, during which the amine groups would be blocked by epoxy functional groups. It is suggested that swelling may be decreased as a result of crosslinking due to reduced elasticity of the structure which hinders swelling in water and prevent water absorption

at the same level of control samples (Tasselli *et al.*, 2013; Patil *et al.*, 2000; Yoon *et al.*, 2003).

Similar to the results shown for HMDI-crosslinked scaffold, epoxy showed higher water absorption ability in comparison with GT. The water absorption of GT-crosslinked scaffolds was 656.2% after 6 hours of incubation in de-ionised water, which is 0.61 times less than the epoxy-crosslinked scaffold. Glutaraldehyde contributes to a higher degree of crosslinking in the structure. Glutaraldehyde molecules are much shorter than epoxide (Sung *et al.*, 1996). A shorter crosslinking agent can lead to higher crosslinking density (Allen *et al.*, 2006). This will ultimately lead to a more compact and tighter structure, less free space between gelatin molecules and hence less water absorption within GT-crosslinked scaffolds (Miles *et al.*, 2005). Shorter GT molecules led to a more compact network comparing with the one crosslinked with longer epoxy molecules. This allows higher water absorption within the structure crosslinked with epoxy compound than GT-crosslinked samples.

3. Iridoid Glucosides (Genipin)

3.1. Introduction

The genipin has a long history for applications such as a herbal medicine in oriental cultures (Akao *et al.*, 1994) and a precursor for the dark blue pigment in the food industry (Touyama *et al.*, 1994). As a crosslinking agent, genipin has been studied as an alternative to the traditional chemical crosslinkers such as GT (Bigi *et al.*, 2002). In comparison with GT, the samples crosslinked with genipin showed similar enzymatic degradation resistance to GT-crosslinked samples (Sung *et al.*, 1998). This shows promising potential of genipin in providing tissue stability at physiological conditions. Liang *et al.*, (2003) reported application of genipin in preparation and crosslinking of gelatin microspheres for drug delivery systems. Genipin-crosslinked microspheres were compared with GT-crosslinked ones and it was found that the former swell significantly less than the latter. This may be due to the bulky heterocyclic structure of genipin that was discussed in Chapter 1, Section 7.4. The study also reported a significantly lower inflammatory reaction after implantation when compared with GT-crosslinked samples (Liang *et al.*, 2003). Liu *et al.*, (2003) used genipin as a crosslinking agent for bone tissue engineering scaffolds, comprising of gelatin and hydroxyapatite. The cytotoxicity of crosslinked-composite with genipin was compared with sample crosslinked with GT and reported that genipin samples were 10,000 times less cytotoxic in the cell viability assays (Liu *et al.*, 2003). Huang *et al.*, (1998) reported applications of genipin as fixing agents for biological tissue applications used as prosthesis. Genipin-fixed samples were compared with GT- and epoxy-fixed specimen. It was reported that genipin and GT-fixed tissues showed a higher resistance against degradation in comparison with epoxy-fixed tissue after subcutaneous implantation in mice (Huang *et al.*, 1998). These results show that by offering comparable enzymatic degradation resistance and better biocompatibility, genipin has the potential to be considered as a viable alternative for crosslinking biomaterials.

3.2. Crosslinking Method

4th generation gelatin scaffolds were crosslinked using the method described by Bigi *et al.*, with some modifications (Bigi *et al.*, 2002). The prepared scaffolds were immersed overnight (16 hours) in Phosphate Buffered Solution (PBS) of genipin with concentration of 1% w/v (0.005% mol/v) under moderate shaking at 20°C. This molar concentration is equivalent to the molar value of 0.50% v/v GT solution used in Chapter 3 and allows direct comparison of these two crosslinkers based on their molar activity. The calculation for determining necessary mass for preparing solution with this concentration is provided in Appendix 3. Yao *et al.*, (2004) reported that 1% w/v genipin concentration resulted in an optimum gelatin crosslinking index of 74% and higher concentration did not lead to a higher crosslinking index (Yao *et al.*, 2004). The scaffolds were repeatedly washed with de-ionised water and frozen before lyophilisation. Lyophilisation was performed under vacuum pressure of 0.250 mbar and temperature of -40°C.

3.3. Results

3.3.1. Visual Description of Scaffolds

Gelatin scaffolds crosslinked with genipin and the internal section of the sample are shown in Figure 4-11-(A) and (B), respectively. As discussed in Chapter 1, Section 7.4 the reaction of genipin with the lysine, hydroxylysine, and arginine residues of proteins such as gelatin results in a dark blue colour seen in Figure 4-11 (Touyama *et al.*, 1994). Genipin solution penetrated through the scaffold as the internal section of scaffold showed uniform blue colour in the depth of the sample as shown in Figure 4-11-(B).

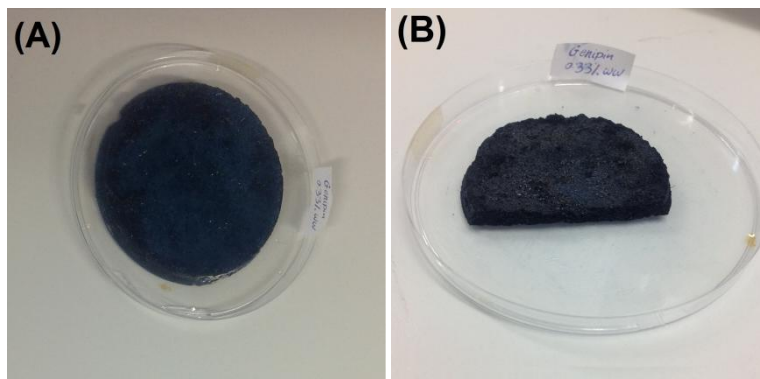


Figure 4-11: Visual features of the 4th generation gelatin scaffolds crosslinked with genipin. (A) The top view of crosslinked scaffold, the scaffold showed the signature dark blue colour that was caused by reaction of genipin with amino acid groups of gelatin at neutral pH, (B) the genipin solution was penetrated in the internal parts of sample and genipin-gelatin reaction was apparent from blue colour in the scaffold internal segment.

Upon close inspection the porosity dispersion of the scaffolds were more irregular and had disordered pore shapes. The edges of the scaffold were covered with cracks and hollow spaces and were not as smooth as scaffolds crosslinked using epoxy. Long duration of soaking (16 hours), accompanied with mild agitation may have resulted in over-swelling of the scaffold, and eventually caused coarser surfaces and edges. In addition, crosslinking gelatin scaffolds using genipin is reported to induce structural changes to the gelatin macromolecular structure (Panzavolta *et al.*, 2011). This is attributed to the slow crosslinking kinetics of genipin relative to the faster rate of gelatin dissolution. Crosslinking at room temperature may have been another factor contributing to irregular and distorted pore shapes. Higher crosslinking temperature has been reported to increase the pore size of the gelatin structure (Sarem *et al.*, 2013). Further discussion regarding the microstructure of the scaffolds would be presented in the SEM analysis segment (Section 3.3.5).

3.3.2. Fourier Transform Infra-Red Spectroscopy (FT-IR)

Figure 4-12 shows the FT-IR spectrum of genipin-crosslinked gelatin scaffolds in comparison with the control samples. Gelatin main FT-IR absorptions assigned to amide I, II, and III, were at 1628, 1539, and 1235 cm⁻¹, respectively (Haroun and El Toumy,

2010; Hashim *et al.*, 2010; Payne *et al.*, 1988; Jackson *et al.*, 1995). For the crosslinked scaffold, the intensity of absorption for amide III band at 1235 cm^{-1} was higher than control sample. Panzavolta *et al.*, (2011) reported a similar FT-IR spectrum of genipin-crosslinked gelatin samples. This is assigned to relatively higher order in samples (Panzavolta *et al.*, 2011).

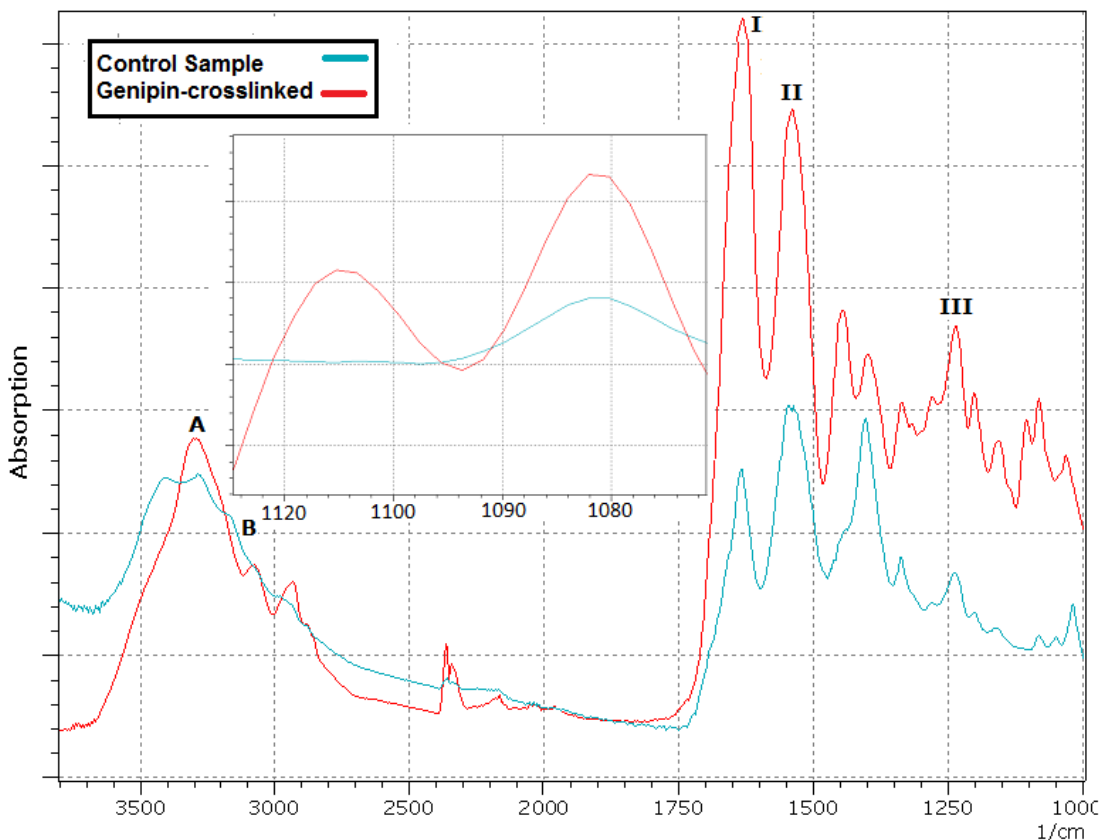


Figure 4–12: The FT-IR spectrum of 4th generation gelatin scaffolds crosslinked with genipin. The inset part of the Figure shows the absorption peak at 1105 cm^{-1} assigned to unreacted genipin.

Reaction of genipin with gelatin includes the conversion of primary amine groups to secondary amines (Mi *et al.*, 2000). This is reflected in the FT-IR spectrum of the crosslinked sample by the decrease in relative absorbance of the amide II peak (at 1550 cm^{-1}) to the absorbance of amide I in the comparison with the control. The newly formed peaks at 1414 cm^{-1} is caused by the ring stretching mode in the genipin molecules and appeared after crosslinking with genipin (Butler *et al.*, 2003). Comparing crosslinked and the control sample spectra showed a new peak at 1105 cm^{-1} which was

absent in the control sample spectrum (The inset part of Figure 4-12). This peak is assigned to the C-O-C stretching of the unreacted genipin olefinic ring (Mi *et al.*, 2000). As discussed in Chapter 1, Section 7.4, the reaction of genipin with gelatin includes a ring opening which includes the substitution of C-O-C bonds in cyclic skeleton ring of genipin with C-N bonds between genipin and gelatin (Sung *et al.*, 1999a). As the crosslinking reaction proceeds, unreacted genipin within the solution would be consumed and thus it is expected that intensity of C-O-C peak be subtle. Observation of this peak at any concentration of genipin can be the sign of excessive genipin accumulation within the reaction vessel. The magnified inset of Figure 4-12 showed that the crosslinked samples may have contained unreacted genipin compounds in this study. However, current concentration of genipin (1% w/v) was chosen deliberately to be able to compare the effect of each crosslinker at similar molar concentration with 0.50% v/v GT. A separate study regarding the optimum concentration of genipin for crosslinking gelatin scaffolds can be the focus of future works.

3.3.3. Mechanical Properties of the Scaffolds

Table 4–5 lists the mechanical properties of the genipin-crosslinked scaffolds, control samples, and the scaffolds crosslinked with GT.

Table 4–5: Mechanical properties of 4th generation gelatin scaffolds crosslinked with genipin. The results were compared with GT-crosslinked scaffolds.

Sample	Tensile Strength (kPa)	Young's Modulus (kPa)	Tensile Strain (%)
Control	80.8 (± 4)	0.9 (± 0.1)	114.8 (± 9)
Genipin	130.8 (± 25)	9.3 (± 1)	15.7 (± 2)
GT	239.5 (± 70)	2.44 (± 0.4)	30.2 (± 5)

The tensile strength of the genipin-crosslinked scaffolds was 130.8 kPa. This was significantly higher than control samples ($p \leq 0.05$). Bigi *et al.*, (2002) showed that tensile strength of the gelatin films crosslinked with the same genipin concentration as this study was 1.20 ± 0.20 MPa (Bigi *et al.*, 2002). This is 9 times higher than the results prepared in this study. The difference may be explained in terms of the effect of porosity on the scaffolds mechanical properties. As discussed earlier in Chapter 3, Section 1.2.3, porosity may lead to an elevated level of local stress across the structure which will lead to structural failure at lower forces (Liu *et al.*, 2006).

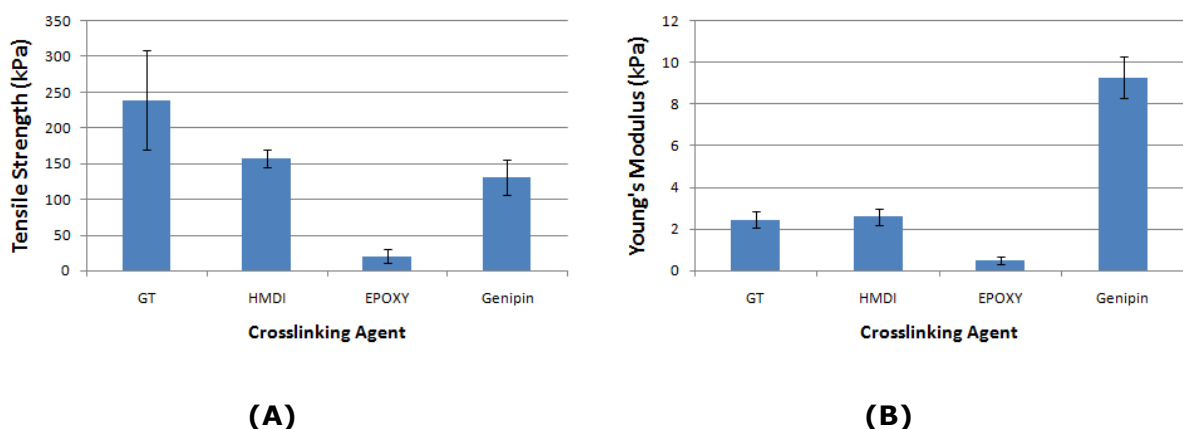
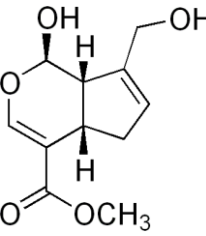
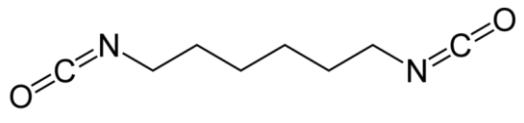
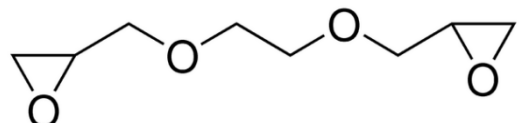


Figure 4–13: The mechanical properties of gelatin scaffolds crosslinked with 4 different crosslinking agents; (A) the tensile strength of scaffolds crosslinked samples, (B) the Young's modulus of crosslinked samples.

Figure 4-13 further compares the mechanical properties of scaffolds crosslinked with 4 alternative crosslinking agents used in this Chapter. GT-crosslinked scaffolds produced the highest tensile strength amongst tested crosslinking agents (Figure 4-13-A). Glutaraldehyde is one of the most reactive crosslinking agents (Khor, 1997). The reaction rate of GT is directly compared with genipin and is showed to be faster (Sung *et al.*, 1999a). This can justify relatively higher tensile strength of GT-crosslinked samples. The epoxy-crosslinked scaffolds, on the other hand, produced the lowest tensile strength amongst the tested samples. When the Young's modulus of samples was compared, the genipin-crosslinked scaffolds showed the highest value (Figure 4-13-B). Table 4-6 makes a comparison amongst the structure of all crosslinking agents used in this study. The epoxy has the longest and genipin has the shortest molecular structure amongst all four crosslinking agents. As discussed earlier in Section 1.3.3 of this Chapter, the molecules chain length can impact elasticity (Mabilleau *et al.*, 2006), brittleness (Patil *et al.*, 2000; Caycik and Jagger, 1992), and crosslinking density (Nakka *et al.*, 2011). Crosslinking using genipin significantly increased the Young's modulus of the scaffold in comparison with the control samples. In comparison with Epoxy, the other three crosslinking agents (i.e.: HMDI, GT, genipin) showed a higher Young's modulus. These sets of results showed the impact of crosslinkers molecular weights on the efficiency of crosslinking and mechanical properties of final products.

Table 4–6: A comparison between the molecular structure of crosslinking agents used in this study.

Compound	Molecular Structure	Number of backbone atoms	Reference
Genipin		-	(Butler <i>et al.</i> , 2003)
GT		5	(Khor, 1997)
HMDI		6	(Khor, 1997)
Epoxy		8	(Sung <i>et al.</i> , 1996b)

However, one should note that the duration of crosslinking for genipin was longer than GT crosslinking (12 hours and 3 hours, respectively). The choice of current crosslinking time is based on the method reported by Bigi *et al.*, (2002) and by considering slow reaction rate of genipin (Sung *et al.*, 1999a). Performing a comparative study with similar crosslinking duration for both GT and genipin in future study may provide a better understanding about relative efficiency of each of these crosslinkers.

3.3.4. Scaffolds Thermal Analysis

Table 4–7 shows the thermal analysis results obtained for the 4th generation gelatin scaffolds crosslinked with genipin. The results of thermal analysis for GT-crosslinked scaffolds are included for comparison. Crosslinking the gelatin scaffolds with genipin increased the denaturation temperature from 48.1°C for the control samples to 87.6°C. This value was higher than the GT-crosslinked scaffold as well as all other crosslinking agents used in this study. Bigi *et al.*, (2002) reported similar results for gelatin film crosslinked using genipin. Increasing the denaturation temperature as a

result of genipin crosslinking shows that genipin can be an effective crosslinking agent (Huang *et al.*, 1998).

Table 4-7: The results of thermal analysis of the 4th generation gelatin scaffolds crosslinked using genipin. Thermal analysis results of scaffold crosslinked using GT are further compared.

Sample	Denaturation Temperature (°C) (T_d)	Enthalpy of Transition (ΔH) (J.g ⁻¹)
Control	48.1 (±6.9)	-25.7 (±16.7)
Genipin	87.6 (±0.3)	-12.0 (±0.2)
GT	84.5 (±1.5)	-16.3 (±0.9)

Genipin-crosslinked scaffolds showed a higher denaturation temperature in comparison with GT-crosslinked samples. As discussed in Chapter 1, Section 7.1, GT-crosslinking occurs through Schiff base formation and aldehydic reactions with amine groups of gelatin, involving the formation of tertiary amines which are more stable than the Schiff base (Bigi *et al.*, 2002; Sung *et al.*, 2001), this may have led to a higher denaturation temperature for the genipin-crosslinked scaffolds. As for the higher denaturation temperature of genipin-crosslinked scaffold comparing with epoxy and HMDI-crosslinked samples, smaller molecular chains and the subsequent lower elastic nature of covalent bonds can be a potential reason for such thermal characteristics (Miles *et al.*, 2005). Chemical crosslinking usually leads to a reduction in the negative value of enthalpy of transition; this was the case for genipin-crosslinked scaffolds where the enthalpy of transition was reduced from -25.7 to 12.0 J.g⁻¹. This is caused by the reduction of hydrogen bonds and the establishment of covalent bonds, as discussed in Chapter 3, Section 1.2.4 (Achet and He, 1995; Dardelle *et al.*, 2011).

3.3.5. Scaffolds Microstructure Analysis

Surface microstructure of the genipin-crosslinked scaffold is shown in Figure 4-14 (A-D). In comparison with the microstructures of the epoxy-crosslinked scaffolds, the samples showed larger and a more distorted structural texture. This is in agreement with the visual features presented earlier (Section 3.3.1). As discussed earlier, the slower reaction kinetics of genipin reaction in comparison with other crosslinking agents may

have caused the distortion and larger pore size (Sarem *et al.*, 2013). The average pore size of the genipin-crosslinked scaffolds was $520\mu\text{m}$ (± 163). The average pore size of the 4th generation scaffolds crosslinked with 0.50% v/v GT was $245\mu\text{m}$. The average pore size of scaffolds crosslinked using HMDI and epoxy were 220 and $389\mu\text{m}$, respectively. This shows a significant increase in the pore size in comparison with both the control and GT-crosslinked scaffolds that have been previously discussed ($p\leq 0.05$). Panzavolta *et al.*, (2011) have attributed genipin crosslinking to induce structural changes to the gelatin macromolecular structure. This effect may have been intensified in this study by long duration of soaking (16 hours) accompanied with mild agitation to cause over-swelling of the scaffold, coarser surfaces and edges.

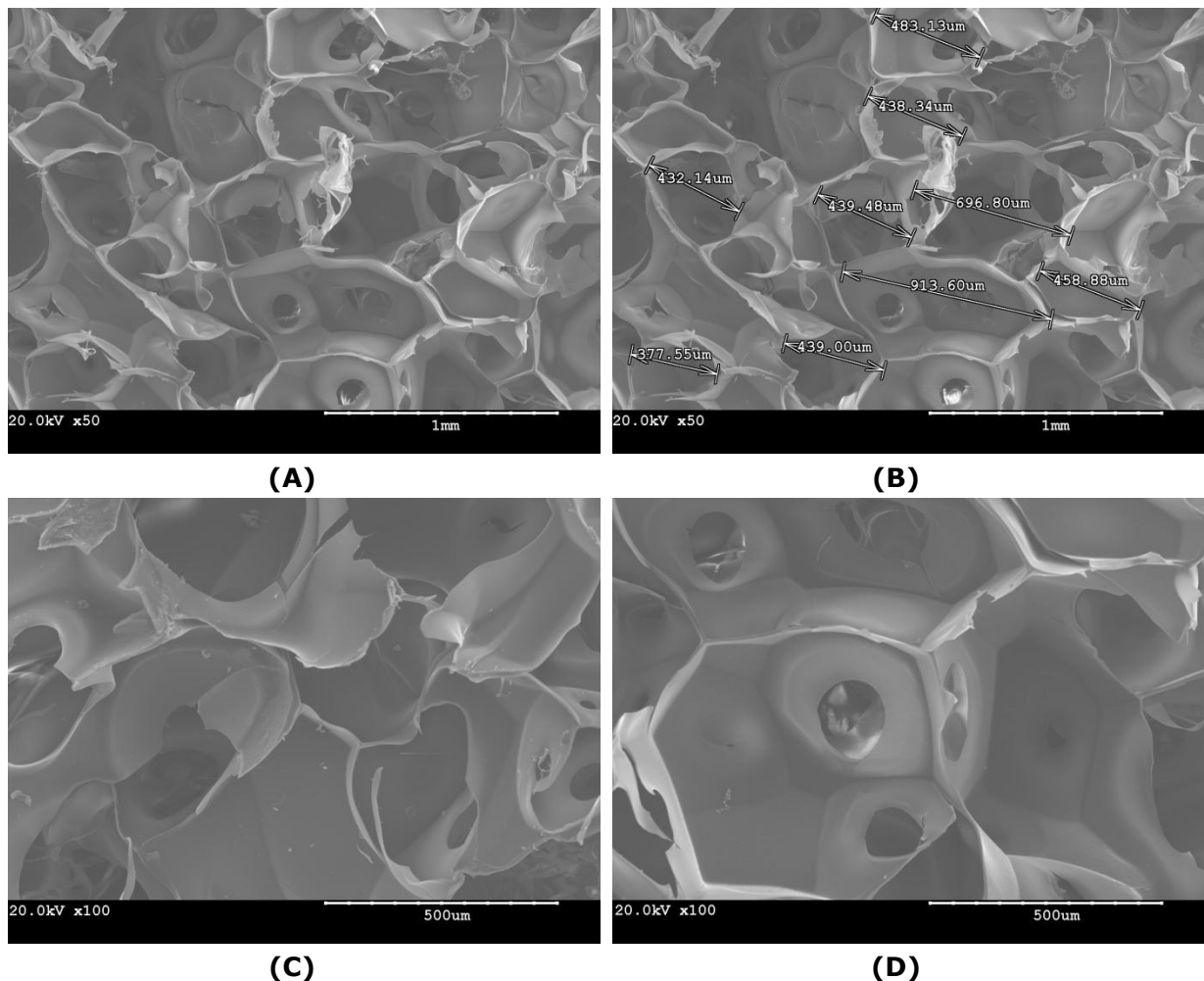


Figure 4-14: SEM images of 4th generation scaffolds crosslinked with genipin at: (A & B) 50x, and (C & D) 100x magnifications. Average pore size of the scaffold was assessed to be $520\mu\text{m}$ (± 163). The images are captured at acceleration voltage of 20kV.

3.3.6. Scaffold Water Absorption

The results of the water absorption capacity of the 4th generation gelatin scaffolds crosslinked with genipin compound are shown in Figure 4-15. The scaffolds crosslinked with genipin showed similar values to the GT-crosslinked samples. After 6 hours incubation in de-ionised water, the sample crosslinked with genipin absorbed 526% of its initial dry weight whilst this value for GT-crosslinked scaffold was 656%. Yao *et al.*, (2004) reported 200% water absorption for gelatin films crosslinked using 1% w/v genipin solution after 24 hours incubation in de-ionised water. Higher water absorption capability reported in this study may be a direct result of more porosity within the structure. The water absorption features of genipin-crosslinked scaffolds was lower than epoxy and HMDI-crosslinked scaffolds and as expected lower than control samples. Genipin does not have a long molecular chain as epoxy and HMDI. Shorter crosslinking molecules lead to a higher crosslinking density within the structure (Allen *et al.*, 2006). Higher crosslink density can lead to fewer available spaces for water molecules accommodation in the structure which lead to less water absorption by genipin crosslinked samples (Miles *et al.*, 2005). Detailed discussion regarding the impact of crosslinking on water absorption is provided in Chapter 3, Section 1.2.6.

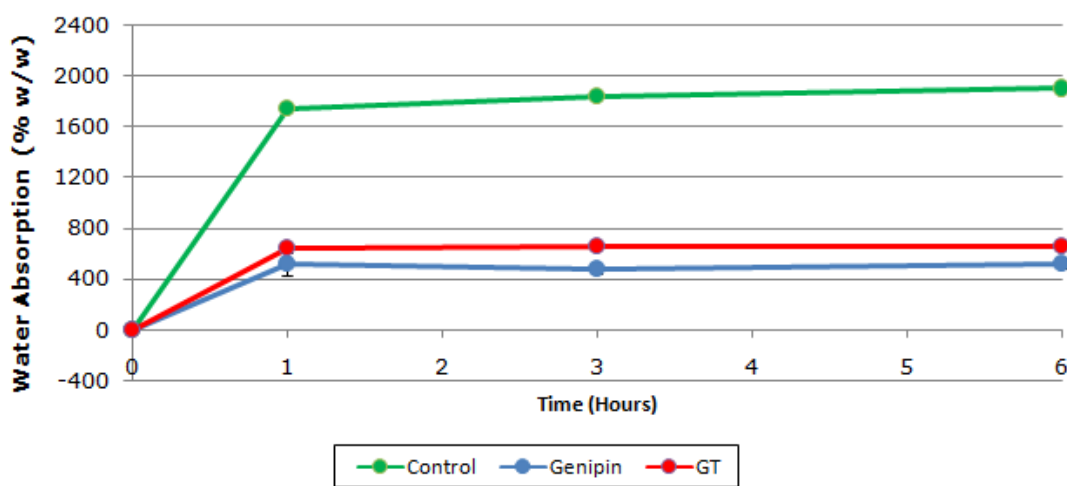


Figure 4-15: Water absorption ability of 4th generation scaffolds crosslinked by genipin compound is compared with GT-crosslinked scaffolds and the control samples.

4. Conclusion

The results of using different types of crosslinking compounds offered some insights into the impact of crosslinkers molecular length and structure on their effectiveness and the sample properties. It was shown that the molecular length and even the type of atoms embedded in the molecular back bone (such as oxygen atoms) had an impact on thermal stability, water absorption, tensile properties, and even the smoothness of the scaffold surface.

Amongst HMDI, Epoxy, and Genipin, the first one was difficult to use, since it required to be processed in a non-aqueous environment (Section 1.2), this required several additional processing steps for the foaming procedure that was used. Genipin and epoxy both offered satisfactory alternatives in terms of microstructure, mechanical strength, and thermal stability. The effectiveness of these crosslinkers was tested through Ninhydrin assays and the results are shown in Figure 4-16. Epoxy-crosslinked samples had the crosslinking index of 39.3% which was lower than genipin at 74.1%. Lower crosslinking index of epoxy compound in comparison with genipin may be due to longer molecular chain of the epoxy which may have hindered diffusion through the scaffold (Sung *et al.*, 1996). A high effectiveness of GT in establishing covalent bonds may explain higher crosslinking index of GT in comparison with all three of these compounds.

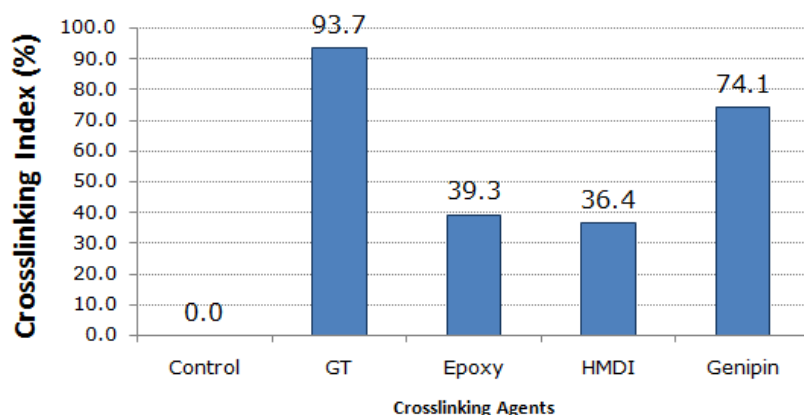


Figure 4-16: A comparison amongst the crosslinking index and tensile strength of the 4th generation gelatin scaffold crosslinked with various crosslinking agents.

In terms of mechanical properties, genipin and HMDI-crosslinked scaffolds had a higher tensile strength than epoxy-crosslinked scaffolds. A comparison amongst the mechanical properties of the scaffold crosslinked with different crosslinking agents was displayed in Figure 4-13. Although, genipin managed to provide a significantly higher tensile strength than epoxy ($p \leq 0.05$), it did not provide a uniform and regular porous structure as compared with epoxy-crosslinked scaffolds. A satisfactory microstructure is crucial for having a successful tissue engineering scaffold (Dehghani and Annabi, 2011). Epoxy-crosslinked scaffold showed a better plastic nature (Table 4-3). Without any intention to ignore the importance of optimal tensile strength, it must be noted that having a less plastic surface structure is not always desirable for cell migration. Less plastic matrices make cell contraction prior to migration more difficult and reduce the rate of cell migration (Griffith and Swartz, 2006). The epoxy-crosslinked scaffolds showed significantly higher flexibility than genipin-crosslinked samples ($p \leq 0.05$). In addition to better flexibility, epoxy samples had higher ability to absorb water than genipin-crosslinked scaffolds. *Wet-ability* of the scaffold at the wound bed is another critical factor to produce a scaffold-wound early bond and the prevention of air pocket formation which can become the sites of bacterial infection (Chvapil, 1982; Yannas and Burke, 1980). Both better flexibility of epoxy-crosslinked scaffolds and higher water absorption allow a better spread over the wound bed and displace the air from the scaffold-tissue interface more effectively than genipin-crosslinked scaffold.

Considering these findings, it was decided to use epoxy as the crosslinking agent of choice for the remainder of research study. To compensate for the lack of scaffold tensile strength, it was decided that a chitosan-gelatin thin layer with a high tensile strength be applied as a backing for the gelatin scaffold so that both the acceptable tensile properties and desirable microstructure/wet-ability can be achieved in a single product.

Chapter 5:

Mechanical Support

(Middle Layer)

Chapter 5 - Mechanical Support, (Middle Layer)

1. Introduction

Considering the lack of mechanical properties in the epoxy-crosslinked scaffolds, in this Chapter a thin membrane of chitosan-gelatin is prepared and characterised to function as a mechanical support for the porous gelatin scaffolds. Gelatin and chitosan are both frequently used as biomaterials in variety of applications. Chitosan is the deacetylated polysaccharide from chitin. Chitin is the second most abundant natural polymer found in nature after cellulose (Rivero *et al.*, 2009). Chitosan or its derivatives pose many advantages including: good film formation, non-toxicity, antibacterial characteristics, and biodegradability (Huang *et al.*, 2007; Jeya Shakila *et al.*, 2012). Similar to gelatin, owing to its similarities to the structure of extracellular matrix, chitosan has been widely studied for tissue engineering applications (Miranda *et al.*, 2011). Application of either chitosan or gelatin individually includes advantages such as fat binding capability, wound healing activities, hydrophilicity, biodegradability, with positive impact on cellular adhesion (Piotrowska *et al.*, 2008; Yang *et al.*, 2004; Zhang *et al.*, 2008; Li *et al.*, 2009b; Awad *et al.*, 2004; Moscato *et al.*, 2008). Several researchers investigate application of gelatin and chitosan together and as a composite structure in bone tissue engineering (Miranda *et al.*, 2011), skin tissue engineering (Mao *et al.*, 2003), and cardiac tissue engineering (Pok *et al.*, 2013). Huang *et al.*, (2005) reported an extensive study on the impact of gelatin addition to the chitosan membrane and the subsequent change in cell response. The addition of gelatin increased the rate of biodegradation and cell adhesion as well as spreading on the surface of the scaffolds (Huang *et al.*, 2005). Chen *et al.*, (2003) explores the potential of a gelatin-chitosan composite as an *in situ* gel forming component for emergency dressing for wounds and burns. *In situ* gel formation may be used for filling hollow spaces through minimally invasive injection. The use of enzymes such as transglutaminase and tyrosinase to crosslink the chitosan-gelatin substrates is reported to provide final products with desirable mechanical strength (Chen *et al.*, 2003). To take advantage of chitosan

antimicrobial features, gelatin - chitosan combination is reported to be used as a thin coating applied directly onto the perishable foods that would melt away during cooking (Gómez-Guillén *et al.*, 2009). Such antimicrobial coating can eliminate food borne pathogens, improve food quality, and extend its shelf life (Kanmani and Rhim, 2014).

2. Membrane Preparation Method

Gelatin-chitosan composite membranes with composition of a 1:1 ratio were prepared by adding 0.22 grams of chitosan to 10 ml de-ionised water and 1 ml acetic acid under moderate heating. In a separate beaker, 0.22 grams of gelatin was dissolved in 5 ml of de-ionised water under moderate heating. Once the components were dissolved completely both solutions were mixed and stirred for 30 minutes. The mixture solution (8g) was cast in a petri dish with 5.5cm in diameter and 0.7cm in height. The molds were placed at 20°C and 65% RH until drying. The membranes were dried after 2 days and were extracted from the petri dish by peeling off.

To crosslink the membranes using epoxy compound, 370 μ l of epoxy compound was directly added to 16ml of the aqueous solution without pH adjustment. The casting and drying conditions of the samples were similar to the control membranes (non-crosslinked samples). The stirring was continued for several minutes to assure an even distribution of epoxy crosslinker before casting. The solution was cast and dried similarly to the control membranes.

In order to assess the impact of gelatin lack of presence, a pure chitosan membranes were prepared. In the acetic acid aqueous solution (10% v/v), 0.35 grams of chitosan was dissolved, the stirring was performed at 1300 rpm at 60°C for 40 minutes. The casting of solution and drying of the material were performed under similar conditions to the composite membrane.

3. Results

3.1. Visual Descriptions of Membranes

Figure 5-1 shows visual features of the chitosan and gelatin-chitosan membranes. Chitosan has a well characterised film-forming feature which is apparent in the Figure 5-1-(A) (Rivero *et al.*, 2009; Bonilla *et al.*, 2013). The prepared membrane showed to be flexible and foldable. The chitosan membranes were transparent, uniform, homogenous, and thin. The average value of 3 thickness measurements using digital micrometer for the pure chitosan membrane conditioned at 95% relative humidity was 80 μm and showed good thickness regularity throughout its surface area ($\pm 14\mu\text{m}$). Figure 5-1-(B) shows a chitosan film crosslinked using the epoxy compound. Addition of epoxy caused the change of transparency of the membrane as well as increase in thickness. Average thickness of the chitosan membrane crosslinked using epoxy was 140 μm ($\pm 6\mu\text{m}$). The impact of gelatin addition to chitosan is shown in Figure 5-1-(C). The gelatin addition did not have an impact on the transparency of the membrane. Lack of change in transparency can show good miscibility between gelatin and chitosan (Pereda *et al.*, 2011). Since gelatin and chitosan are both hydrophilic biopolymers, they are expected to form a homogenous composite (Rivero *et al.*, 2009). Average thickness of gelatin - chitosan membrane was 100 μm ($\pm 30\mu\text{m}$).

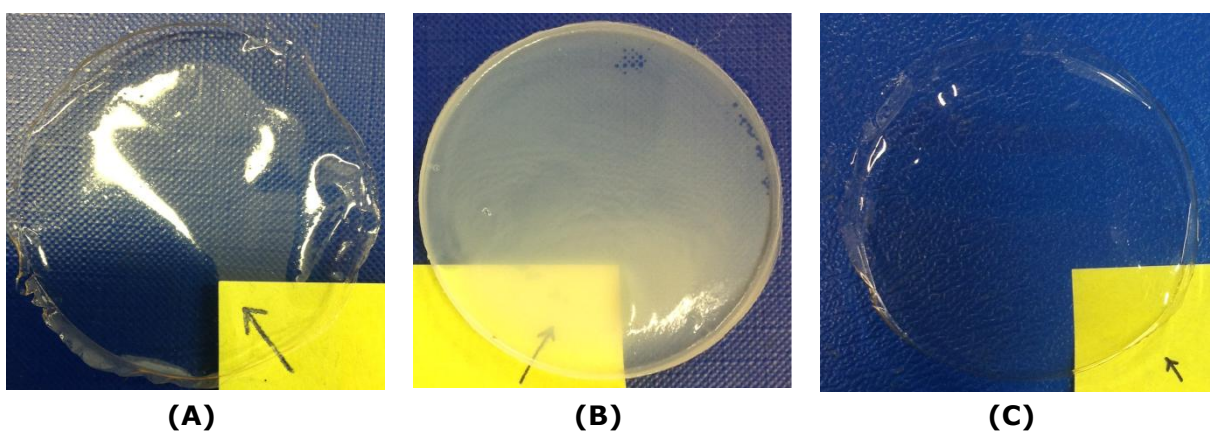


Figure 5-1: Chitosan-based membranes visual descriptions; (A) Pure chitosan membrane without crosslinking, (B) pure chitosan membrane crosslinked using epoxy compound, (C) chitosan-gelatin composite without any crosslinking.

3.2. Fourier Transform Infra-Red Spectroscopy (FT-IR)

Figure 5-2 shows FT-IR spectra of the pure chitosan films and gelatin-chitosan composites in non-crosslinked and crosslinked conditions. The chitosan spectrum showed two strong absorption bands at 1063 and 1149 cm^{-1} which are assigned to C-O and C-O-C symmetrical stretching, respectively (Ostrowska-Czubenko *et al.*, 2009; Huang *et al.*, 2012). The chitosan FT-IR spectrum showed an absorption band at 1280 cm^{-1} which is assigned to the chitosan hydroxyl groups (Butler *et al.*, 2003). Pure chitosan samples also showed a strong absorption intensity at 2868 cm^{-1} causes by chitosan pyranose ring (Pawlak and Mucha, 2003). These absorption peaks are characteristic of the chitosan saccharide structure so verifying the presence of chitosan in the membrane.

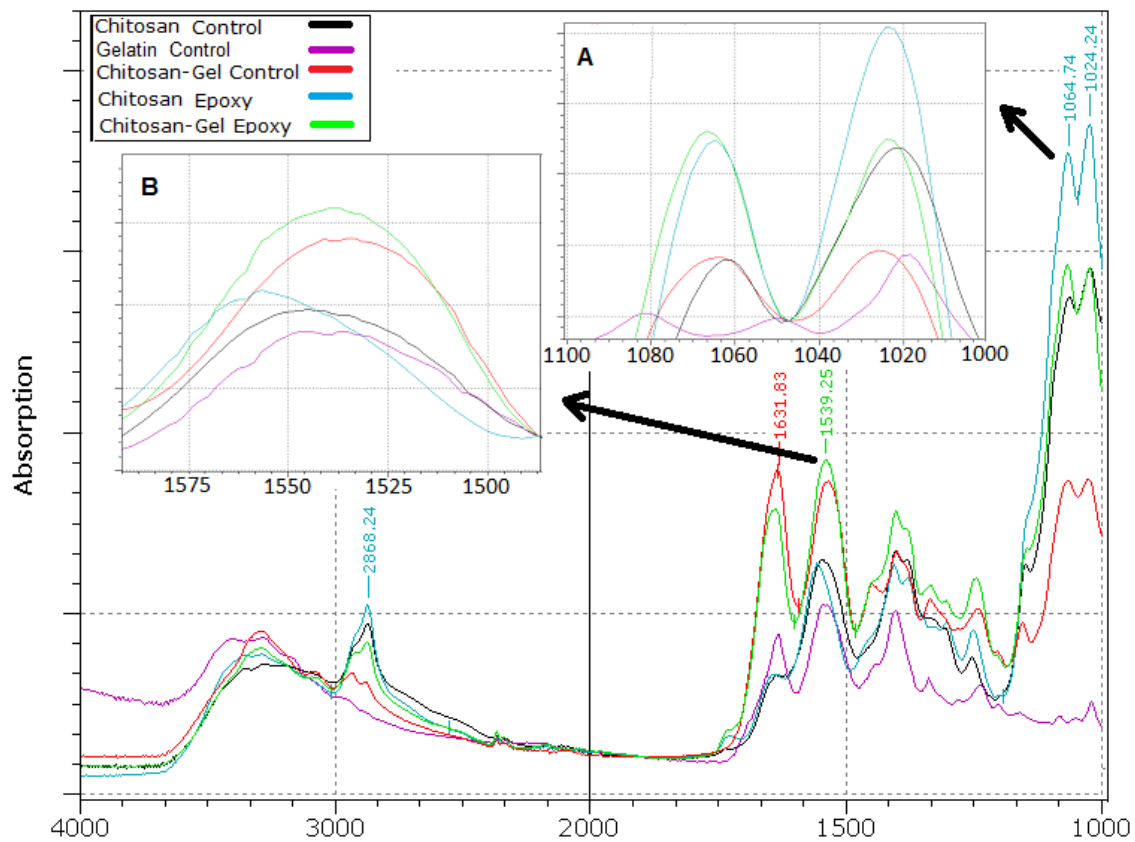


Figure 5-2: FT-IR spectra of pure chitosan and chitosan-gelatin composites in non-crosslinked and crosslinked conditions. The inset (A) shows stronger absorption band at 1070 cm^{-1} in crosslinked samples which is assigned to additional C-O-H groups as a result of crosslinking with epoxy. The inset (B) shows a pronounced shift in amide II absorptions to longer wave number as a result of crosslinking which suggests a structural change after crosslinking.

As discussed earlier in Chapter 3, gelatin spectrum amide absorption bands for amide I, II, and III are located at 1628, 1539, and 1235 cm^{-1} , respectively. In comparison with pure gelatin, the absorption bands affiliated with amide I and II in chitosan spectrum showed a shift toward longer wave numbers. Amide I and II were shown at 1636 and 1544 cm^{-1} resulting from C=O stretching in the acetyl group and -NH₂ bending, respectively (Sarem *et al.*, 2013; Pereda *et al.*, 2011). Upon addition of gelatin into structure, amide I and II absorptions shifted towards the lower wave numbers. Due to the existence of the reactive amine and hydroxyl groups in chitosan, it can be readily altered chemically, and these functional groups play an important role in the formation of inter/intra molecular hydrogen bonds between gelatin and chitosan (Ostrowska-Czubenko *et al.*, 2009; Sagnella *et al.*, 2005). Shift of absorption bands to a lower wave numbers showed interactions between chitosan and gelatin (Sarem *et al.*, 2013). In addition, the gelatin-chitosan composite showed higher intensity in the range of 1500-1700 cm^{-1} which corresponds with the amino and carbonyl moieties. Pereda *et al.*, (2011) reported similar increase in the FT-IR spectrum intensity in this region and concluded that it may be indicative of electrostatic interactions between the gelatin and chitosan. The samples containing chitosan showed an absorption band at 1710 cm^{-1} which may be due to the protonated carboxylic groups in the remaining acetic acid from solution (Butler *et al.*, 2003).

Crosslinked samples had a relatively strong absorption band at 1070 and 1250 cm^{-1} in comparison with the control sample. These two absorption bands are assigned to additional C-O-H and C-O-C functional groups associated with the occurrence of crosslinking (Vargas *et al.*, 2008). A strong absorption band at 2870 cm^{-1} occurs as a result of the C-H bond stretching vibrations (Huang *et al.*, 2012; Natesan *et al.*, 2001). The absorption of crosslinked samples (both chitosan and chitosan-gelatin samples) showed a higher intensity at 2925 cm^{-1} which is the direct result of more alkyl groups (-CH₂ and -CH₃) of the epoxy compound used for crosslinking (Cestari *et al.*, 2012). Comparing the control and crosslinked spectra shows a noticeable shift towards longer

wave numbers for amide I and II absorption peaks. Amide II band of chitosan was shifted from 1545 cm^{-1} in the control sample to 1556 cm^{-1} in the crosslinked sample. As discussed in Chapter 3, Section 1.2.2 changes in the gelatin amide absorption range may be indicative of structural change in the gelatin macromolecules structure (Payne *et al.*, 1988). Such shift suggests the diminished structural integrity in the triple helix structure of gelatin.

3.3. Mechanical Properties of the Membrane

Table 5–1 lists the mechanical properties of gelatin-chitosan membranes in non-crosslinked and crosslinked conditions. Due to high water absorption ability of chitosan, the samples were conditioned at 65% RH instead of 95% RH.

Table 5–1: Mechanical strength of pure chitosan and chitosan-gelatin composite membranes in crosslinked and non-crosslinked conditions. Note that stress unit is changed from kPa to MPa from previous similar tables.

Sample	Tensile Strength (MPa)	Young's Modulus (MPa)	Tensile Strain (%)
Chitosan (Control)	35.7 (± 2)	3.4 (± 0.4)	16.0 (± 2)
Chitosan (crosslinked)	0.9 (± 0.3)	0.2 (± 0)	5.3 (± 1)
Chitosan-Gelatin (control)	26.1 (± 2)	17.3 (± 0.4)	3.9 (± 1)
Chitosan-Gelatin (crosslinked)	1.1 (± 0.3)	0.1 (± 0)	10.9 (± 3)

The results showed that both crosslinked chitosan and crosslinked chitosan-gelatin samples were significantly weaker than their respected control samples ($p \leq 0.05$). As a result of crosslinking, the tensile strength of pure chitosan membranes reduced from 35.7 to 0.9 MPa. Young's Modulus of the membrane was decreased from 3.4 to 0.2 MPa. Deterioration of mechanical strength in the gelatin-chitosan composites after crosslinking has been reported by other researchers (Chen *et al.*, 2003; Pereda *et al.*, 2011; Kostko *et al.*, 2003). This phenomenon is similar to the results observed in crosslinking gelatin scaffolds with epoxy in Chapter 4. Chen *et al.*, (2003) reported the decrease of gelatin-chitosan strength after enzymatic crosslinking. It was suggested that

in the gelatin-chitosan composite, overtime gelatin and chitosan individually forms pockets of gelatin-rich and chitosan-rich regions through gradual molecular rearrangement. This may lead to gelatin and chitosan chains collapse and the loss of strength (Chen *et al.*, 2003). Pereda *et al.*, (2011) reported reduction of chitosan membrane tensile strength as a result of gelatin addition and speculated that it may be due to the impact of gelatin on the reduction of chitosan crystallisation ability. Kostko *et al.*, (2003) speculated that crosslinking chitosan-gelatin composites initially increases the strength of the sample by establishing the covalent grafting of gelatin chains onto chitosan backbones, however the composite may breakdown as a result of a slow diffusion-like process, since the grafted gelatin chains aggregate to form re-natured helical structure. As this slow migration of the gelatin molecular chains is controlled through diffusion, its rate may be increased using plasticisers (Arvanitoyannis *et al.*, 1997). Martucci and Ruseckaite (2010) showed that crosslinking agents with a plasticising effect can cause the reinforcing effect of crosslinkage to be counterbalanced by crosslinker acts as an internal plasticiser (Martucci and Ruseckaite, 2010). Considering the plasticising effect of epoxy due to C-C-O repetition units in the epoxy molecule (Price, 1986; Mabilleau *et al.*, 2006), it may facilitate such rearrangement, counterbalancing the reinforcing effect of crosslinking and caused reduction of strength. Such molecular transitions in the structure of samples may have caused the reduction in the tensile strength reported in Table 5-1.

Crosslinking the membrane using epoxy increased the sample tensile strain and elasticity. The reduction of Young's modulus of the membrane of the samples may be a result of crosslinking using epoxy compound and its long elastic macromolecules which bring more elasticity into the structure and was discussed in details in Chapter 4, Section 2.3.3 (Price, 1986; Mabilleau *et al.*, 2006).

3.4. Membrane Thermal Analysis

A typical thermograph of the chitosan membrane is shown in Figure 5-3 in crosslinked and non-crosslinked conditions. Thermal analysis spectra of chitosan

constituted of two main thermal events: (1) a first peak between 130 and 150 °C, (2) a second peak between 270 and 295 °C. This is common thermal degradation behaviour exhibited by chitosan (Nieto and Peniche-Covas, 1991).

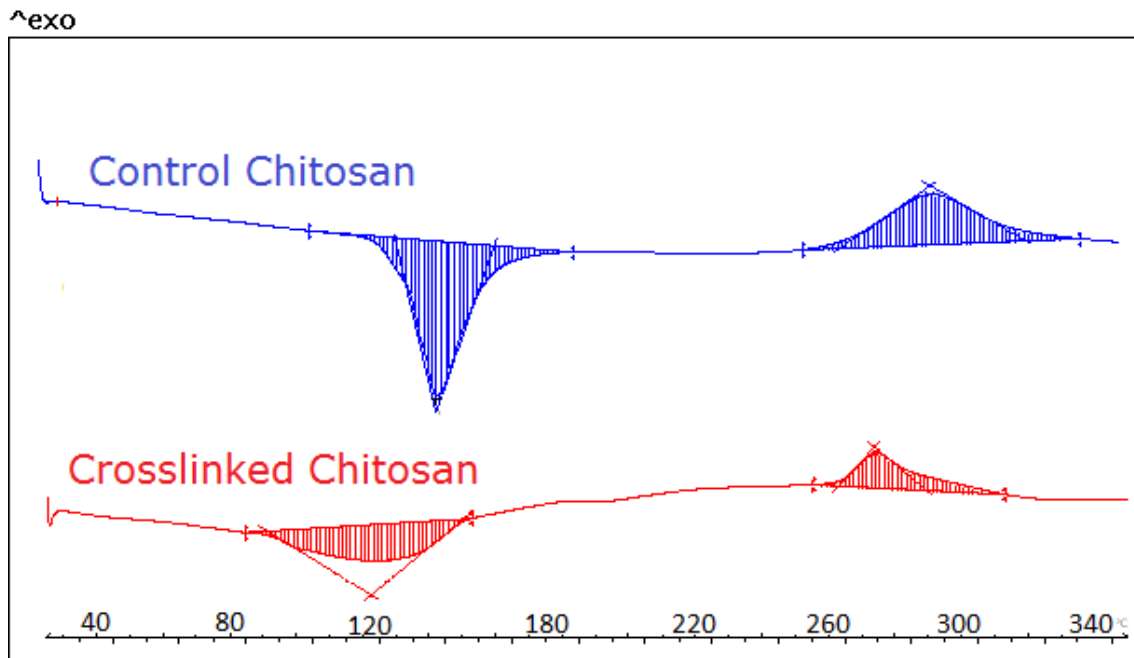


Figure 5–3: A typical thermograph of chitosan consists of two thermal events (Qu *et al.*, 2000). Here, the thermographs of chitosan membranes are shown in the control and crosslinked states as a typical result.

Table 5–2 lists the thermal characteristics of gelatin-chitosan membranes in crosslinked and the control conditions. The first peak in chitosan thermal spectrum is reported to originate from the evaporation of bound water in association with intermolecular hydrogen bonds between chitosan molecules (Yang *et al.*, 2004; Ostrowska-Czubenko *et al.*, 2009). The noticeably high enthalpy of transition of this peak is observed by other researchers and is attributed to high affinity of water to chitosan structure (Nieto and Peniche-Covas, 1991). As a result of gelatin addition to chitosan, this peak shifted from 145 °C to 154 °C. This event can be associated with much stronger interaction between the samples and water as result of gelatin addition (Qu *et al.*, 2000). As a result of crosslinking the negative value of enthalpy of this peak was decreased. This reduction may be due to covalent bond formation and consumption

of hydrogen bond site removal as discussed in details Chapter 3, Section 1.2.4 (Achet and He, 1995; Gill *et al.*, 2010).

Table 5–2: The results of thermal analysis of chitosan membranes and composite of gelatin-chitosan in non-crosslinked and crosslinked states.

Sample	Endothermic Peak		Exothermic Peak	
	Peak Temp. (°C)	Enthalpy of Transition (ΔH) (J.g ⁻¹)	Peak Temp. (°C)	Enthalpy of Transition (ΔH) (J.g ⁻¹)
Pure chitosan (control)	144.6	-199.0	293.2	+121.7
Pure chitosan (crosslinked)	127.3	-105.9	274.2	+53.5
Gelatin-Chitosan (control)	153.9	-218.9	298.0	+48.8
Gelatin-Chitosan (crosslinked)	166.3	-112.0	269.6	+37.3

The second peak is due to chitosan amine group decomposition (Natesan *et al.*, 2001; Guinesi and Cavalheiro, 2006). The fact that there was only one single peak observed at this portion of spectrum may be associated to the homogeneity of gelatin-chitosan membrane (Qu *et al.*, 2000). The second enthalpy of transition was reduced from 122 J.g⁻¹ in the control samples to 54 J.g⁻¹ in the crosslinked samples. Crosslinking of chitosan with epoxy compound consumes amine groups of chitosan leaving less amine group in the samples (Cestari *et al.*, 2012). The reduction in enthalpy of transition after crosslinking may be due to less free amine groups after crosslinking (Tirkistani, 1998). Apart from an enthalpy reduction, the second peak temperature is reduced from 293 °C to 274 °C after crosslinking. The change of the second peak in the chitosan composites can be attributed to two opposing factors: additional bridging through the chitosan after crosslinking which lead to higher thermal stability and, conformation changes of chitosan leading to lower thermal stability (Gill *et al.*, 2010). The reduction of thermal exothermic peak in crosslinked gelatin-chitosan composite may be an indication for the fact that the former was in effect in the case of this study. Epoxy may be able to reduce the recrystallisation of the structure by disrupting, the junction-zones required for this process

(Price, 1986; Arvanitoyannis *et al.*, 1997; Martucci and Ruseckaite, 2010). A weaker ultra-structure may have caused reduction of enthalpy of transition.

3.5. Membrane Water Absorption

Figure 5–4 shows the water absorption abilities of chitosan and chitosan-gelatin membranes in crosslinked and control conditions. A pure chitosan membrane without any crosslinking disintegrated in water, therefore its water absorption capability could not be reported. Disintegration and difficulty in measuring of the pure chitosan membrane is reported by other researcher (Loke *et al.*, 2000). Crosslinked chitosan showed strong water absorption capability and it was the most hydrophilic material studied in this project. The crosslinked chitosan membrane absorbed 4800% of its initial dry weight after 6 hours immersion in de-ionised water. Excellent water absorption capability of chitosan is due to the abundant presence of amine and hydroxyl groups in its structure (Yang *et al.*, 2004; Li *et al.*, 2009b; Hu *et al.*, 2013).

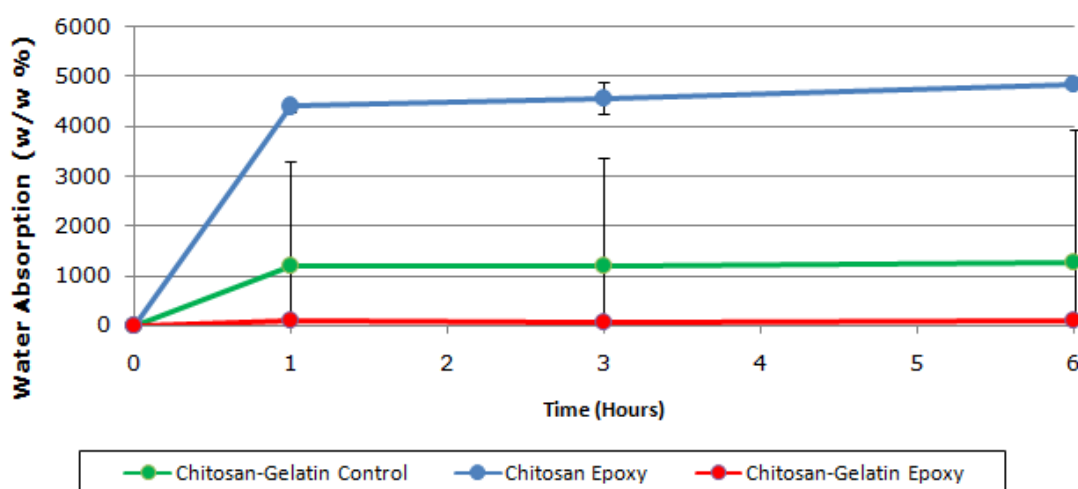


Figure 5–4: Water absorption capability of chitosan and chitosan-gelatin membranes. Pure chitosan membrane in non-crosslinked condition disintegrated in water and its water absorption capability could not be reported.

As a result of gelatin addition to chitosan, the water absorption ability of the membrane was reduced and the obtained values were similar to the results reported for epoxy-crosslinked gelatin scaffolds in Chapter 4, Section 2.3.6. The control chitosan-

gelatin samples absorbed 1300% of their initial dry weight after 6 hours immersion in de-ionised water. The pure gelatin membrane water absorption characteristics are discussed in the next Chapter. Sarem *et al.*, (2013) reported a similar effect of gelatin on the water absorption capability of the chitosan structure. Reduction of the water content as a result of gelatin incorporation in chitosan is believed to be the result of strong interactions between gelatin and chitosan that can displace sites of hydrogen bonding with water (Pok *et al.*, 2013). In this study one of the objectives of middle layer is to assist wound exudate removal from the injury site through water absorption, therefore high water absorption capacity of these samples may facilitate wound healing.

4. Conclusion

Application of chitosan composite above the gelatin scaffold can enhance the water absorption ability of the wound dressing and removal of wound exudates from the wound area. In addition to high water absorption ability of chitosan, application of chitosan-gelatin composite can enhance the mechanical strength of the wound dressing. The gelatin scaffolds prepared in the Chapters 3 and 4 showed a weak mechanical strength. To compensate for this lack of strength, the chitosan was purposefully selected due to its inherent mechanical strength. As the results of mechanical tests showed in Section 3.3, crosslinking chitosan membranes with epoxy caused the tensile strength to decrease. This is against the main purpose of applying chitosan membrane as a mechanical support to the gelatin scaffolds. Thus, it was decided to use chitosan membranes without any crosslinking. However, as it was discussed in water absorption tests (Section 3.5), chitosan membranes without crosslinking are prone to disintegration in contact with water, hence it was decided to sandwich the chitosan membrane between gelatin scaffold and a third membrane to preserve it from disintegration and minimising the impact of water absorption. A simple plasticised gelatin membrane was chosen for the purpose of acting as the third layer and its preparation method is discussed in the next Chapter.

Chapter 6:

Plasticised Cover

(Top Layer)

Chapter 6 - Plasticised Cover, (Top Layer)

1. Introduction

A general introduction into gelatin properties and production methods was given in Chapter 1, Section 6.2. In this Section, an introduction into some of the gelatin applications as a biomaterial will be provided. Large volumes of gelatin are used annually by food and medical industries worldwide. As of 2007, 326000 tonnes of gelatin was produced worldwide and annual growth rate of gelatin production has been 3-4% in the past seven years (Gómez-Guillén *et al.*, 2009). Features such as biodegradability and the possibility of cheap large-scale production turn gelatin into an attractive biomaterial (Koob and Hernandez, 2003). Gelatin was one of the earliest compounds reported to be applied as a biomaterial (Thomazine *et al.*, 2005). Addition of gelatin to other biopolymers such as chitosan, or synthetic polymers such as poly-caprolactone, caused an increase in cell attachment to biomaterial surface (Huang *et al.*, 2005; Lee *et al.*, 2012). This favourable response from cells to gelatin presence may be due to peptide sequences, such as RGDs (known to promote cell adhesion and migration) that remain in gelatin macromolecular structure from its collagen precursor (Hajiali *et al.*, 2011; Miranda *et al.*, 2011; Awad *et al.*, 2004; Moscato *et al.*, 2008). These features cause gelatin to be used for a variety of commercial applications in the pharmaceutical and medical fields, such as sealants for vascular prostheses (Sung *et al.*, 1999a; Young *et al.*, 2005; Elvin *et al.*, 2010), bone-repairing matrices (Azami *et al.*, 2010), blood plasma expander (Dong *et al.*, 2006; Choi *et al.*, 1999), wound healing agents and artificial skin (Noorjahan *et al.*, 2004; Hong *et al.*, 2001), and scaffolds for tissue engineering (Lee *et al.*, 2005; Mao *et al.*, 2003; Yeh *et al.*, 2011). Gelatin-based compound was amongst the first carriers for control drug release (Gómez-Guillén *et al.*, 2009) and antimicrobial compound such as silver-nano particles and nano-clays for biomedical and food packaging (Kanmani and Rhim, 2014). These types of packaging can be used as a replacement for petroleum-based packaging (Ma *et al.*, 2013).

2. Membrane Preparation Method

Glycerol is frequently used to improve plasticity of gelatin-based membrane (Gómez-Guillén *et al.*, 2009; Thomazine *et al.*, 2005). In this study, the gelatin membranes were prepared with addition of glycerol as a plasticiser according to the method described by Ma *et al.*, (2013). A gelatin solution with concentration of 20% w/v was prepared. The Glycerol was added to the solution at a ratio of 0.4:1 glycerol : protein w/w (Ma *et al.*, 2013). The mixture solution (8g) was cast in a petri dish with 5.5cm in diameter and 0.7cm in height. Based on practical observations, the optimum temperature for gelatin casting is 60°C. This casting temperature leads to a membrane that is uniform and with the least amount of voids. The cast membranes were left to dry at 20°C and 65% RH. 48 hours was enough for complete solvent evaporation and drying. The membranes were peeled off from the petri-dishes for storage and characterisations.

3. Results

3.1. Fourier Transformed Infrared Spectroscopy (FT-IR)

Figure 6-1 shows the FT-IR spectra of gelatin membranes with and without glycerol. The gelatin spectrum main absorption bands for amide I, II, III, and A and B were located at 1628, 1539, 1235, 3297, and 3073 cm⁻¹, respectively. The origins of these absorptions were discussed in Chapter 3, Section 1.2.2. In Figure 6-1, three main areas of difference were caused as a result of glycerol presence. Addition of glycerol to the gelatin membranes caused appearance of these absorption bands: a peak at 1050 cm⁻¹ assigned to -C-O stretching, an extra absorption at 1167 cm⁻¹ corresponding with -C-C stretching of 2-hydroxyethyl groups, and a stronger than usual absorption at 2987 cm⁻¹ that corresponds with CH₂ and CH vibrations of the O-methylene (Calvino-Casilda *et al.*, 2011). Moreover a gelatin membrane with the glycerol addition shows a slight shift towards higher wave-numbers in the amide II absorption at 1550 cm⁻¹ in comparison with the gelatin without the glycerol. These changes in FT-IR spectrum of samples suggested a successful incorporation of glycerol within gelatin macromolecules.

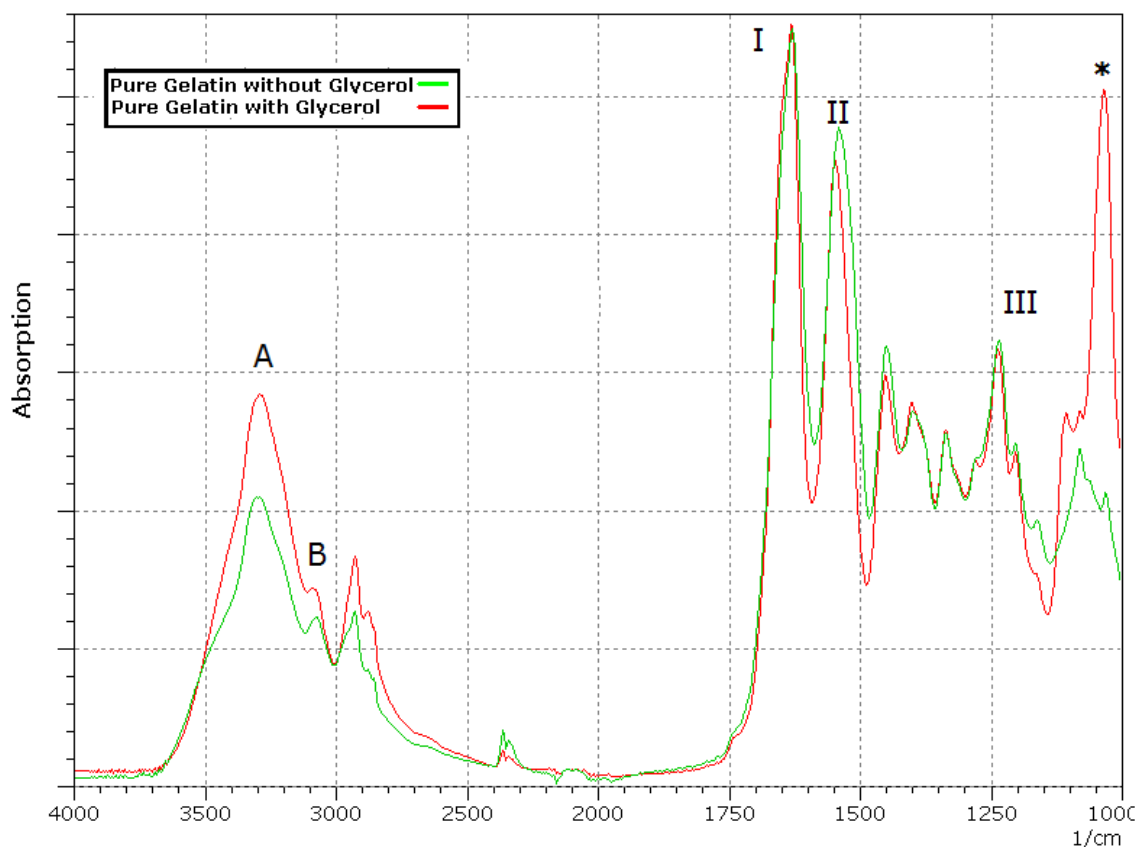


Figure 6–1: The FT-IR spectra of gelatin membranes with and without glycerol. The absorption band at 1050 cm^{-1} is marked with * and indicates incorporation of glycerol in the samples. The gelatin amide I, II, III, A, and B bands are marked in the Figure.

3.2. Mechanical Properties of the Gelatin Membrane

Table 6–1 lists the mechanical properties of the gelatin membrane with and without glycerol addition. Membranes have been crosslinked using the epoxy compound to examine the effect of crosslinking on the mechanical properties of the prepared membranes.

Table 6-1: Mechanical properties of non-crosslinked and crosslinked gelatin membranes prepared in the presence and absence of glycerol as a plasticiser

Sample	Tensile Strength (kPa)	Young's Modulus (kPa)	Tensile Strain (%)
Pure gelatin	3191.3 (± 610)	684.1 (± 401)	19.7 (± 9)
Pure gelatin with glycerol	332.5 (± 113)	5.5 (± 1)	82.0 (± 29)
Gelatin with glycerol crosslinked with epoxy compound	836.0 (± 163)	49.4 (± 6)	19.2 (± 5)

Addition of glycerol to the gelatin membranes significantly reduced the tensile strength of the gelatin membranes ($p \leq 0.05$). Tensile strength of gelatin membrane was reduced from 3191.3 kPa to 332.5 kPa as a result of glycerol addition. Tensile strain was affected in the opposite way as a result of glycerol addition and it was significantly increased ($p \leq 0.05$). Tensile strain of gelatin membrane was increased from 20 % to 82 % as a result of glycerol addition. Reduction of tensile strength and increase in tensile strain as a result of glycerol addition are in agreement with reported results by other researchers (Rivero *et al.*, 2009; Piotrowska *et al.*, 2008; Sobral *et al.*, 2001). The significant decrease of Young's modulus ($p \leq 0.05$) from 684 kPa to 5.5 kPa as a result of glycerol addition is thought to be due to a plasticising effect (Arvanitoyannis *et al.*, 1997). Modifying gelatin membrane less strong and more extendible is due to reduction in interactions between the gelatin chains (Thomazine *et al.*, 2005). Due to their low molecular weight, glycerol molecules are able to be accommodated between gelatin molecules and so act as a lubricant, creating highly mobile regions, improving chain mobility and increase the structures overall plasticity (Díaz *et al.*, 2011; Arvanitoyannis *et al.*, 1997). According to Thomazine *et al.*, (2005) the reduction of the gelatin tensile strength as a result of glycerol incorporation may be due to the reduction of gelatin-gelatin interactions and an increase of the gelatin chains mobility. It is though that upon casting of the membrane, gelatin macromolecules are entangled in a compact and closely packed condition, but glycerol addition allows a structural modification, liberation of compact structure, and causes the consequent decrease in the tensile strength (Arvanitoyannis *et al.*, 1997).

When plasticised membranes are compared, epoxy crosslinking increased the membrane tensile strength. However, crosslinked membrane had significantly lower tensile strength than non-plasticised gelatin membranes ($p \leq 0.05$). Martucci and Ruseckaite, (2010) reported similar results after crosslinking gelatin with a dialdehyde crosslinker with a plasticising effect. In this study it was concluded that the reinforcing effect of the crosslinking is counterbalanced by the crosslinker which may act as an internal plasticiser (Martucci and Ruseckaite, 2010). Thomazine *et al.*, (2005) reported that the incorporation of more than one compound with plasticising effect would exacerbate the reduction of the tensile strength in comparison with the control gelatin sample. This may explain the reduction of tensile strength in gelatin membrane despite crosslinking with epoxy compounds.

3.3. Membrane Thermal Analysis

Table 6-2 lists thermal properties of the gelatin membranes in non-crosslinked and crosslinked states and the effect of glycerol addition to the structure.

Table 6-2: Thermal properties of gelatin membrane and the impact of glycerol addition and crosslinking using epoxy compound on the membrane thermal stability.

Sample	Denaturation Temperature (°C) (T_d)	Enthalpy of Transition (ΔH) (J.g ⁻¹)
Pure gelatin	84.1	-22.2
Pure gelatin with glycerol	65.4	-15.0
Gelatin with glycerol and crosslinked	76.5	-8.1

As a result of the glycerol addition, the denaturation temperature of the membrane was reduced from 84.1°C to 65.4°C. Reduction of the denaturation temperature to 70°C upon the addition of the plasticiser has been observed by other researchers (Sobral *et al.*, 2001). Each glycerol molecule has three hydroxyl groups in its structure. These hydroxyl groups can establish hydrogen bonds with the carboxyl groups of the proteins. It is hypothesised that these hydrogen bonds would replace and disrupt the inter-molecular water bridges in the structures such as collagen triple helix and

weaken inter-protein interactions (Na, 1986). Through the disruption of the hydrogen bonds between the gelatin molecules and increasing polypeptide chains mobility, glycerol can cause the thermal properties of the structure to decrease (Díaz *et al.*, 2011; Thomazine *et al.*, 2005; Sobral *et al.*, 2001). As a result of glycerol addition to gelatin, the negative value of enthalpy of transition was reduced from -22.2 J.g^{-1} to -12.0 J.g^{-1} . It is reported that glycerol decreases the formation of junction zones from which re-natured triple helical structure forms. Enthalpy of transition indicates the required energy for helix to coil transition progress and its value correlates with the available re-natured triple helix in the structure (Achet and He, 1995). A reduction in the number of junction zones which act as precursor to the re-natured triple helix as a result of glycerol addition would lead to reduction of the enthalpy of transition (Arvanitoyannis *et al.*, 1997; Sobral *et al.*, 2001).

Epoxy compound was used to crosslink the gelatin membranes and increased the denaturation temperature from 65°C to 76.5°C . The increase in denaturation temperature is an effect of crosslinking as it was discussed in Chapter 3, Section 1.2.4 (Gratzer *et al.*, 1996). As expected, crosslinking caused the enthalpy of transition to reduce. This is a direct result of covalent bonds formation between gelatin macromolecules as discussed in Chapter 3, Section 1.2.4 (Usha and Ramasami, 2000).

3.4. Water Vapour Permeability

The moisture flux permeability of the wound dress is of great importance in adjusting the function of the wound dress. Too high permeability makes the wound dressing shrink and become too dry, whilst too low permeability would cause liquid build up at the wound and the dressing interface (Yannas and Burke, 1980). The top layer is instrumental in controlling the overall permeability of the wound dressing. To determine the rate of water permeability of the gelatin membranes, water permeability studies were performed according to the standard method SLP 25 described in Chapter 2, Section 2.2.4. Casting 8g of gelatin solution in petri-dishes with diameter of 5.5 cm led to the membrane with diameter of 0.65 mm. The water permeability of the membrane

was $0.25 \text{ mg.cm}^{-2}.\text{6 hour}^{-1}$. The water permeability of the natural skin is reported to be $3 \text{ mg.cm}^{-2}.\text{6 hour}^{-1}$ (Yannas and Burke, 1980). The vapour permeability rate of commercially available film wound dressings described in Chapter 1, Section 5.2, is reported to be $7.5 \text{ mg.cm}^{-2}.\text{6 hour}^{-1}$ (Abdelrahman and Newton, 2011). These values are noticeably higher than the results obtained in this section. An increase of permeability of the membrane can be achieved by increasing the porosity of the structure or reduction of membrane thickness. This may be a focus of future studies.

Chapter 7:

Final Assembled

Wound dressing

Chapter 7 - Final Assembled Wound Dressing

1. Preparation Method

It is reported that lamination of multiple compartments can be used to increase the strength and reduction of the final product extensibility (Badylak *et al.*, 2009). Lamination of porous scaffold with a smooth and continuous surface on one side is reported for limiting the growth of epithelial keratinocytes cells just to the scaffold portion of the wound dressing (Boyce *et al.*, 1988).

In this study, final assembled wound dressing was prepared through a lamination method described by Loke *et al.*, (2000) with some modifications. Wound dressing preparation was begun by solvent casting through orderly casting of each individual membrane in a petri dish with a diameter of 5.5 cm starting with casting of the plasticised cover (Top layer) (Chapter 6 – Section 2), followed by the chitosan-gelatin membrane (Chapter 5 – Section 2), and eventually the gelatin scaffold casting (Chapter 3 – Section 4.1). The time lapse between each casting was 48 hours to allow complete drying of each component. After casting the gelatin scaffold, crosslinking was performed using epoxy compound (Chapter 4 – Section 2.2). Completed wound dressing was obtained by lyophilising the compound for 48 hours. Lyophilisation was performed under vacuum pressure of 0.250 mbar and temperature of -40 °C.

2. Results

2.1. Visual Description of Wound Dressing

Figure 7-1 (A-C) displays the final assembled wound dressing at different orientation and magnifications. The bounded membrane portions of the wound dressing can be readily distinguished from the scaffold section due to their textural differences. Although each of these three segments (i.e.: gelatin top layer, chitosan-gelatin middle layer, and gelatin scaffold) consisted of similar mass of ingredient material (8 grams), different synthesis procedure led to different structural features in each segment. The chitosan-gelatin membrane was located between the two other layers and cannot be

distinguished at the magnifications used in these images (refer to SEM analysis, Section 2.4 of this Chapter).

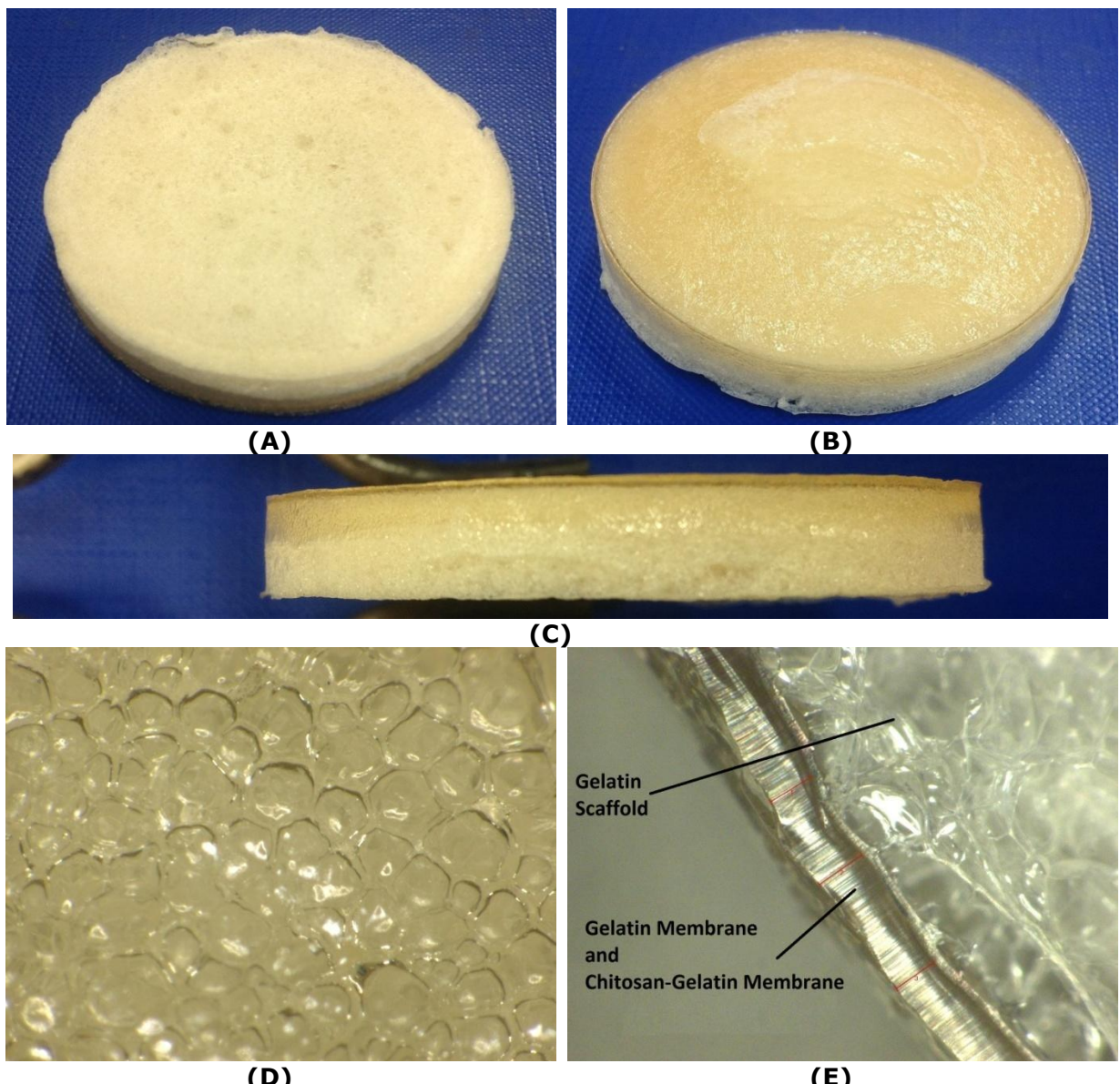


Figure 7-1: Images of prepared multi-layer wound dressing; (A) lower side view of the wound dressing, the gelatin scaffold can be seen attached to the gelatin membranes at the bottom of the image; (B) Top side view of wound dressing with gelatin membrane shown on the top and attached to gelatin scaffold; (C) side view of the wound dressing; (D) Optical microscope image of gelatin backing of wound dressing at 100x magnification, visible contours of the pores were visible through semi transparent gelatin membranes; (E) Optical microscope view of wound dressing cross section at 100x magnification, the middle membrane is not distinguishable from the top membrane at this magnification, however the gelatin scaffold and the membranes can easily be differentiate due to their different structures.

Figure 7-1-C shows the side view of the complete wound dressing. In this orientation the gelatin top membrane and its relative thickness to gelatin scaffold (lower part of image) was noticeable. The membrane and scaffold sections of samples showed good integration since there was no discernible interface and border line between each of them. Figure 7-1-D shows optical microscopic image of the top membrane at 100x magnification (VHX-100, Keyence, Japan). Through the transparent membranes, the visible contours of porosity in the scaffold were visible. The area at which the pores of the scaffold were fused into the membrane was visible. Figure 7-1-E shows a microscopic view of the final assembled wound dressing cross section. The top gelatin and middle gelatin-chitosan layers are not distinguishable at this magnification, however the different textural difference between porous gelatin scaffold (bottom layer) and backing membranes (the two top layers) were visible.

2.2. Mechanical Properties of the Assembled Wound Dressing

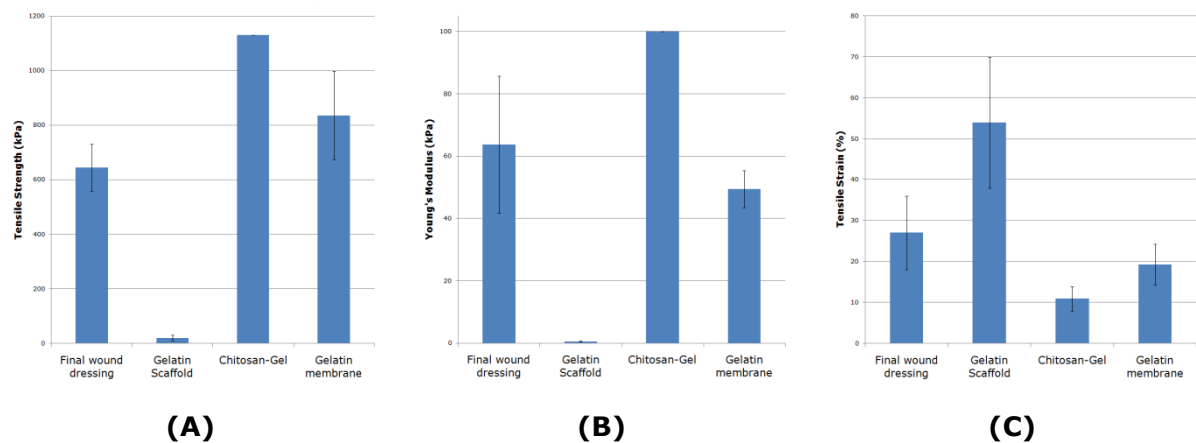


Figure 7-2: Tensile properties of final wound dressing in comparison with the individual components of the structure: (A) tensile strength, (B) Young's modulus, (C) tensile strain.

Table 7-1 lists the tensile properties of the final assembled gelatin wound dressing. Figure 7-2 compares the tensile strength, Young's modulus, and tensile strain of the completed wound dressing with the corresponding properties of each individual component.

Table 7–1: Tensile properties of the final assembled gelatin wound dressing and its individual components.

Sample	Tensile Strength (kPa)	Young's Modulus (kPa)	Tensile Strain (%)
Completed wound dressing	644.4 (± 86)	63.7 (± 22)	27.0 (± 9)
Gelatin scaffold	20.3 (± 9.6)	0.5 (± 0.2)	53.9 (± 16)
Gelatin-Chitosan membrane	1130.0 (± 0.3)	100 (± 0)	10.9 (± 3)
Gelatin membrane	836.0 (± 163)	49.4 (± 6)	19.2 (± 5)

Amongst 3 components, the porous gelatin scaffold showed the lowest tensile strength value and high elasticity (the lowest Young's modulus). On the contrary, the chitosan - gelatin membrane showed the highest tensile strength and its Young's modulus was an order of magnitude higher than each of the individual components. Final wound dressing had significantly higher tensile strength and Young's modulus in comparison with gelatin scaffold ($p \leq 0.05$). This shows the effectiveness of chitosan-gelatin membrane substrate to function as a mechanical support for gelatin scaffold. Rivero *et al.*, (2009) reported that attaching the chitosan membrane to a gelatin membrane in the form of a chitosan-gelatin bilayer increased the tensile strength of the bi-layers as a single entity. As shown in Figure 7–2 the tensile properties of a completed product was between each of the individual components. This behaviour of a laminated composite is reported by Martucci and Ruseckaite, (2010) showing that the tensile strength of the multi-layered gelatin composite is usually between the strength of individual components. The mechanical properties of a laminated composite depend strongly on the quality of adhesion between the laminated membranes. In the next Section the adhesion force between the scaffold and the membranes has studied.

2.3. Adhesion Force of the Membranes

Gas-foamed gelatin scaffold formed matrices with microdomain-like indentations that allowed its adhesion to chitosan-gelatin membrane. In the concept design, it was envisioned that these two structures be peeled off from each other, the residual force of adhesion between scaffold and the two top membranes was measured according to the

test method BS EN ISO 11644 described in Chapter 2, Section 2.2.3. Figure 7-3 shows the rate of change in the force of adhesion as the peeling of the top layer proceeded along the length of the sample. According to the obtained results, the peeling force for the scaffold to be detached from the membrane was between 10 to 15 grams which is the equivalent of 9.8×10^{-2} N to 14.7×10^{-2} N. The bonding of chitosan membrane and the gelatin scaffold may have been achieved by a combination of physical embedding and the electrostatic interactions between the chitosan and gelatin molecules (Pereda *et al.*, 2011). During casting the membranes, gelatin mixture may flow into the pores and interstices to establish mechanical embedding (Liu *et al.*, 2014). In addition to mechanical embedding, short range interaction or Van der Waals forces, are of sufficient magnitude to contribute significantly to the strength of bonding (Sung *et al.*, 1999a). The increase of force after the distance passed 15 mm at the end of experiment may be attributed to gradual increase of detached-sample weight that the hook was lifting from the stub as the test progress.

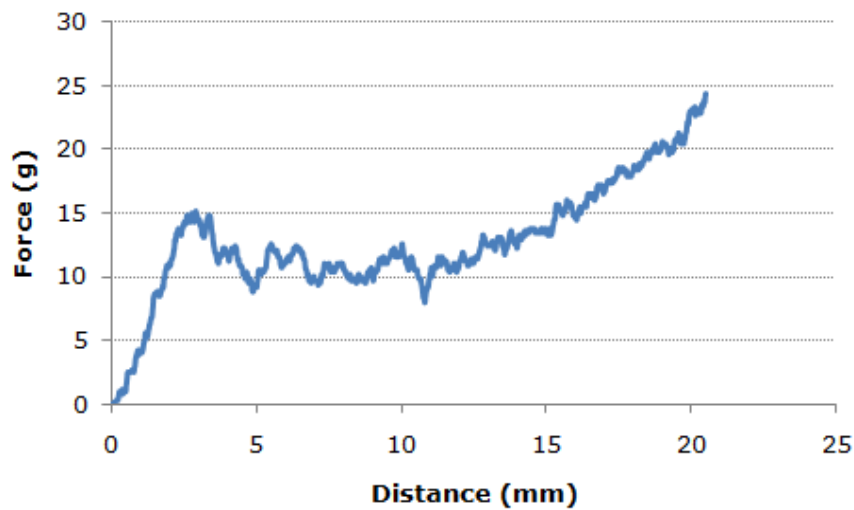


Figure 7-3: The recorded force required for peeling off the gelatin scaffold (bottom layer) from the rest of wound dressing portions (the two top layers).

2.4. Wound Dressing Microstructure Analysis

Figure 7-4 (A & B) shows SEM images of the final wound dressing cross-section at 50x and 100x magnifications. The gelatin porous scaffold can be distinguished from other two top membranes due to its porous structure feature in both Figures. Figure 7-4

shows the cross section at 50x magnification. The combined thickness of the gelatin membrane and the chitosan-gelatin membrane was 300 μm . Figure 7-4-B shows the cross section at 100x magnification. At this magnification the border interface between the gelatin membrane and the chitosan-gelatin membrane was distinguishable. Each membrane showed a thickness close to 120 μm . The interface between these two membranes showed no pore and empty spaces which suggests that they firmly bonded together. Other researchers reported similar compact and dense interface between chitosan-gelatin bilayer indicating good compatibility between the components (Rivero *et al.*, 2009; Pereda *et al.*, 2011). In composites that have close or identical chemical components, it has been suggested that better interaction between their components occurs (Apostolov *et al.*, 2002). In the case of this study, since all three segments of the wound dressing were gelatin-based, the bonding mechanism between segments may be due to the establishment of hydrogen bonds and inter-diffusion of two adjacent segments during casting (Martucci and Ruseckaite, 2010). This may lead to the formation of a compact and uniform structure observed in Figure 7-4.

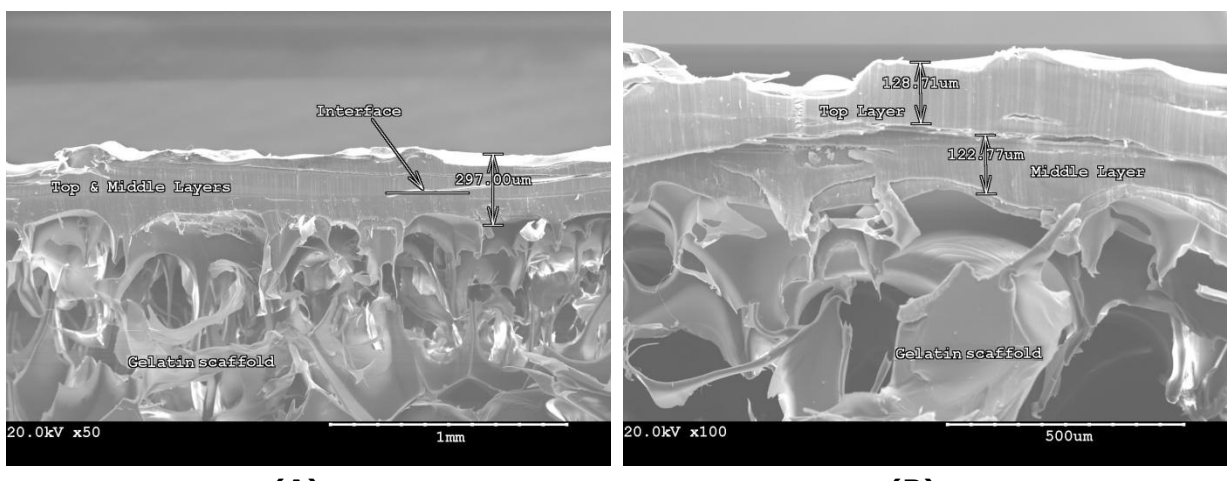


Figure 7-4: The SEM images of the final assembled wound dressing cross section. Porous gelatin scaffold at the bottom is easily distinguishable from the top membranes; (A) SEM image at 50x magnification, the combined thickness of two membranes was 297 μm (B) SEM image at 100x magnification, at this magnification the interface between the top and middle membrane can be distinguished. Each membrane had a thickness of over 120 μm . The images are obtained at 20kV acceleration voltage.

Chapter 8: Conclusion & Future Research Studies

Chapter 8 - Conclusion and Future Research Studies

Conclusion

This study was aimed at achieving following objectives: to produce, optimise, and assemble 3 separately prepared gelatin-based layers for the purpose of application as wound dressing. Each layer needed to be designed specifically to serve a particular functionality such as being biodegradable, porous, water absorbent, and having adequate mechanical strength.

As a conclusion, it can be reported that *in situ* gas foaming method not only is capable of producing porous gelatin scaffolds but also can be successfully optimised for bringing desirable physical and mechanical properties into the final products. As a result of such modifications, the size distribution of pores was successfully reduced from 230-550 μm in the 3rd generation to 180-300 μm in the final optimised batch of samples. In addition, as a result of process optimisation, the maximum achieved tensile strength of the scaffolds crosslinked with GT was increased from 5.4 kPa for the 3rd generation scaffolds to 239 kPa for the 4th generation scaffolds.

To optimise the prepared structures beyond the microstructure of the scaffolds, the impact of different crosslinking agents with different molecular structures was studied. Application of different types of crosslinking compounds provided an insight into the impact of crosslinking agent molecular structure on its functions. It was shown that the molecular length and functional groups may have an important impact on thermal stability, water absorption, tensile properties, and even the smoothness of the scaffold surface. The crosslinking agents such as Epoxy compounds with longer molecular backbone produced structure with denaturation temperature of 80°C, whilst smaller molecules such as genipin produced structures with the denaturation temperature of 88°C. It was also shown that longer crosslinker molecules can lead to a more flexible structure with lower Young's modulus. Such differences may originate from the difference in the crosslinking density in the final product. Crosslinkers with longer

molecules can lead to lower crosslink density within the final structure which can cause lower thermal stability and higher flexibility at the same time (Chapter 4, Sections 3.3.3 and 3.3.4). In the light of such a comparison a better understanding about the impacts of over crosslinking on the porous structure mechanical properties was achieved. It was shown that porous structures are more sensitive to the negative impacts of over crosslinking. Upon applications of highly reactive crosslinking agents such as GT, the tensile strength of the structure can be reduced unintentionally when the crosslinking concentration is raised above a certain critical value. This highlights the well known side effects of over-crosslinking and was attributed to brittleness of the structures. However, in the case of porous structures sharp edges, gaps, and pores were functioning as crack initiation sites and were exacerbating the negative impacts of over crosslinking.

Bonding and assembling prepared layers proved to be a key processing step in order to have a viable prototype with easy handling and practical applications. Trying to increase the porosity of the structure caused the tensile strength of the scaffold to decrease. A multi-layered structure was developed to balance porosity with a high mechanical strength. A chitosan-gelatin membrane was used as a substrate to mechanically support the attached-porous scaffold. The implemented layered-structure strategy managed to increase the overall tensile strength of the wound dressing whilst preserving a desirable microstructure. Overall tensile strength of wound dressing was measured to be 644 kPa which is similar to the tensile strength of human skin (the tensile strength of the skin covering the area of forearm and face is reported to be between 200 - 850 kPa (Diridollou *et al.*, 2000)).

This study highlighted a simple and accessible method of development for wounds dressings. Optimising this method can be continued by following topics for further studies.

Future Research Studies

Improving the Degradation Rate: Tissue engineering scaffolds are considered to be degradable in a period of time and gradually be replaced by the surrounding natural tissue (Böttcher-Haberzeth *et al.*, 2010). However, this degradation and replacement must take place at a desirable pace in accordance with the type of tissue that the scaffolds serve. Considering the high turn-around rate of skin (Gurtner *et al.*, 2008), a wound healing procedure a period of 3 to 14 days for complete degradation may suffice (Enoch and Leaper, 2008). At enzymatic concentration of 2.5 mg/ml almost all of the samples showed the desirable degradation rate (Chapter 3, Section 4.2.7). However at higher concentration of Collagenase (5 mg/ml) the degradation rate was faster than the desired value. Amongst all obtained results, genipin showed high resistance against enzymatic degradation. Genipin has been reported to offer better or comparable resistance against enzymatic degradation than GT (Sung *et al.*, 1998; Liu *et al.*, 2003; Yao *et al.*, 2004). Considering that crosslinking of scaffold using genipin occurred overnight whilst other agents crosslinkings were completed in 3 hours, increasing the crosslinking time may improve the scaffold degradation resistance in future studies. Possible correlation between crosslinking time and degradation rate may be explored to suit the application.

Diffusion Rate and the Impact of Porosity: Apart from facilitating cell migration throughout the structure, porosity of tissue engineering scaffolds is required for enhancing transfer of nutrients and oxygen and removing wastes produced away from the cells (Dehghani and Annabi, 2011). The influence of porosity in the rate of diffusion of nutrients through the scaffold can be a suitable topic for future studies. It is reported that the rate of diffusion of the nutrient is dependent on the scaffold thickness, and concentration of nutrient throughout the wound bed (Yannas and Burke, 1980). Further study is required in determining the ideal thickness and porosity of the scaffold for desirable diffusion rate.

Evaluating the Biocompatibility and Cell Response of Prepared

Prototype: As the next step to advance the prepared prototype towards practical application and further optimising its features as a medical device, the biocompatibility of the product needs to be investigated. Such analysis can be started at *in vitro* scale and can be gradually moved towards animal studies, preclinical, and finally clinical studies. The globally recognised standard for *in vitro* studies on biocompatibility of the medical device is ISO-10993 guidelines. Considering the preparation protocols in this study and application of chemical crosslinker (Epoxy compound) and acetic acid, relevant sections of ISO-10993 standards that should be considered for *in vitro* studies should at least include general cell biocompatibility (ISO 10993-5), investigating the carcinogenicity of product (ISO 10993-3), and blood compatibility of the prototype (ISO 10993-4). The plan to proceed with animal studies and preclinical tests can be carried out after satisfactory results from these *in vitro* analyses. It should be pointed out that general cell biocompatibility analysis and cell culture studies, not only provide valuable details regarding the safety of the prototype, it can reveal the cell response upon contact with the surface of scaffold which is a valuable investigation for any tissue engineering scaffolds.

Chapter 9 - References

- Abdelrahman, T. and Newton, H. (2011) Wound dressings: Principles and practice. *Surgery (Oxford)*. **29** (10), 491-495.
- Abraham, L. C., Zuena, E., Perez-Ramirez, B. and Kaplan, D. L. (2008) Guide to collagen characterization for biomaterial studies. *Journal of Biomedical Materials Research Part B: Applied Biomaterials*. **87B** (1), 264-285.
- Abramo, F., Argiolas, S., Pisani, G., Vannozi, I. and Miragliotta, V. (2008) Effect of a hydrocolloid dressing on first intention healing surgical wounds in the dog: A pilot study. *Australian Veterinary Journal*. **86** (3), 95-99.
- Achet, D. and He, X. W. (1995) Determination of the renaturation level in gelatin films. *Polymer*. **36** (4), 787-791.
- Agache, P. G., Monneur, C., Leveque, J. L., De Rigal, J., (1980) Mechanical properties and Young's modulus of human skin *in vivo*, *Archive of Dermatological Research*, **269**, 221-232.
- Akao, T., Kobashi, M. and Aburada, M. (1994) Enzymatic studies on the animal and intestinal metabolism of geniposide. *Biological and Pharmaceutical Bulletin*. **17** (12), 1573-1576.
- Allen, D. J. and Ishida, H. (2006) Physical and mechanical properties of flexible polybenzoxazine resins: Effect of aliphatic diamine chain length. *Journal of Applied Polymer Science*. **101** (5), 2798-2809.
- Alves, P. M. A., Carvalho, R. A., Moraes, I. C. F., Luciano, C. G., Bittante, A. M. Q. B. and Sobral, P. J. A. (2011) Development of films based on blends of gelatin and poly(vinyl alcohol) cross linked with glutaraldehyde. *Food Hydrocolloids*. **25** (7), 1751-1757.
- Apostolov, A. A., Fakirov, S., Evstatiev, M., Hoffmann, J. and Friedrich, K. (2002) Biodegradable laminates based on gelatin, 1. *Macromolecular Materials and Engineering*. **287** (10), 693-697.
- Apostolov, A. A., Fakirov, S., Hoffmann, J. and Friedrich, K. (2003) Biodegradable laminates based on gelatin, 2. *Macromolecular Materials and Engineering*. **288** (3), 228-234.
- Arvanitoyannis, I., Psomiadou, E., Nakayama, A., Aiba, S. and Yamamoto, N. (1997) Edible films made from gelatin, soluble starch and polyols, part 3. *Food Chemistry*. **60** (4), 593-604.
- Awad, H. A., Quinn Wickham, M., Leddy, H. A., Gimble, J. M. and Guilak, F. (2004) Chondrogenic differentiation of adipose-derived adult stem cells in agarose, alginate, and gelatin scaffolds. *Biomaterials*. **25** (16), 3211-3222.
- Azami, M., Samadikuchaksaraei, A., and Poursamar, A. (2010) Synthesis and characterization of a laminated hydroxyapatite/gelatin nanocomposite scaffold with controlled pore structure for bone tissue engineering. *International Journal of Artificial Organs*. **33** (2), 86-95.

- Badylak, S. F., Freytes, D. O. and Gilbert, T. W. (2009) Extracellular matrix as a biological scaffold material: Structure and function. *Acta Biomaterialia*. **5** (1), 1-13.
- Barbetta, A., Gumerio, A., Pecci, R., Bedini, R. and Dentini, M. (2009) Gas-in-liquid foam templating as a method for the production of highly porous scaffolds. *Biomacromolecules*. **10** (12), 3188-3192.
- Baroni, A., Buommino, E., De Gregorio, V., Ruocco, E., Ruocco, V. and Wolf, R. (2012) Structure and function of the epidermis related to barrier properties. *Clinics in Dermatology*. **30** (3), 257-262.
- Bigi, A., Cojazzi, G., Panzavolta, S., Roveri, N. and Rubini, K. (2002) Stabilization of gelatin films by crosslinking with genipin. *Biomaterials*. **23** (24), 4827-4832.
- Bigi, A., Cojazzi, G., Panzavolta, S., Rubini, K. and Roveri, N. (2001) Mechanical and thermal properties of gelatin films at different degrees of glutaraldehyde crosslinking. *Biomaterials*. **22** (8), 763-768.
- Bigi, A., Panzavolta, S. and Rubini, K. (2004) Relationship between triple-helix content and mechanical properties of gelatin films. *Biomaterials*. **25** (25), 5675-5680.
- Bonilla, J., Atarés, L., Vargas, M. and Chiralt, A. (2013) Properties of wheat starch film-forming dispersions and films as affected by chitosan addition. *Journal of Food Engineering*. **114** (3), 303-312.
- Böttcher-Haberzeth, S., Biedermann, T. and Reichmann, E. (2010) Tissue engineering of skin. *Burns*. **36** (4), 450-460.
- Boyce, S. T., Christianson, D. J. and Hansbrough, J. F. (1988) Structure of a collagen-GAG dermal skin substitute optimized for cultured human epidermal keratinocytes. *Journal of Biomedical Materials Research Part A*. **22**, 939-957.
- Brem, H., Stojadinovic, O., Diegelmann, R. F., Entero, H., Lee, B., Pastar, I., Golinko, M., Rosenberg, H. and Tomic-Canic, M. (2007) Molecular markers in patients with chronic wounds to guide surgical debridement. *Molecular Medicine*. **13** (1-2), 30-39.
- Britan, A., Liverts, M., Ben-Dor, G., Koehler, S. A. and Bennani, N. (2009) The effect of fine particles on the drainage and coarsening of foam. *Colloids and Surfaces A: Physicochemical and Engineering Aspects*. **344** (1-3), 15-23.
- Brohem, C. A., da Silva Cardeal, L. B., Tiago, M., Soengas, M. S., de Moraes Barros, S. B. and Maria-Engler, S. S. (2011) Artificial skin in perspective: Concepts and applications. *Pigment Cell & Melanoma Research*. **24** (1), 35-50.
- Butler, M. F., Ng, Y. and Pudney, P. D. A. (2003) Mechanism and kinetics of the crosslinking reaction between biopolymers containing primary amine groups and genipin. *Journal of Polymer Science Part A: Polymer Chemistry*. **41** (24), 3941-3953.
- Calvino-Casilda, V., Mul, G., Fernández, J. F., Rubio-Marcos, F. and Bañares, M. A. (2011) Monitoring the catalytic synthesis of glycerol carbonate by real-time attenuated total reflection FTIR spectroscopy. *Applied Catalysis A: General*. **409-410** (0), 106-112.
- Catalina, M., Attenburrow, G. E., Cot, J., Covington, A. D. and Antunes, A. P. M. (2011) Influence of crosslinkers and crosslinking method on the properties of gelatin films

- extracted from leather solid waste. *Journal of Applied Polymer Science*. **119** (4), 2105-2111.
- Caycik, S. and Jagger, R. G. (1992) The effect of cross-linking chain length on mechanical properties of a dough-molded poly(methylmethacrylate) resin. *Dental Materials*. **8**, 153-157.
- Cestari, A. R., Vieira, E. F. S., Alves, F. J., Silva, E. C. S. and Andrade Jr., M. A. S. (2012) A novel and efficient epoxy/chitosan cement slurry for use in severe acidic environments of oil wells—Structural characterization and kinetic modelling. *Journal of Hazardous Materials*. **213-214** (0), 109-116.
- Charulatha, V. and Rajaram, A. (2003) Influence of different crosslinking treatments on the physical properties of collagen membranes. *Biomaterials*. **24** (5), 759-767.
- Chen, T., Embree, H. D., Brown, E. M., Taylor, M. M. and Payne, G. F. (2003) Enzyme-catalyzed gel formation of gelatin and chitosan: Potential for in situ applications. *Biomaterials*. **24** (17), 2831-2841.
- Chiou, B., Avena-Bustillos, R. J., Bechtel, P. J., Jafri, H., Narayan, R., Imam, S. H., Glenn, G. M. and Orts, W. J. (2008) Cold water fish gelatin films: Effects of cross-linking on thermal, mechanical, barrier, and biodegradation properties. *European Polymer Journal*. **44** (11), 3748-3753.
- Choi, Y. S., Hong, S. R., Lee, Y. M., Song, K. W., Park, M. H. and Nam, Y. S. (1999) Study on gelatin-containing artificial skin: I. preparation and characteristics of novel gelatin-alginate sponge. *Biomaterials*. **20** (5), 409-417.
- Chuang, T. -., Chen, M. -. and Lin, F. -. (2008) Preparation and surface characterization of HMDI-activated 316L stainless steel for coronary artery stents. *Journal of Biomedical Materials Research Part A*. **85A** (3), 722-730.
- Chvapil, M. (1982) Consideration on manufacturing principles of a synthetic burn dressing: A review. *Journal of Biomedical Materials Research Part A*. **16**, 245-263.
- Covington, A. D. (2009) *Tanning Chemistry, The Science of Leather*. Combridge, UK: Royal Society of Chemistry.
- Dagalakis, N., Flink, J., Stasikelis, P., Burke, J. F. and Yannas, I. V. (1980) Design of an artificial skin. part III. control of pore structure. *Journal of Biomedical Materials Research Part A*. **14**, 511-528.
- Damink, L. H. H., Dijkstra, P. J., Luyn, J. A. V., Wachem, P. B. V., Nieuwenhuis, P. and Feijen, J. (1995) Glutaraldehyde as crosslinking agent for collagen-based biomaterials. *Journal of Materials Science: Materials in Medicine*. **6**, 460-472.
- Dardelle, G., Subramaniam, A. and Normand, V. (2011) Determination of covalent cross-linker efficacy of gelatin strands using calorimetric analyses of the gel state. *Soft Matter*. **7**, 3315-3322.
- De Carvalho, R. A. and Grosso, C. R. F. (2004) Characterization of gelatin based films modified with transglutaminase, glyoxal and formaldehyde. *Food Hydrocolloids*. **18** (5), 717-726.

- Dehghani, F. and Annabi, N. (2011) Engineering porous scaffolds using gas-based techniques. *Current Opinion in Biotechnology*. **22** (5), 661-666.
- Deible, C. R., Petrosko, P., Johnson, P. C., Beckman, E. J., Russell, A. J. and Wagner, W. R. (1998) Molecular barriers to biomaterial thrombosis by modification of surface proteins with polyethylene glycol. *Biomaterials*. **19** (20), 1885-1893.
- Díaz, P., Arratia, C., Vásquez, C., Osorio, F. and Enrione, J. (2011) Effect of glycerol on water sorption of bovine gelatin films in the glassy state. *Procedia Food Science*. **1** (0), 267-274.
- Diridollou, S., Patat, F., Gens, F., Vaillant, L., Black, D., Lagarde, J. M., Gall, Y. and Berson, M. (2000) In vivo model of the mechanical properties of the human skin under suction. *Skin Research Technology*. **6** (4), 214-221.
- Dong, G., Sun, J., Yao, C., Jiang, G. J., Huang, C. and Lin, F. (2001) A study on grafting and characterization of HMDI-modified calcium hydrogenphosphate. *Biomaterials*. **22** (23), 3179-3189.
- Dong, Z., Wang, Q. and Du, Y. (2006) Alginate/gelatin blend films and their properties for drug controlled release. *Journal of Membrane Science*. **280** (1-2), 37-44.
- Dowsett, C., Davis, L., Henderson, V. and Searle, R. (2012) The economic benefits of negative pressure wound therapy in community-based wound care in the NHS. *International Wound Journal*. **9** (5), 544-552.
- Drew, P., Posnett, J. and Rusling, L. (2007) The cost of wound care for a local population in england. *International Wound Journal*. **4** (2), 149-155.
- Elvin, C. M., Vuocolo, T., Brownlee, A. G., Sando, L., Huson, M. G., Liyou, N. E., Stockwell, P. R., Lyons, R. E., Kim, M., Edwards, G. A., Johnson, G., McFarland, G. A., Ramshaw, J. A. M. and Werkmeister, J. A. (2010) A highly elastic tissue sealant based on photopolymerised gelatin. *Biomaterials*. **31** (32), 8323-8331.
- Enoch, S. and Leaper, D. J. (2008) Basic science of wound healing. *Surgery (Oxford)*. **26** (2), 31-37.
- Farris, S., Song, J. and Huang, Q. (2010) Alternative reaction mechanism for the cross-linking of gelatin with glutaraldehyde. *Journal of Agricultural and Food Chemistry*. **58**, 998-1003.
- Fonder, M. A., Lazarus, G. S., Cowan, D. A., Aronson-Cook, B., Kohli, A. R. and Mamelak, A. J. (2008) Treating the chronic wound: A practical approach to the care of nonhealing wounds and wound care dressings. *Journal of the American Academy of Dermatology*. **58** (2), 185-206.
- Franz, M. G., Steed, D. L. and Robson, M. C. (2007) Optimizing healing of the acute wound by minimizing complications. *Current Problems in Surgery*. **44** (11), 691-763.
- Friess, W. (1998) Collagen – biomaterial for drug delivery. *European Journal of Pharmaceutics and Biopharmaceutics*. **45** (2), 113-136.
- Garrison, J. L. (2001) Wound healing: Why hasn't it healed? *Current Surgery*. **58** (4), 357-361.

- Gelse, K., Pöschl, E. and Aigner, T. (2003) Collagens—structure, function, and biosynthesis. *Advanced Drug Delivery Reviews*. **55** (12), 1531-1546.
- Gilkes, J. W. G. (2002) *Studies into the development of an in-situ gelling wound dressing. Thesis (PhD)*, PhD Thesis, Liverpool John Moores University.
- Gill, P., Tohidi Moghadam, T. and Ranjbar, B. (2010) Differential scanning calorimetry techniques: Application in biology and nanoscience. *Journal of Biomolecular Techniques*. **21** , 167-193.
- Giraudier, S., Hellio, D., Djabourov, M. and Larreta-Garde, V. (2004) Influence of weak and covalent bonds on formation and hydrolysis of gelatin networks. *Biomacromolecules*. **5** , 1662-1666.
- Gogolewski, S. and Gorna, K. (2007) Biodegradable polyurethane cancellous bone graft substitutes in the treatment of iliac crest defects. *Journal of Biomedical Materials Research Part A*. **80A** (1), 94-101.
- Gómez-Guillén, M. C., Giménez, B., López-Caballero, M. E. and Montero, M. P. (2011) Functional and bioactive properties of collagen and gelatin from alternative sources: A review. *Food Hydrocolloids*. **25** (8), 1813-1827.
- Gómez-Guillén, M. C., Pérez-Mateos, M., Gómez-Estaca, J., López-Caballero, E., Giménez, B. and Montero, P. (2009) Fish gelatin: A renewable material for developing active biodegradable films. *Trends in Food Science & Technology*. **20** (1), 3-16.
- Gorgieva, S. and Kokol, V. (2011) *Collagen- vs. gelatine-based biomaterials and their biocompatibility: review and perspectives*. Intech. pp. 17-52.
- Gratzer, P. F., Pereira, C. A. and Lee, J. M. (1996) Solvent environment modulates effects of glutaraldehyde crosslinking on tissue-derived biomaterials. *Journal of Biomedical Materials Research*. **31** (4), 533-543.
- Gregg, M. (2001) Wound dressings at the turn of the millennium. *Current Problems in Dermatology*. **13** (2), 86-89.
- Griffith, L. G. and Swartz, A. (2006) Capturing complex 3D tissue physiology invitro. *Nature Reviews*. **7** , 211-224.
- Groeber, F., Holeiter, M., Hampel, M., Hinderer, S. and Schenke-Layland, K. (2011) Skin tissue engineering, *in-vivo* and *in-vitro* applications. *Advanced Drug Delivery Reviews*. **63** (4-5), 352-366.
- Guinesi, L. S. and Cavalheiro, É. T. G. (2006) The use of DSC curves to determine the acetylation degree of chitin/chitosan samples. *Thermochimica Acta*. **444** (2), 128-133.
- Gurtner, G. C., Werner, S., Barrandon, Y. and Longaker, M. T. (2008) Wound repair and regeneration. *Nature*. **453** , 314-320.
- Hajiali, H., Shahghasempour, S., Naimi-Jamal, M. R. and Peirovi, H. (2011) Electrospun PGA/gelatin nanofibrous scaffolds and their potential application in vascular tissue engineering. *International Journal of Nanomedicine*. **6** , 2133-2141.
- Harding, K. (2010) Chronic wounds and their management and prevention is a significant public health issue. *International Wound Journal*. **7** (3), 125-126.

- Hardwicke, J., Schmaljohann, D., Boyce, D. and Thomas, D. (2008) Epidermal growth factor therapy and wound healing; past, present and future perspectives. *The Surgeon*. **6** (3), 172-177.
- Haroun, A. A. and El Toumy, S. A. (2010) Effect of natural polyphenols on physicochemical properties of crosslinked gelatin-based polymeric biocomposite. *Journal of Applied Polymer Science*. **116** (5), 2825-2832.
- Hashim, D. M., Man, Y. B. C., Norakasha, R., Shuhaimi, M., Salmah, Y. and Syahariza, Z. A. (2010) Potential use of fourier transform infrared spectroscopy for differentiation of bovine and porcine gelatins. *Food Chemistry*. **118** (3), 856-860.
- Herskovits, T., Gadegbeku, B. and Jaiillet, H. (1970) On the structural stability and solvent denaturation of proteins. *The Journal of Biological Chemistry*. **245** (10), 2588-2598.
- Hong, S. R., Lee, S. J., Shim, J. W., Choi, Y. S., Lee, Y. M., Song, K. W., Park, M. H., Nam, Y. S. and Lee, S. I. (2001) Study on gelatin-containing artificial skin IV: A comparative study on the effect of antibiotic and EGF on cell proliferation during epidermal healing. *Biomaterials*. **22** (20), 2777-2783.
- Hu, H., Xin, J. H., Hu, H., Chan, A. and He, L. (2013) Glutaraldehyde-chitosan and poly(vinyl alcohol) blends, and fluorescence of their nano-silica composite films. *Carbohydrate Polymers*. **91** (1), 305-313.
- Huang, G., Sun, Y., Xiao, J. and Yang, J. (2012) Complex coacervation of soybean protein isolate and chitosan. *Food Chemistry*. **135** (2), 534-539.
- Huang, L. L. H., Sung, H., Tsai, C. and Huang, D. (1998) Biocompatibility study of a biological tissue fixed with a naturally occurring crosslinking reagent. *Journal of Biomedical Materials Research*. **42** (4), 568-576.
- Huang, R., Chen, G., Sun, M. and Gao, C. (2007) Hexamethylene diisocyanate crosslinking 2-hydroxypropyltrimethyl ammonium chloride chitosan/poly(acrylonitrile) composite nanofiltration membrane. *Journal of Applied Polymer Science*. **105** (2), 673-679.
- Huang, Y., Onyeri, S., Siewe, M., Moshfeghian, A. and Madihally, S. V. (2005) In vitro characterization of chitosan-gelatin scaffolds for tissue engineering. *Biomaterials*. **26** (36), 7616-7627.
- Jackson, M., Choo, L., Watson, P. H., Halliday, W. C. and Mantsch, H. H. (1995) Beware of connective tissue proteins: Assignment and implications of collagen absorptions in infrared spectra of human tissues. *Biochimica Et Biophysica Acta (BBA) - Molecular Basis of Disease*. **1270** (1), 1-6.
- Jayakrishnan, A. and Jameela, S. R. (1996) Glutaraldehyde as a fixative in bioprostheses and drug delivery matrices. *Biomaterials*. **17** (5), 471-484.
- Jeya Shakila, R., Jeevithan, E., Varatharajakumar, A., Jeyasekaran, G. and Sukumar, D. (2012) Comparison of the properties of multi-composite fish gelatin films with that of mammalian gelatin films. *Food Chemistry*. **135** (4), 2260-2267.

- Ji, S., Xiao, S., Luo, P., Huang, G., Li, H., Zhu, S. and Xia, Z. (2011) A new strategy of promoting vascularization of skin substitutes by capturing endothelial progenitor cells automatically. *Medical Hypotheses*. **77** (4), 662-664.
- Kadnaim, A., Janvikul, W., Wichai, U. and Rutnakornpituk, M. (2008) Synthesis and properties of carboxymethylchitosan hydrogels modified with poly(ester-urethane). *Carbohydrate Polymers*. **74** (2), 257-267.
- Kamel, R. A., Ong, J. F., Eriksson, E., Junker, J. P. E. and Caterson, E. J. (2013) Tissue engineering of skin. *Journal of the American College of Surgeons*. **217** (3), 533-555.
- Kanmani, P. and Rhim, J. (2014) Physical, mechanical and antimicrobial properties of gelatin based active nanocomposite films containing AgNPs and nanoclay. *Food Hydrocolloids*. **35** (0), 644-652.
- Khor, E. (1997) Methods for the treatment of collagenous tissues for bioprostheses. *Biomaterials*. **18** (2), 95-105.
- Kim, B., Park, I., Hoshiba, T., Jiang, H., Choi, Y., Akaike, T. and Cho, C. (2011) Design of artificial extracellular matrices for tissue engineering. *Progress in Polymer Science*. **36** (2), 238-268.
- Kiran, E. (2010) Foaming strategies for bioabsorbable polymers in supercritical fluid mixtures. Part I. miscibility and foaming of poly (L-lactic acid) in carbon dioxide + acetone binary fluid mixture. *Journal of Supercritical Fluids*. **54**, 265-307.
- Kittipattanabawon, P., Benjakul, S., Visessanguan, W. and Shahidi, F. (2010) Comparative study on characteristics of gelatin from the skins of brownbanded bamboo shark and blacktip shark as affected by extraction conditions. *Food Hydrocolloids*. **24** (2-3), 164-171.
- Klüver, E. and Meyer, M., (2014) Thermoplastic processing, rheology, and extrudate properties of wheat, soy, and pea proteins. *Polymer Engineering and Science*.
- Knaul, J. Z., Hudson, S. M. and Creber, K. A. M. (1999) Crosslinking of chitosan fibers with dialdehydes: Proposal of a new reaction mechanism. *Journal of Biomedical Materials Research Part B: Applied Biomaterials*. **37** (11), 1079-1094.
- Koli, J. M., Basu, S., Nayak, B. B., Patange, S. B., Pagarkar, A. U. and Gudipati, V. (2012) Functional characteristics of gelatin extracted from skin and bone of tiger-toothed croaker (*otolithes ruber*) and pink perch (*nemipterus japonicus*). *Food and Bioproducts Processing*. **90** (3), 555-562.
- Koob, T. J. and Hernandez, D. J. (2003) Mechanical and thermal properties of novel polymerized NDGA-gelatin hydrogels. *Biomaterials*. **24** (7), 1285-1292.
- Koob, T. J., Willis, T. A., Qiu, Y. S. and Hernandez, D. J. (2001) Biocompatibility of NDGA-polymerized collagen fibers. II. attachment, proliferation, and migration of tendon fibroblasts in vitro. *Journal of Biomedical Materials Research*. **56** (1), 40-48.
- Kostko, A. F., Chen, T., Payne, G. F. and Anisimov, M. A. (2003) Dynamic light-scattering monitoring of a transient biopolymer gel. *Physica A: Statistical Mechanics and its Applications*. **323** (0), 124-138.

- Landsman, A., Taft, D. and Riemer, K. (2009) The role of collagen bioscaffolds, foamed collagen, and living skin equivalents in wound healing. *Clinics in Podiatric Medicine and Surgery*. **26** (4), 525-533.
- Laschke, M. W., Strohe, A., Menger, M. D., Alini, M. and Eglin, D. (2010) In vitro and in vivo evaluation of a novel nanosize hydroxyapatite particles/poly(ester-urethane) composite scaffold for bone tissue engineering. *Acta Biomaterialia*. **6** (6), 2020-2027.
- Leach, J. B., Wolinsky, J. B., Stone, P. J. and Wong, J. Y. (2005) Crosslinked α -elastin biomaterials: Towards a processable elastin mimetic scaffold. *Acta Biomaterialia*. **1** (2), 155-164.
- Lee, J., Yoo, J. J., Atala, A. and Lee, S. J. (2012) Controlled heparin conjugation on electrospun poly(ϵ -caprolactone)/gelatin fibers for morphology-dependent protein delivery and enhanced cellular affinity. *Acta Biomaterialia*. **8** (7), 2549-2558.
- Lee, S. B., Kim, Y. H., Chong, M. S., Hong, S. H. and Lee, Y. M. (2005) Study of gelatin-containing artificial skin V: Fabrication of gelatin scaffolds using a salt-leaching method. *Biomaterials*. **26** (14), 1961-1968.
- Leffler, C. C. and Müller, B. W. (2000) Influence of the acid type on the physical and drug liberation properties of chitosan-gelatin sponges. *International Journal of Pharmaceutics*. **194** (2), 229-237.
- Li, J., Chen, J. and Kirsner, R. (2007) Pathophysiology of acute wound healing. *Clinics in Dermatology*. **25** (1), 9-18.
- Li, L., Yu, Y., Wu, Q., Zhan, G. and Li, S. (2009a) Effect of chemical structure on the water sorption of amine-cured epoxy resins. *Corrosion Science*. **51** (12), 3000-3006.
- Li, Q., Yang, D., Ma, G., Xu, Q., Chen, X., Lu, F. and Nie, J. (2009b) Synthesis and characterization of chitosan-based hydrogels. *International Journal of Biological Macromolecules*. **44** (2), 121-127.
- Liang, H., Chang, W., Lin, K. and Sung, H. (2003) Genipin-crosslinked gelatin microspheres as a drug carrier for intramuscular administration: In vitro and in vivo studies. *Journal of Biomedical Materials Research Part A*. **65A** (2), 271-282.
- Lim, Y., Gwon, H., Shin, J., Jeun, J. P. and Nho, Y. C. (2008) Preparation of porous poly(ϵ -caprolactone) scaffolds by gas foaming process and in vitro/in vivo degradation behavior using γ -ray irradiation. *Journal of Industrial and Engineering Chemistry*. **14** (4), 436-441.
- Linares, H. A. (1996) From wound to scar. *Burns*. **22** (5), 339-352.
- Lionelli, G. T. and Lawrence, W. T. (2003) Wound dressings. *Surgical Clinics of North America*. **83**, 617-638.
- Liu, C. K., Latuna, N. P. and Taylor, M. M. (2014) Preparations of nonwoven and green composites from collagen fibrous networks. *Journal of the American Leather Chemists Association*. **109**, 35-40.
- Liu, B., Yao, C., Chen, Y. and Hsu, S. (2003) In vitro evaluation of degradation and cytotoxicity of a novel composite as a bone substitute. *Journal of Biomedical Materials Research Part A*. **67A** (4), 1163-1169.

- Liu, Q., de Wijn, J. R. and van Blitterswijk, C. A. (1998) A study on the grafting reaction of isocyanates with hydroxyapatite particles. *Journal of Biomedical Materials Research*. **40** (3), 358-364.
- Liu, X., Won, Y. and Ma, P. X. (2006) Porogen-induced surface modification of nano-fibrous poly(L-lactic acid) scaffolds for tissue engineering. *Biomaterials*. **27** (21), 3980-3987.
- Lohre, J. M., Baclig, L., Wickham, E., Guida, S., Farley, J., Thyagarajan, K., Tu, R. and Quijano, C. (1993) Evaluation of epoxy ether fixed bovine arterial grafts for mutagenic potential. *ASAJO Journal*. **39**, 106-113.
- Loke, W. K. and Khor, E. (1995) Validation of the shrinkage temperature of animal tissue for bioprosthetic heart valve application by differential scanning calorimetry. *Biomaterials*. **16** (3), 251-258.
- Loke, W., Lau, S., Yong, L. L., Khor, E. and Sum, C. K. (2000) Wound dressing with sustained anti-microbial capability. *Journal of Biomedical Materials Research*. **53** (1), 8-17.
- Loretta, V. (2007) Stress and wound healing. *Clinics in Dermatology*. **25** (1), 49-55.
- Ma, W., Tang, C., Yin, S., Yang, X. and Qi, J. (2013) Genipin-crosslinked gelatin films as controlled releasing carriers of lysozyme. *Food Research International*. **51** (1), 321-324.
- Mabilleau, G., Stancu, I. C., Honoré, T., Legeay, G., Cincu, C., Baslé, M. F. and Chappard, D. (2006) Effects of the length of crosslink chain on poly(2-hydroxyethyl methacrylate) (pHEMA) swelling and biomechanical properties. *Journal of Biomedical Materials Research Part A*. **77A** (1), 35-42.
- MacNeil, S. (2007) Progress and opportunities for tissue-engineered skin. *Nature*. **445** (22), 874-879.
- Mao, J., Zhao, L., de Yao, K., Shang, Q., Yang, G. and Cao, Y. (2003) Study of novel chitosan-gelatin artificial skin in vitro. *Journal of Biomedical Materials Research Part A*. **64A** (2), 301-308.
- Marston, W., Hanft, J., Norwood, P. and Pollak, R. (2003) The efficacy and safety of dermagraft in improving the healing of chronic diabetic foot ulcers: Results of a prospective randomized trial. *Diabetes Care*. **26**, 1701-1705.
- Martucci, J. F. and Ruseckaite, R. A. (2010) Biodegradable three-layer film derived from bovine gelatin. *Journal of Food Engineering*. **99** (3), 377-383.
- Martucci, J. F., Ruseckaite, R. A. and Vázquez, A. (2006) Creep of glutaraldehyde-crosslinked gelatin films. *Materials Science and Engineering: C*. **435-436**, 681-686.
- Melling, M., Pfeiler, W., Karimian-Teherani, D., Schnallinger, M., Sobal, G., Zangerle, C. and Menzel, E. J. (2000) Differential scanning calorimetry, biochemical, and biomechanical analysis of human skin from individuals with diabetes mellitus. *The Anatomical Record*. **259** (3), 327-333.
- Mendes, A. A., de Castro, H. F., Andrade, G. S. S., Tardioli, P. W. and Giordano, R. d. L. C. (2013) Preparation and application of epoxy-chitosan/alginate support in the

- immobilization of microbial lipases by covalent attachment. *Reactive and Functional Polymers*. **73** (1), 160-167.
- Menke, N. B., Ward, K. R., Witten, T. M., Bonchev, D. G. and Diegelmann, R. F. (2007) Impaired wound healing. *Clinics in Dermatology*. **25** (1), 19-25.
- Meyer, M., Baltzer, H. and Schwikal, K. (2010) Collagen fibres by thermoplastic and wet spinning. *Materials Science and Engineering C*. **30**, 1266-1271.
- Mi, F., Sung, H. and Shyu, S. (2000) Synthesis and characterization of a novel chitosan-based network prepared using naturally occurring crosslinker. *Journal of Polymer Science Part A: Polymer Chemistry*. **38** (15), 2804-2814.
- Michon, C., Cuvelier, G., Relkin, P. and Launay, B. (1997) Influence of thermal history on the stability of gelatin gels. *International Journal of Biological Macromolecules*. **20** (4), 259-264.
- Miles, C. A., Avery, N. C., Rodin, V. V. and Bailey, A. J. (2005) The increase in denaturation temperature following cross-linking of collagen is caused by dehydration of the fibres. *Journal of Molecular Biology*. **346** (2), 551-556.
- Miles, C. A. and Ghelashvili, M. (1999) Polymer-in-a-box mechanism for the thermal stabilization of collagen molecules in fibers. *Biophysical Journal*. **76** (6), 3243-3252.
- Miranda, S. C. C. C., Silva, G. A. B., Hell, R. C. R., Martins, M. D., Alves, J. B. and Goes, A. M. (2011) Three-dimensional culture of rat BMMSCs in a porous chitosan-gelatin scaffold: A promising association for bone tissue engineering in oral reconstruction. *Archives of Oral Biology*. **56** (1), 1-15.
- Moscato, S., Mattii, L., D'Alessandro, D., Cascone, M. G., Lazzeri, L., Serino, L. P., Dolfi, A. and Bernardini, N. (2008) Interaction of human gingival fibroblasts with PVA/gelatine sponges. *Micron*. **39** (5), 569-579.
- Muyonga, J. H., Cole, C. G. B. and Duodu, K. G. (2004) Fourier transform infrared (FTIR) spectroscopic study of acid soluble collagen and gelatin from skins and bones of young and adult nile perch (*Iates niloticus*). *Food Chemistry*. **86** (3), 325-332.
- Na, G. C. (1986) Interaction of calf skin collagen with glycerol: Linked function analysis. *Biochemistry*. **25** , 967-973.
- Na, G. C. (1989) Monomer and oligomer of type I collagen: Molecular properties and fibril assembly. *Biochemistry*. **28** , 7161-7167.
- Nakka, J., Jansen, K. and Ernst, L. (2011) Effect of chain flexibility in the network structure on the viscoelasticity of epoxy thermosets. *Journal of Polymer Research*. **18** , 1879-1888.
- Nam, Y. S., Yoon, J. J. and Park, T. G. (2000) A novel fabrication method of macroporous biodegradable polymer scaffolds using gas foaming salt as a porogen additive. *Journal of Biomedical Materials Research*. **53** (1), 1-7.
- Natesan, S., Baer, D., Walters, T. J., Babu, M. and Christy, R. J. (2010) Adipose-derived stem cell delivery into collagen gels using chitosan microspheres. *Tissue Engineering: Part A*. **16** (4), 1369-1384.

- Natesan, S., Ravichandran, P., Neelakanta Reddy, P., Ramamurty, N., Pal, S. and Panduranga Rao, K. (2001) Collagen-chitosan polymeric scaffolds for the in vitro culture of human epidermoid carcinoma cells. *Biomaterials*. **22** (14), 1943-1951.
- Nieto, J. M. and Peniche-Covas, C. (1991) Characterization of chitosan by pyrolysis-mass spectrometry, thermal analysis and differential scanning calorimetry. *Thermochimica Acta*. **176**, 63-68.
- Noorjahan, S. E. and Sastry, T. P. (2004) An in vivo study of hydrogels based on physiologically clotted fibrin-gelatin composites as wound-dressing materials. *Journal of Biomedical Materials Research Part B: Applied Biomaterials*. **71B** (2), 305-312.
- Nussinovitch, A. (1992) Mechanical properties of hydrocolloid gels filled with internally produced carbon dioxide gas bubbles. *Biotechnology Progress*. **8**, 424-428.
- Olde Damink, L. H. H., Dijkstra, P. J., van Luyn, M. J. A., van Wachem, P. B., Nieuwenhuis, P. and Feijen, J. (1996) Cross-linking of dermal sheep collagen using a water-soluble carbodiimide. *Biomaterials*. **17** (8), 765-773.
- Olsen, D., Yang, C., Bodo, M., Chang, R., Leigh, S., Baez, J., Carmichael, D., Perälä, M., Hämäläinen, E., Jarvinen, M. and Polarek, J. (2003) Recombinant collagen and gelatin for drug delivery. *Advanced Drug Delivery Reviews*. **55** (12), 1547-1567.
- Ostrowska-Czubenko, J. and Gierszecka-Drużyńska, M. (2009) Effect of ionic crosslinking on the water state in hydrogel chitosan membranes. *Carbohydrate Polymers*. **77** (3), 590-598.
- Ovington, L. (2007) Advances in wound dressings. *Clinics in Dermatology*. **25** (1), 33-38.
- Panzavolta, S., Gioffrè, M., Focarete, M. L., Gualandi, C., Foroni, L. and Bigi, A. (2011) Electrospun gelatin nanofibers: Optimization of genipin cross-linking to preserve fiber morphology after exposure to water. *Acta Biomaterialia*. **7** (4), 1702-1709.
- Park, T. G. (2002) Perfusion culture of hepatocytes within galactose-derivatized biodegradable poly(lactide-co-glycolide) scaffolds prepared by gas foaming of effervescent salts. *Journal of Biomedical Materials Research*. **59** (1), 127-135.
- Patil, R. D., Mark, J. E., Apostolov, A., Vassileva, E. and Fakirov, S. (2000) Crystallization of water in some crosslinked gelatins. *European Polymer Journal*. **36** (5), 1055-1061.
- Pauline, B. (2010) Basic science of wound healing. *Surgery (Oxford)*. **28** (9), 409-412.
- Pawlak, A. and Mucha, M. (2003) Thermogravimetric and FTIR studies of chitosan blends. *Thermochimica Acta*. **396** (1-2), 153-166.
- Payne, K. J. and Veis, A. (1988) Fourier transform IR spectroscopy of collagen and gelatin solutions: Deconvolution of the amide I band for conformational studies. *Biopolymers*. **27** (11), 1749-1760.
- Pereda, M., Ponce, A. G., Marcovich, N. E., Ruseckaite, R. A. and Martucci, J. F. (2011) Chitosan-gelatin composites and bi-layer films with potential antimicrobial activity. *Food Hydrocolloids*. **25** (5), 1372-1381.

- Pereira, R. F., Barrias, C. C., Granja, P. L. and Bartolo, P. J. (2013) Advanced biofabrication strategies for skin regeneration and repair. *Nanomedicine*. **8** (4), 603-621.
- Piotrowska, B., Sztuka, K., Kołodziejska, I. and Dobrosielska, E. (2008) Influence of transglutaminase or 1-ethyl-3-(3-dimethylaminopropyl) carbodiimide (EDC) on the properties of fish-skin gelatin films. *Food Hydrocolloids*. **22** (7), 1362-1371.
- Pok, S., Myers, J. D., Madihally, S. V. and Jacot, J. G. (2013) A multilayered scaffold of a chitosan and gelatin hydrogel supported by a PCL core for cardiac tissue engineering. *Acta Biomaterialia*. **9** (3), 5630-5642.
- Porter, D. and Vollrath, F. (2012) Water mobility, denaturation and the glass transition in proteins. *Biochimica Et Biophysica Acta (BBA) - Proteins and Proteomics*. **1824** (6), 785-791.
- Poursamar, S. A., Azami, M. and Mozafari, M. (2011) Controllable synthesis and characterization of porous polyvinyl alcohol/hydroxyapatite nanocomposite scaffolds via an *in situ* colloidal technique. *Colloids and Surfaces B: Biointerfaces*. **84**, 310-316.
- Price, C. A. (1986) The effect of cross-linking agents on the impact resistance of a linear poly(methyl methacrylate) denture-base polymer. *Journal of Dental Research*. **65** (7), 987-992.
- Prochazkova, S., Vårum, K. M. and Ostgaard, K. (1999) Quantitative determination of chitosans by ninhydrin. *Carbohydrate Polymers*. **38** (2), 115-122.
- Puppi, D., Chiellini, F., Piras, A. M. and Chiellini, E. (2010) Polymeric materials for bone and cartilage repair. *Progress in Polymer Science*. **35** (4), 403-440.
- Qu, X., Wirsén, A. and Albertsson, A. -. (2000) Effect of lactic/glycolic acid side chains on the thermal degradation kinetics of chitosan derivatives. *Polymer*. **41** (13), 4841-4847.
- Rabotyagova, O. S., Cebe, P. and Kaplan, D. L. (2008) Collagen structural hierarchy and susceptibility to degradation by ultraviolet radiation. *Materials Science and Engineering: C*. **28** (8), 1420-1429.
- Ramos-e-Silva, M. and Ribeiro de Castro, M. C. (2002) New dressings, including tissue-engineered living skin. *Clinics in Dermatology*. **20** (6), 715-723.
- Reich, G. (2007) *From collagen to leather: the theoretical background, What is collagen?* BASF. pp. 7.
- Ren, L., Tsuru, K., Hayakawa, S. and Osaka, A. (2001) Synthesis and characterization of gelatin-siloxane hybrids Derived through sol-gel procedure. *Journal of Sol-Gel Science and Technology*. **21** , 115-121.
- Ren, L., Wang, J., Yang, F., Wang, L., Wang, D., Wang, T. and Tian, M. (2010) Fabrication of gelatin-siloxane fibrous mats via sol-gel and electrospinning procedure and its application for bone tissue engineering. *Materials Science and Engineering: C*. **30** (3), 437-444.
- Rivero, S., García, M. A. and Pinotti, A. (2009) Composite and bi-layer films based on gelatin and chitosan. *Journal of Food Engineering*. **90** (4), 531-539.

- Ruszczak, Z. (2003) Effect of collagen matrices on dermal wound healing. *Advanced Drug Delivery Reviews*. **55** (12), 1595-1611.
- Sagnella, S. and Mai-Ngam, K. (2005) Chitosan based surfactant polymers designed to improve blood compatibility on biomaterials. *Colloids and Surfaces B: Biointerfaces*. **42** (2), 147-155.
- Saint, S., Elmore, J. and Sullivan, S. (1998) The efficacy of silver alloy-coated urinary catheters in preventing urinary tract infection: A meta-analysis. *American Journal of Medicine*. **105** (1), 236-241.
- Sarem, M., Moztarzadeh, F. and Mozafari, M. (2013) How can genipin assist gelatin/carbohydrate chitosan scaffolds to act as replacements of load-bearing soft tissues? *Carbohydrate Polymers*. **93** (2), 635-643.
- Schoof, H., Apel, J., Heschel, I. and Rau, G. (2001) Control of pore structure and size in freeze-dried collagen sponges. *Journal of Biomedical Materials Research*. **58** (4), 352-357.
- Sezer, A.D. and Cevher, E.(2011) *Biopolymers as wound healing materials: challenges and new strategies*. Intech. pp. 383-415.
- Sherratt, J. A. and Dallon, J. C. (2002) Theoretical models of wound healing: Past successes and future challenges. *Comptes Rendus Biologies*. **325** (5), 557-564.
- Shiroasaki, Y., Tsuru, K., Hayakawa, S., Osaka, A., Lopes, M. A., Santos, J. D., Costa, M. A. and Fernandes, M. H. (2009) Physical, chemical and in vitro biological profile of chitosan hybrid membrane as a function of organosiloxane concentration. *Acta Biomaterialia*. **5** (1), 346-355.
- Sobral, P. J. A., Menegalli, F. C., Hubinger, M. D. and Roques, M. A. (2001) Mechanical, water vapor barrier and thermal properties of gelatin based edible films. *Food Hydrocolloids*. **15** (4-6), 423-432.
- Speit, G., Neuss, S., Schütz, P., Fröhler-Keller, M. and Schmid, O. (2008) The genotoxic potential of glutaraldehyde in mammalian cells in vitro in comparison with formaldehyde. *Mutation Research - Genetic Toxicology and Environmental Mutagenesis*. **649** (1-2), 146-154.
- Stadelmann, W. K., Digenis, A. G. and Tobin, G. R. (1998a) Impediments to wound healing. *The American Journal of Surgery*. **176** (2, Supplement 1), 39S-47S.
- Stadelmann, W. K., Digenis, A. G. and Tobin, G. R. (1998b) Physiology and healing dynamics of chronic cutaneous wounds. *The American Journal of Surgery*. **176** (2, Supplement 1), 26S-38S.
- Stankus, J. J., Guan, J. and Wagner, W. R. (2004) Fabrication of biodegradable elastomeric scaffolds with sub-micron morphologies. *Journal of Biomedical Materials Research Part A*. **70A** (4), 603-614.
- Steed, D. L., Ricotta, J. J., Prendergast, J. J., Kaplan, R. J., Webster, M. W., McGill, J. B. and Schwartz, S. L. (1995) Promotion and acceleration of diabetic ulcer healing by arginine-glycine-aspartic acid (RGD) peptide matrix. *Diabetes Care*. **18** (1), 39-46.

- Stevenson, P. (2010) Inter-bubble gas diffusion in liquid foam. *Current Opinion in Colloid & Interface Science*. **15** (5), 374-381.
- Strodtbeck, F. (2001) Physiology of wound healing. *Newborn and Infant Nursing Reviews*. **1** (1), 43-52.
- Sun, S., Lin, Y., Weng, Y. and Chen, M. (2006) Efficiency improvements on ninhydrin method for amino acid quantification. *Journal of Food Composition and Analysis*. **19** (2-3), 112-117.
- Sung, H., Chen, C., Huang, R., Hsu, J. and Chang, W. (2000) In vitro surface characterization of a biological patch fixed with a naturally occurring crosslinking agent. *Biomaterials*. **21** (13), 1353-1362.
- Sung, H., Cheng, W., Chiu, I., Hsu, H. and Liu, S. (1996a) Studies on epoxy compound fixation. *Journal of Biomedical Materials Research*. **33** (3), 177-186.
- Sung, H., Hsu, C., Lee, Y. and Lin, D. (1996b) Crosslinking characteristics of an epoxy-fixed porcine tendon: Effects of pH, temperature, and fixative concentration. *Journal of Biomedical Materials Research*. **31** (4), 511-518.
- Sung, H., Hsu, C., Wang, S. and Hsu, H. (1997a) Degradation potential of biological tissues fixed with various fixatives: An in vitro study. *Journal of Biomedical Materials Research*. **35** (2), 147-155.
- Sung, H., Hsu, H. and Hsu, C. (1997b) Effects of various chemical sterilization methods on the crosslinking and enzymatic degradation characteristics of an epoxy-fixed biological tissue. *Journal of Biomedical Materials Research*. **37** (3), 376-383.
- Sung, H., Huang, D., Chang, W., Huang, R. and Hsu, J. (1999a) Evaluation of gelatin hydrogel crosslinked with various crosslinking agents as bioadhesives: In vitro study. *Journal of Biomedical Materials Research*. **46** (4), 520-530.
- Sung, H., Huang, R., Huang, L. L. H. and Tsai, C. (1999b) In vitro evaluation of cytotoxicity of a naturally occurring crosslinking reagent for biological tissue fixation. *Journal of Biomaterials Science, Polymer Edition*. **10** (1), 63-78.
- Sung, H., Huang, R., Huang, L. L. H., Tsai, C. and Chiu, C. (1998) Feasibility study of a natural crosslinking reagent for biological tissue fixation. *Journal of Biomedical Materials Research*. **42** (4), 560-567.
- Sung, H., Liang, I., Chen, C., Huang, R. and Liang, H. (2001) Stability of a biological tissue fixed with a naturally occurring crosslinking agent (genipin). *Journal of Biomedical Materials Research*. **55** (4), 538-546.
- Sung, H., Shih, J. and Hsu, C. (1996) Crosslinking characteristics of porcine tendons: Effects of fixation with glutaraldehyde or epoxy. *Journal of Biomedical Materials Research*. **30** (3), 361-367.
- Supp, D. M. and Boyce, S. T. (2005) Engineered skin substitutes: Practices and potentials. *Clinics in Dermatology*. **23** (4), 403-412.
- Susi, H., Ard, J. S. and Carroll, R. J. (1971) The infrared spectrum and water binding of collagen as a function of relative humidity. *Biopolymers*. **10** (9), 1597-1604.

- Tasselli, F., Mirmohseni, A., Seyed Dorraji, M. S. and Figoli, A. (2013) Mechanical, swelling and adsorptive properties of dry-wet spun chitosan hollow fibers crosslinked with glutaraldehyde. *Reactive and Functional Polymers*. **73** (1), 218-223.
- Thomazine, M., Carvalho, R. A. and Sobral, P. J. A. (2005) Physical properties of gelatin films plasticized by blends of glycerol and sorbitol. *Journal of Food Science*. **70** (3), E172-E176.
- Tillet, G., Boutevin, B. and Ameduri, B. (2011) Chemical reactions of polymer crosslinking and post-crosslinking at room and medium temperature. *Progress in Polymer Science*. **36** (2), 191-217.
- Tirkistani, F. A. A. (1998) Thermal analysis of some chitosan schiff bases. *Polymer Degradation and Stability*. **60** (1), 67-70.
- Touyama, R., Takeda, Y., Inoue, K., Kawamura, I., Yatsuzuka, M., Ikumoto, T., Yokoi, T. and Inouye, H. (1994) Studies on the blue pigments produced from genipin and methylamine. I. structures of the brownish-red pigments, intermediates leading to the blue pigments. *Chemical and Pharmaceutical Bulletin*. **42** (3), 668-673.
- Usha, R. and Ramasami, T. (2000) Effect of crosslinking agents (basic chromium sulfate and formaldehyde) on the thermal and thermomechanical stability of rat tail tendon collagen fibre. *Thermochimica Acta*. **356** (1-2), 59-66.
- van den Bosch, E. and Gielens, C. (2003) Gelatin degradation at elevated temperature. *International Journal of Biological Macromolecules*. **32** (3-5), 129-138.
- Vargas, G., Acevedo, J. L., López, J. and Romero, J. (2008) Study of cross-linking of gelatin by ethylene glycol diglycidyl ether. *Materials Letters*. **62** (21-22), 3656-3658.
- Vijayakumar, V. and Subramanian, K. (2014) Diisocyanate mediated polyether modified gelatin drug carrier for controlled release. *Saudi Pharmaceutical Journal*. **22** (1), 43-51.
- Vincent, F. (2005) Wound healing and its impairment in the diabetic foot. *The Lancet*. **366** (9498), 1736-1743.
- Warren, J. (1997) Catheter-associated urinary tract infections. *Infectious Disease Clinics of North America*. **11** (1), 609-622.
- Werdin, F., Tenenhaus, M. and Rennekampff, H. (2008) Chronic wound care. *The Lancet*. **372** (9653), 1860-1862.
- Williamson, D. and Harding, K. (2004) Wound healing. *Medicine*. **32** (12), 4-7.
- Wine, Y., Cohen-Hadar, N., Freeman, A. and Frolow, F. (2007) Elucidation of the mechanism and end products of glutaraldehyde crosslinking reaction by X-ray structure analysis. *Biotechnology and Bioengineering*. **98** (3), 711-718.
- Wong, V. W. and Gurtner, G. C. (2012) Tissue engineering for the management of chronic wounds: Current concepts and future perspectives. *Experimental Dermatology*. **21** (10), 729-734.
- Wu, X., Liu, Y., Li, X., Wen, P., Zhang, Y., Long, Y., Wang, X., Guo, Y., Xing, F. and Gao, J. (2010) Preparation of aligned porous gelatin scaffolds by unidirectional freeze-drying method. *Acta Biomaterialia*. **6** (3), 1167-1177.

- Yang, C., Xu, L., Zhou, Y., Zhang, X., Huang, X., Wang, M., Han, Y., Zhai, M., Wei, S. and Li, J. (2010) A green fabrication approach of gelatin/CM-chitosan hybrid hydrogel for wound healing. *Carbohydrate Polymers*. **82** (4), 1297-1305.
- Yang, J. M., Su, W. Y., Leu, T. L. and Yang, M. C. (2004) Evaluation of chitosan/PVA blended hydrogel membranes. *Journal of Membrane Science*. **236** (1-2), 39-51.
- Yannas, I. V. and Burke, J. P. (1980) Design of an artificial skin. I. basic design principles. *Journal of Biomedical Materials Research Part A*. **14**, 65-81.
- Yao, C., Liu, B., Chang, C., Hsu, S. and Chen, Y. (2004) Preparation of networks of gelatin and genipin as degradable biomaterials. *Materials Chemistry and Physics*. **83** (2-3), 204-208.
- Yeh, M., Liang, Y., Cheng, K., Dai, N., Liu, C. and Young, J. (2011) A novel cell support membrane for skin tissue engineering: Gelatin film cross-linked with 2-chloro-1-methylpyridinium iodide. *Polymer*. **52** (4), 996-1003.
- Yilgör, E., Burgaz, E., Yurtsever, E. and Yilgör, İ. (2000) Comparison of hydrogen bonding in polydimethylsiloxane and polyether based urethane and urea copolymers. *Polymer*. **41** (3), 849-857.
- Yoon, J. J., Kim, J. H. and Park, T. G. (2003) Dexamethasone-releasing biodegradable polymer scaffolds fabricated by a gas-foaming/salt-leaching method. *Biomaterials*. **24** (13), 2323-2329.
- Young, S., Wong, M., Tabata, Y. and Mikos, A. G. (2005) Gelatin as a delivery vehicle for the controlled release of bioactive molecules. *Journal of Controlled Release*. **109** (1-3), 256-274.
- Zeugolis, D. I., Paul, G. R. and Attenburrow, G. (2009) Cross-linking of extruded collagen fibers?A biomimetic three-dimensional scaffold for tissue engineering applications. *Journal of Biomedical Materials Research Part A*. **89A** (4), 895-908.
- Zhang, X., Yang, D. and Nie, J. (2008) Chitosan/polyethylene glycol diacrylate films as potential wound dressing material. *International Journal of Biological Macromolecules*. **43** (5), 456-462.
- Zhao, W., Jin, X., Cong, Y., Liu, Y. and Fu, J. (2013) Degradable natural polymer hydrogels for articular cartilage tissue engineering. *Journal of Chemical Technology & Biotechnology*. **88** (3), 327-339.
- Zhou, J. and Lucas, J. P. (1999) Hygrothermal effects of epoxy resin. part I: The nature of water in epoxy. *Polymer*. **40** (20), 5505-5512.

Appendix 1

Gelatin

Characterisation

Methods

1. Hydroxyproline Content

Hydroxyproline is essential to stabilise collagen triple helical structure and increase protein thermal stability. In addition, it acts to suppress protein aggregation and fibril formation. In the absence of hydroxyproline, the essential triple helical conformation of protein is thermally unstable at well below physiological temperature. Hydroxyproline content in gelatin sample used in this study was assayed using Chloramine T method.

0.31 Grams of gelatin powder was placed in digestion tube and 10 ml of hydrochloric acid (50% v/v) was added to the tube and the lid was immediately closed. The tube was put in oven at 100 °C for 16 hours.

The hydrolysed sample was cool and transferred to a 100 ml volumetric flask and was diluted to the mark with de-ionised water. 2 ml of this solution was extracted and transferred to a separate 100 ml volumetric flask and diluted to the mark.

Standard curve was drawn by means of diluting 100 mg.dm⁻³ hydroxyproline stock solution to 100 ml according to Table A-1. All standards and samples were prepared in triplicate. The blank sample was prepared using de-ionised water.

Table A-1: Prepared standard concentration using 100 mg.dm⁻¹ hydroxyproline solution

Aliquot of stock solution (ml)	0	2.50	5.00	10.00	15.00	20.00
Standard Concentration (mg/L)	0	2.50	5.00	10.00	15.00	20.00

Reaction mixture was prepared by mixing following volume of each ingredient: 0.55 ml of hydrolysed sample (or above-prepared standard) with 1.27 ml of Propanol-2-ol, and 0.88 ml of chloramines T reagent. Chloramine T reagent was prepared by mixing 10 ml of de-ionised water, 0.70 g of chloramines T, and 50 ml of citrate buffer. Citrate buffer was prepared according to following recipe: 17.19 g of sodium acetate anhydrous,

18.75 g of tri-sodium citrate.2H₂O, and 2.75 g citric acid were all dissolved 200 ml of de-ionised water and 200 ml of proponol-2-ol.

Upon mixing sample solution with diluents and chloramines T agent, the mixture left for 5 minutes at room temperature and then 2.30 ml of Ehrlichs reagent was added to the reaction tube. The Ehrlichs reagent was prepared by dissolving 12 g of Dimethylaminobenzaldehyde in 18 ml of perchloric acid; 100 ml of pronol-2-ol was added to this mixture immediately before use.

Upon addition of Ehrlichs reagent, the mixture was vortexed and incubated in a water bath at 70 °C for 10 minutes. The test tubes were cooled to room temperature and the absorbance was read at 555 nm (UV-250IPC, Shimadzu, Japan).

Figure A-1 shows the calibration curve of hydroxyproline stock solution along with the value obtained from commercially available bovine Type-B gelatin used in this study.

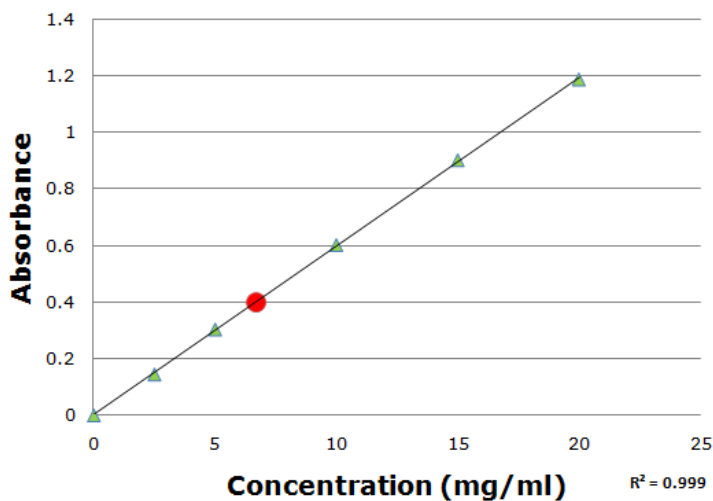


Figure 1: calibration curve used to assess the hydroxyproline content of bovine gelatin sample used in this study, Triangle markers show standard protein hydroxyproline content and red circular marker shows gelatin sample hydroxyproline content.

According to Figure A-1, prepared sample shows absorption of 0.40 which delineates the concentration of 6.70 mg/ml; however, several dilutions were performed

on original sample which needs to be taken into account to obtain actual hydroxyproline content of the sample:

0.31 g of sample is 500 times diluted; thus:

$$6.67 \times 500 = 3350 \text{ mg/ml};$$

The initial volume of HCl in which the gelatin was dissolved was 10 ml (0.01 l), thus:

$$3350 \text{ mg} * \frac{10 \text{ ml}}{1000 \text{ ml}} = 33.50 \text{ mg}$$

This amounts to 0.31 g of gelatin sample which was originally digested in HCl, thus each gram of sample contains (in percentage):

$$(33.50 / 310) \times 100 = \%10.80 \text{ hydroxyproline}$$

Collagen conversion coefficient for gelatin is 8, therefore the collagen content of the gelatin used in this study is equal with:

$$10.80 \times 8 = 86.40 \% \text{ collagen content}$$

2. Protein Content Analysis

Protein content of the gelatin sample used in this experiment was analysed according to Flory-Lowry Method.

Materials:

Complex Forming reagent was prepared as following:

Solution A: 2%w/v Na₂CO₃ in 0.1 M NaOH

Solution B: 1%w/v CuSO₄.5H₂O in distilled water

Solution C: 2 %w/v Na tartrate in distilled water

1 ml of solution B and C was mixed with 98 ml solution A to make 100 ml. The mixing was carried out immediately 1 hour before use. Extra cautious was undertaken for the pH to be around 10 to 10.5.

Standards Sample Preparation: Bovine serum albumin was used as standard protein. A stock solution of bovine serum albumin containing 2 mg/ml protein in distilled water was prepared. The standard solution was thawed in 37°C water bath each time

before use. Standard solutions were prepared by diluting the albumin solution (stock solution) with distilled water as listed in Table A-2:

Table A-2: List of prepared standard solution for gelatin protein content analysis

Stock Solution (μl)	0	50	100	200
Water (μl)	1000	950	900	800
Protein Content ($\mu\text{g/ml}$)	0	100	200	400

Unknown Sample Preparation: 2 mg/ml gelatin aqueous solution was dissolved in distilled water using magnetic stirrer and hotplate at 60°C. Prepared gelatin solution was diluted by taking 50 μl of gelatin solution and adding 950 μl distilled water to reach the final volume to 1000 μl . This places the unknown sample potential protein content in the middle of standard concentration range (Table A-2).

Assay Protocol:

1. Both unknown sample and standard solution were hydrolysed at 100°C for 10 min in heating block.
2. Hydrolysed were cooled to room temperature and 5 ml of freshly mixed complex-forming reagent was added to each sample vial. The solution was left stay at room temperature for 10 minutes.
3. As the reaction is extremely pH sensitive, the solution pH was checked one last time to be above 10.
4. 0.25 ml of Folin reagent (2N) was added to each sample vials and immediately mixed using vortex.
5. The test solutions were incubated at ambient temperature for 30 minutes.
6. The solution absorbance was read at 550 nm (UV-250IPC, Shimadzu, Japan).
7. Standard curve of absorbance as a function of initial protein concentration was plotted and was used to determine the unknown protein concentration.

Figure A-2 show the calibration curve of standard protein sample along with the value obtained from commercially available bovine Type-B gelatin purchased from sigma chemical and used in this study.

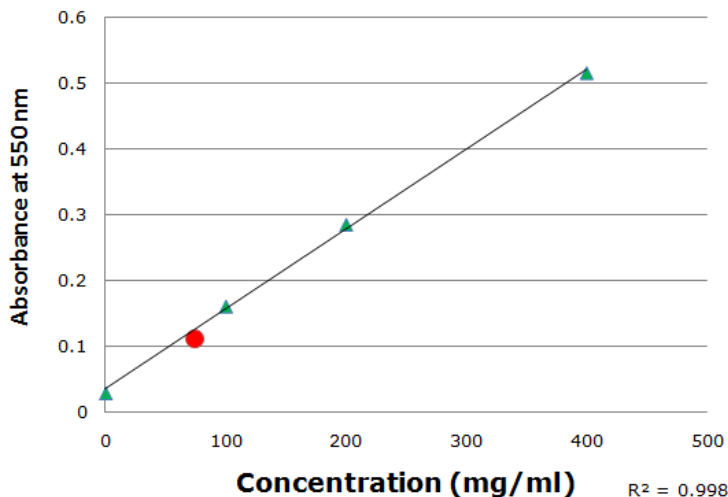


Figure A-2: The standard curve of protein content analysis along with the result of experiments on gelatin sample used in this study. Standard data are shown by triangle marker, whilst the sample protein content result is shown by circular red marker.

According to Figure A-2, prepared sample shows an absorption of 0.107 which delineates the concentration of 75 mg/ml; however, several dilutions were performed on original sample which needs to be taken into account to obtain real protein content of the sample:

10 mg was dissolved in 5 ml of de-ionised and obtained solution is later diluted 20 times, thus:

$$75 \times 20 = 1500 \text{ mg/ml}$$

The initial volume of solution in which the gelatin was dissolved was 5 ml (0.005 l), thus:

$$1500 \text{ mg} * \frac{5 \text{ ml}}{1000 \text{ ml}} = 7.5 \text{ mg}$$

This amounts to 10 mg of gelatin sample, thus each gram of sample contains (in percentage):

$$(7.5 / 10) \times 100 = 75 \% \text{ protein content}$$

The protein content of gelatin samples differs based on their origin and animal source type. For instance the range of reported results for protein content of gelatin samples originate from fish is lower than bovine and porcine gelatin. Bovine and porcine gelatin generally shows higher amount of gelatin content. The value of protein content

reported for bovine and porcine gelatin range between 83 to 88% (Koli *et al.*, 2012, Jeya Shakila *et al.*, 2012).

3. Bloom Index:

Bloom index (also known as gel strength) is one of the most important properties of gelatin and the mechanical integrity of gelatin is determined by its value. The hydrogen bond formation between the water molecules and free hydroxyl groups of amino acid in the gelatin are responsible for the bloom strength (Jeya Shakila *et al.*, 2012).

The bloom index of gelatin sample used in this study was determined according to ISO-9665 standard. Bloom index is a measure of hydrogel stiffness, with higher bloom index indicative of higher gel stiffness. This index is an inherent property of gelatin macromolecules and would be set by several parameters such as manufacturing method and source of gelatin. 7.14% w/w gelatin solution was prepared by adding appropriate amount of gelatin powder to de-ionised water. The containers were covered with parafilm and left at room temperature for 2 hours for gelatin to soak. The containers were heated at 60 degree using magnetic stirrer and hotplate for 15 minutes to dissolve the gelatin completely. The gelatin aqueous solution was immediately poured into standard bloom jar (with standard internal diameter of 59 mm and a capacity of approximately 155 ml). The bloom jars were covered and left for 2 minutes for potential bubble dissipate. The jars were transferred into 10 degree water bath for 16 hours. The gelatin bloom index was determined using TA-XT-Plus texture analyser (Surrey, UK). To perform the experiment standard probe with diameter of 0.5" was used. The probe was programmed to plunges into the conditioned-gelatin surface downward for 4 mm with crosshead speed of 0.5 mm/sec. At this depth the maximum force was read and reported as gelatin bloom index. The results were obtained in triplicate.

The gel strength of commercial gelatins ranges from 100 to 300; fish gelatin typically has a gel strength ranging from as low as zero to 426g, whilst this amount for bovine gelatin or porcine gelatin is between 200 to 300 g. the difference in bloom index of different type of gelatin may possibly be due to the lower content of proline and hydroxyproline. The gelatin used in this study shows the bloom index of 303 g. This amount is in high end range of value reported for bovine gelatin bloom index which will ultimately helps enhance the mechanical properties of final product.

4. Molecular Weight Distribution of Gelatin

Molecular weight of gelatin sample used in this study was determined using SDS - Poly Acrylamide Gel Electrophoresis (SDS-PAGE). Figure A-3 represents a comparison between obtained results and collagen SDS-PAGE gel results reported by other researchers. According to obtained results the gelatin samples has a molecular weight distribution between 100 kDa to 200 kDa. The examined bovine gelatin shows two bands corresponding to approximately 116 and 100 kDa. Skin is made up of skin type I collagen (Olsen *et al.*, 2003) which in turn is made up of two identical α_1 chains and one α_2 chain linked covalently to form a triple helix structure (Gómez-Guillén *et al.*, 2011). Figure A-3-B shows the result of bovine type I collagen SDS-PAGE which reflects three distinct bands designated as γ , β , and α bands. Depending on gelatin manufacturing method these bands may or may not be reflected in the produced gelatin SDS-PAGE results. In case there is any remaining triple helical structure left from collagen, they will be shown as a distinct band on the top part of the gel (known as γ band) around 250kDa (Rabotyagova *et al.*, 2008). Obtained results do not show this band which shows triple helical structure decimation as a result of heat treatment and Basic solution extraction method throughout gelatin manufacturing process. β bands is culmination of covalently linked dimmers of alpha chains and would be reflected around 100 kDa (Gómez-Guillén *et al.*, 2011, Rabotyagova *et al.*, 2008). The third and last band is designated as alpha chains which are fragmented collagen backbones and would appeared after β dimmers.

The molecular range distribution shown for the material used in this study is in agreement with the results reported for commercially available bovine gelatin (Jeya Shakila *et al.*, 2012). The gel preparation protocols, staining, and destaining methods are discussed in the following portion of this section.

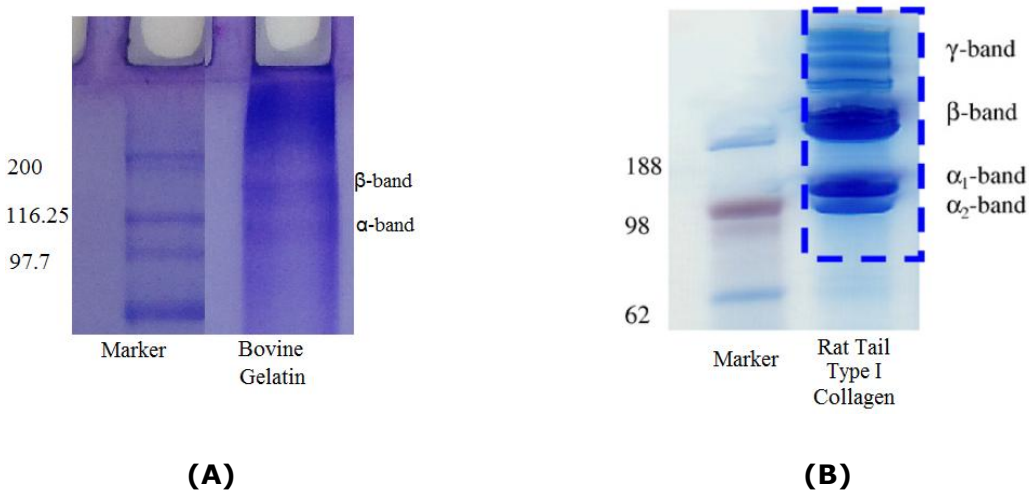


Figure A-3: (A) The result of SDS-PAGE electrophoresis of gelatin sample used in this study (B) SDS-PAGE electrophoresis of type I collagen sample, three distinct bands of γ , β , and α represent trimmer, dimmer, and fragmented collagen alpha chains (Rabotyagova *et al.*, 2008).

Gel Preparation:

Resolving Gel: 10% resolving gel was prepared according to ingredient ratio mentioned in Table A-3. All ingredients except for APS and TEMED were mixed in conical flask and were degassed under vacuum for more than 10 minutes. Upon degassing, TEMED and APS were added to the mixture and the gel was cast immediately. The resolving gel was left to set at ambient temperature for 45 minutes. During setting period the gel was topped by de-ionised water.

Stacking Gel: 5% stacking gel was prepared according to ingredient ratio mentioned in Table A-3. Stacking gel preparation was similar to resolving gel preparation except for the following. Prior to stacking gel casting, the water on the top of resolving gel was removed using paper filter. Immediately after stacking gel casting the comb was inserted into the stacking gel to form sample wells. The resolving gel was left to set at ambient temperature for 45 minutes. During setting period the gel was topped by de-ionised water.

Table A-3: Resolving and stacking gel ingredients

	Resolving Gel (10%)	Stacking Gel (5%)
30% acrylamide	3.3 ml	1.7 ml
1.0 M Tris-HCl	2.5 ml (pH: 8.8)	2.5 ml (pH: 6.8)
10% SDS	0.1 ml	0.1 ml
Distilled water	4.1 ml	5.7 ml
10% APS	50 µl	50 µl
TEMED	5 µl	10 µl

Sample Digestion: Gelatin solution with 4 mg/ml concentration was prepared. 1µl of digested sample solution would be mixed with 20 µl of sample buffer and hydrolysed in 100°C boiling water for 5 minutes. 5 µl of the prepared mixture would be loaded into prepared acrylamide gel well and electrophoresed under 50 volts current. The electrophoreses would be continued until the dye front would reach the base of the gel. The gels would be removed from the cell and stained after 1 hour using Coomassie Brilliant Blue and then destained using mixture of 10 ml methanol and 7 ml acetic acid diluted to 100 ml with de-ionised water.

Appendix 2

Ninhydrin Assay

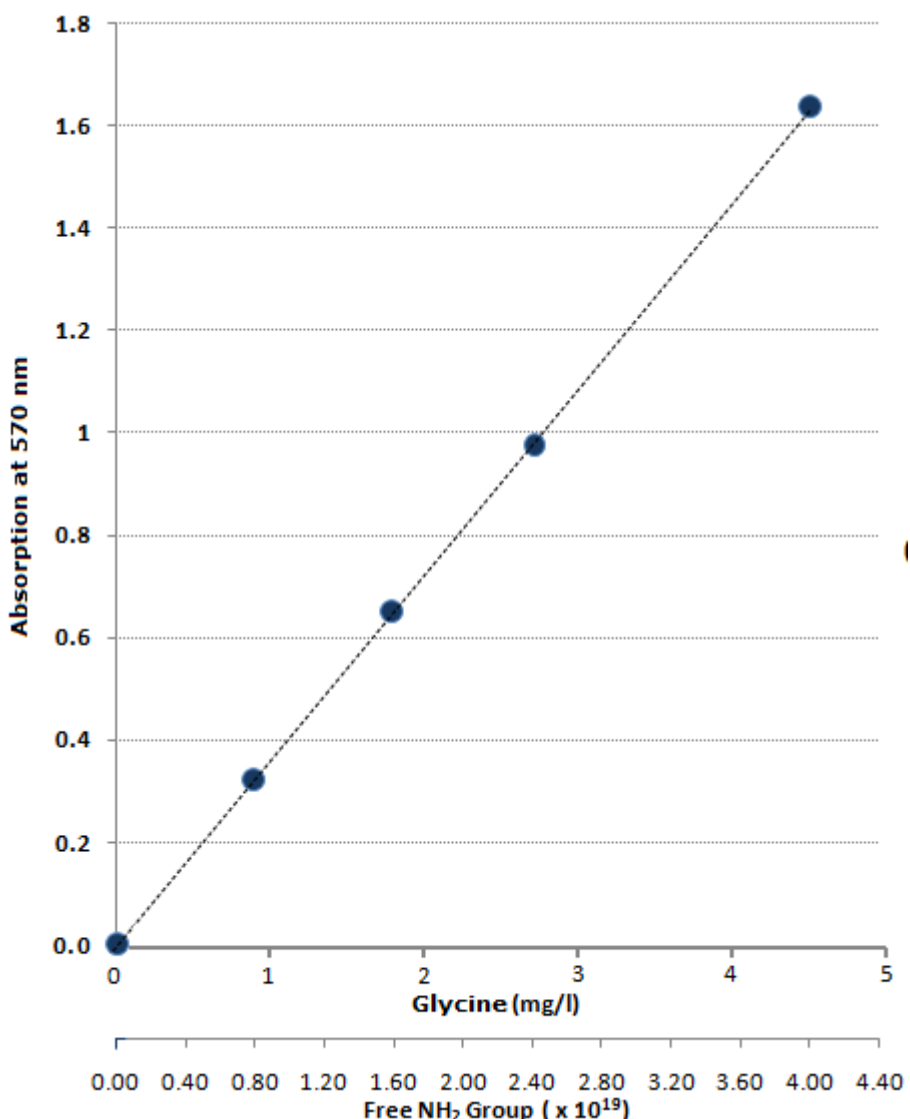


Figure A-4: Standard curve for glycine solution with 0, 1, 2, 3, and 5 mg/l concentrations and schematic representation of glycine molecule structure. The secondary X-axis at the bottom of the diagram shows the number of available free amine group at each concentration of glycine ($R^2=0.999$).

To perform the Ninhydrin assay, gelatin scaffolds were weighed and grounded. 1 ml of deionised water was added to the grounded gelatin scaffold fragments. 1 ml of Ninhydrin reagent was added to gelatin-water mixture. Ninhydrin reagent was prepared according to the following recipe; 2g of Ninhydrin was mixed with 0.3g of Hydrindantin. The mixture was dissolved in 75ml of Dimethyl Sulfoxide (DMSO). The obtained solution was purged with N₂ for 20 minutes to purge the solution from Oxygen. Separately, 25 ml of lithium acetate buffer was prepared by adding 408g lithium acetate in 1 litre of deionised water (pH was adjusted at 5.2). Ninhydrin solution was added and agitated with

Lithium acetate mixture and a dark red colour solution formed. The mixture of gelatin solution and reagent were heated in boiling water for 20 minutes. After heating the test tubes were transferred into a 4 °C water bath and after temperature adjustment, 5ml of 50% v/v ethanol-water solution was added to test tube. The excess non-reacted ninhydrin were oxidised by vortex for 15 seconds. The absorption was measured at 570 nm (UV-250IPC, Shimadzu, Japan). The reagent should be kept in the fridge. It can be stored for about a week after which it will go off by turning into yellow liquid as a result of reaction with air Oxygen.

Glycine was used as a standard to plot calibration curve (Sung *et al.*, 1997a). Each molecule of glycine has only one free amine group. The number of glycine molecules is the same as the number of free amine groups in solution. This fact can be used to link the value of UV absorption to the number of available free amine group in any solution. 0.1 g/l glycine stock solution was prepared and 1, 2, 3, and 5 ml of stock solution were diluted to 100 ml with de-ionised water to obtain 1, 2, 3, and 5 mg/l standard solutions, respectively. Every 1ml of standard solution was added to 1 ml of Ninhydrin reagent. Figure A-4 shows obtained absorption curve for glycine standard concentrations. Second horizontal axis in Figure A-4 shows the number of free amine group corresponding to each concentration. The calculation for the number of free amine groups in 1 mg/l solution is provided in Equation A-1; Glycine molar mass is 75.05 g/mol and Avogadro Number is 6.02×10^{23} .

$$\frac{1 \text{ mg Glycine}}{1 \text{ l}} \times \frac{1 \text{ mole Glycine}}{75050 \text{ mg Glycine}} \times \frac{6.02 \times 10^{23}}{1 \text{ mole Glycine}} = 0.802 \times 10^{19} \frac{\text{Number of Glycin Molecules}}{\text{l}}$$

$$0.802 \times 10^{19} \frac{\text{Glycin Molecules}}{\text{l}} = 0.802 \times 10^{19} \frac{\text{Free amine}}{\text{l}} \quad (\text{Equation A-1})$$

Appendix 3

Crosslinking agent concentration determination

Following calculations were used to determine necessary volume and mass for three alternative crosslinking agents used in this study to be compared against GT.

To prepare HMDI solution with concentration of 0.005% mol/v, 0.803 ml of HMDI was added to 100 ml of Propan-2-ol, this amount was assessed by assuming HMDI molar mass and density as 168.19 g/mol and 1.047 g/ml, respectively. Equation A-2 shows the computation for obtaining suitable amount of HMDI for this study.

$$\frac{0.005 \text{ Mol HMDI}}{100 \text{ ml Propan -2-ol}} \times \frac{168.19 \text{ g HMDI}}{1 \text{ mol HMDI}} \times \frac{1 \text{ ml HMDI}}{1.047 \text{ g HMDI}} = \frac{0.803 \text{ ml HMDI}}{100 \text{ ml Propan -2-ol}} \quad (\text{Equation A-2})$$

To prepare Epoxy solution with concentration of 0.005% mol/v, 2.31ml of epoxy was added to 100ml de-ionised water. Equation A-3 shows relevant calculation for obtaining aqueous solution of epoxy with molar concentration of 0.005% mol/v. To prepare this molar concentration epoxy molar mass and density were assumed as 526 g/mol and 1.14 g/ml, respectively.

$$\frac{0.005 \text{ Mol Epoxy}}{100 \text{ ml de-ionised water}} \times \frac{526 \text{ g Epoxy}}{1 \text{ mol Epoxy}} \times \frac{1 \text{ ml Epoxy}}{1.14 \text{ g Epoxy}} = \frac{2.31 \text{ ml Epoxy}}{100 \text{ ml water}} \quad (\text{Equation A-3})$$

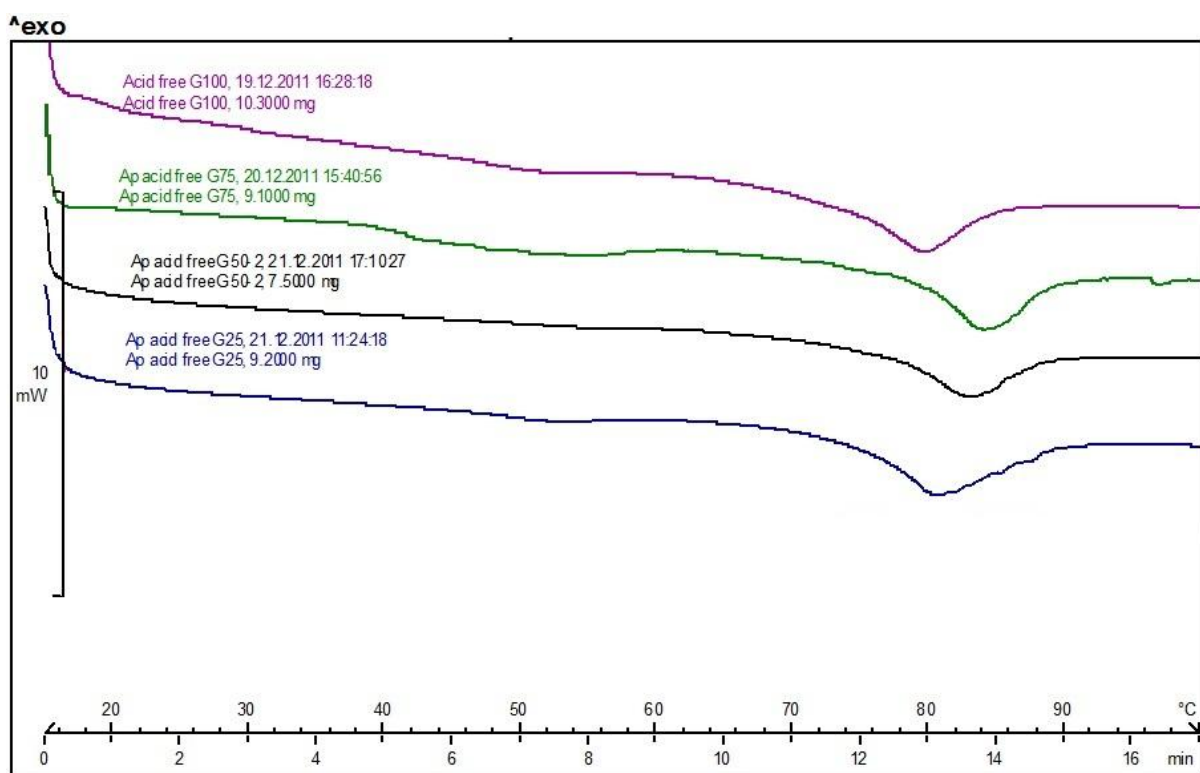
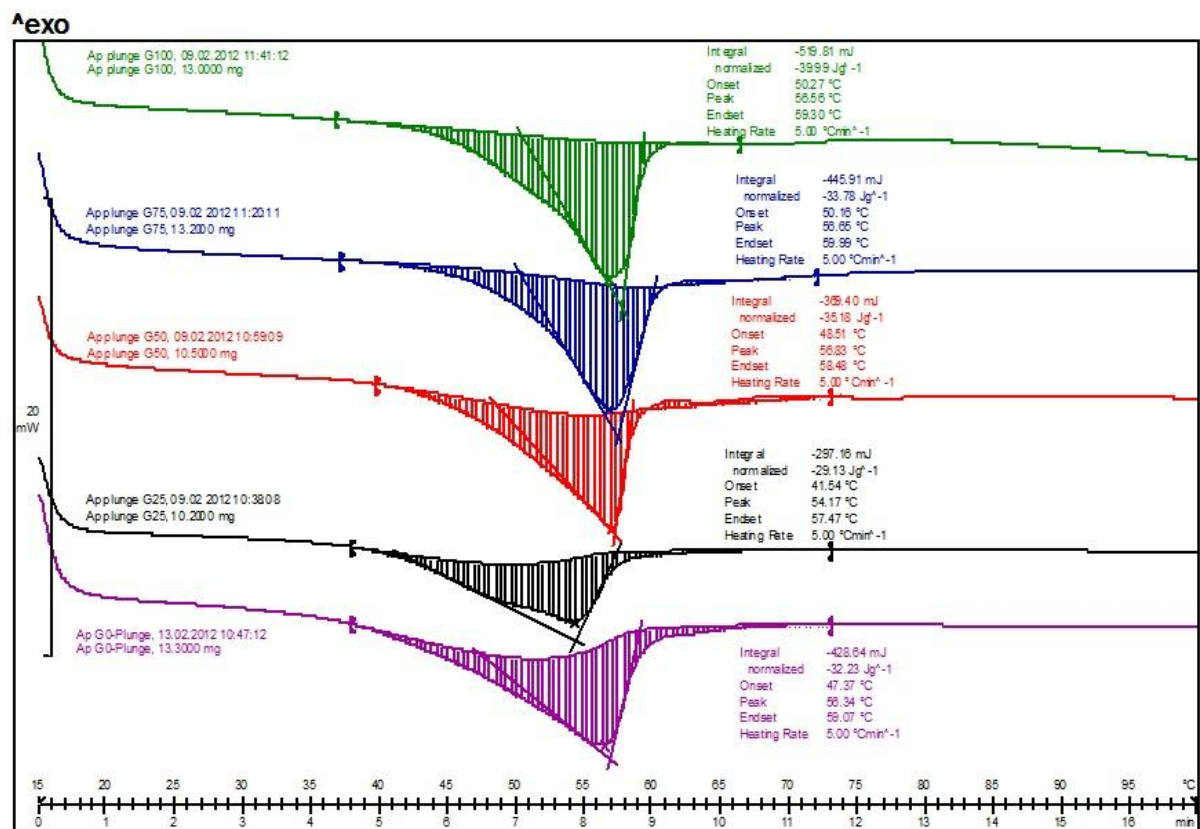
To prepare Genipin solution with concentration of 0.005% mol/v, 1.13g genipin was added to 100ml PBS solution. Equation A-4 shows relevant calculation for obtaining aqueous solution of Genipin. The molar weight of the Genipin used was 226.23 g/mol. Equation 3 shows the calculation used to prepare 0.005% mol/v genipin solution.

$$\frac{0.005 \text{ Mol Genipin}}{100 \text{ ml PBS solution}} \times \frac{226.23 \text{ g Genipin}}{1 \text{ mol Genipin}} = \frac{1.13 \text{ g Genipin}}{100 \text{ ml PBS solution}} \quad (\text{Equation A-4})$$

Appendix 4

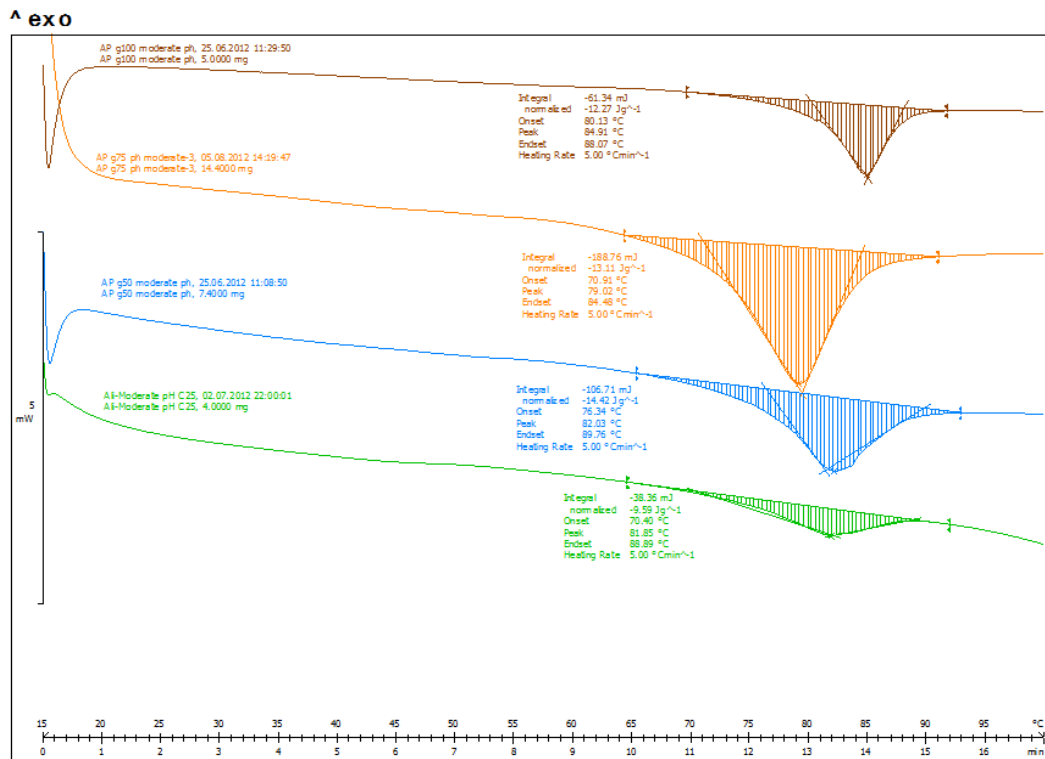
Differential Scanning Calorimetry (DSC) Raw Date

First Generation Scaffolds

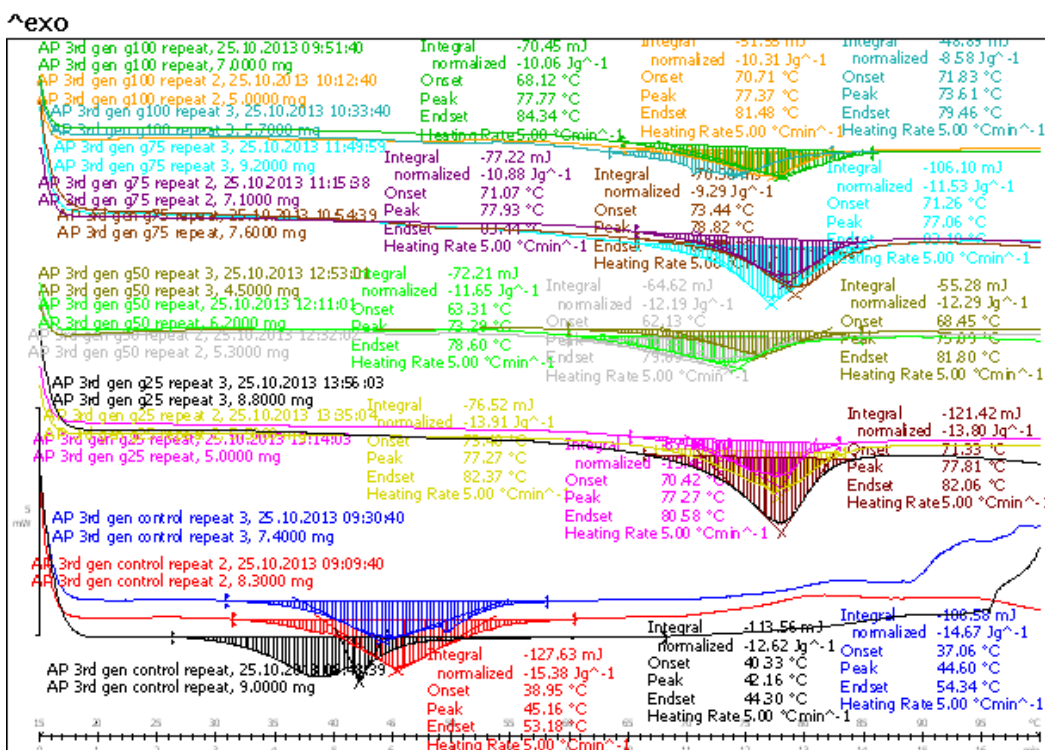
Second Generation Scaffolds pH 2.5¹

¹ This pH was chosen since it shows the importance of pH adjustment for effective GT activity.

Second Generation Scaffolds pH 4.5

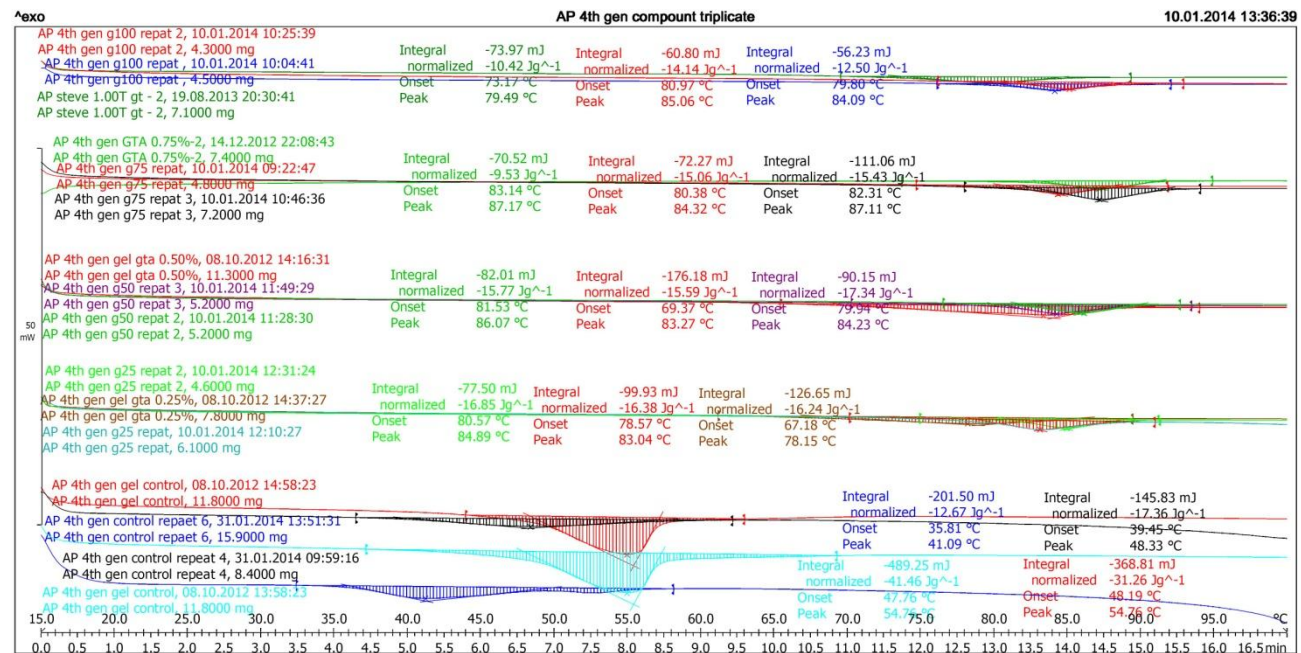


Third Generation Scaffolds

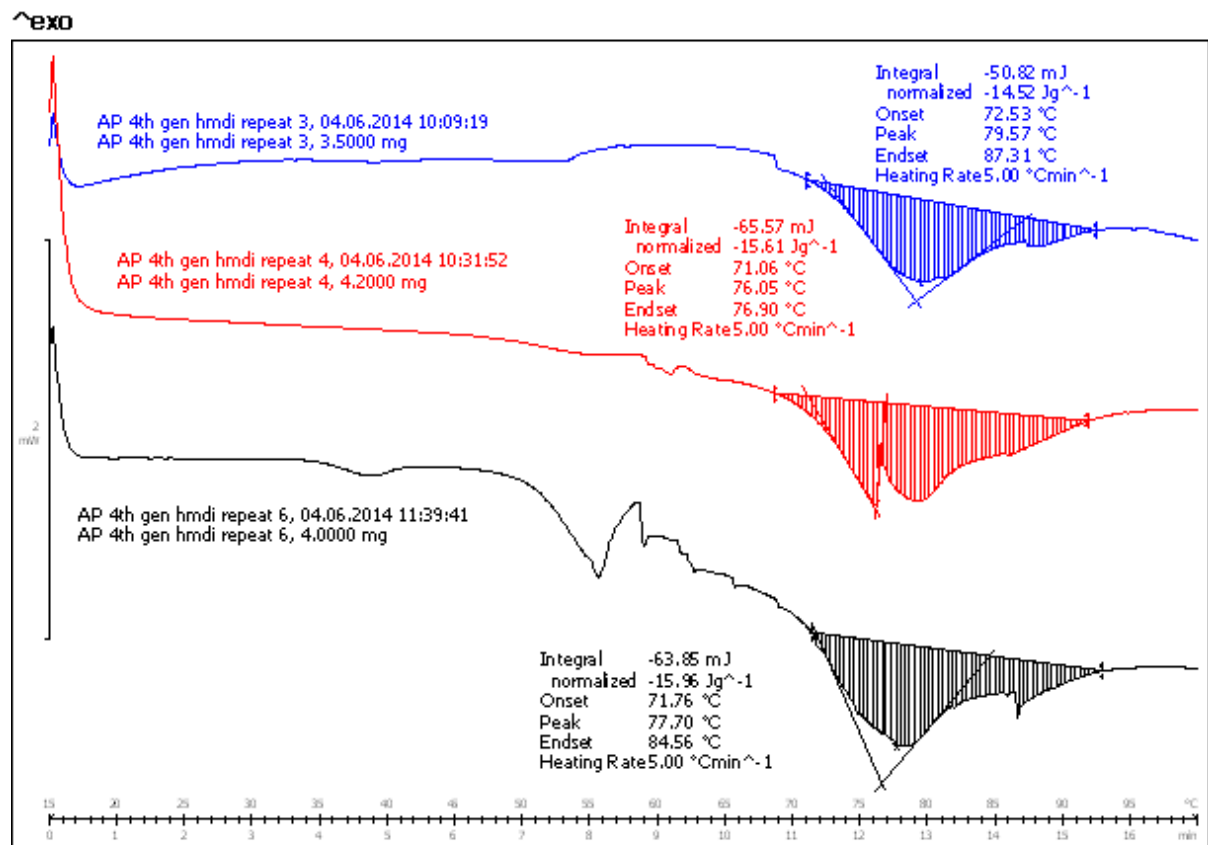


Appendix 4

Fourth Generation Scaffolds



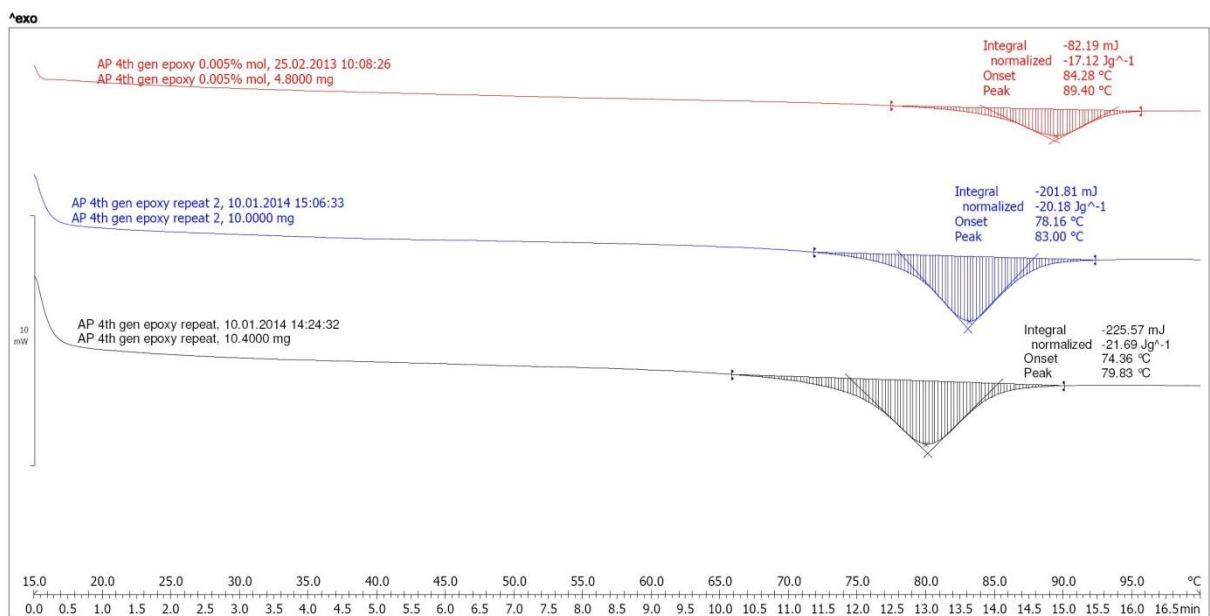
HMDI-crosslinked Scaffolds



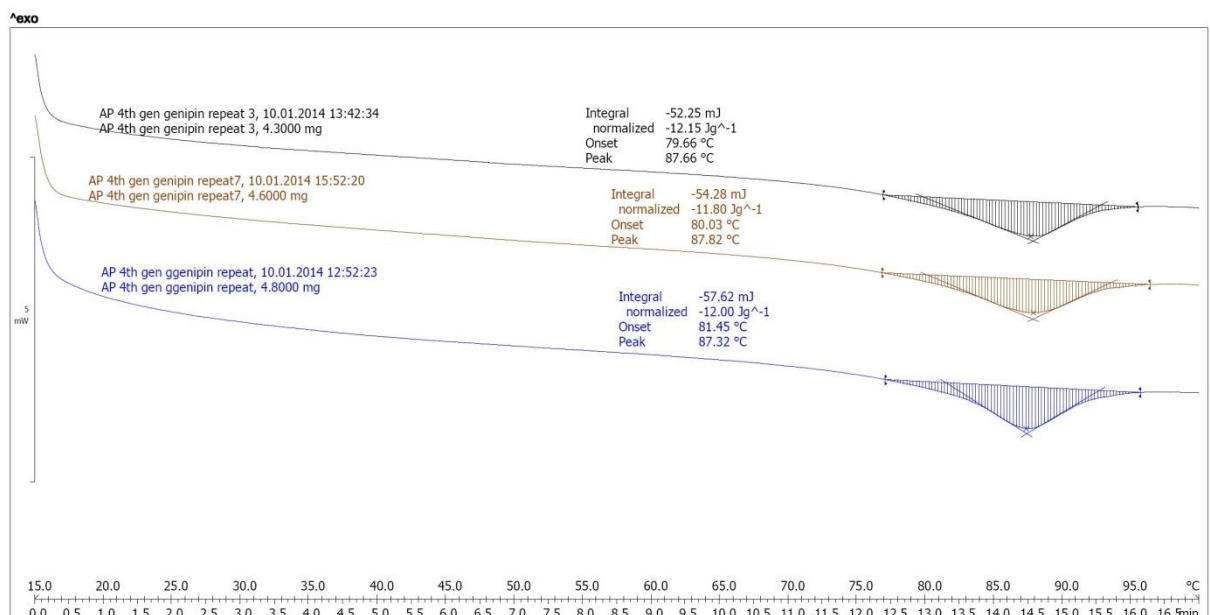
Lab: METTLER

STAR[®] SW 9.10

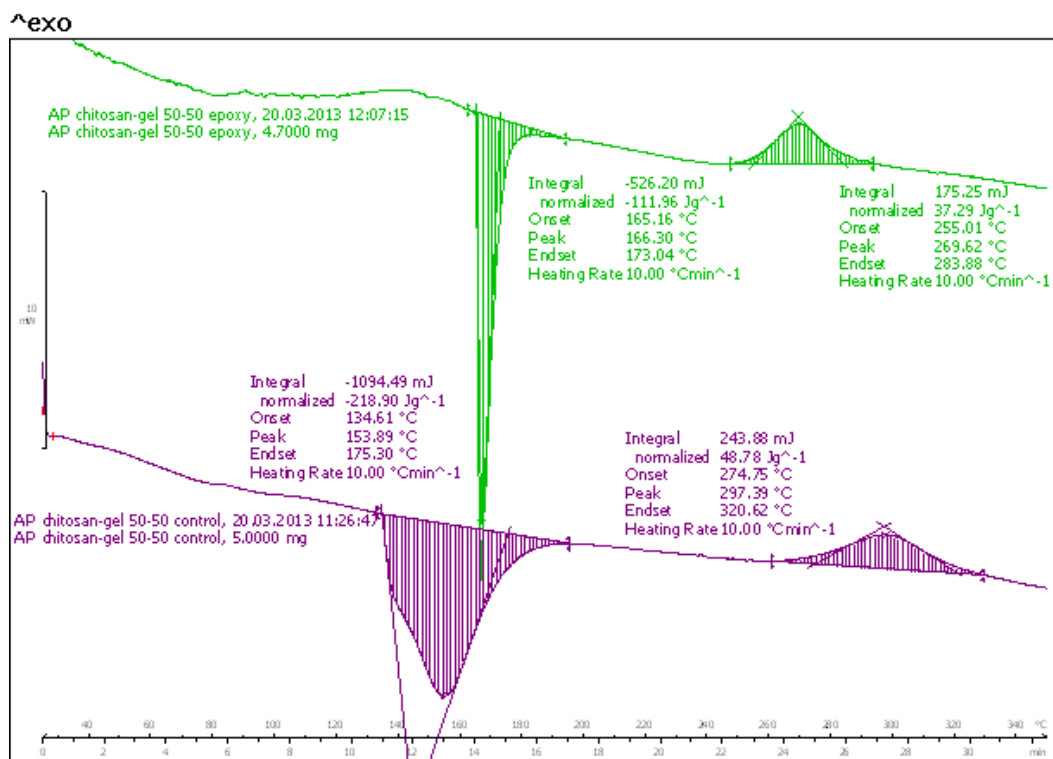
Epoxy-Crosslinked Scaffolds



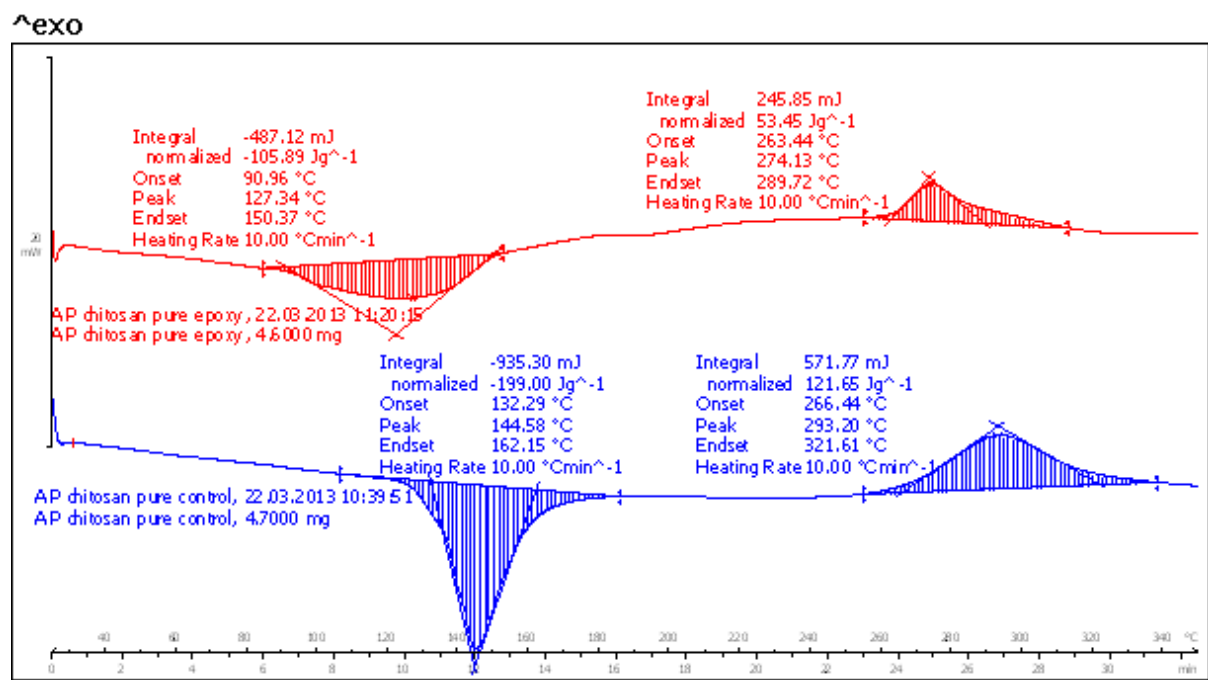
Genipin-Crosslinked Scaffolds



Chitosan-Gelatin Membranes



Pure Chitosan Membrane



Appendix 5

Scientific Contribution up to Present

18th Congress of the European Society of Biomechanics, Lisbon, Portugal,

Title: Porous Gelatin Scaffold Mechanical Behaviour under Cyclic Load as a Function of Water Content

Authors: S. Ali Poursamar, Alexander Lehner, A.P.M. Antunes

Porous gelatin scaffolds have been extensively used for tissue engineering applications. The scaffolds primary role is to act as a means of delivery for seeded cells into the target tissue. It should therefore provide a seeded cellular enclave with adequate mechanical support and suitable conditions for cellular proliferation. Depending on the target tissue, an implanted scaffold would face different loading patterns. Cyclic compressive load prevails within certain tissues such as knee cartilage. Due to their elastic nature, gelatin constructs may be considered a suitable candidate for these *in vivo* applications. However, due to excessive interaction between water and gelatin, characterising their mechanical properties in respect to structure water content is important. Gelatin is highly water absorbent, with the water acting as a plasticiser for gelatin molecules. Higher water content reduces gelatin structural strength but increases its elasticity. In this study porous gelatin scaffolds were subjected to cyclic compressive loading at different water contents.

3rd TERMIS World Congress 2012, 5-8 September 2012, Vienna, Austria

Title: Optimizing gas foaming method to obtain highly porous gelatin scaffolds

Authors: S. Ali Poursamar, Alexander Lehner, A.P.M. Antunes

An ideal tissue engineering scaffold should have a high porosity and inter-connected porous structure. Gas foaming is effective technique in obtaining such structures. In this study, porous gelatin scaffolds were prepared through gas foaming. Acetic acid and sodium hydrogen carbonate were used to produce CO₂ gas within gelatin solution. As result of gas production, gelatin solution turns into foam. Prepared foam crosslinked using Glutaraldehyde and freeze-dried for 24 h before testing. The impact of gelatin Bloom Index on the final product is studied via compressive mechanical testing, SEM analysis, and water absorption. As of any other foaming system, viscosity and rheology of gelatin solution are pivotal in obtaining an optimal porous structure, thus the influence of viscosity changes as a function of solution temperature on the prepared scaffolds macro-structure was also studied. It was shown that at the same temperature, gelatin samples with different bloom indices show different solution viscosities. An ideal viscosity for obtaining optimum scaffold macro-structure is suggested. It was verified that the gelatin bloom index has an impact on scaffold porous micro-texture, mechanical, and physical properties. Preparing porous scaffolds from gelatin with a higher bloom index allows the final structure to show an improved compressive strength, more desirable porous microstructure with better interconnectivity among pores, and a better water absorption capability.

32nd Conference of IULTCS, Istanbul, Turkey, 29-31 May, 2013

Title: A New Variation of Gas Foaming Procedure to Prepare Gelatin Scaffolds for Wound Management

Authors: S. Ali Poursamar, Alexander Lehner, A.P.M. Antunes

In tissue-engineering, scaffolds play a pivotal role in maintaining and promoting new tissue formation. Highly porous gelatin scaffolds can be produced through a gas foaming process. This method is performed within an acidic pH environment which in presence of the correct components causes foam formation. Foaming must be followed by a crosslinking process to stabilise the scaffolds in-vivo and to increase their mechanical properties. In an ordinary gas foaming procedure, foaming and crosslinking steps would be performed separately. This is a long, laborious, and inefficient approach, and in addition, causes matrix pore structure distortion due to prolong interaction with water. Thus performing foaming and crosslinking in one step is desirable. In this study, these two steps were optimised so that they can be performed in a single step. An optimum reaction environment must be maintained to result in maximum possible gassing effects and effective crosslinking at the same time. In this study, the impact of the reaction vessel conditions was examined via mechanical testing, Scanning Electron Microscopy, and thermal analysis. Optimising synthesis procedure makes scaffold microstructure more uniform. Average pore size of the obtained scaffolds was 180 μm . Tensile strength of scaffolds increased as the reaction vessel pH increased, from 40.7 KPa to 100.6 KPa. Increasing the reaction vessel pH from 2 to 4.5, increases the shrinkage temperature of gelatin scaffolds from 54°C to 82°C, respectively. This study showed that optimising crosslinking and foaming together is practical and has remarkable influence on final product properties.

Journal of Material Science and Engineering C, Accepted, Article in Press;

Title: Gelatin Porous Scaffolds Fabricated Using a Modified Gas Foaming Technique: Characterisation and Cytotoxicity Assessment

Authors: S. Ali Poursamar, Javad Hatami, Alexander N. Lehner, Claudia Lobato da Silva, Frederico Castelo Ferreira, A.P.M. Antunes,

The current study presents an effective and simple strategy to obtain stable porous scaffolds from gelatin via gas foaming method. The technique exploits the intrinsic foaming ability of gelatin in the presence of CO₂ to obtain a porous structure stabilised with glutaraldehyde. The produced scaffolds were characterised using physical and mechanical characterisation methods. The results showed that gas foaming may allow the tailoring of the 3-dimensional structure of the scaffolds with an interconnected porous structure. To assess the potential cytotoxicity of using glutaraldehyde as a crosslinker in this method, direct and in-direct cytotoxicity assays were performed at different concentrations of glutaraldehyde. The results indicate the potential of the gas foaming method, in the preparation of viable tissue engineering scaffolds.